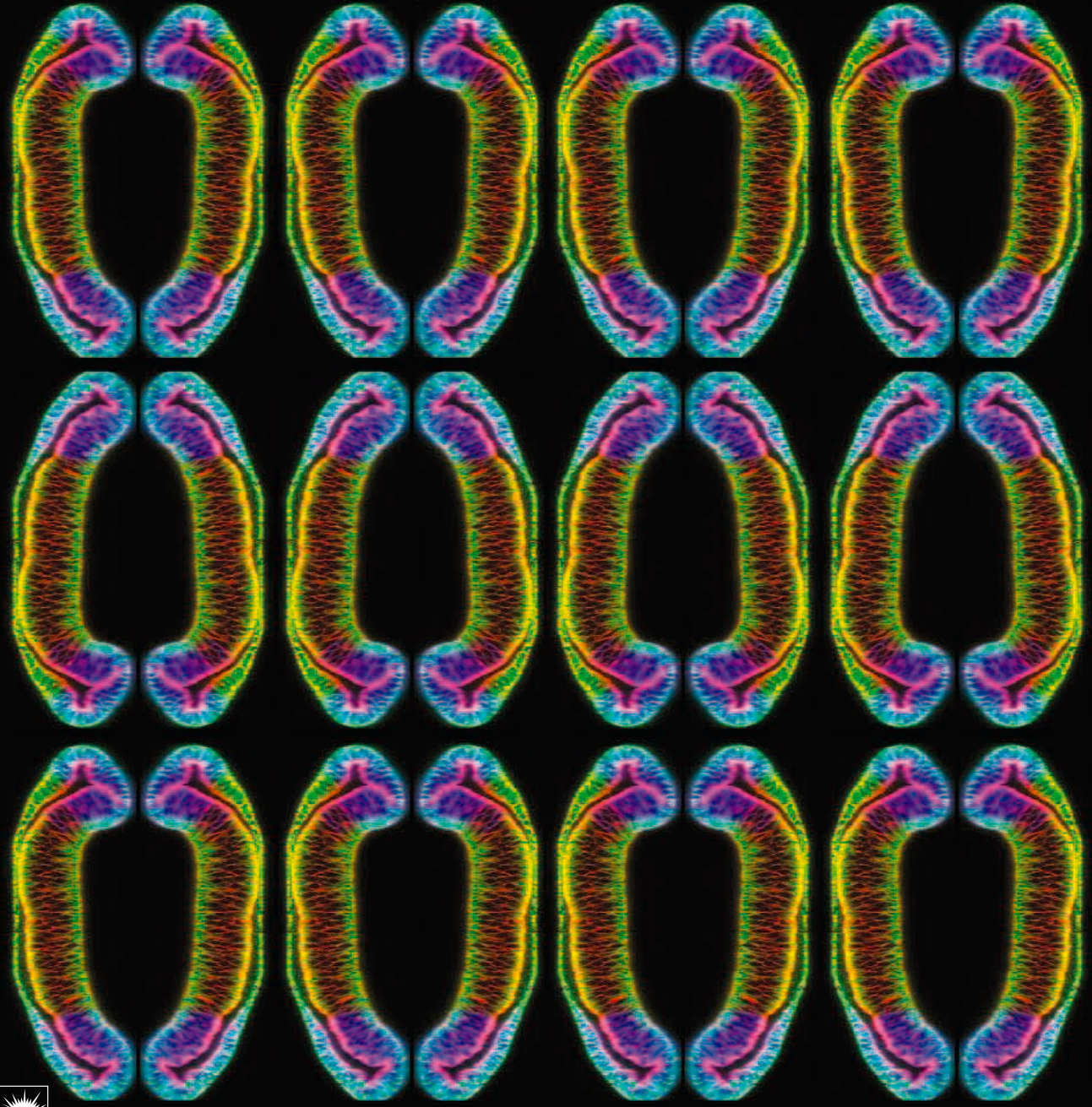


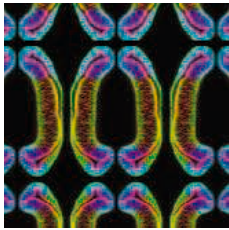


18 March 2005

# Science

Vol. 307 No. 5716  
Pages 1673–1820 \$10





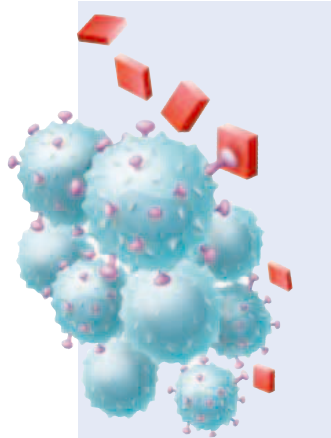
**COVER** Repeated images of an optical cross section through a *Drosophila* wing epithelium very early in development, illustrating that regions lacking a morphogenetic signal (deprived regions shown in blue) also lack a well-organized apical cytoskeleton (yellow band, microtubules and F-actin together). As described on page 1785, extracellular signaling pathways can direct appendage development through position-specific effects on epithelial architecture. [Image: M. Gibson]

## DEPARTMENTS

- 1685 SCIENCE ONLINE
- 1687 THIS WEEK IN SCIENCE
- 1691 EDITORIAL by Hans Wigzell  
A European CDC?
- 1693 EDITORS' CHOICE
- 1698 CONTACT SCIENCE
- 1701 NETWATCH
- 1791 NEW PRODUCTS
- 1792 SCIENCE CAREERS

## NEWS OF THE WEEK

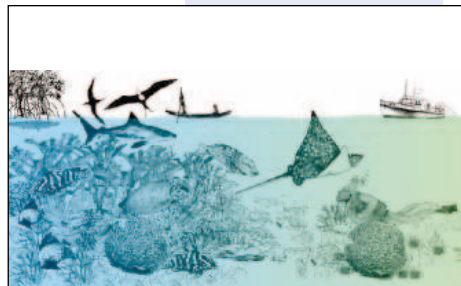
- 1702 **BIOETHICS**  
Anticloning Forces Launch  
Second-Term Offensive  
U.N. Settles on Nonbinding Resolution
- 1703 **CONFLICT-OF-INTEREST POLICY**  
NIH Rules Make Some Pack, Others Plead
- 1705 **EVOLUTION**  
Special Hemoglobin Helped Swim Bladders  
Give Fish Diversity a Lift  
*related Research Article page 1752*
- 1705 SCIENCE SCOPE
- 1706 **GENETICALLY MODIFIED CROPS**  
Safety Research Falls Foul of German Politics
- 1706 **GRADUATE SCHOOLS**  
Drop in Foreign Applications Slows
- 1707 **MARINE GEOLOGY**  
Pursued for 40 Years, the Moho Evades Ocean  
Drillers Once Again
- 1708 **AIDS CLINICAL TRIALS**  
More Woes for Novel HIV Prevention Approach
- 1708 **GENETICS**  
Mutterings From the Silenced X Chromosome
- 1709 **NASA**  
Nominee Wins Quick Praise for His Technical  
Expertise
- 1709 **PLANETARY SCIENCE**  
Enceladus, a Work in  
Progress
- 1711 **DIABETES RESEARCH**  
Researchers Puzzle Over  
Possible Effect of Gleevec
- 1711 **FRENCH SCIENCE**  
INSERM Doubts  
Criminality in Growth  
Hormone Case
- NEWS FOCUS**
- 1712 **DRUG DISCOVERY**  
Magnificent Obsession
- 1715 **HISTORY OF MATHEMATICS**  
'Amateur' Proofs Blend Religion and  
Scholarship in Ancient Japan



1712



1723



1725

- 1716 **PUBLIC HEALTH**  
Provocative Study Says Obesity May Reduce  
U.S. Life Expectancy
- 1718 RANDOM SAMPLES

## LETTERS

- 1720 Combining Parenting and a Science Career  
*C. Djerassi; A. L. Lewis et al.; A. Peekna. Crying "Whorf"*  
*D. Casasanto. Response P. Gordon. Recombinant Virus  
Bank for Gene Delivery K. K. Yokoyama et al.*
- 1722 Corrections and Clarifications

## BOOKS ET AL.

- 1723 **ORNITHOLOGY**  
Nature's Music The Science of Birdsong  
*P. Marler and H. Slabbekoorn, Eds., reviewed by B. Lohr*
- 1724 **APPLIED PHYSICS**  
The Story of Semiconductors  
*J. Orton, reviewed by J. R. Chelikowsky*

## POLICY FORUM

- 1725 **ECOLOGY**  
Are U.S. Coral Reefs on the Slippery Slope  
to Slime?  
*J. M. Pandolfi et al.*

## PERSPECTIVES

- 1727 **CANCER**  
An Anchor for Tumor Cell Invasion  
*S. H. Yuspa and E. H. Epstein Jr.*  
*related Report page 1773*
- 1728 **EVOLUTION**  
Fossil Horses—Evidence for Evolution  
*B. J. MacFadden*
- 1730 **PHYSICS**  
Toward Creating a Rutherford Atom  
*D. M. Villeneuve*  
*related Report page 1757*
- 1731 **CELL BIOLOGY**  
Ras on the Roundabout  
*D. Meder and K. Simons*  
*related Research Article page 1746*
- 1733 **APPLIED PHYSICS**  
Toward Quantum-Information Processing with  
Photons  
*I. A. Walmsley and M. G. Raymer*
- REVIEW**
- 1735 **CELL BIOLOGY**  
The Molecular Requirements for Cytokinesis  
*M. Glotzer*

## SCIENCE EXPRESS [www.sciencexpress.org](http://www.sciencexpress.org)

### NEUROSCIENCE: Target Cell–Dependent Normalization of Transmitter Release at Neocortical Synapses

H. J. Koester and D. Johnston

All synapses between one cortical neuron and any particular target cell have the same calcium response and release probability, indicating that the target cell specifies the synapse type.

### DEVELOPMENTAL BIOLOGY: MicroRNAs Regulate Brain Morphogenesis in Zebrafish

A. J. Giraldez, R. M. Cinalli, M. E. Glasner, A. J. Enright, J. M. Thomson, S. Baskerville, S. M. Hammond, D. P. Bartel, A. F. Schier

In zebrafish embryos, small regulatory RNAs control the movement of cells to form organs and tissues, especially in the nervous system, without determining cell identity.

### MICROBIOLOGY: Nicotinic Acid Limitation Regulates Silencing of *Candida* Adhesins During UTI

R. Domergue, I. Castaño, A. De Las Peñas, M. Zupancic, V. Lockatell, J. R. Hebel, D. Johnson, B. P. Cormack

The low levels of nicotinic acid in the urinary tract trigger expression of an adhesion protein in invading yeast, thus enabling infection.

### ATMOSPHERIC SCIENCE: Assessing Methane Emissions from Global Space-Borne Observations

C. Frankenberg, J. F. Meirink, M. van Weele, U. Platt, T. Wagner

Satellite measurements of the global distribution of methane, an important greenhouse gas, show that tropical rainforests are a surprisingly large source of emissions.



## BREVIA

### 1740 APPLIED PHYSICS: Self-Organized Origami

L. Mahadevan and S. Rica

When a thin object shaped like a leaf or petal is compressed laterally—for example, by growth or heating—coherent spatial waves are produced that lead to self-organized folding.

## RESEARCH ARTICLES

### 1741 PALEOCLIMATE: Southern Hemisphere Water Mass Conversion Linked with North Atlantic Climate Variability

K. Pahnke and R. Zahn

Past changes in mid-depth water formation near Antarctica coincided with both abrupt warming in the Southern Hemisphere and deep water formation in the North Atlantic, implying an atmospheric connection.



1741

### 1746 CELL BIOLOGY: An Acylation Cycle Regulates Localization and Activity of Palmitoylated Ras Isoforms

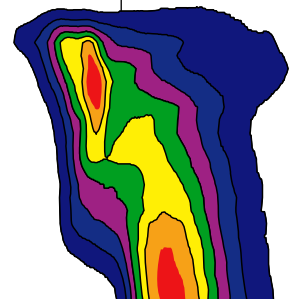
O. Rocks, A. Peyker, M. Kahms, P. J. Verwee, C. Koerner, M. Lumbierres, J. Kuhlmann, H. Waldmann, A. Wittinghofer, P. I. H. Bastiaens

A small signaling protein moves from the plasma membrane to the Golgi apparatus and back, as a lipid is added to and taken off the protein. [related Perspective page 1731](#)

### 1752 EVOLUTION: Evolution of Oxygen Secretion in Fishes and the Emergence of a Complex Physiological System

M. Berenbrink, P. Koldkjær, O. Kepp, A. R. Cossins

The evolution of swim bladders in fish, which inflate with oxygen to control buoyancy, required a series of interrelated changes in hemoglobin, proton transporters, and the development of a complex vascular network. [related News story page 1705](#)



1730 &  
1757

## REPORTS

### 1757 PHYSICS: Microwave Manipulation of an Atomic Electron in a Classical Orbit

H. Maeda, D. V. L. Norum, T. F. Gallagher

Adjusting the frequency of an applied microwave field produces and allows control of a planet-like orbit of an excited electron around a lithium nucleus. [related Perspective page 1730](#)

Contents continued ►

## REPORTS CONTINUED

- 1760 **MATERIALS SCIENCE:** Rheological Measurements of the Thermoviscoelastic Response of Ultrathin Polymer Films  
*P. A. O'Connell and G. B. McKenna*  
 Observing the shape of bubbles inflated in a polymer film shows that thin films can be less flexible than bulk material but still transform to a glass-like state at similar temperatures.

- 1763 **MATERIALS SCIENCE:** The Controlled Evolution of a Polymer Single Crystal  
*X. Liu, Y. Zhang, D. K. Goswami, J. S. Okasinski, K. Salaita, P. Sun, M. J. Bedzyk, C. A. Mirkin*  
 An atomic force microscope coated with a polymer solution is used to nucleate a polymer on a surface, then control and monitor its growth.

### CLIMATE CHANGE

- 1766 **The Climate Change Commitment**  
*T. M. L. Wigley*
- 1769 **How Much More Global Warming and Sea Level Rise?**  
*G. A. Meehl, W. M. Washington, W. D. Collins, J. M. Arblaster, A. Hu, L. E. Buja, W. G. Strand, H. Teng*  
 Two climate models indicate that even if stabilization of greenhouse gases at 2000 or 2005 levels were possible, sea level would still rise 30 cm from thermal expansion alone and much more from glacial melting.

- 1773 **MEDICINE:** Type VII Collagen Is Required for Ras-Driven Human Epidermal Tumorigenesis  
*S. Ortiz-Urda, J. Garcia, C. L. Green, L. Chen, Q. Lin, D. P. Veitch, L. Y. Sakai, H. Lee, M. P. Marinkovich, P. A. Khavari*  
 An abnormal fragment of collagen, a protein that forms a structural matrix outside of cells, causes certain forms of human skin cancer by disrupting the usual controls on cell migration. *related Perspective page 1727*

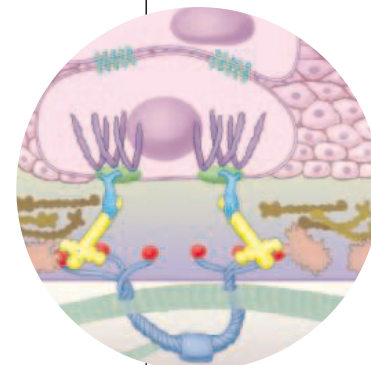
- 1776 **NEUROSCIENCE:** Uncharged tRNA and Sensing of Amino Acid Deficiency in Mammalian Piriform Cortex  
*S. Hao, J. W. Sharp, C. M. Ross-Inta, B. J. McDaniel, T. G. Anthony, R. C. Wek, D. R. Cavener, B. C. McGrath, J. B. Rudell, T. J. Koehnle, D. W. Gietzen*  
 The neurons in the mammalian brain sense which amino acids are missing from the diet by monitoring levels of their uncharged tRNAs, the same system that is used by yeast.

- 1778 **MICROBIOLOGY:** Human Symbionts Use a Host-Like Pathway for Surface Fucosylation  
*M. J. Coyne, B. Reinap, M. M. Lee, L. E. Comstock*  
 The most common microorganism in the human gut coats itself in a sugar molecule identical to one decorating the surface of gut cells and thus escapes immune detection.

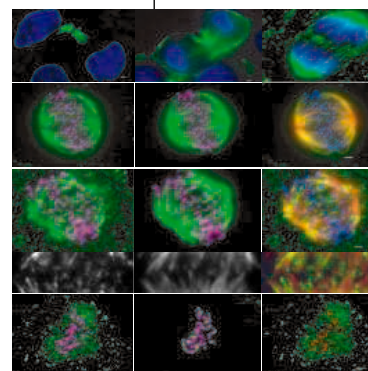
- 1781 **CELL BIOLOGY:** A Mitotic Septin Scaffold Required for Mammalian Chromosome Congression and Segregation  
*E. T. Spiliotis, M. Kinoshita, W. J. Nelson*  
 During cell division, a polymerizing GTP-binding protein helps chromosomes bunch together and then move to the appropriate daughter cell.

### DEVELOPMENTAL BIOLOGY

- 1785 **Extrusion and Death of DPP/BMP-Compromised Epithelial Cells in the Developing *Drosophila* Wing**  
*M. C. Gibson and N. Perrimon*
- 1789 **Extrusion of Cells with Inappropriate Dpp Signaling from *Drosophila* Wing Disc Epithelia**  
*J. Shen and C. Dahmann*  
 Cells in fly wings lacking an important signaling pathway have abnormal cytoskeletons and so are pushed out of the normal flat tissue as blebs, but contrary to early assumptions, they do not die.



1727 &  
1773



1781



ADVANCING SCIENCE, SERVING SOCIETY

SCIENCE (ISSN 0036-8075) is published weekly on Friday, except the last week in December, by the American Association for the Advancement of Science, 1200 New York Avenue, NW, Washington, DC 20005. Periodicals Mail postage (publication No. 484460) paid at Washington, DC, and additional mailing offices. Copyright © 2005 by the American Association for the Advancement of Science. The title SCIENCE is a registered trademark of the AAAS. Domestic individual membership and subscription (51 issues): \$135 (\$74 allocated to subscription). Domestic institutional subscription (51 issues): \$550; Foreign postage extra: Mexico, Caribbean (surface mail) \$55; other countries (air assist delivery) \$85. First class, airmail, student, and emeritus rates on request. Canadian rates with GST available upon request, GST #1254 88122. Publications Mail Agreement Number 1069624. Printed in the U.S.A.

Change of address: allow 4 weeks, giving old and new addresses and 8-digit account number. Postmaster: Send change of address to Science, P.O. Box 1811, Danbury, CT 06813-1811. Single copy sales: \$10.00 per issue prepaid includes surface postage; bulk rates on request. Authorization to photocopy material for internal or personal use under circumstances not falling within the fair use provisions of the Copyright Act is granted by AAAS to libraries and other users registered with the Copyright Clearance Center (CCC) Transactional Reporting Service, provided that \$15.00 per article is paid directly to CCC, 222 Rosewood Drive, Danvers, MA 01923. The identification code for Science is 0036-8075/83 \$15.00. Science is indexed in the Reader's Guide to Periodical Literature and in several specialized indexes.

Contents continued ►



### More Science, Less Friction

Simulation study shows how a motor oil ingredient protects engines from wear.

### The Consummate Sperm Protein

Newly discovered protein is crucial for sperm-and-egg fusion.

### Cluster Computing Gets Closer

New study shows that an alternative route to quantum computing is feasible.



Plan your industry move carefully.

## science's next wave [www.nextwave.org](http://www.nextwave.org) CAREER RESOURCES FOR YOUNG SCIENTISTS

### US: Tooling Up—The Job-Offer Checklist *D. Jensen*

A job in industry has much to offer, but look before you leap.

### US: The 2005 National Postdoc Association Meeting *J. Austin*

Next Wave Editor Jim Austin reports from this year's NPA meeting in San Diego.

### CANADA: Dirty Bombs and Other Career Stories of a Defense Scientist *A. Fazekas*

A young researcher working with Canada's Radiological Analysis and Defense group shares her story.

### EUROPE: European Science Bytes *Next Wave Staff*

Read the latest funding, training, and job market news from Europe.

### MiSciNET: Profile—Margaret Hiza Redsteer *A. Sasso*

A Native American geologist with the U.S. Geological Survey has had to endure many hardships.

### MiSciNET: Bridges to Native American Students in Community Colleges Program *G. Kuehn*

New Mexico State University aims to increase the number of Native American students with degrees and working in biomedical research.

## science's sage ke [www.sageke.org](http://www.sageke.org) SCIENCE OF AGING KNOWLEDGE ENVIRONMENT

### PERSPECTIVE: The Genetic Basis of Aging—An Evolutionary Biologist's Perspective *D. N. Reznick*

Analyses of aging in model organisms offer a limited view of how senescence occurs.

### NEWS Focus: How Low Can You Go? *R. J. Davenport*

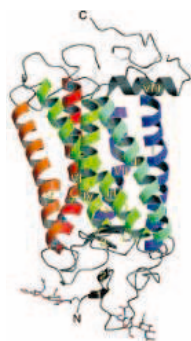
Molecule might improve statins' cholesterol-depleting power.

### NEWS Focus: Outrunning Alzheimer's Disease *M. Leslie*

Exercise curbs  $\beta$  amyloid buildup in mice.



Evolution and aging.



Crystal structure of rhodopsin.

## science's stke [www.stke.org](http://www.stke.org) SIGNAL TRANSDUCTION KNOWLEDGE ENVIRONMENT

**TEACHING RESOURCE: Structure of G Protein-Coupled Receptors and G Proteins** *R. Iyengar*  
Lecture materials for a graduate-level course are provided.

**CONNECTIONS MAP OVERVIEW: Ethylene Signaling Pathway** *A. N. Stepanova and J. M. Alonso*  
New evidence suggests the MAPK6 module may not contribute to ethylene responses.

**CONNECTIONS MAP OVERVIEW: Arabidopsis Ethylene Signaling Pathway** *A. N. Stepanova and J. M. Alonso*

New results prompt removal of some components of the pathway.

Separate individual or institutional subscriptions to these products may be required for full-text access.

**GrantsNet**  
[www.grantsnet.org](http://www.grantsnet.org)  
RESEARCH FUNDING DATABASE

**AIDScience**  
[www.aidsience.com](http://www.aidsience.com)  
HIV PREVENTION & VACCINE RESEARCH

**Members Only!**  
[www.AAASMember.org](http://www.AAASMember.org)  
AAAS ONLINE COMMUNITY

**Functional Genomics**  
[www.sciencegenomics.org](http://www.sciencegenomics.org)  
NEWS, RESEARCH, RESOURCES

## Collagen as Oncoprotein

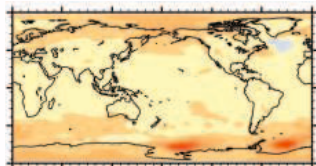
Patients with an inherited skin disorder called recessive dystrophic epidermolysis bullosa (RDEB) often develop squamous cell carcinoma, a form of skin cancer that is common in the general population. RDEB is caused by mutations in the gene encoding the extracellular matrix (ECM) protein collagen VII, but the role of collagen in cancer development has been unclear. **Ortiz-Urda et al.** (p. 1773; see the Perspective by **Yuspa and Epstein**) now show that RDEB patients who develop cancer express an aberrant, truncated version of collagen VII that confers tumorigenic properties to skin cells, by enhancing their ability to invade surrounding tissue. In mice, tumor induction can be blocked by administration of antibodies targeting this collagen fragment. These results highlight the critical role of the ECM in tumorigenesis and suggest that ECM proteins may be valuable therapeutic targets for certain forms of cancer.

## The Good Food Sense

Some animals can recognize that a meal is deficient in amino acids, and thus reject such offerings within 20 minutes. This behavioral response to amino acid deficiency in omnivores has been known for some time, but the nutrient sensor has eluded discovery. **Hao et al.** (p. 1776) found that an ancient amino acid sensing mechanism found in yeast is conserved in the neurons of the anterior piriform cortex. This amino acid chemosensory brain area projects to neural circuits controlling food intake.

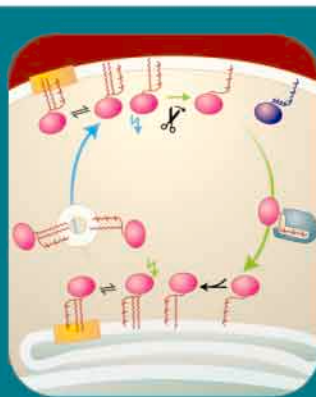
## Thermal Inertia and Climate

If the emission of greenhouse gases were to stop today, their associated global warming would continue because of the long lifetime of the gases in the atmosphere and thermal inertia of the ocean, and sea level rise would continue because of thermal expansion. Two modeling studies address these issues. **Wigley** (p. 1766) discusses the long-term climate warming commitment we have made already, as well as that which would occur under the still highly optimistic scenario of no further rise in the rate of greenhouse gas emissions. **Meehl et al.** (p. 1769) quantify how much more global warming and sea level rise (just from thermal expansion) could be expected had greenhouse gas concentrations been frozen at their 2000 levels. Both studies conclude that even in these best-case scenarios, temperatures



## Letting Ras Know Where It's At

The correct spatial organization of cellular signaling molecules is crucial to ensuring proper biological response. Some signaling proteins, such as the Ras guanine triphosphatases, are modified by lipids that direct their localization to the plasma membrane and to intracellular membranes of the Golgi complex. Ras proteins are thought to acquire these lipid moieties while transiting through the secretory pathway. **Rocks et al.** (p. 1746, published online 10 February 2005, see the Perspective by **Meder and Simons**) now find that Ras becomes depalmitoylated at the plasma membrane, releasing the protein to the cytoplasm. Released Ras that is redistributed to the Golgi becomes repalmitoylated and subsequently transported to the cell surface, where the acylation cycle begins again. These changes in palmitoylation correlate with Ras signaling and provide a mechanism for controlling Ras protein intracellular distribution.



will rise by as much as 0.5°C and sea level will rise by tens of centimeters, not including any melting from ice sheets and glaciers.

## Radio-Controlled Electrons

Although atoms are often depicted with discrete electrons orbiting the nucleus, electrons are more properly described as delocalized clouds. However, under the right excitation conditions, the classical model can pertain. When electrons are excited sufficiently that the level spacing is much smaller than the total energy, they can occupy several levels at once. This delocalization in energy leads to a corresponding localization in space, and temporarily the electrons resemble classical orbiting particles. **Maeda et al.** (p. 1757, published online 10 February 2005, see the Perspective by **Villeneuve**) have stabilized Li atoms in this state by applying a microwave field tuned to the orbiting frequency. They further show that by adjusting the microwave frequency, they can fine-tune the period and radius of the electron orbit, along with the corresponding binding energy.

## Probing Polymer Creep and Crystallization

The motion of polymer chains in thin films is complex; the presence of a free surface should allow for greater degrees of freedom in their motion, but the reduced dimension of the film restricts mobility. These effects are reflected in the glass

transition temperature and the rheology of the films. **O'Connell and McKenna** (p. 1760) use the inflation of a bubble to measure the compliance of thin polymer films. While they see no changes in the glass transition temperature, they do see dramatic changes in the film's elasticity. For polymers that can partially crystallize, the crystallization process is relatively slow. The morphologies that form depend on the processing conditions, the orientations of chains before solidification, and residual stresses. **Liu et al.** (p. 1763) have devised an atomic force microscope that can deliver polymer chains and take images at the same time, thus allowing for exquisite control and observation of the crystallization.

## Breaking Up Is Hard To Do

Proper cell division—the formation of two daughter cells from a single mother cell—involves mitosis, during which duplicated chromosomes are separated, and cytokinesis, the separation of the two daughter cells. **Glotzer** (p. 1735) reviews what is known

CONTINUED ON PAGE 1689

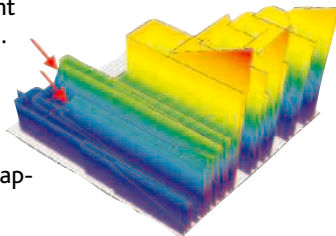
about the cellular mechanisms involved in cytokinesis in a variety of cellular systems. Coordination of cytokinesis with chromosome congression and segregation is critical for proper cell division. In a Report, **Spiliotis et al.** (p. 1781) describe their study of a conserved family of binding proteins known as the septins that localize to the metaphase plate during mammalian mitosis. Septin depletion disrupted the accumulation of chromosomes and their segregation and led to defects in cytokinesis. These defects correlated with a failure of CENP-E, a mitotic motor and mitotic checkpoint regulator, to localize correctly on congressing chromosomes. Mammalian septins may thus form a mitotic scaffold that coordinates chromosome congression and segregation with cytokinesis.

## Change Down Under

The ocean process most commonly associated with global climate change is the formation of deep water in the North Atlantic, but a growing body of observations and model results implicate other parts of the ocean, particularly in the Southern Hemisphere. **Pahnke and Zahn** (p. 1741) examine the role of Antarctic Intermediate Water (AAIW), which forms in the southern mid-latitudes and is found at depths between 500 and 100 meters, in redistributing heat and fresh water within the deeper oceans. Changes in AAIW formation during the last 340,000 years were coupled to variations in North Atlantic deep water formation and climate change in the Antarctic. The contemporaneous responses implicate the atmosphere in forcing the climate changes.

## The Eyes—and the Swimbladder—Have It

Teleost fishes maintain buoyancy using a gas-inflated swimbladder. Oxygen is pumped into the swimbladder by means of a complex arrangement of veins and arteries, known as the *rete mirabile*, and special pH sensitive "root-effect" hemoglobins, which also have low specific buffer values. A  $\text{Na}^+/\text{H}^+$  exchanger regulates the intracellular pH of red blood cells. Many fish also have an ocular *rete mirabile* to support the high metabolic activity of the avascular fish retina. **Berenbrink et al.** (p. 1752) use phylogenetics, the biochemistry and structure of hemoglobins, and details of the activity of the  $\text{Na}^+/\text{H}^+$  exchanger in extant fishes to explain the evolution of this complex system. Root-effect hemoglobins must have appeared before the *rete mirabile*. The ocular *retia*—which required the presence of the  $\text{Na}^+/\text{H}^+$  exchanger—likely evolved 100 million years before the swimbladder *retia*, whose appearance correlates with significant adaptive radiation in teleost fish.



## Sugary Coating

How do humans tolerate the presence of billions of bacteria in the gut without mounting an inflammatory response? **Coyne et al.** (p. 1778) analyze the most common bacterial genus found in the human intestine (*Bacteroides*) and show that these organisms decorate their capsular polysaccharides and surface glycoproteins with L-fucose. L-Fucose is abundant on the surface of intestinal epithelial cells, and *Bacteroides* stimulates intestinal epithelial cells to express fucosylated molecules. This molecular mimicry allows *Bacteroides* to be tolerated by the host.

## The Right Stuff for Wing Formation

Animal organs and appendages are comprised of cells with different morphologies. For example, the *Drosophila* wing primordium displays cells that are squamous, cuboidal, or columnar. What are the molecular determinants for this cell variation? **Gibson and Perrimon** (p. 1785) examine this question by screening flies with defects in epithelial cell morphogenesis in the wing. Mutation of a signaling receptor produced a wing defect in which cells are extruded from the epithelial surface. Contrary to earlier work that implicated this signaling pathway in cell survival, it appears that the signaling pathway is instead involved in epithelial organization, and any subsequent cell death is a secondary effect. Similar conclusions are also reached by **Shen and Dahmann** (p. 1789).



### RESEARCH GRANT AWARDS

**Five-Year named Chairs for Senior and Junior Faculty**, maximum of \$1,100,000 over a five-year period.

**One-Time Start-Up Cost Grant**, maximum of \$1,000,000.

**Individual Grants**, maximum of \$200,000 per year, research grants for basic or clinical research on spinal cord injury and disease.

### Postdoctoral & Graduate Student Fellowship Awards

Applicants must be associated with a New Jersey Institution and may collaborate with researchers out-of-state and country.

Application form and details at: [www.state.nj.us/health/spinalcord/](http://www.state.nj.us/health/spinalcord/)

Application form and details from: **New Jersey Commission on Spinal Cord Research**  
PO Box 360

Market and Warren Streets  
Trenton, New Jersey 08625-0360  
Tel: 609-292-4055

E-mail: [njcscri@doh.state.nj.us](mailto:njcscri@doh.state.nj.us)

Closing Date for Grant Applications:  
**June 8, 2005**

**Q:** How can I organize and protect my back issues of *Science*?

**A:** Custom-made library file cases!



Great gift idea!

Designed to hold 12 issues and covered in a rich burgundy leather-like material, each slipcase includes an attractive label with the *Science* logo.

One ..... \$15  
Three ..... \$40  
Six ..... \$80

Send order to:  
**TNC Enterprises Dept.SC**  
P.O. Box 2475  
Warminster, PA 18974

Specify number of slippases and enclose name, address and payment with your order (no P.O. boxes please). Add \$3.50 per slipcase for shipping and handling. PA residents add 6% sales tax. Cannot ship outside U.S.

**Credit Card Orders:** AmEx, VISA, MC accepted. Send name, number, exp. date and signature.

**Order online:**  
[www.tncenterprises.net/sc](http://www.tncenterprises.net/sc)

**Unconditionally Guaranteed**

## A European CDC?

Infectious diseases have made an unfortunate comeback. After the Second World War, the development of new vaccines and discoveries of efficient antibiotics meant to many that lethal infectious disorders were enemies of the past. But, not surprisingly, nature has hit back. We now face an increasing number of deadly drug-resistant bacteria, including the mycobacterium that causes tuberculosis, as well as staphylococci. Around 1% of the world population is now infected with HIV. The severe acute respiratory syndrome (SARS) epidemic of 2003 demonstrated just how enormous the social and economic effects of such new infectious diseases can be, and a global avian flu pandemic hovers on the horizon. Moreover, the communicable nature of these diseases is exacerbated by modern travel.

Hence, the decision taken by the European Union (EU) in April 2004 to create a European Center for Disease Prevention and Control (ECDC) is commendable. But what is the potential capacity of the center to fulfill its important mission? The ECDC will start operating in May 2005 in Stockholm, Sweden. The center shall “identify, assess and communicate current and emerging threats to human health from communicable diseases,” surely a broad mission to cover. The budget for the center is put at approximately 5, 15, and 30 million euros for 2005, 2006, and 2007, respectively. Compared to a present budget for the U.S. Centers for Disease Control (CDC) of around \$4 billion, this budget is hardly inspiring. Even in 2007, the ECDC budget will be less than those of many national disease centers in Europe, and that dictates a stringent policy regarding priorities for deciding which tasks can best be performed by the agency. The current instructions put major emphasis on the operation of surveillance networks and the provision of technical and scientific expertise to the 25 member states. And although the directives repeatedly emphasize the need for the ECDC to provide scientific expertise to the EU, the center will lack laboratories of its own and be devoid of regulatory power.

The director of the ECDC, Zsuzsanna Jakab, will be crucial in shaping the policy and position of the agency within the EU. Jakab, from Hungary, is a former politician with a long administrative background at the regional office of the World Health Organization (WHO) in Copenhagen. In contrast to most directors of disease centers around the world, Jakab lacks medical expertise and scientific background in the field. But her knowledge of EU and WHO bureaucracies may prove invaluable for skillful navigation around the archipelagos of political complexity. However, equally vital for a successful ECDC will be the new director’s ability to create an attractive environment for scientists of high quality.

The response to the ECDC has generally been positive. Of course, concerns continue about its power to fulfill an ambitious mission on a minimal budget. It is also unclear how existing projects within the present EU budget concerning public health and communicable diseases will be affected. Scientific experts often require strong ongoing links to research in order to maintain their expertise. Can Jakab construct such an environment in an institute without labs? Perhaps she can; France and Ireland, for example, have disease centers that are considered to function quite well without laboratories. However, as a putative hub of expertise among EU member states, the lack of infrastructure at the ECDC could pose a challenge to its mission.

Harmony among states with regard to rules for handling epidemics of infectious diseases in the EU region is critical, especially in an emergency. Without regulatory power, the ECDC will somehow have to support this cause by relying on other devices. That will be a challenge: Several EU countries defend their rights to have their own laws for handling infectious diseases, whereas others support a common European law. And with an impending avian flu epidemic on its radar screen, the ECDC will have to move swiftly to coordinate EU strategies for handling a potential crisis.

So, what are we left with? A European variant of the U.S. CDC, with a much more restricted role as the coordinating center for networks of surveillance, based largely on independent national agencies. An external evaluation will no doubt be needed in a few years to measure the effectiveness of this European model. Given such formidable challenges, is it conceivable that the ECDC could emerge as a leading international scientific institution in the control of infectious diseases? We look forward, hopefully, to that possibility.

**Hans Wigzell**

Hans Wigzell is Director for Medical Innovation at the Karolinska Institute, Stockholm, Sweden, and Scientific Advisor to the Swedish Government.



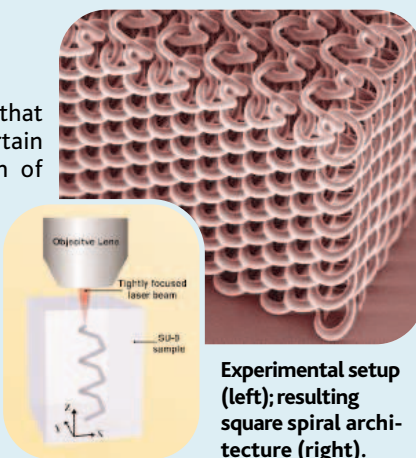


edited by Stella Hurtley

## MATERIALS SCIENCE

## Spiral Photonic Crystals

Photonic crystals are periodic dielectric structures that have a band gap that stops the propagation of a certain frequency range of light. Through the inclusion of defects or cavities, photonic crystals can be designed to trap or guide light and are thus of considerable interest for use in optics and communications. Three-dimensional photonic crystals have been designed from theory, but most have a complex structure that cannot be fabricated using traditional layer-by-layer approaches. Seet *et al.* use direct laser writing to fabricate circular and square spiral architecture structures. The process works through the curing or hardening of a polymeric photoresist as it absorbs multiple photons from a tightly focused laser beam. In previous systems, a liquid photoresist has been used, but because of shrinkage that occurs on curing, this method limits the resolution that can be obtained. The photoresist SU-8, by contrast, is solid both before and after processing and undergoes only small refractive index and density changes upon curing, making the writing process more uniform. Because of the self-supporting nature of the material, complex defect structures could be engineered into the periodic crystals. — MSL



Experimental setup (left); resulting square spiral architecture (right).

*Adv. Mater.* 17, 541 (2005).

nuclear envelope defects and concomitantly other defects, such as those in histone modification, are rescued—effectively reversing the cellular aging process. These findings may provide an avenue of hope for potential therapies aimed at this distressing, though extremely rare, condition. In addition, detailed understanding of the cellular aging process will be important in helping to combat the symptoms of aging in the general population. — SMH

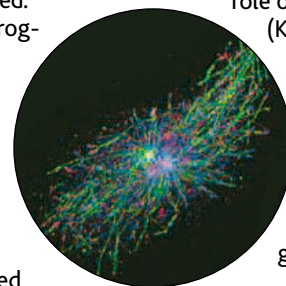
*Nature Med.* 7, 235 (2005).

## CELL BIOLOGY

## Division of Labor

Eukaryotic cells contain a dynamic array of cytoskeletal elements—microtubules—that organize key events in the cell's life cycle, including cell division. The regulation of microtubule polymerization and depolymerization, processes that both occur at the so-called plus ends of microtubules, must therefore be carefully controlled.

Mennella *et al.* looked at the role of two kinesins (KLPs) and how they cooperate to control appropriate microtubule dynamics. KLP10A targeted micro-



Motor protein KLP10A (red) follows EB1 (blue) to the ends of a subset of microtubules (green).

tubules via the microtubule plus-end tracking protein EB1 and stimulated microtubule catastrophe—a process in which a growing microtubule suddenly changes its behavior and shrinks rapidly. KLP59C also stimulated microtubule depolymerization, but by sup-

## ECOLOGY/EVOLUTION

## Preserving the Reserves

Protected areas of tropical forests harbor some of the greatest concentrations of terrestrial biodiversity, and the maintenance of this wealth depends in part on the integrity of the surrounding unprotected habitat. The effectiveness of protected areas for conservation of ecosystems

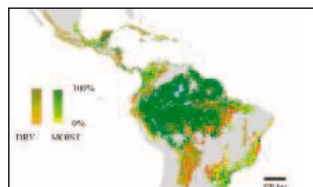
and biodiversity is a continual source of anxiety for conservationists, especially when such areas are remote and difficult to monitor. Using satellite data, DeFries *et al.* have completed a global assessment of the extent of forest loss within and around nearly 200 protected areas in the tropics over the past 20 years. The capacity of surrounding buffer zones to enhance the effective size of protected areas has diminished in most cases over this period, and there has been a near-universal trend toward increasing isolation of protected areas. This trend has been especially sharp in Asian tropics and in dry tropical forests, where the protected areas themselves have often suffered habitat loss. As the surrounding areas become decreasingly effective as buffer zones, the management of protected areas will need to focus more sharply on the ecological interactions at the boundary if biodiversity is not to be further eroded. — AMS

*Ecol. App.* 15, 19 (2005).

## CELL BIOLOGY

## Reversing the Signs of Aging

Progeria is a devastating disease in which the normal processes of aging appear to be alarmingly accelerated. Hutchinson-Gilford progeria is caused by a mutation in one of the nuclear lamin genes that leads to the production of a truncated form of lamin A (De Sandre-Giovannoli *et al.*, *Science* 27 June 2003, p. 2055; published online 17 April 2003). Nuclear lamins line the inner nuclear membrane and help to maintain nuclear integrity. Cells taken from progeric patients display nuclear abnormalities, including severe morphological defects in the nuclear envelope. Now Scaffidi and Misteli show that simple expression of wild-type lamin does not rescue this cellular phenotype. Instead, suppressing the expression of the mutant lamin "cures" the



Logging in the tropics (bottom); forestation decline (red) in Latin America (top).



pressing a process termed rescue—when the behavior of a shrinking microtubule is converted to growth. Both motors were found at the plus ends of distinct subpopulations of microtubules (KLP10A on polymerizing microtubules and KLP59C on depolymerizing microtubule). Thus, there appears to be a division of labor within cells between these two molecular motors to locally control microtubule dynamics. — SMH

*Nature Cell Biol.* 7, 235 (2005).

**APPLIED PHYSICS**

**Canceling Brownian Motion**

One problem in trapping small particles or cells in solution for further study is the ever-present jostling caused by Brownian motion. Cohen and Moerner have developed an anti-Brownian electrophoretic, or ABEL, trap that cancels Brownian motion. Particle movement was followed via fluorescence microscopy. Images were acquired and processed in real time, and the resulting analysis

was used to apply voltages to a set of four electrodes, which create a gap of 10 to 15  $\mu\text{m}$  around the particle. The applied electric fields create electrophoretic drift that cancels Brownian motion in the

plane. Excursions of polystyrene nanospheres of more than 5  $\mu\text{m}$  from the center of the trap were rare. — PDS

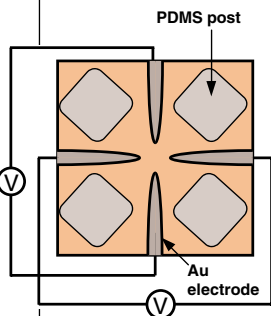
*Appl. Phys. Lett.* 86, 093109 (2005).

**GEOLOGY**

**On Top of the World**

The Himalayas and Tibet now have Earth's highest elevation, approaching 5 km above sea level on average, but it has been unclear how long this has been the case. One hypothesis is that within the past 5 to 10 million years, the dense lower crust and upper mantle of Tibet have detached and sunk, allowing an influx of hotter, less dense mantle that produced rapid uplift in this region. Some recent evidence based on elevation ranges of fossil plants, however, has implied that elevations were already high 15 to 20 million years ago. Currie *et al.* used a different approach to determine paleoelevations—the oxygen isotopes in carbonate minerals deposited in ancient lakes on the leeward (northern) side of the Himalayas. The basic idea is that as air masses encounter mountains, they rise, producing rain and snow, which decreases the  $^{18}\text{O}/^{16}\text{O}$  ratio of water vapor in the air mass. Higher mountains lead to further reductions in this ratio. The data from the ancient lakes are consistent with the plant fossil data and imply that the Himalayas have been about 5 km high for about 15 to 20 million years. Although a detached slab of crust is not ruled out, their high uplift may require another explanation. — BH

*Geology* 33, 181 (2005)



**ABEL trap.**

was used to apply voltages to a set of four electrodes, which create a gap of 10 to 15  $\mu\text{m}$  around the particle. The applied electric fields create electrophoretic drift that cancels Brownian motion in the

**HIGHLIGHTED IN SCIENCE'S SIGNAL TRANSDUCTION KNOWLEDGE ENVIRONMENT**



**It Takes Two**

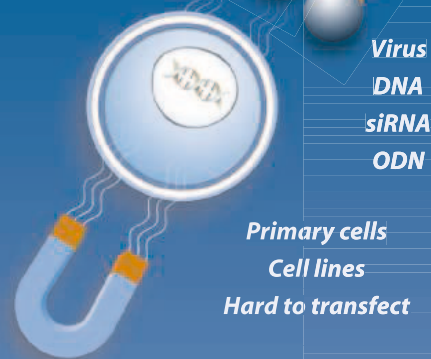
The prevailing model of olfaction is that individual neurons express only one odorant receptor (OR). Goldman *et al.* challenge this view by finding that one olfactory receptor neuron (ORN) in the *Drosophila* sensilla in the maxillary palp (a fly olfaction organ) expresses two highly divergent *Or* genes. Seven *Or* genes were expressed in the six types of neurons found in maxillary palp sensilla. In a receptor-to-neuron map of the ORNs in the maxillary palp, three *Or* genes were expressed in the pb2 class of sensilla. Each class of sensilla consists of an A- and a -B type neuron. To determine if the genes were expressed in the A or B neuron, the *Or*-specific promoters were used to express the proapoptotic protein Reaper, causing selective cell death in only one of the two neurons. When *Or33c* or *Or85e* promoters were used, the surviving neuron was pb2B. Thus, both *Or33c* and *Or85e* appear to be expressed in the pb2A neuron. *Or85e* and *Or33c* transcripts were present in the same ORN in three different species of fly. The combined receptors may be specific for unidentified odorants, potentially increasing further the complexity and specificity of odorant perception. — NG

*Neuron* 45, 661 (2005).

**Magnetofection™**

**The New & Original Transfection Technology**

Highly efficient  
Innovative  
Simple & Rapid



**Three unique & powerful reagents:**

**PolyMag**

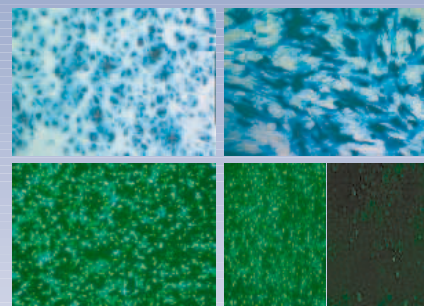
For all nucleic acids, and all transfection conditions

New **SilenceMag**

The most powerful transporter of siRNA even with very low doses

**CombiMag**

Unique solution for all vectors: Viruses & Transfection reagents



Please visit our website for more data  
[www.ozbiosciences.com](http://www.ozbiosciences.com)



**OZ Biosciences**  
contact@ozbiosciences.com  
Tel: +33 4 91 82 81 72  
Fax: +33 4 91 82 81 70

CREDIT: COHEN AND MOERNER, APPL. PHYS. LETT. 86, 093109 (2005)



## EDUCATION

### Space Flight's Untold History

The Soviet Soyuz 5 mission in 1969 wasn't one to boast about. The craft reentered Earth's atmosphere nose first and nearly burned up before righting itself.

Cosmonaut Valentinovich Volynov then shattered his teeth during the rough, off-target landing. Little-known facts and behind-the-scenes stories like this one typify the Encyclopedia Astronautica, a massive space-flight compendium from enthusiast Mark Wade.

Offering contributions by Wade and other writers, the encyclopedia can satisfy readers' hunger for, say, biographical details on the German rocket pioneer Hermann Oberth or maps of the Soviets' Baikonur Cosmodrome. Intriguing historical entries put a new spin on some familiar events. For example, in one article Wade summarizes the evidence that the race to the moon, which seemed like a runaway win for the Americans, was a squeaker. The Soviets planned secret launches into lunar orbit and onto the surface; only when both efforts failed at the last minute did they begin to deny they were competing. The site also covers recent space developments, such as the launch of the Delta IV Heavy (above) in 2004, the first large-payload rocket the United States has introduced since the 1960s.

[www.astronautix.com](http://www.astronautix.com)

## RESOURCES

### Life in the Colonies

Known as the "moss animals," bryozoans are tough to categorize. Some of the colony-forming creatures resemble fronds or shaggy shrubs, whereas others, such as the Australian species *Triphyllozoon munitum* (below), could pass for corals. Find out more at the site



Recent and Fossil Bryozoa, hosted by paleontologist Philip Bock of Deakin University in Burwood, Australia. Fossil bryozoan skeletons can form whole limestone layers, and some modern species have become pests because they stick to ships' hulls or clog intake pipes. Visitors can brush up on bryozoan taxonomy or browse full-text versions of more than 30 classic publications. The site also offers the notebooks of bryozoologist extraordinaire Sidney Harmer (1862–1950), former head of natural history at the British Museum.

[www.civgeo.rmit.edu.au/bryozoa/default.html](http://www.civgeo.rmit.edu.au/bryozoa/default.html)



## TOOLS

### A Human Gene Master List

If you search several genome databases for information about a particular human gene, the results won't always match. That's because the various sites apply different criteria to pinpoint genes and often marshal different evidence to infer their functions. To straighten out these discrepancies, genome mavens have crafted a master catalog of nearly 15,000 of our genes that almost certainly code for proteins. The Consensus CoDing Sequence project involved organizations such as the National Center for Biotechnology Information, the University of California, Santa Cruz, and the European Bioinformatics Institute and entailed comparing the latest gene rosters compiled by researchers and by computers. Experts weeded out problem sequences such as pseudogenes, which lack a corresponding protein. Recent estimates suggest that humans might carry up to 10,000 more genes, but many of these didn't make the cut because of insufficient evidence.

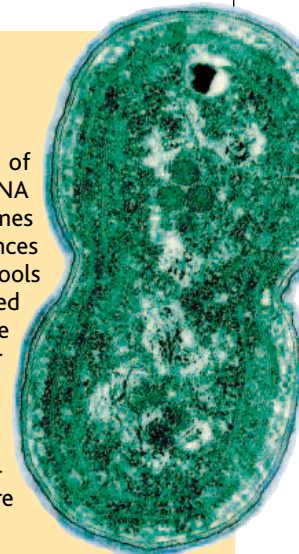
[www.ncbi.nlm.nih.gov/projects/CCDS](http://www.ncbi.nlm.nih.gov/projects/CCDS)

## DATABASE

### Microbial Get-Together

This new clearinghouse from the U.S. Department of Energy can help researchers analyze the deluge of DNA data on microorganisms. Integrated Microbial Genomes stashes nearly 300 draft or completed genome sequences from archaea, bacteria, and other bugs, along with tools for sifting through the data. Visitors can get acquainted with all 2526 protein-coding genes carried by the marine cyanobacterium *Synechococcus* (right), for example. Besides basic information about the gene, its protein, and its function, you can summon diagrams illustrating which biochemical pathways the gene influences. Browsing tools make it easy to pinpoint similar genes in different organisms and compare them side by side.

[img.jgi.doe.gov/v1.0/main.cgi](http://img.jgi.doe.gov/v1.0/main.cgi)



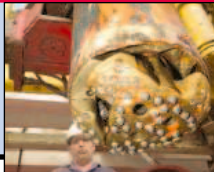
## LINKS

### Surfing the Rocks

Somewhere on the Web lurks a list of accepted and rejected scientific names for dinosaurs and an introduction to soil liquefaction, which occurs when water-logged dirt loses its strength during an earthquake. You'll find these and more than 3000 other Web sites on earth sciences, geography, and related fields at Geo-Guide, a portal sponsored by two German universities. Geo-Guide is heavy on institutional sites, but it also includes plenty of databases, primers, and educational offerings for everyone from the general public to professionals.

[www.geo-guide.de](http://www.geo-guide.de)

Send site suggestions to [netwatch@aaas.org](mailto:netwatch@aaas.org). Archive: [www.sciencemag.org/netwatch](http://www.sciencemag.org/netwatch)



### BIOETHICS

## Anticlone Forces Launch Second-Term Offensive

The once-solid political coalition in the United States that opposes any form of human cloning is showing signs of splintering over strategy. Supporters of cloning research are paying close attention to the rift, first reported in the *Washington Post* last week, wondering whether it may work to their advantage or lead to new laws restricting research that stretches ethical boundaries.

One camp, led by Senator Sam Brownback (R-KS) and pro-life groups, seeks to renew the fight to pass a comprehensive ban on all cloning of human embryos. Brownback, who plans to reintroduce legislation this week, and others have tried to capitalize on the near-universal aversion to the notion of cloning a human to also ban the use of somatic cell

nuclear transfer (SCNT) to create early-stage embryos for research. Citing SCNT's potential to elucidate and perhaps treat diseases such as Parkinson's, research and patient groups have thwarted such legislative efforts to date.

In recent months a new camp has emerged, led by Leon Kass, chair of the President's Council on Bioethics, and Eric Cohen, editor of the conservative bioethics journal *The New Atlantis*.

Frustrated that Congress has repeatedly failed to pass anticloning measures, they call for a broader ban on novel reproductive approaches, including cloning humans. Arguing that seman-



**Private citizen.** Leon Kass says he is pushing for new legislation as a private citizen, not as head of the President's Council on Bioethics.

tics have trumped ethics in the cloning debate thus far, they also want to "delink" restrictions on novel reproduction from those on research cloning by dealing with them in separate bills—an approach that those in favor of research cloning have advocated in the past.

One of several position papers Kass and others have discussed during informal meetings, recently posted on a Web site,\* calls first

for legislation that would protect "the Dignity of Human Procreation." It seeks to ban reproductive cloning and other procedures including transferring a human embryo into an animal or using sperm or eggs from fetuses to create a child. A "ban on all human cloning does nothing to prevent other ways of making children that would be unwise or unethical," explains Cohen. (An aide to Brownback says the senator will introduce additional legislation soon that would outlaw ethically questionable reproductive methods.)

The document recommends lobbying for a second law that would ban "the creation of any human embryo [through cloning or IVF] solely for research and destruction." It's this tactic, in particular, that has divided the two anticloning camps. Brownback and others say that delinking reproductive and research cloning would give supporters of research cloning a political advantage. "Tactically, [the first] might pass, and you would weaken the case for the other," says David Prentice, senior fellow at the conservative Family Research Council.

Others say the new proposals are unlikely to change the political deadlock. "Congress could pass a ban on reproductive cloning with or without these other prohibitions, and we're going to stay divided on the research cloning," says Kathy Hudson, director of the Johns Hopkins University Genetics and Public Policy Center in Washington, D.C.

But Kass argues in an e-mail that a clarified debate on basic morals could win "a very broad range of people, left and right"—including support from scientists. "Far from undermining the

\* [blog.bioethics.net/2005/03/kass-agenda-bioethics-for-second-term.html](http://blog.bioethics.net/2005/03/kass-agenda-bioethics-for-second-term.html)

## U.N. Settles on Nonbinding Resolution

In an attempt to break nearly 4 years of deadlock, the United Nations General Assembly passed a nonbinding resolution last week urging member countries to draft laws that forbid human cloning. However, the vague wording of the measure and the fact that it doesn't require countries to act means it will have little impact, either on attempts to clone humans or on researchers who hope to use nuclear transfer techniques, which involve the creation of a cloned embryo, as part of research into disease.

The text, which was approved on 8 March, says member states are "called upon to prohibit all forms of human cloning inasmuch as they are incompatible with human dignity and the protection of human life." Representatives from countries that had pushed for a ban on all human nuclear transfer experiments, whether for reproductive or research purposes, called the vote a victory. But if it is a victory, it is a

hollow one, says Christian Much, legal adviser at the German mission to the United Nations. "This will be forgotten 6 months from now," he says. "It was the cheap way out after countries realized there was no way to reach a consensus."

A German and French proposal to draft an international ban on attempts to clone a human received wide support in 2001. But efforts to draft a treaty fell apart when the United States and several other countries insisted that any treaty must ban so-called therapeutic cloning, in which nuclear transfer technology is used to create lines of embryonic stem cells for research. But in a mirror of the stalemate that has scuttled U.S. legislation on the issue (see main text), countries with laws permitting human nuclear transfer research, including the United Kingdom, said they would not endorse such a treaty. Three years of debate followed, ending in deadlock (*Science*, 29 October 2004, p. 797). The final vote on the nonbinding resolution was 84 in favor to 34 against, with 37 abstentions.

—GRETCHEN VOGEL

CREDIT: M. SPENCER GREEN/AP PHOTO

1712  
T cell  
blocker  
blocked



1715  
Geometric  
offerings



1716  
Obesity  
and life  
expectancy



effort to ban all human cloning, I think the new agenda builds on its core principles,” added Cohen in an e-mail. “Should we produce human embryos solely as research tools, and should we begin down the road of making babies in radical new ways. ... This is the debate America deserves.”

As a third prong in its self-identified “offensive,” the document suggests that the National Institutes of Health fund research

into methods of obtaining stem cells that do not require the destruction of an embryo (*Science*, 24 December 2004, p. 2174).

Kass thinks time is of the essence: “We have today an Administration and a Congress as friendly to human life and human dignity as we are likely to have for many years to come,” the document says. “[These goals] allow us to respond to the inability to pass the cloning ban not by yielding ground

but by seizing the initiative.”

Others warn against new laws governing an ever-changing scientific landscape and suggest that the research community should continue to police itself. “A blanket opposition [to advanced biotechnical procedures] could throw out things that could be beneficial and ... nonobjectionable,” said David Magnus, director of the Stanford Center for Biomedical Ethics. **—ELI KINTISCH**

## CONFLICT-OF-INTEREST POLICY

# NIH Rules Make Some Pack, Others Plead

The ethics crackdown announced last month at the National Institutes of Health continues to reverberate across the Bethesda, Maryland, campus. Last week, three federal scientists whose consulting came under fire last year announced their departures. A group of senior scientists urged NIH Director Elias Zerhouni to adopt a more modest ethics plan. And rank-and-file researchers say the stringent new rules are upending their lives, perhaps even to the point of divorce.

Last week, National Cancer Institute (NCI) pathologist Lance Liotta and research partner Emanuel Petricoin of the Food and Drug Administration announced they're leaving shortly to head a new proteomics center at George Mason University (GMU) in Fairfax, Virginia. And the National Heart, Lung, and Blood Institute's Bryan Brewer, who the *Los Angeles Times* has suggested improperly endorsed a cholesterol drug, is retiring from NIH and joining a nearby hospital. NIH ethics officials had approved their outside activities. These cases helped trigger a ban on health-related consulting by NIH staff, even for non-profits, and stringent limits on owning stock (*Science*, 11 February, p. 824).

Liotta and Petricoin co-invented a new method for detecting ovarian cancer by analyzing patterns of proteins found in blood. The approach led to a new clinical proteomics program at their two agencies. But the pair ran into trouble for consulting with a competitor to a firm that held an NCI cooperative agreement they oversaw (*Science*, 28 May 2004, p. 1222).

Liotta and Petricoin declined comment on their job move. GMU associate dean for research Vikas Chandhoke says the two men will be “strongly encouraged” to consult: “It's very healthy for science as well as faculty development.”

Meanwhile, NIH's intramural Assembly

of Scientists released an alternative to what its leader, ethicist Ezekiel Emanuel, calls the agency's “draconian” rules. Their proposal would allow biomedical stock ownership and limited consulting by most intramural scientists. NIH Deputy Director Raynard Kington says NIH and the Department of Health and Human Services (HHS) will consider these comments, but that “the basic rules ... are not going to change.”

The weeks since the new rules were announced have been very stressful, say NIH



**New academics.** NIH's Lance Liotta (left) and FDA's Emanuel Petricoin are headed for George Mason University.

staffers. Scientists had until 4 March to end prohibited outside activities or request an extension. But biochemist Herbert Tabor of the National Institute of Diabetes and Digestive and Kidney Diseases is still waiting to confirm a temporary decision that he can continue a 30-year stint as editor-in-chief of the *Journal of Biological Chemistry*. And Ashani Weeraratna of the National Institute on Aging had to cancel a trip to New York City to speak at an international melanoma symposium

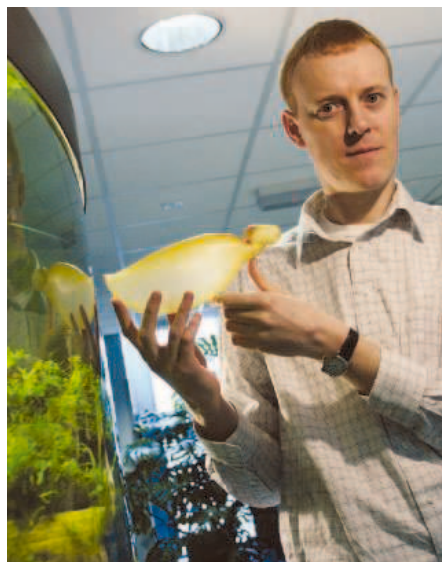
because NIH failed to approve her acceptance of a \$200 train ticket. It was “embarrassing” and a “hardship” for the organizers, wrote Weeraratna in a comment to HHS.

Researchers also point to problems with NIH's plan to allow them to perform scholarly activities as federal employees. For example, Robert Nussbaum, a lab chief at the National Human Genome Research Institute and past president of the American Society of Human Genetics, is seeking an exception to serve on the society's board on his own time. Nussbaum says, “I realized it wouldn't work” as part of his day job because he wants to help the society raise funds and educate members about the political process. Another scientist worries about the propriety of reviewing grant proposals for work on human embryonic stem cells for a foundation, because federal funds cannot be used for some of this work. “They should have asked [us] what the impact would be on the ground,” says the scientist, who requested anonymity.

Michael Brownstein, a 33-year veteran of the National Institute of Mental Health, says he is considering extreme measures to preserve his investments. Brownstein retired last fall because of “commitments I wanted to keep” with companies and foundations; he is moving to the Venter Institute. But his wife, neuroscientist Eva Mezey, still works at NIH. Because even biotech stocks owned by a senior employee's spouse are now verboten under the new NIH rules, the couple is weighing a divorce to avoid a July deadline for divesting. “It's a real option for us. Pretty stupid,” Brownstein says. **—JOCELYN KAISER**

# Special Hemoglobin Helped Swim Bladders Give Fish Diversity a Lift

Scuba divers wear air-filled dive vests to move up and down in the water column. Researchers have now used the fish family tree to piece together how the piscine equivalent, an internal air sac called a swim bladder, evolved a complex capillary network and special hemoglobin molecule to inflate it with oxygen. Moreover, according to the proposal presented on page 1752 by Michael Berenbrink of the University of Liverpool, United Kingdom, and his colleagues, these innovations helped fish expand their species diversity. “The scenario developed presents a fascinating picture of the evolution and radiation of fish,” says Bernd Pelster, an animal physiologist at the University of Innsbruck, Austria.



**Buoyancy compensator.** Michael Berenbrink has reconstructed the evolution of swim bladders such as the one he holds.

Herring and other fish with primitive swim bladders must surface and gulp air to keep their bladders full and their bodies buoyant. The more sophisticated species use oxygen in the blood, an advance that freed them from their air tether and allowed for the expansion into the deep ocean. These species depend upon a network of blood vessels to concentrate oxygen in their swim bladder. However, high oxygen concentrations usually inhibit the release of oxygen from the blood. To get around this problem, these fish have a special Root-effect hemoglobin, a form of the protein that releases its oxygen cargo even when concentrations of the gas are high.

This new hemoglobin evolved before the

swim bladder's capillary network, according to Berenbrink, a comparative animal physiologist. He and his Liverpool colleague Andrew Cossins reconstructed the history of the self-contained swim bladder by looking for its prerequisite components, such as the hemoglobin. The researchers studied species, ranging from sharks to dolphinfish, that represented the different stages of fish evolution.

According to the new study, the Root-effect hemoglobin evolved once in primitive fish. Although the molecules function at high oxygen concentrations in sharks, lungfishes, and even tetrapods, they are most efficient at releasing oxygen in those conditions in codfish and other modern fish. Next came a capillary network that supplied oxygen to fish eyes, allowing them to see better. This also evolved just once, about 250 million years ago, and depended upon the Root-effect hemoglobin. From that point, the hemoglobin was essential to fish.

About 100 million years later, a similar capillary network, this one supplying oxygen to the swim bladder, finally began showing up. This network arose four times in different fish groups, the researchers found.

“It's one of the few examples of our understanding of the evolution of a complex organ from simpler parts,” says Albert Bennett, an evolutionary physiologist at the University of California, Irvine. “They have done an excellent job of teasing apart what happened when.”

Over millions of years, the swim bladder's capillary network came and went in various species, adds Berenbrink. In those species in which the network disappeared, the Root-effect hemoglobins became less essential, he says.

The development of a self-contained swim bladder enabled fish to invade new waters and diversify, according to the researchers. As evidence, Berenbrink contrasts the 198 species of elephant fishes, all with the complex swim bladder, with a close relative that lacks this swim bladder and has just eight species.

Some remain skeptical, however. “To postulate that oxygen secretion is the reason for the diversity of fish ... that might be an overstatement,” says Axel Meyer, an evolutionary biologist at the University of Konstanz in Germany. The hypothesis rests on the questionable accuracy of the fish family tree, adds John H. Postlethwait of the University of Oregon, Eugene.

Still, he and others are impressed by the new study's breadth. “The paper nicely demonstrates the power of an integrated approach,” says Pelster. “I am convinced this paper will stimulate scientists from other areas.” —ELIZABETH PENNISI

## Tsunami Survivors Sue

PARIS—About 60 European survivors of the 26 December 2004 tsunami and relatives of victims have sued the U.S. and Thai governments for failing to issue appropriate warnings before the monster waves came ashore. A preliminary hearing is expected next month on the suit, which was filed 4 March in a New York district court and targets the Pacific Tsunami Warning Center in Hawaii.

Patricio Bernal, executive secretary of the U.N.'s Intergovernmental Oceanographic Commission, says the center “was not in a position to issue a tsunami warning” for the Indian Ocean because the region lacks a monitoring network.

—CHARLENE CRABB

## Mammalian RNAi Library Set Up

A team of scientists and drug companies is creating a publicly accessible RNA-interference library for studies on 30,000 mouse and human genes.

The RNAi Consortium is a collaboration among six institutes and hospitals affiliated with the Massachusetts Institute of Technology and Harvard University, four companies, and a Taiwanese academic consortium. The Taiwan group and the companies—Bristol-Myers Squibb, Eli Lilly and Co., Novartis, and Sigma-Aldrich—are footing most of the \$18 million bill.

The library, announced this week, will house tens of thousands of small RNA molecules embedded in lentiviral vectors that can infect cells. The RNA molecules, in turn, can shut down genes with a complementary sequence, allowing scientists to discern gene functions.

—JENNIFER COUZIN

## EPA Issues Mercury Rule

The U.S. Environmental Protection Agency this week announced its first regulation of mercury emissions from coal-fired power plants, the largest source of mercury pollution in the United States. The controversial regulation would allow power companies to trade pollution credits, an approach that EPA claims will cut emissions by 70% by 2018.

Environmentalists say that faster, better progress could be made by mandating industry-wide reductions (*Science*, 11 February, p. 829). They also argue that the Clean Air Act prohibits trading of hazardous pollutants such as mercury. “There's a very strong prospect of litigation” within the 60-day time limit, says John Walke of the Natural Resources Defense Council in Washington, D.C.

—ERIK STOKSTAD

## GENETICALLY MODIFIED CROPS

## Safety Research Falls Foul of German Politics

**BERLIN**—Researchers at two government-funded labs in Germany have had to withdraw from projects involving the safety of genetically modified (GM) plants after their bosses, officials in the agriculture ministry, said the work was inappropriate. The ban came despite the fact that the projects won funding from another government department—the ministry of research and education—in a nationwide competition for projects studying GM plant safety.

The showdown is the latest example of political hostility toward GM research in Germany, says Jörg Hacker of the University of Würzburg, a vice president of the federal research agency DFG. Even so, he says, the cancellation of specific projects is unprecedented: “To my knowledge, it’s the first time such a thing has happened.” The projects involved “one of the core concerns of the ministry,” he adds, to improve the safety of GM plants.

Agriculture and consumer protection minister Renate Künast, a Green Party member of the left-leaning governing coalition and the researchers’ ultimate boss, is openly skeptical of gene technology. Last



**Nein.** Agriculture ministry, headed by Renate Künast, pulled scientists from research on genetically modified canola.

year, her ministry proposed a law that holds anyone who plants GM crops financially liable if neighboring fields are contaminated with genetically altered pollen. Scientists have complained that the law, which received final approval from the Bundestag in December, essentially prevents all field research with GM plants (*Science*, 25 June 2004, p. 1887).

The researchers leading the projects, Joachim Schiemann of the Institute for Plant Virology, Microbiology, and Biosafety in Braunschweig and Reinhardt Töpfer of the Federal Center for Cultivated Plant Breeding

Research in Siebeldingen, hoped to optimize a method for removing antibiotic-resistance genes from GM plants. During the genetic alteration process, antibiotic-resistance genes are commonly introduced as markers. Their presence in GM plants is often cited by opponents of the technology as a potential danger to consumers and the environment. A spokesperson for the agricultural ministry says the projects could lead to products that would later need

to be evaluated by the institutes in question, and the ministry acted to prevent potential conflicts of interest.

The researchers were not available for comment, but a member of Schiemann’s consortium, Inge Broer of the University of Rostock, says the research will go on. Her group will take over the project, she says, “but we have enough other work to do. It would be better if the [agriculture ministry] researchers did it themselves.” If the government hopes to properly assess the safety of GM crops, she says, they will need qualified experts in the field. —GRETCHEN VOGEL

## GRADUATE SCHOOLS

## Drop in Foreign Applications Slows

The number of foreign students applying for graduate studies in the United States has declined for the second year in a row, according to a survey released last week by the Council of Graduate Schools (CGS). But after a 28% fall last year that was widely attributed to a tightening of U.S. visa policies, this year’s drop of 5%—combined with a similar pattern in the United Kingdom—has some university administrators looking at external factors as the primary cause.

CGS’s survey of 450 U.S. institutions shows that applications from the two biggest sources of students, China and India, are down 13% and 9%, respectively. But a 6% rise from the

Middle East undermines the theory that the fight against terrorism has tarnished America’s reputation as a welcoming country. That finding also “counters the concern that visa changes (geared toward individuals from

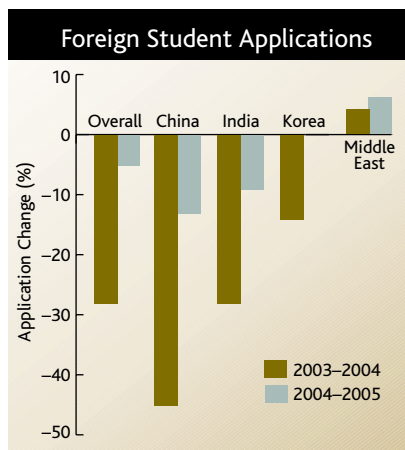
predominantly Muslim nations) would disproportionately discourage students from these countries,” says Heath Brown, co-author of the study.

The Asian numbers point to increasing domestic opportunities in the region, says Peggy Blumenthal, president of the Institute for International Education in New York City. “A U.S. degree is not the only guarantee of a good job and successful career,” she says. Her analysis is

bolstered by numbers from the U.K. Universities and Colleges Admissions Service, which last month reported a 26% drop in Chinese applications as part of a 5% decline in undergraduate applications this year from non-E.U. countries. The same trend is reflected in the number of Asian students who enrolled at U.K. institutions in fall 2004. A survey by Universities UK found that some campuses reported a drop of more than 50% in enrollments by Chinese students compared with 2003 figures.

No matter what the short-term figures show, “there’s no denying that U.S. universities face increasing global competition for the best students, particularly in the sciences and engineering,” says CGS president Debra Stewart. In response, the council wants U.S. graduate schools to step up efforts to attract both international and domestic applicants. Stewart warns that “we will never return to the day when the top 1% of every country’s students will want to come to the United States.”

—YUDHIJIT BHATTACHARJEE



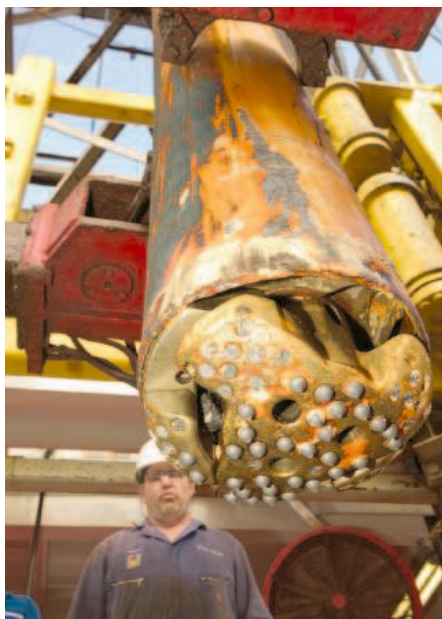
**U.S.-bound.** The number of applications from China and India continues to fall, but the Middle East shows the opposite trend.



# Pursued for 40 Years, the Moho Evades Ocean Drillers Once Again

Hopes were running high early last month that geophysicists had finally come within striking distance of a decades-old goal. Drillers aboard the *JOIDES Resolution* in the mid-North Atlantic were making steady progress down through hundreds of meters of rocky ocean crust toward the legendary Mohorovičić discontinuity, or simply the Moho, the boundary between the thin veneer of Earth's crust and the 2900-kilometer-thick mantle.

But as drilling proceeded with unparalleled ease through 700 meters of crust, then 1000 meters, and even 1400 meters, the



**No (drilling) problem.** Despite trouble-free drilling aided by new technology, the crust-mantle boundary remains beyond reach.

Moho was a no-show. Seismic probing had put it at a depth of 1 kilometer or less just off the Mid-Atlantic Ridge, but drilling cores never showed any sign of the predicted fresh mantle rock. It seems Earth is more complicated than the best geophysical tools had suggested, says Jay Miller, the onboard project manager during the 4 months of drilling. But he and colleagues are still game to return to the hunt.

Ambitions of reaching the Moho drove the first scientific deep-sea drilling effort, Project Mohole, in the early 1960s. Funded by the U.S. National Science Foundation (NSF), oceanographers eventually tested a system for drilling to the Moho where it is closest to the surface, in the deep sea. Croatian geophysicist Andrija Mohorovičić

(1857–1936) had found that seismic waves moved faster below a depth of about 35 kilometers beneath the European continent than they did above, presumably reflecting the iron-rich mineralogy of mantle rock. But beneath the oceans, where the crust is thinner, the Moho lies less than 10 kilometers beneath the unindented sea, Mohole researchers pointed out. That might put the mantle—the sole source of the magmas that form the crust—within reach of drilling.

Project Mohole ended in a bureaucratic and fiscal fiasco, but by the late 1960s, NSF had launched a broadly based ocean drilling program that continues in the international Integrated Ocean Drilling Program (IODP) (*Science*, 18 April 2003, p. 410). Since Mohole, oceanographers looking to reach the deep crust or the Moho have taken their drills to places where the crust is particularly thin. One such thin spot lies at the intersection of the Mid-Atlantic Ridge—where new crust forms—and the Atlantis Fracture Zone at about 30°N. The stress and strain of moving tectonic plates has sliced through the upper ocean crust and dragged it off to expose the lower crust.

Seismometers placed on the sea floor above the thinned spot picked up waves from explosive charges set off near the ocean bottom. The waves sped up to mantlelike velocities whenever they passed much below a depth of 700 meters. “My interpretation was they would reach fresh [mantle rock], certainly by a kilometer,” says seismologist John Collins of the Woods Hole Oceanographic Institution in Massachusetts (WHOI).

After running through a dozen drill bits in 54 days of drilling through 1415 meters of solid rock, however, scientists onboard *Resolution* had recovered nothing that looked like the underlying mantle. “I’m surprised,” says Collins. Possibly, he says, his vertical, two-dimensional seismic picture missed an unexpected deepening of the Moho off to one side: “Perhaps they were unfortunate in where they drilled.” WHOI colleague and seismologist Robert Detrick adds that identifying deep rock “is a hard call to make based on seismic velocity alone.” Rocks of different compositions can have the same seismic velocity, he notes: “It’s a problem that plagues seismology.”

Undaunted, oceanographers are ready to try again. The latest drilling shows that “we now have the technology to deliver deep holes,” says Miller, who is with IODP at Texas A&M University in College Station. For that matter, the new hole “is just sitting there waiting” to be reentered.

—RICHARD A. KERR

## Forgiving Science Majors

The chair of a House spending panel that oversees several U.S. civilian science agencies says he wants to do something “dramatic” to attract more students into science, math, and engineering.

Last week Representative Frank Wolf (R-VA) won endorsements from presidential science adviser John Marburger and National Science Foundation Director Arden Bement, both new to his panel’s jurisdiction, for a bill he’s drafting. It



would forgive interest on college loans for students earning science-related majors and working for 3 years in the field until their salaries exceeded four times the median U.S. income (\$32,000). Borrowing an idea from former House Speaker Newt Gingrich, Wolf said he’s looking for ways to reverse the one-way flow of students from engineering to political science or business. “I think it’s the right kind of program,” said Marburger, calling it a “creative idea.” Bement went even further: “I’ve read Newt’s book, and I liked it.”

—JEFFREY MERVIS

## New Threat to Station Science

An effort to reduce the number of shuttle flights needed to build the international space station could be bad news for researchers. A possible cut from 28 to as few as 15 flights could jeopardize the centrifuge, now being built in Japan and designed to provide important animal data about variable gravity on places such as the moon and Mars. Other animal research facilities also might get the ax, although players on Capitol Hill are gearing up to protect station science.

NASA spokesperson J. D. Harrington says the new science plan will be released next month. In the meantime, he says, “we’re assessing all science needs to see if they are aligned with the exploration objectives” set out by President George W. Bush in January 2004. The shuttle is due to resume flying in May after a more than 2-year hiatus following the Columbia tragedy.

—ANDREW LAWLER

## AIDS CLINICAL TRIALS

## More Woes for Novel HIV Prevention Approach

Clinical trials of a promising new AIDS prevention strategy, already derailed in Cambodia and Cameroon, suffered two more setbacks last week. The studies aim to test whether the drug tenofovir can thwart HIV if people at high risk of becoming infected take one pill every day. Tenofovir, an anti-HIV drug on the market since 2001, has relatively few side effects and stays in the body for an unusually long time.

Citing ethical concerns, Cambodia stopped a tenofovir prophylaxis study in sex workers in August 2004; Cameroon halted a similar trial in February. Then on 11 March, Family Health International (FHI), the North Carolina-based

nonprofit that organized the Cameroon trial, announced that it was pulling the plug on a Nigerian study of sex workers, this time citing technical, not ethical, concerns. Just a day earlier, critics of a study in Thailand involving injecting drug users (IDUs) held a press conference to attack a pending tenofovir study there, charging that the trial, funded by the U.S. Centers for Disease Control and Prevention (CDC) in Atlanta, Georgia, “ignores international ethical standards.”

FHI determined that the research team running the Nigerian trial, which started enrolling participants in September 2004, “is not at this

point able to comply with all of the standards that have been established for conducting this study.” The study team had problems with record-keeping and other technical issues, says Ward Cates of FHI, which decided to cut its losses. “The juice wasn’t worth the squeeze,” Cates says. (The Bill and Melinda Gates Foundation funded FHI to conduct its tenofovir prophylaxis trials, two of which are still under way in Ghana and Malawi.)

In Thailand, the Thai

Drug Users’ Network and other AIDS advocates blasted several aspects of the study. Approved by both U.S. and Thai authorities and run by Thai researchers, the study plans to enroll 1600 uninfected IDUs who visit 17 different methadone clinics. Critics insist that drug users who participate should receive clean needles and syringes to help prevent HIV infection. They also allege that it’s “coercion” to recruit people at methadone clinics, as some fear they must join the study to receive the heroin substitute. They further worry that IDUs who test positive for HIV either during the screening process or the trial itself will not receive AIDS drugs from government programs, which they claim discriminate against them.

Jordan Tappero, head of the CDC program in Bangkok, notes that both U.S. and Thai law prohibit providing sterile injection equipment, but that Thai pharmacies and convenience stores sell needles and syringes without a prescription at low cost. He also disputes the charge that Thailand does not provide anti-HIV drugs to infected drug users. “That’s just a misunderstanding,” he says. As for coercion, social workers, not clinic staff, will recruit people to the study, he says. Tappero and co-workers are continuing discussions with the critics, and he hopes the study can start as planned within the next 2 months. “This community needs a prevention intervention, and tenofovir could be a great tool,” says Tappero. “The only way to evaluate it is a clinical trial.”

—JON COHEN



**Trial tribulations.** Criticisms of a tenofovir study in Thailand are off the mark, says Jordan Tappero, who heads the U.S. CDC program there.

## GENETICS

## Mutterings From the Silenced X Chromosome

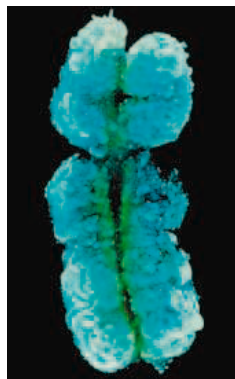
A large-scale survey of the X chromosome has revealed that genes once thought to be silenced in women are sometimes expressed—and that their degree of expression varies from woman to woman. Researchers are now scrambling to figure out whether this previously unknown source of genetic individuality accounts for any significant differences among women.

The X and Y chromosomes define the human sexes, with males having one of each and females having two X’s. During a woman’s development, a murky process called X inactivation almost completely shuts down the second X chromosome to ensure that men and women have the same relative degree of genetic activity. Five years ago, however, geneticists Laura Carrel, now at Pennsylvania State University College of Medicine in Hershey, Huntington Willard, now at Duke University in Durham, North Carolina, and colleagues showed that about 25% of the genes they

analyzed on the “inactivated” X actually escaped deactivation to some degree.

The new work extends that finding to the full repertoire of genes on that X chromosome. An estimated 250 genes are not turned off, says Willard. What’s more, for about 10% of these escapees, the level of gene expression differs among women, he and his colleagues report in the 17 March issue of *Nature*. He and Carrel measured the activity of 94 X chromosome genes in skin cells from 40 women. Depending on the woman, a gene that had escaped inactivation might function at anywhere between 10% and 75% capacity, they found.

“Females are walking around with variability in their [X chromosome gene]



**Genetic escapes.** Some “silenced” X chromosome genes remain active.

expression,” says Evan Eichler of the University of Washington, Seattle. “This will have some impact on how we think about disease.”

Carrel and Willard relied in part on the sequence of the X chromosome, which was described in full in the same issue of *Nature* by Mark Ross of the Wellcome Trust Sanger Institute in Cambridge, United Kingdom, and 250 colleagues. The 155 million bases contain 1098 genes and unusually large numbers of repetitive sequences called LINE1 elements, which seem to play a role in the X-

inactivation process. “Now that we’ve got the sequence of both sex chromosomes, we can do a very detailed comparison [to] really ask the differences between male and female,” says Ross.

—ELIZABETH PENNISI

CREDIT (TOP TO BOTTOM): MALCOLM LINTON; BIOPHOTO ASSOCIATES/PHOTO RESEARCHERS INC.

NASA

## Nominee Wins Quick Praise for His Technical Expertise

President George W. Bush has tapped an aerospace engineer with an undergraduate physics degree to lead NASA. His choice of Michael Griffin, announced on 11 March, won immediate plaudits from both Democrats and Republicans, signaling a likely swift confirmation by the Senate. That will be the easy part: Once he is on the job, Griffin will immediately face a host of pressing budgetary and programmatic decisions.

Griffin's chief asset is his technical expertise. That contrasts with his predecessor, Sean O'Keefe, whose strength was his political prowess. With a Ph.D. in aerospace engineering and an undergraduate textbook on the discipline, Griffin has earned a reputation as a low-key and methodical thinker who's done stints in government, industry, and academia. Although he lacks the high-level connections of O'Keefe, who was a protégé of Vice President Dick Cheney, Griffin, who heads the space department at Johns Hopkins's Applied Physics Laboratory (APL) in Laurel, Maryland, is thoroughly familiar with many components of NASA. "I am pleased President Bush is sending us a nominee with a strong technical background," says Senator Kay Bailey Hutchison (R-TX), who chairs the space and science panel on the Commerce Committee. "I look forward to ... having a smooth nomination process through our committee."

Other lawmakers and many scientists also praised the 55-year-old Griffin. "This is good news," says Stamatios Krimigis, the APL department head emeritus. "Mike has always expressed his support for the science mission of NASA." APL's space work focuses on solar physics and outer solar system exploration, two areas facing cuts in the president's 2006 budget request (*Science*, 11 February, p. 832).

Griffin is well suited to carrying out the vision that President Bush spelled out in January 2004. He was a chief of exploration at NASA during the agency's aborted attempt in the early 1990s to get a similar effort off the ground, and he has been skeptical of the space station and space shuttle—two programs the White House is eager to finish and close down by the next decade in order to proceed



**Science-centered.** Michael Griffin heads the space department at Johns Hopkins's Applied Physics Lab.

with the lunar and Mars missions. "It is beyond reason to believe that [the space station] can help to fulfill any objective, or set of objectives, for space exploration that would be worth the \$60 billion remaining to be invested in the program," he told the House Science Committee last year. (Griffin could not be reached for comment for this article.)

Yet Griffin is also a strong proponent of robotic space science. In 2003, he told the same panel that "scientific research devoted to using space assets to improve our understanding of Earth's

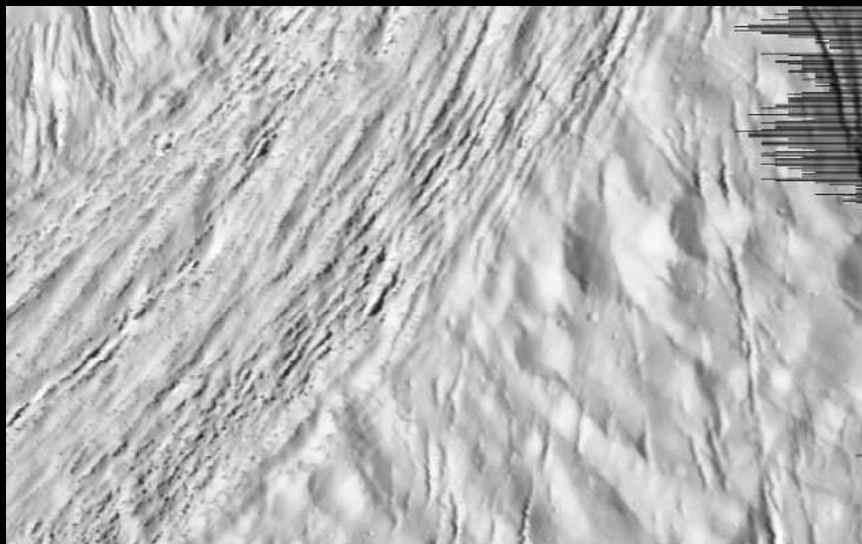
environment, our solar system, and the cosmos beyond will always, and should always, receive due attention in the allocation of

resources." He went on to praise the Hubble Space Telescope, noting that as a young engineer he was involved in the project. "Certain unmanned space systems having little connection with human space flight will be supported—as they are today—because of their inherent scientific or utilitarian value," he added. "There is no inherent conflict between manned and unmanned space programs, save that deliberately promulgated by those seeking to play a difficult and ugly zero-sum game."

A test of that position will come soon enough, given O'Keefe's decision not to send the shuttle again to service the telescope. The same day that the White House announced Griffin's nomination, the National Academies released its final report on Hubble calling for a shuttle flight to upgrade the instruments.

Griffin also will be forced to take a stand on more earthly matters, including a proposal to cut 15% of NASA's workforce in coming years. That plan has upset many lawmakers, some with large NASA facilities in their districts. So although Griffin's technical expertise may go far, his ability to lead the \$16 billion space agency will rest ultimately on his political acumen.

—ANDREW LAWLER



### PLANETARY SCIENCE

## Enceladus, a Work in Progress

As the Cassini spacecraft orbiting Saturn looped by the icy 500-kilometer moon Enceladus again last week, it found yet more terrains beaten up by still-mysterious tectonic processes. This time Cassini focused on a side of Enceladus still bearing the pockmarks of ancient impacts; elsewhere, the surface has been wiped clean of craters by cracking, ridging, and smoothing. Now it's obvious that even recognizably old terrain has been reworked repeatedly. In places, "it

looks like someone had applied an egg slicer to it," says Cassini imaging team member Torrence Johnson of the Jet Propulsion Laboratory in Pasadena, California. Apparently, says Johnson, again and again over great spans of time Enceladus had the internal energy to rework at least parts of its surface. Such a small body should have cooled to a state of geologic stupor long ago. Planetary scientists will be searching for the source of its evident energy.

—RICHARD A. KERR

## DIABETES RESEARCH

# Researchers Puzzle Over Possible Effect of Gleevec

Can a targeted cancer drug help treat diabetes? That's a question two independent teams of Italians are asking after giving leukemia patients the drug Gleevec and watching their preexisting diabetes regress. One 70-year-old woman improved so dramatically that she could no longer be classified as a type 2 diabetic, three physicians reported last week in the *New England Journal of Medicine*. "We don't know exactly what's going on," says Enzo Bonora, the endocrinologist at the University of Verona who treats her.

Similar observations popped up in the November 2004 *Journal of Clinical Oncology*. There, Italian doctors at the University of Rome "La Sapienza" described seven patients with type 2 diabetes and chronic myelogenous leukemia (CML), a cancer susceptible to Gleevec (and the same disease afflicting Bonora's patient). Six experienced enough improvement in diabetes to reduce medications or insulin dosages. The only patient whose diabetes didn't ease, the team says, was also the only one whose leukemia didn't respond to Gleevec. Since his first patient, Bonora has treated two others whose diabetes also improved.

The cohort is tiny, Bonora stresses, and should be viewed cautiously. And some physicians can't corroborate the results.

Brian Druker of Oregon Health and Science University in Portland, a leukemia specialist who helped develop Gleevec, says three or four diabetics with CML have been treated in his center, although he doesn't recall any change in their diabetes while on the drug. "But it's hard to ignore what other people have seen just because we haven't seen it," says Druker, who hopes that physicians will "track down" what's happened in the patients who improved.

Gleevec was designed to disable a defect specific to CML, in a protein called a tyrosine kinase, although it affects other protein kinases as well. Among those kinases are some that help control insulin signaling and how responsive the body is to insulin secreted by the pancreas—both common defects in type 2 diabetes. But the Italians can't say whether an effect on insulin signaling is behind the unusual observations.

Gleevec also hits a protein kinase called platelet-derived growth factor, which some doctors suspect may spur conditions, such as atherosclerosis, that are common complications of diabetes. Two recent mouse studies by Mark Cooper and colleagues at the Baker Heart Research Institute in Melbourne, Australia, showed that Gleevec helped animals with diabetes-induced atherosclerosis and diabetes-induced kidney disease. Cooper theorized that Gleevec's effects on platelet-derived growth factor might explain the results, although he couldn't say for sure.

Bonora plans to ask Novartis, the Basel, Switzerland, company that manufactures Gleevec, whether it might test its drug in type 2 diabetes

patients. Although Novartis finds the results "very intriguing," wrote Novartis spokesperson Kim Fox in an e-mail, "we do not have any studies in Gleevec in type 2 diabetes, and are not planning any at this time." —JENNIFER COUZIN



**New use?** A handful of diabetes patients on Gleevec improved.

## FRENCH SCIENCE

## INSERM Doubts Criminality in Growth Hormone Case

**PARIS**—An expert report that came to light last week questions whether it makes sense to prosecute 12 French scientists and doctors as criminals because they treated children in the mid-1980s with contaminated human growth hormone. The French medical research agency INSERM prepared the report and submitted it last year to a drawn-out investigation. It argues that criminal charges are not justified because doctors and lab personnel were not negligent, even though they used material from human brains infected with Creutzfeldt-Jakob disease (CJD), the human form of mad cow disease. The report was made public by the aggrieved families of CJD victims, who suggest that the medical establishment quietly works against them.

The report concludes, "it is not reasonable to expect the players involved in the production of growth hormone to have guessed there was a possible risk of CJD from a treatment used since the 1960s" without a single incidence of disease. It alleges a lack of "good laboratory practice"—not just in France but also in the United States and the United King-

dom. Before 1985, pediatric endocrinologists and prion experts rarely got together, it says. The first mention of a transmission risk was a letter sent by Alan Dickinson, an expert on scrapie, the sheep form of the disease, to the British health ministry in 1977: It "never left the office to which it was addressed," the report claims.

A total of 968 children were treated in France with high-risk batches of human growth hormone between December 1983 and June 1985. So far, 101 have died from CJD and several others are infected, says Jeanne Goerrián, president of the Association of Growth Hormone Victims. In 1991, magistrate Marie-Odile Bertella-Geffroy began a criminal investigation, which should be completed this year.

Former health minister Bernard Kouchner asked INSERM in 2002 for data on the CJD problem in France since 1980. But the report INSERM submitted digressed, charges Bernard Fau, lawyer for the victims. "Not only was INSERM doing the examining magistrate's job, but it cleared the 12 of

all responsibility," Fau says. The accused 12 include Fernand Dray, who was in charge of purifying the material at the Pasteur Institute, and pediatrician Jean-Claude Job, formerly of the St. Vincent de Paul Hospital in Paris.

INSERM chief Christian Bréchet rejects the accusation of meddling as "unjustified." The report, which INSERM submitted to Bertella-Geffroy and the government last April, was prepared by an international committee of experts that included U.S. experts Stanley Prusiner, who won the Nobel Prize for his work on the CJD prion, and Paul Brown, formerly of the U.S. National Institutes of Health in Bethesda, Maryland.

In 2003, the French courts threw out a similar criminal case involving the use of HIV-tainted blood (*Science*, 27 June 2003, p. 2019). "But we are now sure [the growth hormone case] will come to trial and will be the first public health case to do so," says Fau. The proceedings could start in early 2006 and would last several months.

—BARBARA CASASSUS

Barbara Casassus is a writer in Paris.

Converting an idea for a new MS drug into the real thing turns out to be much harder than a pair of Dartmouth researchers ever imagined—but they refuse to let it go

# Magnificent Obsession

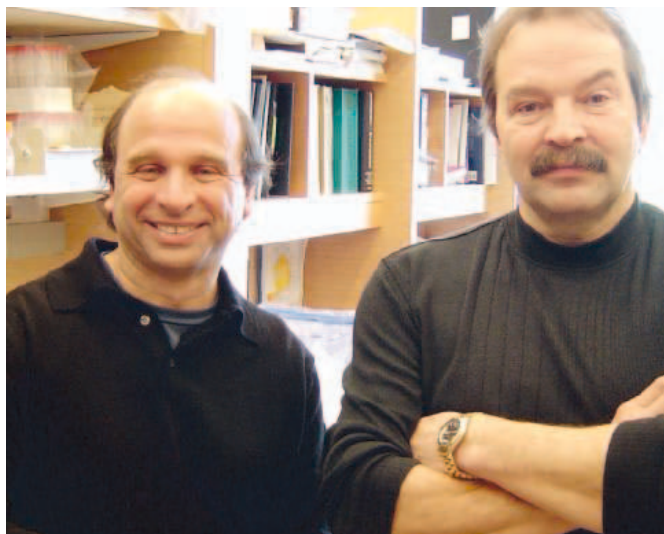
**LEBANON, NEW HAMPSHIRE**—Near the Vermont–New Hampshire border, where highway signs warn of occasional moose crossings, the Dartmouth-Hitchcock Medical Center looms like a mountain behind a wall of fir trees. It offers, among other services, up-to-date therapy for about 1200 New Englanders who suffer from the autoimmune disease multiple sclerosis (MS). The man who directs the MS clinic, a motorcycle enthusiast and painter named Lloyd Kasper, is a veteran of academic medicine and a pioneer in an enterprise that the federal government is pushing strongly these days: “translational research,” which aims to move basic findings into clinical practice. Kasper and a Dartmouth colleague, Randolph Noelle, set out in the 1990s to invent a new drug. Their experience on the frontier between research and business illustrates just how difficult and frustrating negotiating this alien territory can be.

The Dartmouth researchers thought they had found a way to block the biochemistry that spurs MS. The disease relentlessly attacks nerve tissues, slowly robbing many patients of the ability to walk, see, speak, or even think. Today’s drugs can slow its course but cannot halt it.

In his Dartmouth lab, Noelle discovered a way to block contact between certain T cells and other immune cells using an antibody called anti-CD154. An immunologist at Columbia University, Seth Lederman, independently made this discovery at the same time. Over the next several years, Noelle, Lederman, and others found that CD154 was overexpressed in a number of autoimmune diseases, and that blocking it in animals eased symptoms remarkably. A better MS drug seemed tantalizingly close.

But neither Noelle nor Kasper had an inkling, when they became captivated by this immunologic pathway, of how their dream of turning it into a medicine would consume them. Today, 14 years after Noelle began this work, his drug, anti-CD154, is in limbo.

After years of stop-and-go clinical work, concerns about the safety of anti-CD154 left the company with which they partnered jittery. Kasper and Noelle had little choice but to defer to business decisions. They are all too aware that once a company buys a discovery, “you lose control,” says Noelle. The



**Long haul.** Fourteen years into an MS drug project, Dartmouth’s Lloyd Kasper (left) and Randolph Noelle are still chasing their dream.

Dartmouth pair, still convinced their discovery can transform the lives of MS patients, are beside themselves with frustration.

“This is enough to put you on psychotropic drugs,” says Noelle, reclining in a duct-taped leather chair in his seventh-floor office, swinging a black loafer on and off his foot. But not enough, it seems, to prompt either Noelle or his friend of 20 years to capitulate, even as their options for reviving the drug dwindle.

Noelle and Kasper are just two of the thousands of scientists being urged by the government to translate lab work into medical therapies. The 1980 Bayh-Dole Act encouraged university involvement in commercialization; in 2003, National Institutes of Health Director Elias Zerhouni formalized NIH’s effort with an R&D “roadmap” that places a premium on translational research.

Academics are increasingly eager to develop marketed products. A survey from

the Association of University Technology Managers (AUTM) in Northbrook, Illinois, counted almost 8000 new patent applications filed in the fiscal year 2003 by academic scientists and nearly 4000 patents issued.

## Thrill of discovery

In 1991, Noelle discovered a way to disable a recently discovered molecule that helps orchestrate the dance between helper T cells and various other immune cells. The molecule, called a ligand, binds to a specific receptor on the cell’s surface—in this case, CD40. When Noelle used an antibody to block the expression of CD40 ligand, he disrupted the interaction between T cells and immune cells expressing CD40. That seemed to prevent immune cells from proliferating and producing inflammation and antibodies that may attack the body’s own tissues.

Noelle soon learned that he was running neck-and-neck with other scientists, including one who beat him to the patent office. Lederman had identified CD40

ligand and designed an antibody that dampened its effects, the fruition of what he calls “one of the most fascinating and exhilarating experiences” of his life. (A Seattle company, Immunex, now owned by Amgen in Thousand Oaks, California, was involved in some of the early discoveries as well but didn’t pursue the antibodies commercially.)

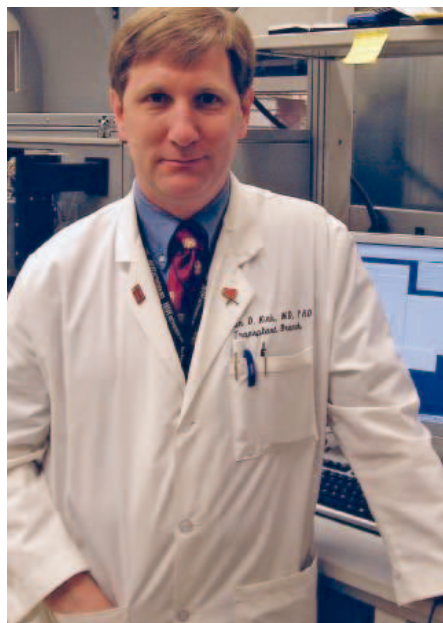
Interest in the therapeutic potential of the antibody, alternatively called anti-CD40 ligand or anti-CD154, increased in part because it fit neatly with observations in medicine. Doctors had noticed that CD154 is overexpressed in autoimmune diseases such as lupus and MS. They also suspected that it was involved in attacks launched by a healthy immune system against a transplanted organ.

Convinced that the CD154 findings could have commercial value, Lederman filed for a patent, followed 3 months later by Noelle. Both scientists also began hunt-

ing for companies to help finance the work. Lederman hooked up with Biogen, a biotechnology company in Cambridge, Massachusetts, and Noelle, with Idec Pharmaceuticals in San Diego, California. After obtaining exclusive licenses, the companies followed up with big investments. The first task was to convert the mouse antibodies that had been used in test-tube studies into a human form that would be accepted by the human immune system. Humanizing the antibodies cost more than \$1 million. In the mid-1990s, animal testing began.

Hopes for CD154-based therapy soared further when a series of experiments at the University of Wisconsin, Madison, strongly hinted that the drug might prevent rejection of a transplanted organ. At first, “nobody was thinking [anti-CD154] would be all that promising” in transplant patients, says David Harlan, who with his youthful, slightly freckled colleague Allan Kirk conducted the monkey studies. They were funded by the U.S. Navy. (Both Kirk and Harlan are now at NIDDK, the National Institute of Diabetes and Digestive and Kidney Diseases in Bethesda, Maryland.) Monkeys given anti-CD154 after a kidney transplant were able to retain the kidney without traditional immunosuppression, even after anti-CD154 was withdrawn. One animal experienced a rejection episode and spontaneously recovered, something “we’d never seen,” says Harlan.

All the monkeys eventually rejected their new kidneys, but in some cases only after several years. Still, keeping a kidney transplant without standard immunosuppression



**Believer.** Transplant doctor Allan Kirk wants to keep testing anti-CD154 in organ recipients.

## The Players

**Idec**  
 SAN DIEGO, CALIFORNIA

**Randolph Noelle,**  
Dartmouth College  
Licensed drug to Idec

**Lloyd Kasper,**  
Dartmouth College

Tested Idec's drug in multiple sclerosis patients

**David Wofsy,**  
University of California, San Francisco

Tested Idec's drug in lupus patients

**Biogen**  
 CAMBRIDGE, MASSACHUSETTS

**Seth Lederman,**  
Columbia University  
Licensed drug to Biogen

**Allan Kirk,**  
National Institute of Diabetes and Digestive and Kidney Diseases

Tested Biogen's drug in transplant patients

was unprecedented. The news spurred NIH to form a \$144 million clinical trials network, the Immune Tolerance Network, in 1999, to test similar drugs in people.

As clinical trials of anti-CD154 took shape, Idec grew concerned that Lederman's patent, awarded in 1995, conflicted with the application from Noelle and Dartmouth, which the U.S. Patent and Trademark Office hadn't yet ruled on. The patent office apparently agreed. In 1999, unable to sort out who owned what regarding anti-CD154, it declared an “interference” between the two claims. Noelle lost the initial case, and Idec appealed on his behalf, defending Noelle's priority based on his lab notes.

Years of court battles ensued, costing tens of millions of dollars in legal fees. In March 2004, a federal appeals court ruled in favor of Biogen and Columbia, which owns Lederman's patent. They can claim royalties on any anti-CD154 antibody to human cells, including Noelle's, should it reach the market.

Before the patent battle reached its climax, both companies had set up clinical trials to test anti-CD154 in neglected diseases such as lupus. Biogen and Idec “did something that took courage, ... which is to devote some scientific attention and meaningful resources to a disease that's usually ignored,” says David Wofsy, a lupus specialist at the University of California, San Francisco, who led lupus trials of the Idec-Dartmouth drug. “It is precisely fear of the unexpected problems that develop when you go into these areas that keeps companies from doing it.”

Idec and Biogen had another factor to consider: With similar antibodies in hand, they were in a flat-out race. Idec, which lagged slightly behind, “knew that if Biogen finished their development program and got their drug approved before Idec got to the [U.S. Food and Drug Administration] FDA, Idec would have nothing,” says Wofsy. “Time was of the essence.”

### A punishing setback

The Dartmouth group initially saw no show-stoppers. Kasper began enrolling the first of 15 MS patients for a trial in 1999. In four sessions spaced weeks apart, each volunteer received an hourlong infusion of anti-CD154. At the same time, Biogen and Idec were running trials of their drugs in lupus and the platelet disorder immune thrombocytopenic purpura; Biogen was also testing its antibody in kidney transplant patients.

Then, months after the MS trial began, disaster struck. Two volunteers in a 28-person Biogen lupus trial suffered heart attacks. In the Biogen transplant trials, which included seven patients, an obese, bedridden woman died of a pulmonary embolism. In all, roughly 10 of the 100 patients taking the Biogen drug experienced clotting, says Akshay Vaishnav, the company's senior director for medical research.

What caused the excess clotting remains a mystery. One theory is that, in addition to binding to certain T cells, the Biogen drug also binds to and activates platelets, which help blood to clot. But “we extensively studied that” after the trials “and could not

prove” that platelet binding was the culprit, says Burt Adelman, Biogen’s executive vice president for research and development.

FDA immediately halted trials with both the Biogen and Idec antibodies. But 9 months later, the agency concluded that the Idec drug seemed safe, and those trials resumed, including the one at Dartmouth. After extensive, failed efforts in animals to understand the side effects of its antibody, Biogen decided to abandon it.

Kasper completed his phase I MS trial in June 2001. The only significant possible side effect occurred in a man who struggled for 3 weeks with the flu. He recovered.

Like most early trials, the study in MS patients assessed safety, not effectiveness. But Kasper and Kathleen Ryan, a nurse who coordinated the trial, say they saw hints of great promise in the antibody. “This small cohort of people ... did phenomenally well,” says Kasper, who saw “uniform stabilization” in all the patients for at least 6 months. Some went 2 years with stable magnetic resonance imaging scans and no relapses, he says.

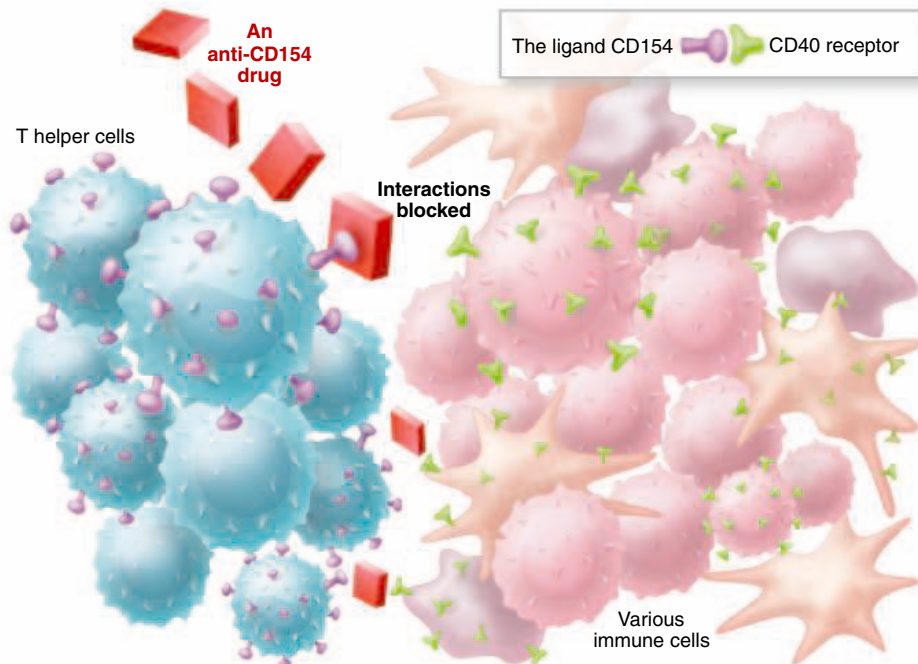
The Dartmouth team garnered nearly \$7 million from NIH and the Immune Tolerance Network for a 40-person phase II trial with a placebo group. But it had only randomized one patient when trouble struck in another anti-CD154 trial. A 62-year-old woman in an Idec study of Crohn’s disease developed a blood clot in her leg. She needed emergency vascular surgery. In June 2002, FDA again halted all the anti-CD154 trials.

After a year of reviewing the data, FDA concluded that the blood clot was probably not linked to the drug because the patient had pre-existing risk factors for clotting. At least two other Idec patients, both in their 80s, had also suffered blood clots, but FDA couldn’t definitively link them to the drug either, says Kasper. In 2003, FDA gave Idec the go-ahead.

By then, however, the dealmakers of the pharmaceutical industry had intervened. One day in late June 2003, Noelle turned on his computer and was startled to learn that Idec and Biogen had merged. The company was now based at Biogen’s headquarters in Cambridge and renamed Biogen/Idec. Years of legal wrangling were rendered irrelevant, because the merger meant that Biogen/Idec now jointly controlled the intellectual property.

In November 2003, Noelle and Kasper learned that the company was halting development of Idec’s anti-CD154 drug, citing safety concerns. Biogen executive Adelman says the danger signal from Idec’s drug was perhaps “softer” than the one from Biogen’s, but there was “still a signal.”

The Biogen and Idec drugs had been tested in 300 patients with kidney transplants, MS, lupus, Crohn’s disease, psoriasis, and immune thrombocytopenic purpura.



**How it works.** An anti-CD154 antibody stops T cells and other key immune cells from intermingling, with the aim of keeping cell proliferation and inflammation in check.

The largest trials were in lupus, but the Idec drug was not effective, says Wofsy. The Biogen lupus trial was halted early, but its leaders reported that the drug, given at double the doses in the Idec lupus trials, worked in several patients and reduced antibodies linked to lupus kidney flares. Anti-CD154 did not substantially help the seven transplant patients who tried it. Unlike marketed autoimmune and transplant drugs which must be given continuously, the new therapies were designed to be given for several months and then withdrawn. Noelle and others suspect that may have made them less appealing to business executives.

#### Rescue missions

Kasper and Noelle, who have a deep personal stake in anti-CD154, aren’t its only cheerleaders. Despite the lackluster response to anti-CD154 among the seven transplant patients who received it, many transplant doctors consider the therapy an extremely promising way to prevent organ rejection. It’s “the most significant drug in transplant,” says Kirk, now the chief of transplants at NIDDK. Kirk’s belief was bolstered, perhaps, by the experience of his cousin, who was dying of lupus-induced kidney disease before entering a Biogen trial. She’s been stable ever since. “There’s no way that this pathway is not important in a lot of immune responses,” says Kirk. “We just need to figure it out.”

In the months after Biogen/Idec dropped the drug, Noelle and Kasper began looking for ways to revive it. They argued that the clotting that brought down Biogen’s drug

shouldn’t taint the Idec drug, pointing out that FDA had allowed clinical trials of Idec’s therapy to proceed. Furthermore, in early 2004, Noelle and Kasper learned from published research out of Massachusetts General Hospital in Boston that combining a drug very similar to Biogen’s with a powerful anti-inflammatory drug prevented asymptomatic blood clots in monkeys. Noelle and Kasper traveled to Cambridge and suggested to a group of Biogen/Idec executives that the company co-administer anti-CD154 with an anti-inflammatory drug.

Biogen/Idec executives were unwilling to take any more chances. Adelman says he believes that pharmaceutical companies must be conservative. “In drug development,” he notes, “where you know that you have a risk and you don’t understand what’s driving that risk, I don’t know how you can go forward.” (In a sign of how volatile drug risks can be, on 28 February, Biogen/Idec and Elan Pharmaceuticals in South San Francisco, California, suspended sales of a new MS drug they had jointly developed. The drug, Tysabri, was linked to a rare and life-threatening neurological disease in two patients.)

Biogen/Idec, says Adelman, is now partnering with the U.K. subsidiary of a Belgian company, UCB, to begin the multiyear process of developing differently structured—and, he hopes, safer—anti-CD154 antibodies.

The Dartmouth pair believes Biogen/Idec saw only the risks and not the potential enormous benefits of a drug everyone was still learning to use. “It’s not a decision

based upon the science,” says Noelle.

Even after the company had pulled its support, Noelle and Kasper saw a way to keep going. NIH and Idec had signed a contract that guaranteed that no matter what Idec chose to do with anti-CD154, it would supply NIH with the drug.

The researchers asked NIH to demand that Biogen/Idec live up to the promise. But they learned that even if NIH exercised this option, someone would need to indemnify the clinic in case problems arose. Dartmouth declined. NIH said it wasn't set up to provide such insurance. “Dartmouth did consider suing NIH” to get the drug but “didn't warm up to that idea,” says Noelle.

Giving up, he says, is not an option. It's a stubbornness other academics can relate to. “You never know how long to persist,” says Judah Folkman, a cancer biologist at Harvard Medical School and Children's Hospital in Boston, who has been trying to push an anti-cancer therapy forward for 20 years. There's a “fine line between persistence and obstinacy in research,” he says. “If you work for 10 years on something and succeed, it's highly valued. On the other hand, if by 11 years you have not yet succeeded, they say, ‘He's obstinate, ... wedded to a theory, pigheaded.’”

#### Looking ahead, and back

Hope in anti-CD154 is still running strong. Kirk's lab and Harlan's spent a year creating a new anti-CD154 antibody—which may have different surface markers from those of either the Biogen or Idec drug, although it still targets CD154—from scratch. They have tested it in monkeys, and it appears effective—but it also causes some blood clotting.

Now, Kirk and Harlan want to humanize their antibody and distribute it to scientists “to try and figure out the complications,” says Harlan. A third colleague, heart transplant surgeon Richard Pierson III of the University of Maryland Medical System in Baltimore, Maryland, who has studied anti-CD154 in primates, is waiting to hear whether NIH will endorse his request for \$12.5 million to create a new, humanized anti-CD154 antibody and test it further in monkeys.

Robert Goldstein, chief scientific officer of the Juvenile Diabetes Research Foundation in New York City, is another enthusiast. “This keeps hitting the list” of promising drugs, says Goldstein. His deep-pocketed advocacy group is making inquiries about anti-CD154's potential use in kidney and islet cell transplants. He's considering what might be done to revive one of the existing anti-CD154 antibodies or create a new one. But “going forward without [the company's] help may complicate life enormously,” Goldstein says. Biogen/Idec, after all, still controls the intellectual property.

Determined to prove that the Idec-

Dartmouth drug is safe, Noelle is testing a theory that the Idec drug, unlike the Biogen drug, doesn't bind to platelets. He's asked a Dartmouth platelet expert to conduct a series of experiments to determine whether this is the case and expects results any day now.

Kasper still has his multimillion-dollar NIH grant for an MS clinical trial with anti-CD154. But Biogen/Idec is no longer making the antibody. Like a movie stuck midway, its characters frozen in time, the trial could continue—but, says Noelle, “for the minor detail of not having any drug.” —JENNIFER COUZIN

## History of Mathematics

# “Amateur” Proofs Blend Religion And Scholarship in Ancient Japan

A 300-year-old Japanese art form presents some surprising mathematical discoveries on elegant wooden tablets

**TOKYO**—When Japan was isolated from the rest of the world, a unique brand of mathematics flourished in the country's shrines and temples. Amateur mathematicians crafted geometric theorems on elegant wooden tablets called sangaku (literally “mathematical tablets”) and offered them to the gods. Remarkably, some of those theorems predate by more than a century the work of Western mathematicians.

Next month the Nagoya City Science Museum will present an exhibition of 130 sangaku from Japan's Edo Period (early 17th to mid-19th centuries). Assembling the show was a labor of love by Hidetoshi Fukagawa, a high school math teacher in central Japan, who has written the definitive texts on the unusual art form. “It's a really remarkable phenomenon, showing that ordinary people of that time studied mathematics purely for enjoyment,” says Fukagawa about the san-

gaku, which were hung up at shrines and temples and often beautifully illustrated with miniatures of women in kimonos, teachers and pupils studying, and landscapes.

Their appeal crosses the oceans. The exhibition “is a unique occasion to see one of the great treasures of Japanese culture,” says Freeman Dyson, a mathematician at the Institute for Advanced Study in Princeton, New Jersey. “I wish I could come to Japan.”

The sangaku tradition flourished in an era when Japan was closed to outside influences and at peace both internally and with its neighbors. That calm meant that the samurai—traditionally schooled not only in swordsmanship but also literature, philosophy, sciences, and the arts—could turn their attention from martial to more intellectual matters. Adds Fukagawa, “There was no academia as we know it. So samurai, farmers, and merchants all felt free to study mathematics.”



**Artistic math.** Illustrated mathematical tablets, or sangaku, include straightforward geometrical problems as well as suggestions for estimating the height of distant peaks (above). An exhibition opens next month in Nagoya, Japan.



The amateur mathematicians built upon an existing tradition of hanging wooden tablets with poetry or paintings in Shinto shrines and Buddhist temples, painting or engraving sangaku that typically give the result of a problem but not the proof. “Ostensibly, the tablets were left as gifts to the gods,” Fukagawa explains. “In reality, people were showing off and challenging others to work out the proof.”

The vast majority of the problems involve plane geometry. But some involve calculating volumes of solids and others deal with algebra-like equations. The sangaku crafters typically included their names and the dates they hung the tablets.

Once Japan ended its isolation in the mid-1800s, the government encouraged the study of the European mathematical tradition as part of its push to catch up to the West technologically and economically. The archaic Chinese characters of Japanese mathematics fell into disuse, and the sangaku tradition disappeared. The rediscovery of sangaku is due in large part to 61-year-old Fukagawa, who holds a degree in mathematics and who has spent nearly 40 years teaching high school math in Aichi Prefecture. Looking for material to enliven his classes, he stumbled upon sangaku. “At the time, no Japanese mathematician had studied sangaku in any depth,” he says.

His first step was to teach himself the archaic Chinese characters used on the tablets. The more sangaku Fukagawa deciphered, the more impressed he became with their sophistication. Japanese mathematicians were less enthralled, however, so Fukagawa started contacting geometers in other countries. His search led to a number of collaborations. In 1989 he and Daniel Pedoe of the University of Minnesota, Twin Cities, co-authored *Japanese Temple Geometry Problems*, which remains the most complete monograph on sangaku in any language. In 2002 he and John Rigby of Cardiff University in Wales published *Traditional Japanese Mathematics Problems from the 18th and 19th Centuries*.

The first book describes a number of Western geometrical theorems that were solved independently in Japan. One notable example is Soddy’s hexlet, a theorem published in 1936 by Frederick Soddy, a British chemistry Nobel laureate, involving a complex construction of spheres within a sphere. Fukagawa and Pedoe found that the identical solution had been inscribed on a sangaku placed at a shrine in Kanagawa Prefecture in 1822. (The tablet is lost but is described in a written text.)

Even so, the mathematical significance of the sangaku tradition is an open question. Hikosaburo Komatsu, a mathematician at the Science University of Tokyo who studies Japan’s indigenous math, agrees that their existence “shows that knowledge of math among ordinary citizens of that time was quite high.” But the tablet format limits results so that



“mathematically, sangaku are not very deep,” he says. Serious Japanese mathematicians were producing much more significant theoretical work at the time, he notes. Still, Peter Wong, who grew up in Hong Kong and now teaches mathematics at Bates College in Lewiston, Maine, says the sangaku “open up

**Sleuth.** Hidetoshi Fukagawa has written the definitive text on sangaku.

all sorts of questions” about how laypeople developed sufficient mathematical skills to tackle nontrivial problems.

Fukagawa hopes further study will provide some answers. About 900 sangaku are known to remain, and dozens more that have been lost are known from written references. Only last year, during a visit to a shrine in Mie Prefecture, Wong used his knowledge of Chinese characters to point out a sangaku that Fukagawa had overlooked. Fukagawa also hopes the exhibition, which runs from 19 April to 26 June, will stimulate interest in the topic and yield additional sangaku. —DENNIS NORMILE

## Public Health

# Provocative Study Says Obesity May Reduce U.S. Life Expectancy

The rising incidence of obesity, especially among children and teenagers, is leading to a variety of diseases that could depress average life span

In the 1980s and 1990s, the late maverick economist Julian Simon infuriated environmentalists by arguing that free markets and scientific progress were constantly improving human life rather than pushing the world toward ecological ruin, social collapse, and famine. A key example was life expectancy at birth, which Simon showed had been steadily rising for centuries. Using that as a metric, he repeatedly claimed that in the 21st century, “humanity’s condition will improve in just about every material way.”

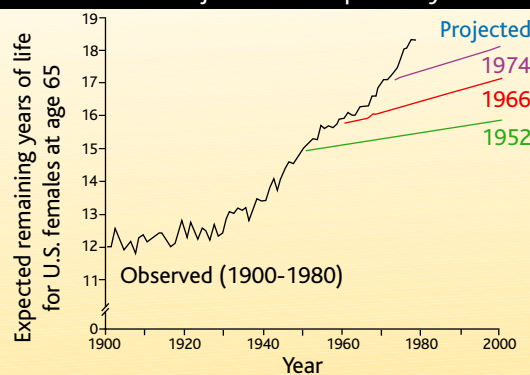
Not so, says a 10-person research team led by S. Jay Olshansky of the University of Illinois, Chicago, and David S. Ludwig of Children’s Hospital in Boston, Massachusetts. In

a study published in the 17 March *New England Journal of Medicine*, the team predicts that U.S. life expectancy “could level off or even decline” by 2050.

The culprit, though, is not environmental heedlessness but the very market-driven affluence that Simon celebrated, because it has fostered an explosive rise in obesity, and especially childhood obesity. That rise, the research team argues, has already offset increasing life expectancy “by 0.33 to 0.93 year for white males,” with similar offsets for women and other races. Assuming that current trends continue and that no big technical fixes emerge, Olshansky says, “we have strong reason to believe this number will rise rapidly in the coming decades.”

That conclusion is likely to be controversial. Critics argue that it is based on a partial reading of the evidence. “Obesity is indeed a problem,” says James Vaupel, director of the Max Planck Institute for Demographic Research in Rostock, Germany. “But on the other side there are extraordinary advances being made as a result of biomedical research.” Moreover, he says, “the United States has seen a slowdown in life expectancy, but in other countries it’s going up fairly rapidly—about 3 months per year in places like France and Japan.”

### Observed and Projected Life Expectancy



**End of an era?** Average years remaining for U.S. females at age 65 rose steadily, in spite of projections to the contrary.

To Olshansky, the continuing increases in those countries may mean only that they have not yet reached U.S. obesity levels. If the projections in the *New England Journal* article come true, he notes, the next generations will be the first in recorded history to die younger and sicker than their parents—a public-health catastrophe.

But there may be more immediate consequences as well. In 2004 the Social Security Administration estimated that by 2078 female and male life expectancy will jump from their current levels of, respectively, 79.9 and 74.5 years to 89.2 and 85.9 years. That rapid increase, which will increase disbursements, is one of the motors driving the current debate over the program's potential insolvency. "Those projections are made from mathematical models," Olshansky says. "If you look at actual people now, I believe you see very quickly that this is not going to happen. The 'benefit,' if you can call it that, is that Social Security will be in less trouble, because fewer people will be alive to collect it."

#### What goes up ...

In the 20th century, U.S. life expectancy climbed from 47 to its present height, a rise unprecedented in human history. The fastest part of the increase occurred in the first few decades of the century, as improved sanitation and nutrition dramatically reduced infant and child mortality. Because a child who avoids death from measles may go on to live for decades more, whereas an older person who avoids death from the same cause will only live a little longer, reducing childhood mortality has a disproportionately large impact on overall life expectancy.

Now, if the *New England Journal* authors are correct, the unprecedented rise in life expectancy will be followed by an equally unprecedented fall. In the 1999–2002 period, according to a Centers for Disease Control and Prevention (CDC) analysis last year, some 16% of U.S. children from 6 to 19—more than 1 out of 8—were overweight, a proportion that has more than tripled in the past 30 years. (Overweight is defined as a body mass index, or BMI—weight in kilograms divided by the square of height in meters—for age and gender at or above the 95th percentile of CDC's baseline growth charts.) Another 15% were at risk for becoming overweight (a BMI between the 85th and 95th percentiles of CDC's growth charts). (For adults, a BMI of 30 or above is considered "obese," and between 25 and 30 is "overweight.")

Because the health effects of obesity can take decades to appear and childhood obesity is a relatively new phenomenon, researchers have relatively little firsthand information on the impact that being overweight in childhood has on the incidence of disease in later life. Instead they make projections from the consequences of obesity on life expectancy for adults. "Obesity is not like running through a minefield, which kills you all at once or lets



**A growing health burden.** One in eight U.S. youths is now overweight.

you run through it unscathed," says David Allison, a biostatistician at the University of Alabama, Birmingham, and a co-author of the *New England Journal* paper. "Instead, your risk increases over time. What you die of is the accumulated effects from years of obesity."

In a typical study, the Netherlands Epidemiology and Demography Compression of Morbidity Research Group analyzed data from the Framingham Heart Study to find in January 2003 that obesity led to declines in life expectancy of 7.1 years for 40-year-old female nonsmokers and 5.8 years for 40-year-old male nonsmokers. The next day, Allison's research team released a study arguing that life expectancy for extremely obese white 20-year-olds (BMIs of 45 or more) is 13 years lower than that for people of normal weight. "The younger you become obese, the more years of life you lose," Allison says. "That's not at all surprising. If you become obese as a child, the impact should be even greater."

#### Conservative assumptions

For the *New England Journal* study, Olshansky says, "we tried to answer a simple question: What would life expectancy be like in the U.S. if obesity did not exist?" Basing their estimates on data from CDC's big National Health and Nutrition Examination Surveys, they assumed, for simplicity's sake, that all overweight or obese people had BMIs of either 30 or 35, respectively. The assumption

had the additional beneficial effect of making the calculation "very conservative," Olshansky says, because it implicitly excluded the impact of higher BMIs. "The proportion of extremely obese is rising very rapidly—things are really moving in the wrong direction—and we ultraconservatively eliminated that." The researchers also assumed that obesity had no effect before the age of 20 or after 85, both of which "we know are not true."

Although Olshansky stresses that the estimate is "a first-pass approximation," he believes the effect is large enough to demonstrate "that trends in obesity in younger ages will lead to significantly higher rates of mortality in the future—we will lose 2 to 5 or more years [of life expectancy] in the coming decades" if the obesity epidemic continues unchecked. Another way of expressing this impact is to note that curing all forms of cancer would only add 3.5 years to average U.S. life expectancy. Rising obesity would more than cancel that out.

Perhaps so, says Vaupel of the Max Planck Institute. But on a global level the United States is an outlier—life expectancy is continuing to rise elsewhere. "That suggests to me that this is a localized problem that could be addressed by appropriate public-health policies," Vaupel says. As he has argued (*Science*, 10 May 2002, p. 1029), demographers have repeatedly predicted that increases in life expectancy will level off. "And they've always been wrong. Olshansky himself wrote in 1990 [*Science*, 2 November 1990, p. 634] that life expectancy would never exceed 85 on average without major breakthroughs. Well, in 2003, Japanese female life expectancy reached 85.33."

To team co-leader Ludwig, the *New England Journal* paper is a "call to action when action could still make a difference." The explosion in obesity, he says, will occur in three phases. The first is increased prevalence. "For the first decade or so, very little occurs—you just have a lot of heavy kids." In the second phase, the rising prevalence is "translated into actual diseases. Then, after yet another period of time, the third phase comes, when those diseases come to translate into lower life expectancy. Right now, we're at the beginning of the second phase. ... The first wave of children diagnosed with type 2 diabetes in adolescence is now reaching their late 20s, and we're just starting to see [circulatory problems leading to] amputations, kidney failure requiring dialysis, and increased mortality."

—CHARLES C. MANN

# RANDOM SAMPLES

Edited by Greg Miller



## No Head Blow for Tut

Fifteen minutes in an x-ray scanner have quelled decades of speculation that King Tutankhamun was done in by a blow to the head.

Previous 2D x-ray studies of King Tut's mummy had revealed two bone fragments in the boy-king's cranium and apparent thinning at the back of the skull, which some took as signs of a partially healed blow. Along with Tut's young age at death (19) and suspected intrigue within the royal family, the skull's state fueled theories that Tut was murdered before being entombed in 1352 B.C.E.

In January a team led by Egyptologist Zahi Hawass of Egypt's Supreme Council of Antiquities did a computed tomography scan of the mummy and called in three international experts to help them pore over the 3D images. On 8 March, the team announced its conclusion: Tut's skull shows no signs of a blow to the head—partially healed or otherwise—during his lifetime. The team says the suspicious fragments most likely were created by the embalmers or by archaeologist Howard Carter's team, which discovered the mummy in 1922.

Philosopher and Egyptologist Bob Brier of Long Island University in Brookville, New York, and a proponent of the murder theory, accepts the conclusions of the scanning team. However, he's not ready to rule out foul play. "The case is not closed," Brier says. "You cannot say he wasn't poisoned; you cannot say he wasn't stabbed."

## Taxonomy, Turkish Style

Who knew that taxonomic nomenclature could undermine national unity? The Turkish Ministry of Environment and Forestry did, apparently, and earlier this month it changed the Latin names of three animals to expunge "divisive" references to two ethnic minorities: Kurds and Armenians.

Turkey's relationship to Kurds and Armenians has long been tense. The government opposes Kurdish separatists and disputes Armenian claims that the Ottoman Empire, modern Turkey's predecessor, had a policy of ethnic cleansing in Eastern Turkey in

### Divisive fox?

the early 20th century.

Henceforth, the ministry declared in a 4 March statement, *Vulpes vulpes kurdistanica*, a Turkish subspecies of the red fox, will be referred to simply as *Vulpes vulpes*. The wild sheep *Ovis armeniana* becomes *Ovis orientalis anatolicus*, and the deer *Capreolus capreolus armenius* is now *Capreolus capreolus capreolus*. The statement alleges that the original names were given with "ill intent."

That seems far-fetched, says Andrew Polaszek, executive secretary of the International Commission on Zoological Nomenclature (ICZN), the body responsible for establishing species naming conventions. Polaszek says changing a species name for

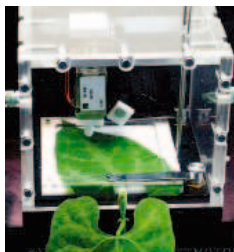
political reasons is verboten. But he adds that the Turkish changes probably don't violate ICZN rules because the new names are scientifically acceptable alternatives.

However, taxonomists note that the ministry overlooked some microbial species whose names could be considered similarly divisive. "I certainly hope that the Turkish politicians don't discover the *Azotobacter armeniacus*, *Cystobacter armeniacus*, [or] *Actinoplanes armeniacus*," says George Garrity, a microbiologist at Michigan State University in East Lansing.

## Probing Plant Defenses

Many plants send out a silent SOS when they are attacked by leaf-munching predators, releasing volatile chemicals that attract wasps and other insectivores to feast on the attackers. But scientists have been unsure what triggers the plant's cry for help: the damaged leaf, or something in the attackers' saliva.

So scientists at the Max Planck Institute for Chemical Ecology in Jena, Germany, designed an ersatz worm, a computer-driven arm that punches small holes in a pinned-

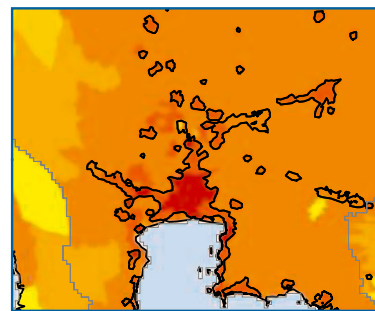


Automated muncher.

down leaf, inflicting systematic damage over hours. In contrast to previous studies in which suddenly slashing leaves with razor blades or scraping them with sand-

paper failed to trigger the chemicals' release, the researchers found that lima bean plants subjected to the "MecWorm" released all the same compounds as plants subjected to attack by hungry insects or snails. The team reports its findings in the March issue of *Plant Physiology*.

Now that the plant's role has been confirmed, co-inventor Axel Mithöfer says the tool should enable scientists to design controlled experiments that home in on exactly how plants detect and fend off hungry caterpillars.



## Urban Expansion

Urban areas cover 3% of Earth's land, far more than previously thought, according to a new map that combines census numbers with satellite imaging of nighttime lights. The map, a result of Columbia University's Global Rural-Urban Mapping Project, reveals dense settlements stretching beyond Bangkok, Thailand (above), a dramatic contrast to the more centralized urban centers found in many other parts of the world.



Edited by Yudhijit Bhattacharjee

**JOBS**

**Follow the money.** Peter Jahrling, a veteran of U.S. bio-defense research, has left the



U.S. Army Medical Research Institute of Infectious Diseases (USAMRIID) in Fort Detrick, Maryland, to lead a high-containment lab being built by

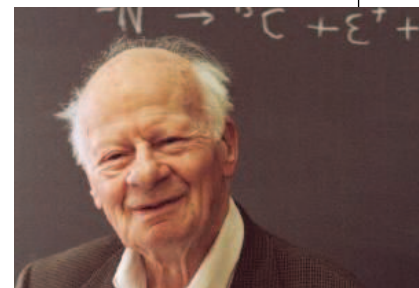
the National Institute of Allergy and Infectious Diseases (NIAID). The \$105 million lab is also on the Fort Detrick campus.

Jahrling, 58, spent 32 years at USAMRIID, working on exotic viruses such as Ebola, Marburg, and monkeypox, before his departure in January. He strongly opposes destruction of the last known stocks of variola, the smallpox virus, which he studied at the Centers for Disease Control and Prevention in Atlanta, Georgia.

A traditional biodefense stronghold, USAMRIID has been eclipsed by NIAID and its billions in new money since 9/11 (*Science*, 14 June 2002, p. 1954).

**DEATHS**

**Shining star.** Nobelist Hans Bethe, who helped develop the atomic bomb and later became an advocate for the control of



nuclear weapons, died at his home in Ithaca, New York, on 6 March. He was 98.

Raised in Germany, Bethe fled from the Nazis and came to Cornell University in 1935. During World War II, J. Robert Oppenheimer put him in charge of theoretical physics for the bomb effort, where he made important contributions. Bethe later urged several U.S. presidents to restrict proliferation, efforts that helped lead to the atmospheric test ban in 1963 and controls on antiballistic missile systems in 1972.

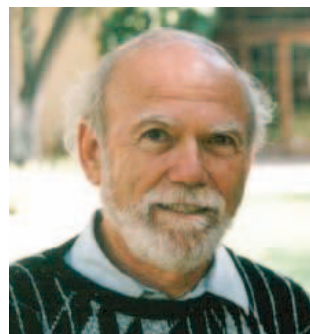
Bethe's work on nuclear reactions in the sun won him the Nobel Prize in 1967. He also worked with Richard Feynman on quantum electrodynamics, a theory of the electromagnetic force, and wrote a seminal paper on so-called order-disorder transitions in alloys. After retirement, he collaborated with John Bahcall of the Institute for Advanced Study in Princeton, New Jersey, to explain why only a portion of neutrinos emanating from the sun were detected upon reaching Earth.

"He brought clarity to an amazing number of fields of science—especially in astrophysics—where he had to work in the face of uncertainty," says Cornell astrophysicist Edwin Salpeter.

Jahrling's exit is another "dramatic loss" for the institute, says Heinz Feldmann of Canada's National Microbiology Laboratory in Winnipeg. But the move will also foster collaboration between the new lab and USAMRIID, says Colonel Erik Henchal, commander of the Army lab.

**Linear thinker.** Caltech physicist Barry Barish says that he's ready to lead the design group for the International Linear Collider—once organizers work out details such as the source of his salary. "Assuming that happens, I'm going to take [the job]," Barish says.

Currently the director of the



gravitational-wave-detection effort known as LIGO, Barish will spend 80% of his time heading the collider project, a proposed multibillion-dollar electron-positron machine that many consider crucial to the future of high-energy physics. Barish hopes the team will be based in North America, suggesting that Vancouver, British Columbia, would be a good choice "because of the visa situation [in the United States]."

According to Barish, the collider's design group will aim for a "strawman" design this year and a more fleshed-out version by the end of 2006.

Got any tips for this page? E-mail [people@aaas.org](mailto:people@aaas.org)

**IN THE PUBLIC EYE**

**Driven.** Representative Bob Inglis (R-SC), who returned to Congress this year after a self-imposed exile, is a staunch conservative and budget hawk. But as the new chair of the House Science Committee's research panel, Inglis sounds a lot like a free-spending liberal when he talks about the importance of funding basic science.



"We need to stop simple spending and start thoughtful investing," Inglis declared last week at a hearing—his first as chair—on the president's 2006 request for the National Science Foundation (NSF), which he decried as woefully inadequate. A proponent of free trade, Inglis says that U.S. companies rely on innovation to stay ahead of the competition—and that federally funded research

is the key first step in that process.

Inglis, a 45-year-old lawyer who stepped down after three terms in the 1990s and reclaimed his old seat in November, says he took the science committee post to advance his passion for the so-called Smart Car, the next generation of pollution-free vehicles. (The auto industry is a major employer in his district.) But he's also eager to learn about NSF and the other federal civilian science agencies under the committee's jurisdiction.

CREDITS (TOP TO BOTTOM): COPYRIGHT 1996 MICHAEL OKONIEWSKI; PHOTO COURTESY OF USAMRIID; SOURCE: BARRY BARISH/CALTECH; HOUSE SCIENCE COMMITTEE

## Combining Parenting and a Science Career

**THE SOBERING NEWS FOCUS ARTICLE "FAMILY MATTERS: Stopping tenure clock may not be enough"** (Y. Bhattacharjee, 17 Dec. 2004, p. 2031) shows how little has changed in the last 20 years to make child rearing possible for a woman scientist who receives her Ph.D. or M.D. around age 27, completes her postdoc near her 30th birthday, and is then off on a 6-year race toward academic tenure with 60- to 80-hour work weeks.

The only new incentive for early parenting mentioned is a pilot program by the National Institute of Allergy and Infectious Diseases to "enable principal investigators (PIs) to hire a technician for up to 2 years to assist a postdoc in their lab who has primary caregiving responsibilities." I would suggest that such funds might be used more flexibly and more effectively when directed specifically to the mother herself.

Why not make available—on a competitive basis related to professional promise or performance—4-year grants (at a level of about \$20,000 to \$25,000 per year) for domes-

U.S. National Academy of Sciences. But even though foundation heads, university presidents, and government officials commented in glowing terms when I approached them, all felt that financial implementation should come from someone else's purse. Has the time finally come to once more raise the issue?

**CARL DJERASSI**

Department of Chemistry, Stanford University, Stanford, CA 94305-5080, USA.

### Reference

1. C. Djerassi, *Science* **239**, 10 (1988).

**IN HIS NEWS FOCUS ARTICLE "FAMILY MATTERS: stopping tenure clock may not be enough"** (17 Dec. 2004, p. 2031), Y. Bhattacharjee discusses the negative impact of childbearing on junior faculty due for a tenure decision. This issue affects women at every rung of the academic ladder. While there is abundant evidence for the health benefits of early childbearing and sustained breast-feeding for both mother and baby, the scientific "training period" now extends into what are likely to be the last reliably fertile years of a woman's life. An anxious new mother cannot be fully effective unless she can be at her

infant's side at short notice. Thus, if women are to succeed in science without sacrificing their health or their chances of having healthy children, academic institutions must give this issue high priority. We suggest that the single best approach is to provide safe, affordable, easily accessible infant care.

Despite espousing "family-friendly" policies, many institutions either do not offer infant day-care or provide only a limited number of spaces. Many off-site facilities will not accept

infants, leaving few viable options when the maternity leave is over—usually in 12 weeks or less in the United States. Attention to this issue will encourage the healthy development of a balanced career and family life, while promoting gender equity in the academic pursuit.

The primary barriers to adequate on-site infant care appear to be cost and liability. Rather than building centralized child-care facilities, we suggest that institutions build or renovate existing smaller spaces on-site, to be used as child-care cooperatives, run by the users. This would be more cost-effective and would ensure access to the infant at short notice. In addition to space,

## Letters to the Editor

Letters (~300 words) discuss material published in *Science* in the previous 6 months or issues of general interest. They can be submitted through the Web ([www.submit2science.org](http://www.submit2science.org)) or by regular mail (1200 New York Ave., NW, Washington, DC 20005, USA). Letters are not acknowledged upon receipt, nor are authors generally consulted before publication. Whether published in full or in part, letters are subject to editing for clarity and space.

the institutions should provide basic financing and administrative support to coordinate resources for the project. As for liability issues, it should be possible to completely indemnify the institution and make these co-op facilities self-insured.

Some may wonder how academic institutions can garner the resources to initiate adequate child-care programs. The question really should be, how much do institutions have to lose in time and productivity before taking such steps to benefit scientists as well as science?

**AMANDA L. LEWIS,<sup>1</sup> TASHA K. ALTHEIDE,<sup>2</sup>**

**AJIT VARKI,<sup>3</sup> KAREN ARDEN,<sup>4</sup> NISSI M. VARKI<sup>5</sup>**

<sup>1</sup>Biological Sciences Division, <sup>2</sup>American Cancer Society Postdoctoral Fellow, <sup>3</sup>Department of Medicine, <sup>4</sup>Section of Molecular Genetics, Ludwig Institute, <sup>5</sup>Department of Pathology, University of California, San Diego, La Jolla, CA 92093, USA.

**THE WELCOME ARTICLE "FAMILY MATTERS: stopping tenure clock may not be enough"** (Y. Bhattacharjee, 17 Dec. 2004, p. 2031) deserves further comment. As a person with a Ph.D. (physics) who has been employed in academia, in a government lab, in R&D departments of two private-sector firms, and self-employed since 1992, perhaps I can provide some perspective.

The tenure system is not just unfriendly to women. These days, two-career families are the norm, and thus, the tenure system is unfriendly to families with children.

The private sector has its own problems with family-friendliness. For example, a former boss once informed his department of his new policy that required all vacation days to be taken in week-long minimum increments scheduled at the beginning of the year. A private discussion followed, in which I pointed out that two working parents with three kids simply cannot do that; most of our vacation days get used up 1 to 2 days at a time tending to family emergencies.

Initiatives such as stopping the tenure clock, part-time positions, and others mentioned in the article are steps in the right direction. Nevertheless, rethinking the whole tenure system should not necessarily be ruled out.

Looking back over the years, I've had many a guilt-trip over whether pursuing my

“ **While there is abundant evidence for the health benefits of early childbearing and sustained breast-feeding for both mother and baby, the scientific "training period" now extends into what are likely to be the last reliably fertile years of a woman's life.** ”

—LEWIS ET AL.

tic child-care support? A woman scientist would be eligible to apply as soon as she has secured a postdoctoral or junior academic position, but actual payment and start of the 4-year grant would only commence a couple of months before the expected birth of the baby, which would have to occur within 3 to 4 years of the date the grant was approved. This support might attract women into demanding scientific careers when they are otherwise not prepared to do so because of their desire for childbearing and child care in the home.

When I made this suggestion in 1988 (1), I received many enthusiastic letters from readers who ranged from female graduate students to two female members of the

scientific interests came at the expense of our kids by somewhat limiting the time I could spend with them, and whether they would have been better off if I had chosen a simpler way of making a living. In the end, the benefits of providing an intellectually rich environment became clear. All three turned out well.

ANDRES PEEKNA

Innovative Mechanics, Inc., 5908 North River Bay Road, Waterford, WI 53185-3035, USA.

## Crying "Whorf"

SOME OF THE MOST STRIKING DISCOVERIES IN the study of language and cognition are also the hardest to interpret. Peter Gordon's Report on innumeracy in a remote Amazonian tribe is no exception ("Numerical cognition without words: evidence from Amazonia," 15 Oct. 2004, p. 496). Although this study invokes a fascinating question about the relation between language and numerical cognition, the data presented do not support Gordon's answer.

Gordon reports that the Pirahã of Brazil lack words in their language for numbers greater than two and also appear unable to match exact quantities larger than two or three. He takes this coincidence to be evi-

dence for a version of the Whorfian hypothesis (*I*) that he calls strong linguistic determinism: If you don't have a word in your language, you can't entertain the concept. Two fundamental problems render Gordon's results uninterpretable.

First, the study fails to compare Pirahã speakers' exact quantity matching performance to performance on a control task, or to performance in an appropriate control group. In this case, appropriate control subjects might be members of another tribe whose culture and habitat are similar to the Pirahã's, but whose language includes exact number words. Suppose that their performance turned out to be indistinguishable from that of the Pirahã speakers, despite their enhanced number vocabulary? Suitable controls might be difficult to implement for practical reasons, but without them it is impossible to tell whether Gordon's results reveal a limitation of the Pirahã's numerical competence or only a limitation of the tasks used to measure their competence.

A second shortcoming is the failure to provide evidence that the Pirahã's impoverished number vocabulary causes their (putative) numerical incompetence. The core of strong linguistic determinism appears to be a causal relation between language and concepts.

Gordon writes that the availability of number words "enables exact numeration" in speakers of some languages and that the lack of counting words "precludes" exact numeration in speakers of other languages like Pirahã. Yet this causal claim is simply not supported, nor is it potentially supportable by the experiments reported in this paper. It is often challenging to demonstrate causation experimentally, and researchers must sometimes argue cause from correlational evidence that is structured so as to make one direction of the causal arrow seem overwhelmingly more plausible than the other. How is this accomplished in Gordon's study? The results are consistent with the Whorfian claim that Pirahã lack number concepts because they lack number words, but results are no less consistent with the opposite claim, which is arguably more plausible. Gordon's data suggest that keeping track of large exact quantities is not critical for getting along in Pirahã society. In the absence of any environmental or cultural demand for exact enumeration, perhaps the Pirahã never developed this representational capacity—and consequently, they never developed the words.

There are good reasons why the Whorfian hypothesis fell into disrepute. Many of the linguistic and behavioral studies that have sought to validate it are badly flawed (2). These days,

Looking for a  
**job?**

- Job Postings
- Job Alerts
- Resume/CV Database
- Career Advice
- Career Forum

**NEW**

**ScienceCareers.org**

We know science



## BILL & MELINDA GATES foundation

### REQUEST FOR PROPOSALS (RFPs)

#### Research consortia to accelerate the development of preventive HIV/AIDS vaccines

The Bill & Melinda Gates Foundation is seeking research proposals to apply new technologies, concepts, and approaches to the design of safe and effective preventive vaccines against HIV/AIDS, in the context of the Scientific Strategic Plan of the Global HIV/AIDS Vaccine Enterprise.

To achieve that purpose, the foundation will initially fund a number of consortia or centers targeting three different priority areas identified in the Scientific Strategic Plan of the Enterprise, namely:

- Design of immunogens that induce broadly reactive neutralizing antibodies (**RFP GH-HTR-05-01**).
- Design of immunogens that induce persistent high levels of cell-mediated immunity (**RFP GH-HTR-05-02**).
- Standardization and development of laboratory assays to comparatively measure the immunogenicity of HIV vaccine candidates in pre-clinical and clinical trials (**RFP GH-HTR-05-03**).

The foundation is interested in innovative approaches to solve the problems associated with the development of an HIV/AIDS vaccine.

Proposals should be conceived as complementary to and not duplicative of ongoing efforts which are currently being supported by other organizations.

Deadline for submission of Letter of Inquiry: **April 1, 2005**

Details of the RFPs can be found at the following Web site:  
<http://www.gatesfoundation.org/GlobalHealth/HIVAIDSTB/HIVAIDS/Vaccines>

the Whorfian hypothesis is experiencing a renaissance, and cognitive science is finally finding ways to pose the Whorfian question clearly (3). But crying “Whorf!” when there’s no Whorfian effect in sight only clouds the issue.

DANIEL CASASANTO

Massachusetts Institute of Technology, Department of Brain & Cognitive Sciences, 77 Massachusetts Avenue, NE20-457, Cambridge, MA 02139, USA. E-mail: djc@mit.edu

#### References

1. B. L. Whorf, *Language, Thought, and Reality: Selected Writings of Benjamin Lee Whorf*, J. B. Carroll, Ed. (MIT Press, Cambridge, MA, 1956).
2. S. Pinker, *The Language Instinct* (Harper, New York, 1994), pp. 55–82.
3. D. Gentner, S. Goldin-Meadow, Eds., *Language in Mind: Advances in the Study of Language and Thought* (MIT Press, Cambridge, MA, 2003).

### Response

**IN MY REPORT, I ASKED WHETHER THERE ARE** some concepts that cannot be translated from one language to another and if this could preclude speakers of one language from entertaining the untranslatable concepts of another. Casasanto paraphrases this position as “if you don’t have a word in your language, you can’t entertain the concept,” which is almost certainly false (for example, most people have a concept of the thing on top of a trolley car that connects to the cables, but few people know its name, including me) and is much more general than I intended.

Casasanto criticizes my research design for not employing a “control group,” which would require finding a tribe exactly like the Pirahã, except that they would have words for exact numbers. Even if such a tribe could be found, they would not constitute a “control group” in the strict sense, but a comparison group. Members of a culture that could count with exact number words would not be comparable to the Pirahã, precisely because they could count. If the comparison tribe were to perform perfectly on my tasks, one could still argue that they differed in important respects from the Pirahã on dimensions other than numerical competence. If the comparison tribe performed no better on the tasks than the Pirahã, then the conclusions would still be ambiguous. One could not be sure that the comparison tribe failed for exactly the same reasons as the Pirahã. This is not to say that such a comparison group would be unhelpful, but the interpretation of results would not be straightforward.

Casasanto’s second criticism concerns my failure to show causation between the lack of number words and lack of numerical abilities in the Pirahã. He cites my report as claiming that “the lack of counting words ‘precludes’ exact enumeration...” and appears to equate “precludes” with “causes.” But these are not the same thing. I do not claim that lack of number words directly causes the lack of number concepts, because this assumes a kind of causal directionality that is not realistic. Casasanto suggests that causality might be reversed: “perhaps the Pirahã never developed this representational capacity—and consequently, they never developed the words.”

In framing the issues in this way, Casasanto changes the debate into one about cultural history, which is totally irrelevant to an argument about synchronic cognitive ability. The question is not how the Pirahã culture might or might not have evolved, but what the consequences are of being born into the culture, as it currently exists. To ask what is the cause of the Pirahã, as a culture, not acquiring exact numerical representations is an exercise in imagining all of the counterfactual possible worlds in which the Pirahã might have acquired such knowledge. The failure of each of those possible worlds to become the actual world then becomes the “cause” of the missing concepts. Casasanto writes as if there were one and only one such counterfactual state of affairs that can be pinned down as the final cause of Pirahã innumeracy, but that is surely wrong.

My own position does not entail a simple cause-and-effect mechanism whereby possession of words for numbers provides all of the necessary and sufficient conditions for the acquisition of exact numerical concepts. It is unlikely that the acquisition of numerical concepts can be characterized in terms of unidirectional cause-and-effect relations. Word meanings tend to be embedded within systems of knowledge. To know the meanings of integers is to know about the basic arithmetic relations between them, which in turn requires some symbolic representation of the integers themselves. In the absence of core components of a system, it is unlikely that the system will develop to its full potential and might emerge relatively unchanged from its original form. I suggest that Pirahã numerical competence emerges with the innate numerical systems of small exact number competence and large number approximation. If we go chasing our tails to find single causal

explanations, then I think we will be forever chasing those tails without resolution.

PETER GORDON

Department of Biobehavioral Sciences, Teachers College, Columbia University, 525 West 120th Street Box 180, New York, NY 10027, USA.

## Recombinant Virus Bank for Gene Delivery

**VIRAL VECTORS HAVE BEEN DEVELOPED AS** therapeutic agents for the introduction of exogenous genes into living cells (1), and clinical trials of gene therapy and the use of viral vectors in the laboratory have been reported with increasing frequency during the past decade (2–4).

We have established a Recombinant Virus Bank at RIKEN BioResource Center in Japan to supply researchers with more than 300 infectious recombinant viruses and 500 recombinant vectors with replication-competent viruses (RCVs) free, which should help to ensure the safety of recombinant viruses and vectors in laboratory experiments and in pre-clinical trials of human gene therapy. The Bank includes recombinant viruses that carry cDNA for cytokines, regulators of the cell cycle, transcription factors, enzymes, and apoptosis-related proteins. We have already dispatched more than 730 recombinant viruses or vectors to scientists worldwide through our database (see [www.brc.riken.jp/lab/dna/rvd/](http://www.brc.riken.jp/lab/dna/rvd/)). To maintain high-quality stocks of recombinant viruses and related vectors, these genetic materials have been subjected to stringent quality control (5–7). They are distributed to scientists who have a material transfer agreement (MTA) with the Bank. The Bank is a non-profit organization, and the only charges are for handling and shipping. The Recombinant Virus Bank should be useful to large numbers of molecular biologists, as well as in human gene therapy.

KAZUNARI K. YOKOYAMA,\* TAKEHIDE MURATA, HIDEYO UGAI, ERIKA SUZUKI, MIHO TERASHIMA, YUKARI KUJIME, SANAE INAMOTO, MEGUMI HIROSE, KUMIKO INABE, TAKAHITO YAMASAKI

Gene Engineering Division, Department of Biological Systems, BioResource Center, RIKEN, 3-1-1 Koyadai, Tsukuba Ibaraki 305-0074, Japan.

\*To whom correspondence should be addressed. E-mail [kazu@brc.riken.jp](mailto:kazu@brc.riken.jp)

#### References

1. D.T. Curiel, J. T. Douglas, *In Vector Targeting for Therapeutic Gene Delivery* (Wiley-Liss, Hoboken, NJ, 2002).
2. See [www.advisorybodies.doh.gov.uk/genetics/gtac/publications.htm](http://www.advisorybodies.doh.gov.uk/genetics/gtac/publications.htm).
3. K. Fukuda *et al.*, *Cancer Res.* **63**, 4434 (2003).
4. E. Seo *et al.*, *Cancer Res.* **65**, 546 (2005).
5. H. Ugai *et al.*, *Jpn. J. Cancer Res.* **93**, 598 (2002).
6. H. Ugai *et al.*, *Biochem. Biophys. Res. Commun.* **300**, 448 (2003).
7. E. Suzuki *et al.*, *Oncol. Rep.* **11**, 173 (2004).

### CORRECTIONS AND CLARIFICATIONS

**ScienceScope:** “Italy pulls out of Global Fund” (4 Feb., p. 655). The item incorrectly reported that the Italian government was withholding its contribution to the Global Fund this year. In fact, Italy decided in late January to allocate 180 million euros for 2004–05 to the fund, a partnership of private and public bodies fighting AIDS, tuberculosis, and malaria. *Science* regrets the error.

**News of the Week:** “Cash-short schools aim to raise fees, recruit foreign students” by E. Marshall (4 Feb., p. 656). The vice chancellor of Oxford University was incorrectly identified. His name is John Hood.

## ORNITHOLOGY

### Sweet Bird Most Musical

Bernard Lohr

Sweet bird, that shunn'st the noise of folly,  
Most musical, most melancholy!  
—John Milton, *Il Penseroso*

Describing and deciphering the enormous variety and complexity of sounds that birds produce was Luis Felipe Baptista's lifelong passion. Sadly, Baptista, the curator of ornithology at the California Academy of Sciences, passed away in June of 2000, leaving the field without his keen enthusiasm and broad-ranging expertise. He was widely admired for his prolific research record, which included important contributions to the fields of song learning, conservation bioacoustics, and the parallels between birdsong and music. He also possessed a well-known desire to bring the sometimes arcane and highly technical arena of birdsong biology to a more general audience. After his untimely death, a large group of his many colleagues and friends convened a conference in his honor. *Nature's Music: The Science of Birdsong* grew out of that symposium.

The editors, Peter Marler (University of California, Davis) and Hans Slabbekoorn (Leiden University, the Netherlands), have drawn on contributors with a wide range of backgrounds and expertise. Marler, whose pioneering work helped establish and guide the study of birdsong as a discipline, starts the volume off with an overview of the field's history. Well-organized, comprehensive summaries of past and current progress on the topics of song learning in birds, the diversity and plasticity of birdsong, auditory perception, vocal production, and the evolution of avian song are provided by well-known experts in these areas. In addition, accomplished younger investigators contribute several of the 14 chapters. These include Slabbekoorn's review of the ecology of birdsong; Jeffrey Podos and Stephen Nowicki's chapter on performance limits, which elegantly integrates mechanism and evolution in the context of song diversity; and Erich Jarvis's discussion of the neuro-

biology of the songbird (oscine) brain, perhaps the most lucid account of current work in this intensively studied and intricate field.

A major attraction of *Nature's Music* comes in the form of scattered brief essays—48 in all—that offer details and perspectives from additional authors whose work bears directly on the issues at hand. Another highlight is the inclusion of two compact discs that contain samples of many of the sounds discussed in the text. Culled from audio archives (including those of the Cornell Laboratory of Ornithology and the British Library of Wildlife Sounds) as well as recordings by individual authors, such auditory examples are long overdue in a book of this type. I hope that future books will continue this welcome trend and perhaps even include DVDs with short video clips or affiliated interactive Web pages to facilitate firsthand glimpses of the study sites, species, and methodology of some of the systems and subjects under review.

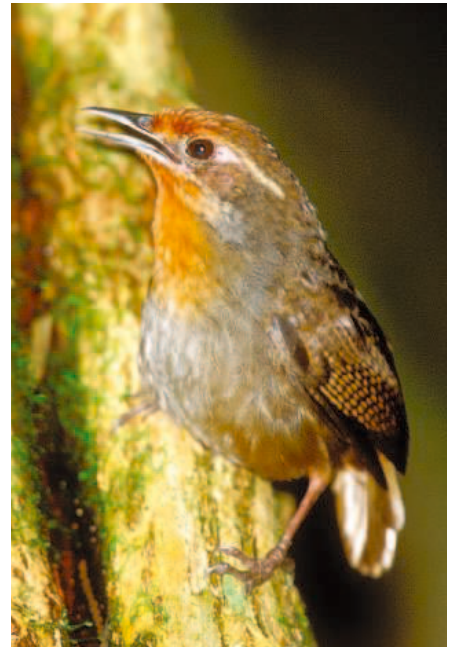
The editors have made a concerted effort to balance the technical nature of the material with the desire to accommodate a more general audience. As a whole, the volume succeeds admirably, although some sections (particularly in chapters that consider questions of biological mechanisms) are still likely to be too specialized for general readers. Another minor shortcoming of the volume is the repeated description of some well-studied processes in birdsong. The developmental stages of song learning, for instance, are recounted in detail in no fewer than four chapters. Some redundancy, however, is unavoidable in a multi-authored volume, and the book generally strikes an excellent balance between brevity and thoroughness.

The contributors do not shy away from controversy. Donald Kroodsma, for example, issues a challenge to those who suggest large song repertoires are a consequence of sexual selection. Kroodsma remains unconvinced that existing direct experimental data demonstrate female choice for larger repertoires in a natural context. Although his criticism is general, he selects—as he did in an earlier critique of song playback

designs—studies of other eminent birdsong biologists as specific examples. Because those researchers are more than capable of defending their conclusions and viewpoints, an interesting and vigorous debate is sure to ensue.

*Nature's Music* outlines a number of important areas for future work. Several contributors stress the need for a greater emphasis on comparative studies, especially in parrots, hummingbirds, and suboscine passerines—all groups now known to show at least some vocal learning. Several authors make a compelling case for renewed emphasis in the relatively neglected area of bird calls (usually shorter, acoustically simpler vocalizations) as distinguished from song;

**Nature's Music**  
The Science  
of Birdsong  
Peter Marler and  
Hans Slabbekoorn, Eds.  
Elsevier Academic Press,  
San Diego, 2004. 543 pp.  
+ 2 CD-ROMS. \$74.95,  
£49.95. ISBN 0-12-  
473070-1.



**Melodic marcel.** The tuneful notes of the musician wren (*Cyphorhinus arada*) inspire investigation into the complexity of birdsong.

indeed, an entire chapter is devoted to this end. Calls occur in numerous contexts and were commonly thought to be nonlearned, although there is now ample evidence in some species to dispute this generality. Lastly, there is a need for a more intensive application of songbird studies to conservation efforts, particularly in the emerging field of conservation bioacoustics (pioneered in part by Baptista). Chapters by Sandra Gaunt and Archibald McCallum, Slabbekoorn, and Robert Dooling all address some aspects of this increasingly important issue, especially the use of song as an environmental indicator and the potential effects of noise on vocal signaling.

The reviewer is in the Department of Psychology, University of Maryland, College Park, MD 20742. E-mail: blohr@psyc.umd.edu

CREDIT: EDSON ENDRIGO/AVESFOTO



Future work on avian song must also grapple with the many contradictions and counterexamples that impede an easy explication of general principles. The challenge is to learn how exceptions to the rule—the “exuberant cacophony” or “exquisite nonstereotypy” of some bird-song—may enhance our understanding of the underlying mechanisms, developmental trajectories, adaptive functions, and evolution of song in birds. *Nature's Music* provides a comprehensive review of these issues and amply conveys the wide-ranging interests and enthusiasm about birdsong championed by Baptista. A fitting tribute to his science and mentoring, the volume offers a generally approachable yet complete and timely review of avian song.

10.1126/science.1108290

## APPLIED PHYSICS

# Shining a Light on Semiconductors

James R. Chelikowsky

In *The Story of Semiconductors*, John Orton attempts to tell you everything you ever might want to know about semiconductors: the science, the economics, the people, the culture, and the history. Of course, he cannot do all of this in any detail while keeping the book's size and scope tractable, but he does an excellent job in addressing most of these matters.

The book shines when the author presents the “people” side of semiconductors. Orton, a semiconductor researcher who retired from the University of Nottingham, names names, gives dates, provides pictures, and recounts interesting anecdotal stories. He does so in a witty, informal, and eminently readable fashion. For example, the book contains a paragraph on the controversies surrounding Nikola Tesla and the development of wireless communications. Orton notes that in an 1893 lecture to the U.S. National Electric Light Association Tesla outlined all the features necessary for a wireless communication system, including the means to provide selectivity. Given that Tesla clearly pioneered these key ideas, why do histories of radio generally not credit him for his contributions? Orton starts with what some people probably already know: that Tesla was not a good advocate for this technology because

The reviewer is at the Institute for Computational Engineering and Sciences, University of Texas, Austin, TX 78712, USA. E-mail: jrc@ices.utexas.edu

he was commercially naive and reluctant to publish his research findings. What readers may not have previously realized is that Tesla's commercial benefactor at the time was someone not very interested in promoting wireless technologies. George Westinghouse “had a vested interest in AC power transmission along wires and was all too keen to keep Tesla's [wireless] work from reaching practical application!”

Orton's technological history of semiconductor inventions includes many interesting details. Some are well known, such as the famous prognostication Gordon Moore, a founder of Intel, made in 1965—the prediction that the number of components on an integrated circuit would double every year. Moore's law has been largely obeyed for the past three decades (though Orton notes that the annual increase is actually about 1.6) and provides a reliable guide to the near future. But how many people outside of the field know Craford's law? As Orton explains, this law quantifies progress in developing the efficiency of light-emitting diodes: the luminous efficiency of such diodes should increase by a factor of ten each decade. Craford's law, like Moore's, has held for the past 30 years, but we are now approaching the limiting efficiency of 100%.

A figure in the book charts the progress from the first light-emitting diodes of the early 1970s, based on GaAsP, to today's AlGaInP/GaP combinations. Readers are guided along the arduous path of how efficient light-emitting diodes were developed. Orton's account will disabuse anyone who believes that progress in materials synthesis and characterization is a minor issue in semiconductors. The light-emitting diodes of the 1970s were inefficient and had few applications, whereas—largely through materials advances—diodes now are routinely employed in traffic lights and will likely replace the incandescent light bulb.

The author is not timid about addressing some of the major economic and social issues surrounding such topics as the Japanese successes in the explosive development of the microelectronics industry during the 1970s. In seeking the key to the Japanese success when American start-up companies like Texas Instruments, Fairchild, Hewlett-Packard, and Intel were clearly a leading and innovative force, Orton recognizes the usual suspects. The Japanese government imposed a “controlled competition” on companies like NEC, Hitachi, and Fujitsu, and Orton contrasts this policy with the *laissez faire* or



**The first transistor (1947).** To obtain power gains, Walter Brattain had to reduce the separation of the two metal point contacts on the germanium crystal to under 50  $\mu\text{m}$ .

“uncontrolled warfare” of the American system. But he also claims that there was more to the Japanese success than government planning, factors such as the planning of product development within companies: “The essential philosophy was one of starting with a product which was perceived to be marketable and thinking backwards to define a research and development programme designed to realize precisely this.” He goes on to strengthen his case by noting cultural circumstances such as the Japanese lifestyle and the urge to develop a “home-made” telecommunications industry.

If there is a shortcoming to the book, it lies in the discussions of the underlying science of semiconductors. To avoid an overly technical narrative, Orton has placed the more specialized and mathematical details in boxes of text and figures. He asserts that the book may be read without resort to these boxes, the main text being complete in itself. One suspects that this will not be true, save for those trained in the field. Of course, this complaint is a bit unfair. As noted in the preface, *The Story of Semiconductors* is not a substitute for a scientific text. It decidedly is not, but it is a fun book to read.

10.1126/science.1108867

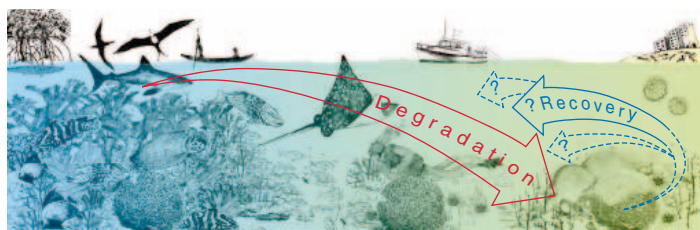
Visit our Books *et al.*  
home page  
[www.sciencemag.org/books](http://www.sciencemag.org/books)

## ECOLOGY

# Are U.S. Coral Reefs on the Slippery Slope to Slime?

J. M. Pandolfi,<sup>1\*</sup> J. B. C. Jackson,<sup>3,4</sup> N. Baron,<sup>5</sup> R. H. Bradbury,<sup>6</sup> H. M. Guzman,<sup>4</sup> T. P. Hughes,<sup>7</sup> C. V. Kappel,<sup>8</sup> F. Micheli,<sup>8</sup> J. C. Ogden,<sup>9</sup> H. P. Possingham,<sup>2</sup> E. Sala<sup>3</sup>

Coral reefs provide ecosystem goods and services worth more than \$375 billion to the global economy each year (1). Yet, worldwide, reefs are in decline (1–4). Examination of the history of degradation reveals three ways to challenge the current state of affairs (5, 6). First, scientists should stop arguing about the relative importance of different causes of coral reef decline: overfishing, pollution, disease, and climate change. Instead, we must simultaneously reduce all threats to have any hope of reversing the decline. Second, the scale of coral reef management—with mechanisms such as protected areas—



The slippery slope of coral reef decline through time.

Enhanced online at [www.sciencemag.org/cgi/content/full/307/5716/1725](http://www.sciencemag.org/cgi/content/full/307/5716/1725)

has been too small and piecemeal. Reefs must be managed as entire ecosystems. Third, a lack of clear conservation goals has limited our ability to define or measure success.

Large animals, like turtles, sharks, and groupers, were once abundant on all coral reefs, and large, long-lived corals created a complex architecture supporting diverse fish and invertebrates (5, 6). Today, the most degraded reefs are little more than rubble, seaweed, and slime. Almost no large animals survive, water quality is poor, and large corals are dead or dying and being replaced by weedy corals, soft corals, and

seaweed (2, 7, 8). Overfishing of megafauna releases population control of smaller fishes and invertebrates, creating booms and busts. This in turn can increase algal overgrowth, or overgrazing, and stress the coral architects, likely making them more vulnerable to other forms of stress. This linked sequence of events is remarkably consistent worldwide (see top figure, this page).

Even on Australia's Great Barrier Reef (GBR), the largest and best-managed reef in the world, decline is ongoing (9). Australia's strategy, beginning with the vision to establish the world's largest marine park in 1976, is based on coordinated management at large spatial scales. Recently more than one-third of the GBR was zoned "no take," and new laws and policies to reduce pollution and fishing are in place (10). Evaluating benefits of increased no-take zones will require detailed follow-up, but smaller-scale studies elsewhere support increased protection. Two neighboring countries, the Bahamas (11) and Cuba (12), have also committed to conserve more than 20% of their coral reef ecosystems. By contrast, the Florida Keys and main Hawaiian Islands are far further down the trajec-

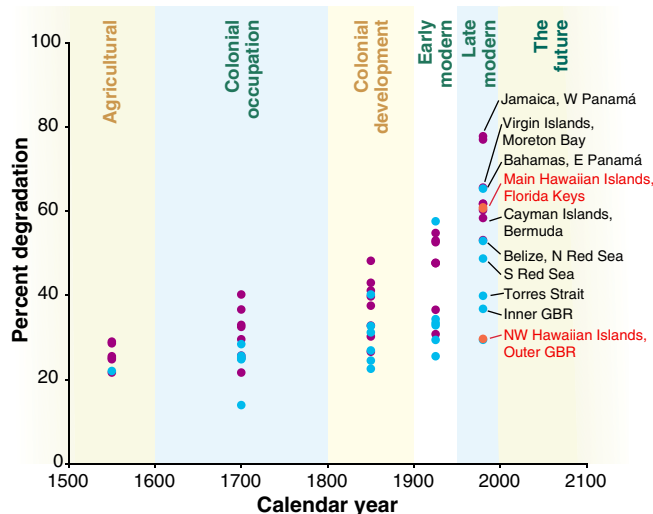
tory of decline (see bottom figure, this page), yet much less action has been taken.

What is the United States doing to enhance its coral reef assets? In the Florida Keys National Marine Sanctuary, the Governor and the National Oceanic and Atmospheric Administration (NOAA) agreed in 1997 to incorporate zoning with protection from fishing and water quality controls (13). But only 6% of the Sanctuary is zoned no take, and these zones are not strategically located. Conversion of 16,000 cesspools to centralized sewage treatment and control of other land-based pollution have only just begun. Florida's reefs are well over halfway toward ecological extinction and much more impaired than reefs of Belize and all but one of the

Pacific reefs in the figure below (6). Large predatory fishes continue to decrease (14), reefs are increasingly dominated by seaweed (15, 16), and alarming diseases have emerged (17).

Annual revenues from reef tourism are \$1.6 billion (1), but the economic future of the Keys is gloomy owing to accelerating ecological degradation. Why? Without a clear goal for recovery, development and ratification of the management plan became a goal in itself.

Reefs of the northwest Hawaiian Islands have been partially protected by isolation from the main Hawaiian Islands (which show



Past and present ecosystem conditions of 17 coral reefs, based on historical ecology (6). The method consists of determining the status of guilds of organisms for each reef with published data, performing a multivariate, indirect gradient analysis on the guild status database, and estimating the location of each reef along a gradient of degradation from pristine to ecologically extinct reefs. Green, Caribbean sites; blue, Australian and Red Sea sites; red, U.S. reefs from the most recent cultural period.

<sup>1</sup>The Centre for Marine Studies and Department of Earth Sciences, <sup>2</sup>Department of Mathematics and School of Life Sciences, The University of Queensland, St. Lucia, QLD 4072, Australia. <sup>3</sup>Center for Marine Biodiversity and Conservation, Scripps Institution of Oceanography, La Jolla, CA 92093, USA. <sup>4</sup>Smithsonian Tropical Research Institute, Balboa, Republic of Panamá. <sup>5</sup>National Center for Ecological Analysis and Synthesis, Santa Barbara CA. <sup>6</sup>Centre for Resource and Environmental Studies, Australian National University, Canberra, ACT 0200, Australia. <sup>7</sup>Centre for Coral Reef Biodiversity, School of Marine Biology, James Cook University, Townsville, QLD 4811, Australia. <sup>8</sup>Hopkins Marine Station, Stanford University, CA 93950–3094, USA. <sup>9</sup>Florida Institute of Oceanography, St. Petersburg, FL 33701, USA.

\* Author for correspondence. E-mail: [j.pandolfi@uq.edu.au](mailto:j.pandolfi@uq.edu.au)

## A ROADMAP FOR REVERSING THE TRAJECTORY OF DECLINE OF U.S. CORAL REEFS

Threat (time frame)	Critical first step	Results	Benefits
Overfishing (years)	Immediate increase of cumulative no-take areas of all U.S. reefs to >30%; reduce fishing efforts in adjacent areas	Increase in short-lived species, such as lobsters, conch, parrotfish, and sea urchins	Economic viability to lost or weakened fisheries; reduction in algal competition with corals
Overfishing (decades)	Establishment of large fish, shark, turtle, and manatee breeding programs; mandatory turtle exclusion devices (TEDs) and bycatch reduction devices (BRDs)	Increase in megafauna populations	Return of key functional components and trophic structure
Pollution (years-decades)	Stringent controls over land-based pollution	Increase in water quality	Reduction in algal competition with corals; reduced coral disease
Coastal development (years-decades)	Moratorium on coastal development in proximity to coral reefs	Increase in coral reef habitat	Increase of coral reef populations (i.e., reduced mortality)
Global change (decades)	International engagement in emission caps	Reduction in global sea surface temperatures and CO <sub>2</sub>	Lower incidence of coral bleaching; increase calcification potential

degradation similar to that of the Florida Keys) and are in relatively good condition (see figure at the bottom of page 1725). Corals are healthy (2, 18), and the average biomass of commercially important large predators such as sharks, jacks, and groupers is 65 times as great (19) as that at Oahu, Hawaii, Maui, and Kauai. Even in the northwestern islands, however, there are signs of decline. Monk seals and green turtles are endangered (20, 21); large amounts of marine debris are accumulating, which injure or kill corals, seabirds, mammals, turtles, and fishes (2, 18, 22); and levels of contaminants, including lead and PCBs are high (18).

Until recently, small-scale impacts from overfishing and pollution could be managed locally, but thermal stress and coral bleaching are already changing community structure of reefs. Impacts of climate change may depend critically on the extent to which a reef is already degraded (8, 23). Polluted and overfished reefs like in Jamaica and Florida have failed to recover from bouts of bleaching, and their corals have been replaced by seaweed (2). We believe that restoring food webs and controlling eutrophication provides a first line of defense against climate change (8, 23); however, slowing or reversing global warming trends is essential for the long-term health of all tropical coral reefs.

For too long, single actions such as making a plan, reducing fishing or pollution, or conserving a part of the system were viewed as goals. But only combined actions addressing all these threats will achieve the ultimate goal of reversing the trajectory of decline (see the table above).

We need to act now to curtail processes adversely affecting reefs. Stopping overfishing will require integrated systems of no-take areas and quotas to restore key functional groups. Terrestrial runoff of nutrients, sediments, and toxins must be greatly reduced by wiser land use and coastal development. Reduction of emissions of greenhouse gases are needed to reduce coral bleaching and disease. Progress on all fronts

can be measured by comparison with the past ecosystem state through the methods of historical ecology to determine whether or not we are succeeding in ameliorating or reversing decline. Sequential return of key groups, such as parrot fish and sea urchins that graze down seaweed; mature stands of corals that create forest-like complexity; and sharks, turtles, large jacks, and groupers that maintain a more stable food web (4, 5, 6, 24) constitutes success.

This consistent way of measuring recovery (see the figure at the bottom of page 1725) and the possibility of short-term gains set a benchmark for managing other marine ecosystems. Like any other successful business, managing coral reefs requires investment in infrastructure. Hence, we also need more strategic interventions to restore species that provide key ecological functions. For example, green turtles and sea cows not only once helped maintain healthy seagrass ecosystems, but also were an important source of high-quality protein for coastal communities (25).

Our vision of how to reverse the decline of U.S. reefs rests on addressing all threats simultaneously (see the table above). By active investment, major changes can be achieved through practical solutions with short- and long-term benefits. Short-lived species, like lobster, conch, and aquarium fish will recover and generate income in just a few years, and benefits will continue to compound over time. Longer-lived species will recover, water quality will improve, and the ecosystem will be more resilient to unforeseen future threats. Ultimately, we will have increased tourism, and the possibility of renewed sustainable extraction of abundant megafauna. One day, reefs of the United States could be the pride of the nation.

## References

1. D. Bryant *et al.*, *Reefs at Risk. A Map-Based Indicator of Threats to the World's Coral Reefs* (World Resources Institute, Washington, DC, 1998).
2. C. R. Wilkinson, *Status of Coral Reefs of the World:*

2004 (Global Coral Reef Monitoring Network and Australian Institute of Marine Science, Townsville, Australia, in press); vol. 1 is available at [www.gcrmn.org/status2004.asp](http://www.gcrmn.org/status2004.asp).

3. T. A. Gardener *et al.*, *Science* **301**, 958 (2003).
4. D. R. Bellwood, T. P. Hughes, C. Folke, M. Nyström, *Nature* **429**, 827 (2004).
5. J. B. C. Jackson *et al.*, *Science* **293**, 629 (2001).
6. J. M. Pandolfi *et al.*, *Science* **301**, 955 (2003).
7. T. P. Hughes *et al.*, *Science* **265**, 1547 (1994).
8. N. Knowlton, *Proc. Natl. Acad. Sci. U.S.A.* **98**, 5419 (2001).
9. Great Barrier Reef Marine Park Authority, *Overview: The current status of the Great Barrier Reef*, [www.gbrmpa.gov.au/corp\\_site/info\\_services/publications/sotr/overview/index.html](http://www.gbrmpa.gov.au/corp_site/info_services/publications/sotr/overview/index.html)
10. Great Barrier Reef Marine Park Authority, New Policy Web site: [www.gbrmpa.gov.au/corp\\_site/management/zoning/publications.html](http://www.gbrmpa.gov.au/corp_site/management/zoning/publications.html)
11. D. R. Brumbaugh *et al.*, *Proceedings of the Forum 2003 Conference*, Nassau, Bahamas, 30 June to 4 July 2003 (College of the Bahamas, Nassau, Bahamas, 2003).
12. R. Estrada *et al.*, *El sistema nacional de areas marinas protegidas de Cuba* [Center for Protected Areas (CNAIP), Havana, Cuba, 2003].
13. Florida Keys National Marine Sanctuary, *Draft Management Plan/Environmental Impact Statement* (Department of Commerce, National Oceanic and Atmospheric Administration, Washington, DC, 1995), vol. 1, pp. 1–323.
14. J. A. Bohnsack, *Gulf Caribbean Res.* **14**, 1 (2003).
15. W. C. Jaap *et al.*, *Environmental Protection Agency/National Oceanographic and Atmospheric Administration (NOAA) Coral Reef Evaluation and Monitoring Project: 2002 Executive Summary* (Report of the Florida Fish and Wildlife Conservation Commission, Tallahassee, and the University of Georgia, Athens, 2003).
16. J. W. Porter *et al.*, in *The Everglades, Florida Bay, and Coral Reefs of the Florida Keys: An Ecosystem Handbook*, J. W. Porter and K. G. Porter, Eds. (CRC Press, Boca Raton, FL, 2002), pp. 749–769.
17. C. D. Harvell *et al.*, *Science* **296**, 2158 (2002).
18. J. Maragos, D. Gulko, Eds., *Coral Reef Ecosystems of the Northwestern Hawaiian Islands: Interim Results Emphasizing the 2000 Surveys* (U.S. Fish and Wildlife Service and Hawaii Department of Land and Natural Resources, Honolulu, HI, 2002).
19. A. M. Friedlander, E. E. DeMartini, *Mar. Ecol. Prog. Ser.* **230**, 253 (2002).
20. International Union for the Conservation of Nature and Natural Resources, *Red List of Threatened Species*, available at [www.redlist.org](http://www.redlist.org).
21. NOAA, [www.nmfs.noaa.gov/prot\\_res/species/](http://www.nmfs.noaa.gov/prot_res/species/).
22. C. Safina, *Eye of the Albatross* (Holt, New York, 2003).
23. T. P. Hughes *et al.*, *Science* **301**, 929 (2003).
24. T. Elmquist *et al.*, *Front. Ecol. Environ.* **1**, 488 (2003).
25. J. B. C. Jackson, *Coral Reefs* **16**, S23 (1997).

10.1126/science.1104258

## Supporting Online Material

[www.sciencemag.org/cgi/content/full/307/5716/1725/DC1](http://www.sciencemag.org/cgi/content/full/307/5716/1725/DC1)

## An Anchor for Tumor Cell Invasion

Stuart H. Yuspa and Ervin H. Epstein Jr.

Studies of skin cancer in the mouse provide experimental proof that tumors develop in multiple steps. Among these steps are initiation, promotion, and progression. Individuals prone to developing cutaneous tumors and other skin diseases due to inherited mutations have illuminated a number of cellular pathways that are involved in cancer susceptibility. For example, mutations in DNA-repair genes in xeroderma pigmentosum predispose to several cancers, and mutations in genes of the Hedgehog signaling pathway predispose to basal cell carcinoma. Other examples include mutations in  $\beta$ -catenin (an adhesion protein and transcription factor) that predispose to hair follicle tumors (pilomatricoma); mutations in the *CYLD* gene (encoding a regulator of protein degradation in the NF- $\kappa$ B pathway) that predispose to head and neck tumors (cylindroma); and mutations in the cell cycle regulator *INK4A* (*p16*) that predispose to familial melanoma. On page 1773 of this issue, Ortiz-Urda *et al.* (1) link another hereditary skin disease to a mechanism for cancer invasion by studying patients with mutations in the anchoring molecule collagen VII. Mutations in collagen VII cause recessive dystrophic epidermolysis bullosa, a blistering skin disorder. Ortiz-Urda and co-workers report that these patients are predisposed to developing invasive skin cancers, but only if they express a crucial part of the collagen VII molecule.

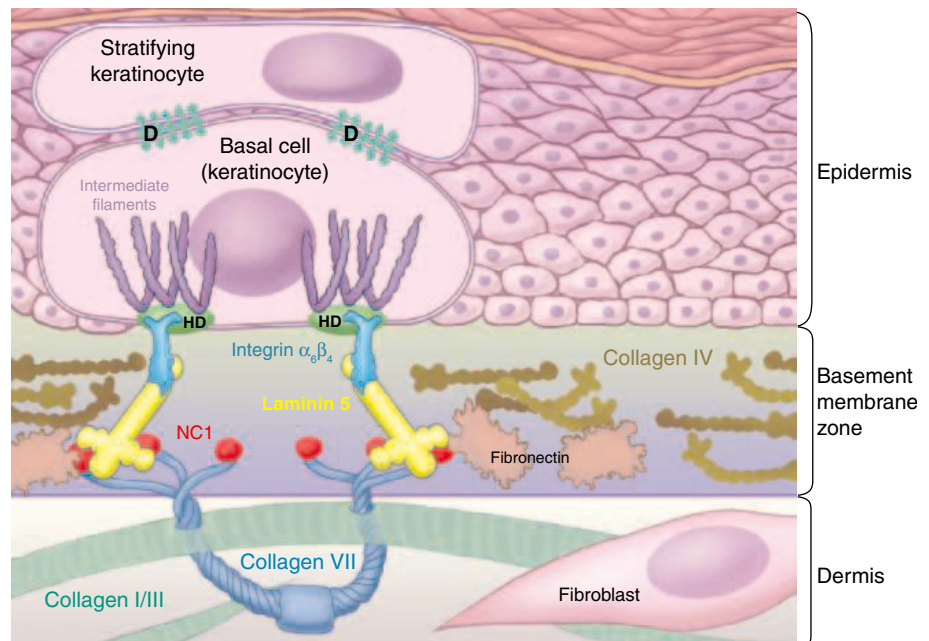
Epidermolysis bullosa describes a heterogeneous group of diseases characterized by fragile skin. These diseases are associated with mutations in at least 10 different genes encoding proteins that form the basement membrane zone of skin, the point where the epidermis and dermis meet (see the figure) (2). Crucial to the anchoring of the epidermis to the dermis are a series of protein inter-

actions: Keratin intermediate filaments of basal skin cells (keratinocytes) are connected to hemidesmosomes that interact with laminin 5, which is bound to collagen VII (see the figure). Collagen VII forms bundles of anchoring fibrils that extend from the basement membrane into the dermis.

Mutations in collagen VII cause dystrophic epidermolysis bullosa, the cruellest member of this disease assemblage. Even mild trauma splits off the epidermis from the underlying dermis, resulting in severe scarring, deformities of the extremities, and chronic nonhealing wounds. A unique feature of this disease is the development of highly aggressive metastatic cutaneous squamous cell carcinoma (SCC), which is

fatal in about half of these patients. The cellular pathways that predispose to these SCCs remain undefined, but the following have been implicated: mutations in the *p53* gene, suppression of *p16<sup>INK4a</sup>* activity, increased collagenase activity, and an increase in basic fibroblast growth factor in the plasma of some patients (3, 4).

In their new study, Ortiz-Urda *et al.* address the question of why more than half of patients with recessive dystrophic epidermolysis bullosa develop SCC, whereas the remainder do not. These authors previously developed a model in which normal human keratinocytes were transduced with retroviruses carrying two aberrant genes—an oncogenic Ras allele, and a mutant I $\kappa$ B gene that blocks activation of the master transcription factor NF- $\kappa$ B—and then were grafted intradermally or subcutaneously into immunocompromised mice (5). Transduction of normal human keratinocytes with these two genes transformed them into invasive SCC tumor cells. In their new work, Ortiz-Urda and colleagues analyzed keratinocytes obtained



**Intimate connections.** An adhesion complex in the basement membrane zone of skin anchors the epidermis to the dermis. Stratifying skin cells (keratinocytes) are connected by desmosomes (D) to basal keratinocytes. Hemidesmosomes (HD) anchor basal keratinocytes to the basement membrane principally through the interaction of laminin 5 with the  $\alpha_6\beta_4$  integrin receptor. This interaction also relays signals from the epidermal and extraepidermal environments to a network of keratin intermediate filaments. Anchoring of the epidermis to the dermis depends on the interaction of laminin 5 with the NC1 domain of collagen VII, the major component of fibrils that extend from the basement membrane zone into the dermis (10). Patients with the blistering skin disease recessive dystrophic epidermolysis bullosa, who carry mutations resulting in deposition of the NC1 fragment of collagen VII, develop SCC. In contrast, those patients carrying mutations that block production of collagen VII do not develop these cutaneous cancers (7).

S. H. Yuspa is in the Laboratory of Cellular Carcinogenesis and Tumor Promotion, National Cancer Institute, National Institutes of Health, Bethesda, MD 20892, USA. E-mail: sy12j@nih.gov. E. H. Epstein Jr. is in the Department of Dermatology, University of California, San Francisco, CA 94108, USA. E-mail: epsteine@derm.ucsf.edu



from 12 patients with recessive dystrophic epidermolysis bullosa. They show convincingly that susceptibility to developing invasive SCC, both clinically and experimentally, depends strictly on the retention of part of the collagen VII protein. Keratinocytes from patients carrying mutations that abrogate the deposition of collagen VII do not develop into invasive SCC, whereas those from patients with mutations that result in deposition of a crucial fragment of collagen VII do become cancerous.

Collagen VII is produced primarily by keratinocytes, with perhaps a small contribution from dermal fibroblasts. The collagen VII molecule has a characteristic central glycine-rich, triple-helical collagenous domain, with noncollagenous domains at its amino and carboxyl ends. Keratinocytes from patients with mutations that specifically leave intact the amino-terminal non-collagenous domain (NC1) of collagen VII, and more specifically the fibronectin III-like repeats within the NC1 domain (FNC1) that bind to laminin 5, developed into invasive SCC. Furthermore, introduction of either the NC1 or FNC1 domains into patient keratinocytes deficient in collagen VII restored a predisposition to tumorigenesis, whereas introduction of NC1 without the fibronectin repeats did not. Interestingly, antibodies that specifically recognized the FNC1 domain of collagen VII either prevented tumor development or suppressed tumor invasion when administered to mice with SCC tumors caused by Ras/IκB-transformed keratinocytes from normal individuals. Invasion studies *in vitro* confirmed the *in vivo* findings and further revealed that interaction of FNC1 with laminin 5 was required for the invasive phenotype to develop.

What do these results tell us about epidermolysis bullosa and SCC? First, they suggest an explanation for why chronic wounds seldom develop into SCC in patients with mutations in adhesion complex proteins that are closer to the epidermis (for example, laminin 5, hemidesmosomal proteins, and intermediate filament proteins). Keratinocytes harboring such mutations lack an intact adhesion complex between the NC1 domain of collagen VII and laminin 5 and the hemidesmosomes. Hence, these keratinocytes are not tethered to the dermis and may not receive the stromal signals that they would need to migrate to and invade the dermal layer. Laminin 5 is the ligand for  $\alpha_6\beta_4$  integrin, a signaling receptor on the surface of basal keratinocytes. Hence, interactions between collagen VII and laminin 5 may be the conduit for stromal signals that direct the migratory and invasive behaviors of epidermal tumors (6).

Ortiz-Urda *et al.* also show that boosting

production of NC1 enhances the invasiveness of transformed keratinocytes from normal individuals, and of keratinocytes from patients with other skin diseases. A central regulator of collagen VII expression is transforming growth factor- $\beta$  (TGF- $\beta$ ) (7), which enhances invasion and metastasis of established squamous cell tumors and other epithelial neoplasms (8). The new work suggests that the relationship between collagen VII and TGF- $\beta$  is worth exploring further. There are also two possible clinical applications of the current study. Attempts to restore collagen VII locally using gene therapy in patients with dystrophic epidermolysis bullosa are under active investigation (9). The authors caution that for certain patients, restoration of collagen VII containing the NC1 domain could increase their risk of developing SCC, particularly in those who lack production of collagen VII. On the other hand, the good news is that the NC1 domain could be a therapeutic target for treating invasive SCC and other cancers.

However, a therapeutic molecule that binds to the NC1 domain must block the molecular interactions required for tumor invasion while leaving intact those required for anchoring the epidermis to the dermis. We are faced with a possible Pyrrhic victory as we contemplate the epithelial-stromal interface: perhaps winning the battle against SCC but losing the battle against the disfiguring skin defects of dystrophic epidermolysis bullosa.

References

1. S. Ortiz-Urda *et al.*, *Science* **307**, 1773 (2005).
2. L. Pulkkinen, J. Uitto, *Matrix Biol.* **18**, 29 (1999).
3. J. L. Arbiser *et al.*, *Mol. Med.* **4**, 191 (1998).
4. J. L. Arbiser *et al.*, *J. Invest. Dermatol.* **123**, 788 (2004).
5. M. Dajee *et al.*, *Nature* **421**, 639 (2003).
6. M. M. Mueller, N. E. Fusenig, *Nature Rev. Cancer* **4**, 839 (2004).
7. M. J. Calonge, J. Seoane, J. Massague, *J. Biol. Chem.* **279**, 23759 (2004).
8. A. B. Glick, *Cancer Biol. Ther.* **3**, 276 (2004).
9. D. T. Woodley *et al.*, *Nature Med.* **10**, 693 (2004).
10. J. R. McMillan, M. Akiyama, H. Shimizu, *J. Dermatol. Sci.* **31**, 169 (2003).

10.1126/science.1110346

EVOLUTION

# Fossil Horses— Evidence for Evolution

Bruce J. MacFadden

Thomas Huxley, an early advocate of Darwinian evolution, visited the United States in 1876 on a lecture tour. Huxley had planned to talk about evidence for evolution based on a fragmentary sequence of fossil horses from Europe. One of Huxley's first stops was at Yale, where he studied the fossil horse collection assembled by the paleontologist O. C. Marsh during expeditions to the western territories. Huxley was so taken with the definitive evidence provided by Marsh's fossil horse collection that he used this evolutionary sequence as the focal point for his subsequent talk to the New York Academy of Sciences (1).

Since the late 19th century, the 55-million-year (My) phylogeny of horses (Family Equidae)—particularly from North America—has been cited as definitive evidence of long-term “quantum” evolution (2), now called macroevolution. Macroevolution is the study of higher level (species, genera, and above) evolutionary patterns that occur on time scales ranging from thousands to millions of years. The speciation, diversification, adaptations, rates of change, trends, and extinc-

tion evidenced by fossil horses exemplify macroevolution.

The sequence from the Eocene “dawn horse” *Eohippus* to modern-day *Equus* has been depicted in innumerable textbooks and natural history museum exhibits. In Marsh's time, horse phylogeny was thought to be linear (orthogenetic), implying a teleological destiny for descendant species to progressively improve, culminating in modern-day *Equus*. Since the early 20th century, however, paleontologists have understood that the pattern of horse evolution is a more complex tree with numerous “side branches,” some leading to extinct species and others leading to species closely related to *Equus*. This branched family tree (see the figure) is no longer explained in terms of predestined improvements, but rather in terms of random genomic variations, natural selection, and long-term phenotypic changes (3).

The Equidae, a family within the odd-toed ungulate Order Perissodactyla (which includes rhinoceroses, tapirs, and other closely related extinct groups), consists of the single extant genus *Equus*. Depending upon interpretation, it also includes several subgenera, 8 to 10 species, and numerous subspecies (4). On the basis of morphological differences, *Equus* is separated into two or

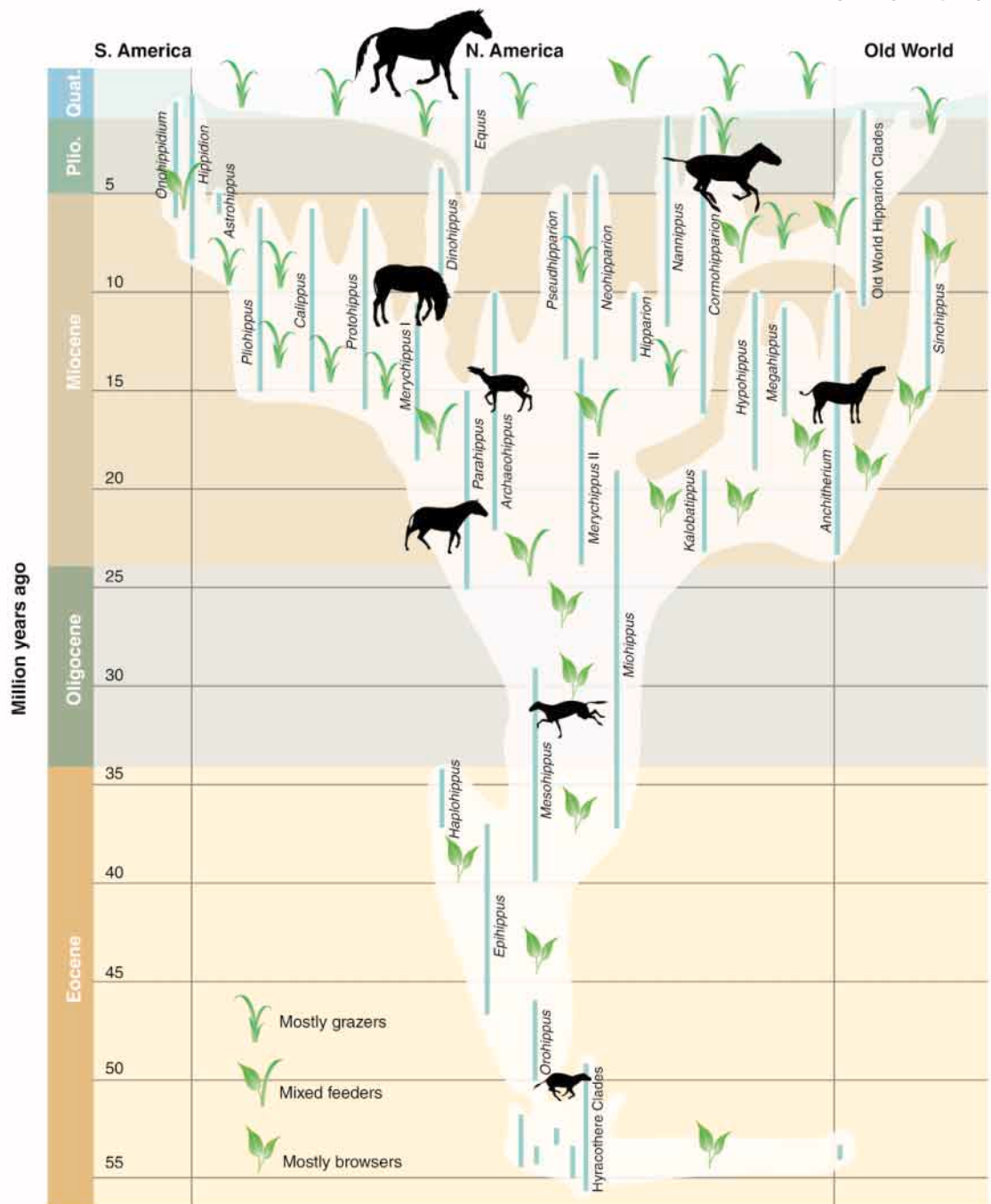
The author is in the Florida Museum of Natural History, University of Florida, Gainesville, FL 32611, USA. E-mail: bmacfadd@flmnh.ufl.edu

three deep clades within the genus. These include caballines (domesticated horse, *E. caballus*); zebras (three species recognized); and asses, donkeys, and related species. Recent studies of mitochondrial DNA indicate two deep clades within *Equus*, namely, the caballines and the zebras/asses (5). These deep clades split ~3 million years ago (Ma) in North America and subsequently dispersed into the Old World. *Equus* became extinct in the New World ~10,000 years ago, probably as a result of multiple factors including climate change and hunting by early humans. In the Old World, although its range contracted, *Equus* persisted and was then domesticated in central Asia about 6000 years ago from a stock similar to Przewalski's wild horse, *E. caballus* (sometimes considered its own species, *E. przewalskii*) (4).

The single modern genus *Equus* stands in marked contrast to a highly diverse adaptive radiation of the Family Equidae over the past 55 My that resulted in some three dozen extinct genera and a few hundred extinct species (3). Although the overall branched pattern of horse phylogeny (see the figure) has remained similar for almost a century, new discoveries and reinterpretation of existing museum fossil horse collections have added to the known diversity of extinct forms. Recent work reveals that Eocene "hyracotheres" horses, previously known as "eohippus" or *Hyracotherium*, include an early diversification of a half-

dozen genera that existed between 55 and 52 Ma in North America and Europe (6). New genera have recently been proposed for the complex middle Miocene radiation (7), although the validity of these genera is still debated.

Horse teeth frequently preserve as fos-



**Adaptive radiation of a beloved icon.** Phylogeny, geographic distribution, diet, and body sizes of the Family Equidae over the past 55 My. The vertical lines represent the actual time ranges of equid genera or clades. The first ~35 My (Eocene to early Miocene) of horse phylogeny are characterized by browsing species of relatively small body size. The remaining ~20 My (middle Miocene until the present day) are characterized by genera that are either primarily browsing/grazing or are mixed feeders, exhibiting a large diversification in body size. Horses became extinct in North America about 10,000 years ago, and were subsequently reintroduced by humans during the 16th century. Yet the principal diversification of this family occurred in North America. Although the phylogenetic tree of the Equidae has retained its "bushy" form since the 19th century [for example, see (2, 3)], advances in knowledge from fossils have refined the taxonomy, phylogenetic interrelationships, chronology, and interpretations of the ancient ecology of fossil horses.

sils and are readily identifiable taxonomically. They serve as objective evidence of the macroevolution of the Equidae. Horse teeth have undergone considerable changes over the past 55 My. The tempo of this morphological evolution has sometimes been slow and at other times rapid (2, 3).

Primitive Eocene through early Miocene (between 55 and 20 My) horses had short-crowned teeth adapted for browsing on soft, leafy vegetation. During the later Miocene (between 20 and 15 Ma), horses underwent explosive adaptive diversification in tooth morphology. Shorter crowned browsers,

which inhabited forests and open-country woodlands, declined in diversity during this time (8). In contrast, many other clades of horses evolved high-crowned teeth adapted for grazing on the extensive grasslands of more open-country biomes, which spread during the Miocene (25 to 15 Ma). Once high-crowned teeth evolved, some clades underwent a secondary adaptation, that is, they went from being grazers to being mixed feeders with diets consisting of grass and some leafy plants (9). Studies of carbon isotopes preserved in fossil horse teeth indicate that before ~7 Ma, early tropical and temperate grasslands of the world consisted primarily of grasses that used the C<sub>3</sub> photosynthetic pathway, whereas today these grasslands consist mostly of C<sub>4</sub> grasses (10).

In many fossil groups, the trend toward larger body size in ancestral-descendent sequences has been termed “Cope’s rule.” Early Eocene hyracothere horses classically have been compared in size to a small dog (~10 to 20 kg), although house-cat-sized

species have been discovered more recently. At the other end of the evolutionary spectrum, wild modern *Equus* attains a body size of ~500 kg (3, 4). Although the 55-My-old fossil horse sequence has been used as a classic example of Cope’s rule, this notion is now known to be incorrect. Rather than a linear progression toward larger body size, fossil horse macroevolution is characterized by two distinctly different phases. From 55 to 20 Ma, primitive horses had estimated body sizes between ~10 and 50 kg. In contrast, from 20 Ma until the present, fossil horses were more diverse in their body sizes. Some clades became larger (like those that gave rise to *Equus*), others remained relatively static in body size, and others became smaller over time (3).

Fossil horses have held the limelight as evidence for evolution for several reasons. First, the familiar modern *Equus* is a beloved icon that provides a model for understanding its extinct relatives. Second, horses are represented by a relatively continuous and widespread 55-My evolution-

ary sequence. And third, important fossils continue to be discovered and new techniques developed that advance our knowledge of the Family Equidae. The fossil horse sequence is likely to remain a popular example of a phylogenetic pattern resulting from the evolutionary process.

#### References

1. C. Schuchert, C. M. LeVene, O. C. Marsh *Pioneer in Paleontology* (Yale Univ. Press, New Haven, CT, 1940).
2. G. G. Simpson, *Major Features of Evolution* (Columbia Univ. Press, New York, 1953).
3. B. J. MacFadden, *Fossil Horses: Systematics, Paleobiology, and Evolution of the Family Equidae* (Cambridge Univ. Press, New York, 1992).
4. R. M. Nowak, *Walker’s Mammals of the World, 5.1 Online* (Johns Hopkins Univ. Press, Baltimore, 1997).
5. E. A. Oakenfull, H. N. Lim, O. A. Ryder, *Conserv. Genet.* **1**, 341 (2000).
6. D. J. Froehlich, *Zool. J. Linn. Soc.* **134**, 141 (2002).
7. T. S. Kelly, *Contrib. Sci. Nat. Hist. Mus. Los Ang. Cty.* **455**, 1 (1995).
8. C. M. Janis, J. Damuth, J. M. Theodor, *Proc. Natl. Acad. Sci. U.S.A.* **97**, 7899 (2000).
9. B. J. MacFadden, N. Solounias, T. E. Cerling, *Science* **283**, 824 (1999).
10. T. E. Cerling *et al.*, *Nature* **389**, 153 (1997).

10.1126/science.1105458

## PHYSICS

# Toward Creating a Rutherford Atom

David M. Villeneuve

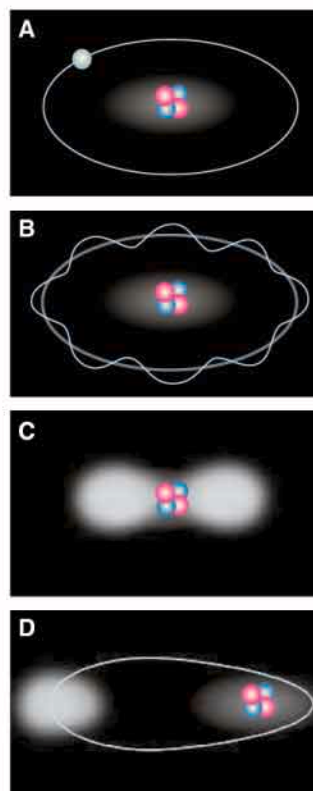
The early 20th century saw a rapid evolution in the concept of the atom (see the first figure). In 1911, Ernest Rutherford proposed that the atom resembled a tiny solar system, with most of the mass concentrated in a nucleus, and electrons revolving around it in planetary orbits (see the first figure, panel A). Although his model has been supplanted by quantum mechanics, Maeda *et al.* show on page 1757 of this issue (1) that it is possible to make Rutherford atoms in the laboratory.

Doubts about the Rutherford model were raised soon after he proposed it. The emission spectrum of hydrogen was known to have a regular progression of lines, and Johannes Rydberg had shown in 1888 that these lines could be fit to a simple algebraic formula. The Rutherford model could not explain this behavior.

In 1913, Niels Bohr postulated that the angular momentum of the electrons must be quantized. This quantization led to discrete orbits (see the first figure, panel B), which were labeled by an integer quantum number

and explained Rydberg’s formula. When Bohr’s model was supplanted by quantum mechanics as we know it today, the concept of the electron as a planet was replaced by a mathematical wave function that was not directly observable. The electron orbits became fuzzy clouds (see the first figure, panel C).

**Evolution of the concept of atomic structure.** (A) In the Rutherford model, an electron orbits a massive nucleus in a planetary orbit. (B) In the Bohr model, the electron is partly a wave that can only go in discrete orbits. (C) In the quantum mechanical picture, the electron is spread out within an orbital. (D) In the Rydberg atom, the electron is localized into a small volume and follows an almost classical orbit, as demonstrated by Maeda *et al.* (1).



Quantum mechanics has been highly successful in predicting the structure of atoms and molecules, giving birth to notions such as quantum teleportation and quantum computing. It is so precise that experiments have been proposed to look for tiny changes in the fundamental constants as the universe ages over a period of years (2). Yet we know that objects in the macroscopic world that

we inhabit are not fuzzy clouds. Electrons are real particles that travel through wires and form images on television screens. So where does the quantum world end and our everyday classical world begin?

This question is being addressed by scientists who try to construct atoms that resemble classical objects. Maeda *et al.* (1) show that this approach can yield atoms that behave like Rutherford’s miniature solar system.

To make a Rutherford atom, one must first localize the electron cloud, that is, confine it to a small volume. In quantum mechanics, this is achieved by creating a coherent superposition of states, called a wave packet (see the second figure). For example, a femtosecond laser pulse is a superposition of many sine waves that add constructively only in

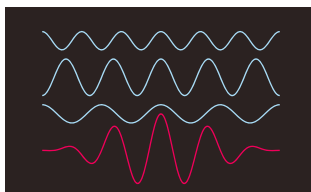
The author is with the National Research Council of Canada, 100 Sussex Drive, Ottawa, Ontario, Canada K1A 0R6. E-mail: david.villeneuve@nrc.ca

the middle of the pulse.

To make their Rutherford atom, Maeda *et al.* (1) exploit the fact that the highly excited states of the hydrogen atom, called Rydberg states (see the first figure, panel D) (3), provide a range of quantum states whose energy spacing is almost uniform, as the notes on a piano are almost

uniformly spaced in frequency. When many of these states are added together, the resulting electron wave function briefly becomes localized. However, the energy spacing of the Rydberg atom is not perfectly uniform, and the wave packet quickly begins to fall apart because of dispersion (the same process that spreads white light into a rainbow).

Highly excited Rydberg atoms are tenuous things. Even blackbody radiation from the walls of the vacuum chamber, or the electric field from a flashlight battery, can knock the electron out of its orbit. Such atoms can be tens of nanometers in size, approaching



**Localizing an electron.** A localized wave packet forms via a coherent superposition of states; the red wave packet is the sum of the three blue sine waves.

the size of features on silicon chips. Their orbital periods are slower than those of unexcited atoms by six orders of magnitude.

Rydberg atoms are thus sufficiently big and slow that the time scale of the electron motion is slowed from optical to microwave frequencies. They provide a test bed to learn about the murky

boundary between quantum mechanics and the macroscopic world.

Maeda *et al.* create their Rydberg atoms from a beam of lithium atoms. They use a series of laser pulses to excite the atoms to successively higher energy levels. The authors demonstrate that a linearly polarized microwave field can counteract the dispersion and can hold the wave packet together for thousands of orbits around the nucleus, just as a sheepdog keeps a herd of sheep together. They can speed up the wave packet's orbit or slow it down by sweeping the microwave frequency up or down. They can

even knock the electron wave packet out of the atom by applying a brief electric pulse at just the right moment.

Rydberg atoms are like a quantum playground. They allow single photons to be non-destructively detected (4) and can encode information as qubits for quantum computing (5). But Rydberg atoms may also have more practical applications. A gas of Rydberg atoms can spontaneously ionize and form an ultracold plasma (6). And techniques learned from experiments like those reported by Maeda *et al.* may lead to methods for cooling antimatter atoms (7).

#### References

1. H. Maeda, D. V. L. Norum, T. F. Gallagher, *Science* **307**, 1757 (2005); published online 10 February 2005 (10.1126/science.1108470).
2. M. Fischer *et al.*, *Phys. Rev. Lett.* **92**, 230802 (2004)
3. T. F. Gallagher, *Rydberg Atoms* (Cambridge Univ. Press, Cambridge, 1994).
4. G. Nogues *et al.*, *Nature* **400**, 239 (1999).
5. J. Ahn *et al.*, *Phys. Rev. Lett.* **86**, 1179 (2001).
6. M. P. Robinson *et al.*, *Phys. Rev. Lett.* **85**, 4466 (2000).
7. G. Gabrielse *et al.*, *Phys. Rev. Lett.* **89**, 213401 (2002).

10.1126/science.1110367

## CELL BIOLOGY

# Ras on the Roundabout

Doris Meder and Kai Simons

**P**roliferation and differentiation are the cell's most fundamental responses to extracellular stimuli. The two outcomes are poles apart: Proliferating cells divide into more of the same kind, whereas differentiating cells undergo profound changes in shape, subcellular organization, and metabolic activity that are often accompanied by a block in proliferation. Yet they can be initiated by the same key regulators and with identical effector molecules. The differential signaling output is fundamentally dependent on the spatial organization of the signaling molecules and their regulators within the cell. How signaling molecules are targeted to different cellular compartments is an important but poorly understood challenge for the cell. On page 1746 of this issue, Rocks *et al.* shed light on this challenge with their report that Ras signaling molecules modified by addition of palmitoyl groups (palmitoylation) continuously cycle between the plasma membrane and the Golgi complex (1).

The major signaling cascade for cell proliferation and differentiation is the

mitogen-activated protein kinase (MAPK) cascade, which receives stimuli from growth factors and hormones that are transmitted to the cell through tyrosine kinase receptors. The key regulator of this pathway is the guanosine triphosphatase (GTPase) Ras. Mutations in Ras occur in human cancers, and oncogenic Ras isoforms transform cultured cells. Mammals have three different Ras genes that give rise to four highly homologous proteins differing only in the carboxyl terminus that anchors them to cellular membranes. All Ras isoforms are modified with a farnesyl group (farnesylation). In addition, N-Ras is acylated with one palmitoyl group and H-Ras with two, whereas K-Ras4B contains a polybasic stretch of amino acids in its carboxyl terminus (its splice variant K-Ras4A carries a single palmitoyl group like N-Ras). Despite their identical effector binding domains, the different signaling pathways regulated by Ras isoforms have been attributed to differences in subcellular localization. K-Ras4B is confined to the plasma membrane, whereas H-Ras and N-Ras have also been detected in the Golgi. Originally, Ras signaling was believed to occur exclusively at the plasma membrane, but recent data suggest that the Golgi serves as an additional signaling

platform (2). How the different Ras signaling pathways are segregated in different cellular compartments remains unclear.

Rocks *et al.* focused their investigation on the two Ras isoforms that are palmitoylated: H- and N-Ras. Fluorescently labeled H- and N-Ras expressed in cultured canine kidney cells were localized to the plasma membrane and to the Golgi membranes. After photobleaching of the Golgi area, fluorescence was regained by accumulation of unbleached molecules from other compartments. Similarly, when fluorescence was selectively activated in the plasma membrane, the Golgi also became labeled over time. The finding of retrograde flow from the plasma membrane to the Golgi is important, because Ras was previously believed to pass through the Golgi only on its way out to its final destination in the plasma membrane (3).

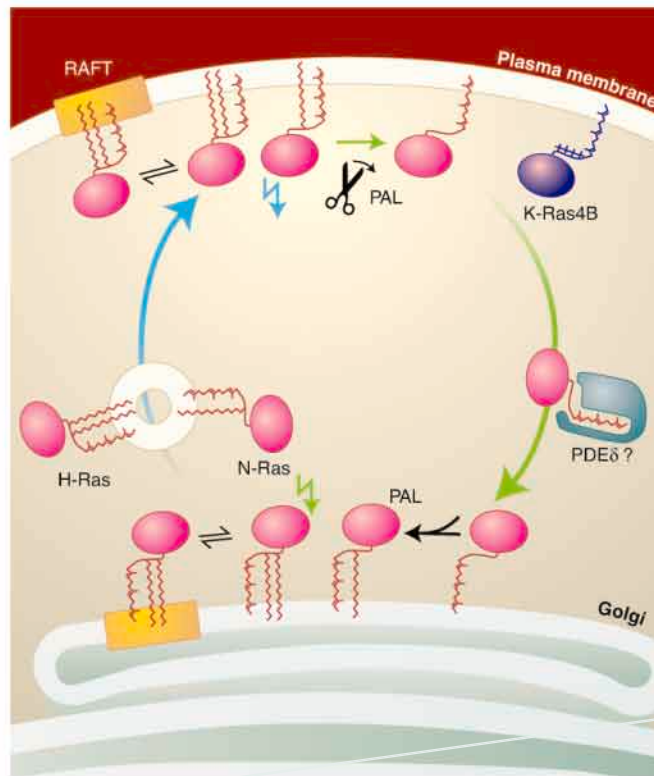
Interestingly, the recovery kinetics were faster for N-Ras carrying one palmitoyl group than for H-Ras carrying two, indicating the involvement of palmitoylation in this process. Indeed, inhibition of palmitoylation abolished Ras trafficking from the plasma membrane to the Golgi. Given that palmitoylation is a reversible form of protein modification, Rocks *et al.* tested whether depalmitoylation was also a prerequisite for exchange of Ras between the plasma membrane and Golgi. To this end, two fluorescently labeled N-Ras molecules were chemically synthesized, one in which the palmitate was attached by a cleavable thioester bond and the other in which the

The authors are at the Max Planck Institute of Molecular Cell Biology and Genetics, 01307 Dresden, Germany. E-mail: meder@mpi-cbg.de, simons@mpi-cbg.de



thioether bond could not be cleaved. When these two proteins were microinjected into canine kidney cells, the first one behaved like wild-type N-Ras and cycled between the plasma membrane and Golgi. In contrast, the depalmitoylation-defective variant was randomly distributed to all cellular membranes and did not display movement between the plasma membrane and Golgi. The authors therefore argue that it is the depalmitoylation-repalmitoylation cycle that defines the specific distribution of Ras between the plasma membrane and Golgi. Ras is depalmitoylated at the plasma membrane and subsequently “falls out” of the plasma membrane into the cytosol. Then it becomes randomly inserted into the membranes of cellular organelles and finds itself kinetically trapped in the Golgi, where it is repalmitoylated and thus again becomes stably anchored to the membrane. Although palmitoylated Ras joins the vesicular secretory pathway from the Golgi to the plasma membrane, retrograde transport in the opposite direction is probably not vesicular. It is unclear whether farnesylated Ras diffuses freely in the cytosol, or whether it is bound to a chaperone (as is the case for Rab and Rho GTPases). A possible chaperone candidate is PDE $\delta$ , a structural homolog of Rho-GDI (guanine nucleotide dissociation inhibitor), which binds to the carboxyl terminus of H-Ras in vitro and in vivo (4).

The depalmitoylation-repalmitoylation cycle is not a unique feature of H- and N-Ras; it also operates for other palmitoylated proteins such as GTPase activating protein GAP-43, heterotrimeric GTP-binding protein subunit G $\alpha_{i1}$ , and endothelial nitric oxide synthase. Current research is investigating whether this cycle is linked to Ras activation and signaling. Earlier studies showed that upon stimulation with epidermal growth factor (EGF), Ras is initially activated at the plasma membrane, but that this activation is transient and is usually followed by a more sustained activation of Ras in the Golgi (2). Ras activation is typically detected with the fluorescently tagged molecule RafRBD (the Ras binding domain of the downstream target Raf), which binds only to the GTP-loaded



**A cellular compartment of one's own.** The largely homologous Ras proteins H-, N-, and K-Ras regulate distinct signaling pathways. These proteins are able to regulate separate signaling pathways because they inhabit different compartments within the cell. Whereas K-Ras4B is exclusively available for signaling at the plasma membrane, N-Ras and H-Ras cycle between the plasma membrane and Golgi depending on whether they carry a palmitoyl group or not. An increased rate of depalmitoylation leads to accumulation of N- and H-Ras in the Golgi, whereas increased palmitoylation leads to their accumulation at the plasma membrane. Palmitoylated Ras isoforms are incorporated into secretory vesicles for anterograde transport from the Golgi to the plasma membrane. Because depalmitoylation correlates with detachment from the plasma membrane, retrograde transport from the plasma membrane to the Golgi is nonvesicular and possibly involves a farnesyl-binding chaperone such as PDE $\delta$ . A second level of spatial organization comes from the subcompartmentalization of the Golgi membranes and plasma membrane into different domains separated by lipid rafts (orange). Doubly palmitoylated H-Ras has an affinity for lipid rafts that is modulated according to its activation state.

active form of Ras but does not discriminate between the different Ras isoforms. To assess H-Ras and N-Ras activation separately, Rocks *et al.* used fluorescence lifetime imaging as a measure of fluorescence resonance energy transfer between H- or N-Ras tagged with cyan fluorescent protein and RafRBD tagged with yellow fluorescent protein. Activated H-Ras was first detected at the plasma membrane and appeared at the Golgi only after a 15-min delay, whereas activated N-Ras was observed at the Golgi immediately after activation at the cell surface. The kinetics of Ras activation thus mimic the kinetics of the plasma membrane–Golgi cycle and suggest that, in this case, Ras is loaded with GTP at the plasma membrane and then is trans-

ported to the Golgi in its activated form. However, the cycle seems to operate independently of the activation state of Ras, so that GTP loading could also occur in the Golgi.

The subcellular site of Ras activation is determined by the localization of specific guanine nucleotide exchange factors (GEFs) and GAPs. In T lymphocytes, low-grade stimulation of the T cell receptor activates an alternative signaling pathway that acts simultaneously on a Golgi-resident Ras-GEF and a plasma membrane-resident Ras-GAP and thus leads to activation of N-Ras exclusively in the Golgi (5). To keep activated Ras in the Golgi for sustained signaling, scaffolds that bind to the activated protein and keep it in place are most likely needed. Such effector-mediated stabilization in the membrane has been described for Rab GTPases (6). Recently, the first Golgi-resident Ras effector (7) and a Golgi-associated MAPK scaffold (8) were identified. Nonetheless, the function of the palmitoylation cycle might go beyond targeting Ras to different cellular compartments and may provide a way to tune Ras signaling. Depalmitoylation ensures removal of Ras-GTP from the plasma membrane, leading to transient plasma membrane signaling, as others have reported (2). Furthermore, changing the rates of palmitoylation or depalmitoylation would shift Ras either to the Golgi or to the plasma membrane and thus prime the signaling cascade with a high number of Ras molecules in the location where activation is needed.

The palmitoylation cycle provides a way to allocate Ras signaling pathways to different subcellular compartments. A second level of subcompartmentalization comes from the possible partitioning of Ras isoforms into different membrane domains. Such dynamic assemblies could vary in their concentration of activated tyrosine kinase receptors or downstream effectors and targets, and consequently could mediate distinct signaling outputs. Two principal Ras activators have affinities for membrane lipid rafts, ordered assemblies composed of sphingolipids with saturated, long-chain fatty acids and cholesterol that are dynamically segregated from the bulk of the membrane due to the immiscibility of their lipids with those of the rest of the membrane (see

the figure). T cell receptors activate their signaling pathways from lipid rafts (9), and signaling by EGF receptors is differentially regulated by raft lipids. The ganglioside  $G_{M3}$  inhibits EGF receptor autophosphorylation by binding to its extracellular domain, but administration of another ganglioside ( $G_{D1a}$ ) enhances EGF-mediated signaling by increasing dimerization of EGF receptors, thus priming them for binding to EGF (10).

Of the four Ras isoforms, only H-Ras with its two palmitoyl chains has a definite affinity for lipid rafts, depending on its activation state. The current interpretation is that H-Ras is in dynamic equilibrium between at least two types of small (10 to 15 nm) membrane domains. One domain is formed by lipid-lipid interactions and is cholesterol dependent, whereas the other is stabilized mostly by protein-protein interactions and is cholesterol independent. H-Ras is thought to be shifted from the former to the latter when loaded with GTP (11). The assemblies formed by GTP-loaded H-Ras are dependent on galectin-1, a cytosolic protein that binds to galactose moieties as well as to H-Ras and plays a crucial part in Ras signaling (12). Another admittedly speculative view is that galectin-1 organizes GTP-loaded H-Ras into cholesterol-independent raft nanoclusters from which signals are relayed. But the question is how. It is possible that galactosylceramide when flipped to the cytosolic lipid leaflet could serve as a raft anchor for galectin-1.

The importance of membrane domains in Ras signaling is obviously an open issue. The question raised here is whether transiently specialized raft assemblies could form through protein-lipid and protein-protein interactions that do not result in the accumulation of other raft markers. Their formation would not be restricted to the plasma membrane but could take place equally in Golgi membranes, which contain all of the components needed for raft assembly. The rapid time scale of the interaction between Ras and Raf (11), followed by depalmitoylation and dissociation from the membrane, will further complicate the analysis of these nanoscale Ras signaling platforms.

Ras proteins have been identified and characterized and their posttranslational modifications established for more than 25 years. With more than 25,000 PubMed entries, Ras proteins are probably the most extensively studied signaling molecules ever. Nonetheless, the individual roles of the different isoforms in cell proliferation, differentiation, and oncogenic transformation are still not understood, nor are the signaling outputs of their specific effector pathways. Unfortunately, good tools for selectively

assessing the function of a single Ras isoform without resorting to overexpression experiments are still missing. Thus, the spatiotemporal analysis of endogenous Ras signaling remains a big challenge for the future. Why is Ras signaling localized to the Golgi? One advantage of the Golgi is its close proximity to the nucleus, the ultimate destination for activated MAPK. Computer modeling of the MAPK signaling cascade predicts a strong attenuation of the phosphorylation signal from the plasma membrane toward the nucleus (13). Signaling from the Golgi would bring the process closer to the target site and therefore would be especially suited for transcriptional regulation.

The paper by Rocks *et al.* is an important piece in the Ras puzzle but it is also of much more general value, because it describes a targeting mechanism that has not received much attention by researchers in the protein sorting field. It could well be that there are many more proteins that are sorted by reversible

posttranslational modifications and that cycle between different cellular sites. On the roundabouts as well as at the exits, there are probably more surprises to come.

#### References

1. O. Rocks *et al.*, *Science* **307**, 1746 (2005); published online 10 February 2005 (10.1126/science.1105654).
2. V. K. Chiu *et al.*, *Nature Cell Biol.* **4**, 343 (2002).
3. A. Apolloni, I. A. Prior, M. Lindsay, R. G. Parton, J. F. Hancock, *Mol. Cell Biol.* **20**, 2475 (2000).
4. V. Nancy, I. Callebaut, A. El Marjou, J. de Gunzburg, *J. Biol. Chem.* **277**, 15076 (2002).
5. I. Perez de Castro, T. G. Bivona, M. R. Philips, A. Pellicer, *Mol. Cell Biol.* **24**, 3485 (2004).
6. M. Zerial, H. McBride, *Nature Rev. Mol. Cell Biol.* **2**, 107 (2001).
7. N. Y. Mitin *et al.*, *J. Biol. Chem.* **279**, 22353 (2004).
8. S. Torii, M. Kusakabe, T. Yamamoto, M. Maekawa, E. Nishida, *Dev. Cell* **7**, 33 (2004).
9. P. W. Janes, S. C. Ley, A. I. Magee, *J. Cell Biol.* **147**, 447 (1999).
10. Y. Liu, R. Li, S. Ladisch, *J. Biol. Chem.* **279**, 36481 (2004).
11. J. F. Hancock, R. G. Parton, *Biochem. J.*, in press
12. B. Rotblat *et al.*, *Cancer Res.* **64**, 3112 (2004).
13. B. N. Kholodenko, *Trends Cell Biol.* **12**, 173 (2002).

10.1126/science.11116551

#### APPLIED PHYSICS

## Toward Quantum-Information Processing with Photons

Ian A. Walmsley and Michael G. Raymer

The emerging field of quantum technology uses individual atoms, molecules, and photons to construct new kinds of devices. Quantum objects are not limited to the binary rules of conventional computing, but can be in two or more logical states at once. When a group of objects collectively occupy two or more states at once, they are said to be entangled. Photons interact very weakly with their environment, and therefore entangled states of photons hold considerable promise for applications ranging from imaging and precision measurement to communications and computation.

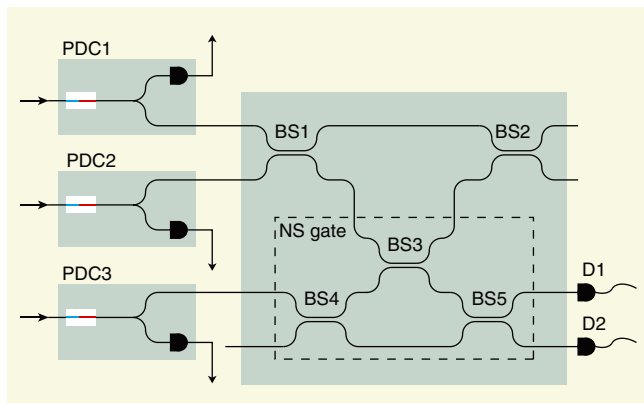
In every quantum-information processing scheme, bits of information must be stored in the states of a set of physical objects, and there must be a physical means to effect an interaction between these quantum bits (qubits). But when one tries to use individual photons to store and process information, a problem arises: Photons interact extremely weakly or not at all, and it might thus seem unlikely that they can be used directly for quantum-information processing.

Remarkably, a scheme for effective quantum interactions between photons has been invented that does not require the photons to interact physically. When a group of photons are in an entangled state, the measurement of one or more of these photons' states causes the state of the remaining photons to "collapse." Such a state collapse can be viewed as an effective interaction between the remaining photons (1). The nature of the interaction depends on the outcomes of the measurement on each observed (ancilla) photon. The occurrence of certain predetermined outcomes of the ancilla measurements signals (heralds) the effective interaction of the remaining photons.

This approach can be used to implement "heralded" quantum logic gates in a scheme called linear-optical quantum computing (see the first figure). Substantial progress toward linear-optical quantum computing has been made, such as the design (2) and demonstration (3) of a teleportation gate and of a controlled-not (C-NOT) logic gate (4), and the preparation of entangled states of two photons (5). But serious challenges remain.

When using photons as qubits to encode information, each photon must be created in one of two distinct quantum states or in a superposition of these two states. If the photons occupy more states in an uncontrolled

I. A. Walmsley is at the Clarendon Laboratory, University of Oxford, Oxford OX1 3PU, UK. E-mail: walmsley@physics.ox.ac.uk M. G. Raymer is with the Department of Physics and Oregon Center for Optics, University of Oregon, Eugene, OR 97403, USA. E-mail: raymer@uoregon.edu



**Quantum computing based on single-photon wave packets.** Three heralded sources of pure state photons (PDC1 to PDC3, left) feed into a cascade of beam splitters (BS1 to BS5), where they interfere. The three beam splitters in the dashed box implement a linear-optical quantum conditional sign-shift gate (NS gate), an element of the quantum C-NOT gate. The phase difference between the paths linking BS1 and BS2 is shifted conditionally upon detection of a photon at D1 and no photon at D2.

way, the scheme for effecting interactions among photons described above will fail. The quantum states of a photon are characterized by their spectrum, pulse shape, time of arrival, transverse wave vector, and position. All of these variables must be controlled precisely to ensure that only two distinct quantum states are present.

The linear-optical quantum-computing scheme relies on two-photon interference. When two photons are incident from opposite sides of a beam splitter (see the second figure), the quantum nature of photons leads to a counterintuitive effect, named after Hong, Ou, and Mandel (6). If photons behaved as classical particles, they should both exit the same port, either the upper or the lower (see the second figure, top panel), 50% of the time, and at opposite ports the other 50%. The latter event, in which both detectors should fire together, can occur in two ways: Either both photons are reflected, or both are transmitted (see the second figure, bottom panel). For identical photons, these two events cancel each other out, and the two detectors never fire together. Such a cancellation cannot occur for classical particles.

For linear-optical quantum logic devices to operate properly, the input photons must not carry any distinguishing information and must not be in a statistical mixture of states of different character. What is needed is a source that creates photons in controlled, “pure” quantum states, such that each photon has the same temporal and spatial shape.

The main strategy to create such pure photons is to structure (“engineer”) the quantum vacuum, that is, to reduce the number of possible ways in which a newly created photon can fill a previously empty space. This notion is the basis of several

recent experiments that use single atoms in cavities to build a single-photon source (7, 8). When an atom is confined in a high-quality optical cavity, it emits photons with well-defined frequency and spatiotemporal extent. Cavity-controlled photon emission has also been accomplished with solid-state sources, and the Hong-Ou-Mandel effect has been observed with these (9). In principle, these sources should be able to create photons “on demand”—that is, a single, pure photon should be available at the

push of a button—but much practical development remains to be done for this to be the case.

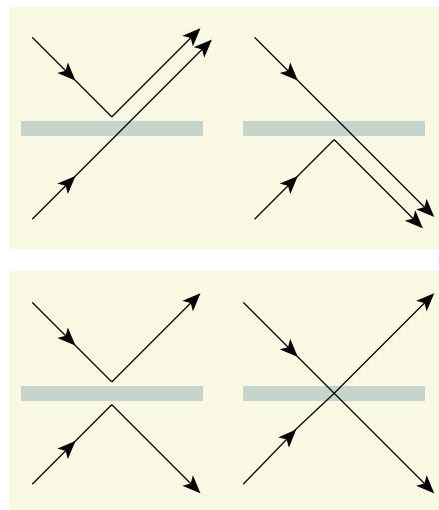
Single photons can also be generated by “photon splitting.” In this process, a single (say, blue) pump photon may split at random into a pair of (red) daughter photons traveling in different directions, or beams. The detection of one photon then heralds the imminent arrival of the second photon. Such “twin” beams may be generated in certain nonlinear optical crystals by a process called “parametric downconversion.” The spatial and temporal correlations of the photons in each pair are determined by the characteristics of the pump beam and

by the internal structure of the nonlinear crystal. Unfortunately, in most practical situations, the resulting photon pairs are entangled, so that detection of the herald photon leaves the other photon in a statistically random (rather than a pure) state. Because the photons are not pure, they will not interfere at a beam splitter (10).

Vacuum engineering can be used to improve the control of the downconversion process. By placing the nonlinear crystal or other medium in a low-loss optical cavity, analogous to putting an atom in a cavity, the frequency of the emitted photons can be controlled (11). A good configuration for producing pure photons is a medium with a periodically structured linear refractive index, which creates an optical cavity that is shorter than the medium itself (12).

An alternative method, which works without a cavity, is to structure the nonlinear properties of the medium in a periodic pattern. With this method, called quasi-phase matching, nonentangled photon pairs can be generated (13). The measurement of one of the twins then yields information only about the presence of the other, not about any other property. The photon thus prepared is pure and suitable for linear-optical quantum computing.

Micropatterned structures for photon downconversion can be fabricated in an optical waveguide that is compatible with optical-fiber systems and that can be scaled up, allowing large numbers of identical photons to be created in a compact device. These and other approaches for creating clean, pure photons are at the forefront of quantum optics research and will lead to new quantum technologies, many of which are yet to be envisioned.



**Photons at a beam splitter. (Top)** Two processes lead to both photons exiting the same port. These never cancel each other out, and the photons therefore bunch together at the output. **(Bottom)** Two processes lead to one photon exiting each of the upper and lower ports. In the case of identical photons, these processes cancel one another out.

## References

1. E. Knill, R. Laflamme, G. J. Milburn, *Nature* **409**, 46 (2001).
2. T. B. Pittman, M. J. Fitch, B. C. Jacobs, J. D. Franson, *Phys. Rev. A* **68**, 032316 (2003).
3. S. Gasparoni, J.-W. Pan; P. Walther, T. Rudolph, A. Zeilinger, *Phys. Rev. Lett.* **93**, 020504 (2004).
4. J. L. O’Brien, G. J. Pryde, A. G. White, T. C. Ralph, *Nature* **426**, 264 (2003).
5. P. G. Kwiat, E. Waks, A. G. White, I. Appelbaum, *Phys. Rev. A* **60**, R773 (1999).
6. C. K. Hong, Z. Y. Ou, L. Mandel, *Phys. Rev. Lett.* **59**, 2044 (1987).
7. A. Kuhn M. Hennrich, G. Rempe, *Phys. Rev. Lett.* **89**, 067901 (2002).
8. J. McKeever *et al.*, *Science* **303**, 1992 (2004).
9. C. Santori, D. Fattal, J. Vukovi, G. S. Solomon, Y. Yamamoto, *Nature* **419**, 594 (2002).
10. W. P. Grice, A. B. U’Ren, I. A. Walmsley, *Phys. Rev. A* **64**, 063815 (2001).
11. Z. Y. Ou, Y. J. Lu, *Phys. Rev. Lett.* **83**, 2556 (1999).
12. M. G. Raymer, B. Smith, J. Noh, I. A. Walmsley, K. Banaszek, Paper WF3 in *Frontiers in Optics/Laser Science XIX Conference*, 5 to 9 October 2003, Tucson, AZ (Optical Society of America, Washington, DC, 2003).
13. A. B. U’Ren, K. Banaszek, I. A. Walmsley, *Quant. Inf. Comput.* **3**, 480 (2003).

10.1126/science.1107451

# The Molecular Requirements for Cytokinesis

Michael Glotzer

After anaphase onset, animal cells build an actomyosin contractile ring that constricts the plasma membrane to generate two daughter cells connected by a cytoplasmic bridge. The bridge is ultimately severed to complete cytokinesis. Myriad techniques have been used to identify proteins that participate in cytokinesis in vertebrates, insects, and nematodes. A conserved core of about 20 proteins are individually involved with cytokinesis in most animal cells. These components are found in the contractile ring, on the central spindle, within the RhoA pathway, and on vesicles that expand the membrane and sever the bridge. Cytokinesis involves additional proteins, but they, or their requirement in cytokinesis, are not conserved among animal cells.

Cell multiplication involves cell growth and an ordered sequence of events: replication of the genome, chromosome segregation, and cell division. Although many aspects of cell growth, cell cycle regulation, and chromosome replication and segregation are understood at the molecular and, increasingly, the atomic level, cell division, also called cytokinesis, is less well understood. However, a molecular outline is emerging. Animal cells use a contractile ring that is attached to the plasma membrane to create a cleavage furrow that partitions the cell into two lobes (Fig. 1A). The contractile ring is a network of actin and myosin filaments, and the motor activity of myosin translocates actin filaments to drive its constriction. Contractile ring assembly is directed by the RhoA guanosine triphosphatase (GTPase), which induces actin nucleation and activates myosin. The contractile ring assembles in a position dictated by the position of the anaphase spindle, perhaps through local regulation of RhoA activity. The contractile ring and the central spindle probably sterically hinder simple fission of the plasma membrane. Instead, vesicle insertion appears to be necessary ultimately to achieve division of the plasma membrane.

Here, I introduce the core protein machines that are important for animal cell cytokinesis in divergent animal species (e.g., vertebrates, nematodes, and insects). The well-characterized machines that regulate cytokinesis fall into five broad categories (Fig. 1B): (i) components of the central spindle, (ii) RhoA and its regulators and direct effectors, (iii) nonmuscle myosin II, (iv) actin and direct regulators of its assembly into filaments, and (v) factors required

for trafficking and fusion of membrane vesicles. As might be expected for a process that requires the coordinated action of microtubules, actomyosin, and membrane fusion, some proteins required for cytokinesis fall into more than one category. Some, but not all, of these machines also regulate cytokinesis in fungi and *Dictyostelium*.

## The Cytokinetic Machinery

*The central spindle: a set of microtubule-based machines.* Anaphase onset marks the beginning of cytokinesis. The proteolytic destruction of cyclins inactivates mitotic kinases and permits dephosphorylation and activation of several proteins that are critical for assembly of the central spindle, a set of antiparallel microtubules that become bundled between the separating chromosomes during anaphase and serve to concentrate key regulators of cytokinesis (Fig. 2). The components of the central spindle have acquired a bewildering nomenclature that is summarized in Fig. 2. One of these proteins, PRC1, is a microtubule-associated protein (MAP) with microtubule-bundling activity. PRC1 localizes primarily to the central spindle and is required for central spindle organization and cytokinesis in most animal cells (1–3). The kinesin-4 family member, KIF4, interacts with PRC1 and restricts the localization of PRC1 to a narrow region in the center of the anaphase spindle (4). During metaphase, PRC1 is inhibited from binding to microtubules by phosphorylation on Cdk1 sites (1). Cdk1/cyclin B also inhibits microtubule bundling by the centralspindlin complex, which consists of the kinesin-6 family member MKLP1 and the Rho family GTPase activating protein (GAP), CYK-4 (5). During anaphase, centralspindlin becomes highly concentrated in the central spindle, apparently where microtubule plus ends overlap (6–8). Central spindle assembly requires complex

formation between MKLP1 and CYK-4, and the MKLP1/CYK-4 complex but not the individual subunits has microtubule bundling activity in vitro (6).

Localization of centralspindlin depends on another complex that concentrates on the central spindle, the aurora B kinase complex (9, 10). Aurora B function requires interactions with incenp, survivin, and a poorly conserved subunit, CSC-1 (11–16). Inhibition of aurora B kinase activity results in cytokinesis defects that are similar to those caused by depletion of MKLP1. Centralspindlin localization may not be the sole function of aurora B. A combination of the strong phenotype caused by defects in central spindle assembly and the existence of parallel pathways for furrow formation may obscure an early, central spindle-independent role for aurora B. The relevant substrates of aurora B remain to be identified, although aurora B can phosphorylate CYK-4 in vitro and this phosphorylation may indirectly affect its GTPase activation function (17).

Numerous proteins become concentrated on the central spindle during anaphase and telophase. These include proteins, such as NuSAP (nucleolar spindle-associated protein), orbit, and the tumor suppressor BRCA2, that affect the organization of the central spindle and/or progression of cytokinesis (18–20). Currently, it is not clear whether these are core components that are required for cytokinesis in diverse species.

Activation of central spindle assembly in early anaphase has implications for formation of the contractile ring. In *Drosophila*, for example, cells lacking the MKLP1 subunit of centralspindlin do not form a contractile ring (21). This phenotype may reflect interactions of components of centralspindlin with factors that regulate RhoA activation. However, depletion of the orthologous protein in *Caenorhabditis elegans* or human cells does not prevent furrow formation; in *C. elegans*, this difference is caused by a redundant pathway for furrow formation (22).

*The RhoA pathway: the key switch for cytokinesis.* A central player in contractile ring assembly is the RhoA GTPase module (Fig. 3). RhoA, like most ras-related GTPases, is regulated by factors that promote nucleotide exchange [guanine nucleotide exchange factors (GEFs)] and nucleotide hydrolysis (GAPs). There appears to be one critical GEF for RhoA in cytokinesis, known as ECT2 (23, 24).

Research Institute of Molecular Pathology, Dr. Bohr-Gasse 7, A-1030 Vienna, Austria. E-mail: mglotzer@imp.univie.ac.at

Depletion of ECT2 blocks furrow formation as does depletion of RhoA, although in vitro this GEF is not RhoA specific (22, 23). The identity of the GAP for RhoA in cytokinesis is not completely clear. CYK-4 is an attractive candidate, because it is localized to the midbody at a late stage in cytokinesis, a site where inactivation of RhoA could be required for the final steps of cytokinesis (25). However, genetic evidence suggests that CYK-4 regulates Rac proteins (26). Perhaps CYK-4 regulates both GTPases; indeed, it has GAP activity for RhoA, Rac, and Cdc42 in vitro (25). Interestingly, an interaction has been detected between the *Drosophila* orthologs of the GEF and the putative GAP for RhoA, namely ECT2/Pebble and CYK-4/RacGAP50C (8). Localization of this RhoGEF may direct local RhoA activation to sites in the cell cortex adjacent to the central spindle (8). This complex is reminiscent of the breakpoint cluster region protein in that it contains both RhoGAP and RhoGEF domains. Localization of ECT2 to the central spindle may not be essential to activate RhoA, because RhoA

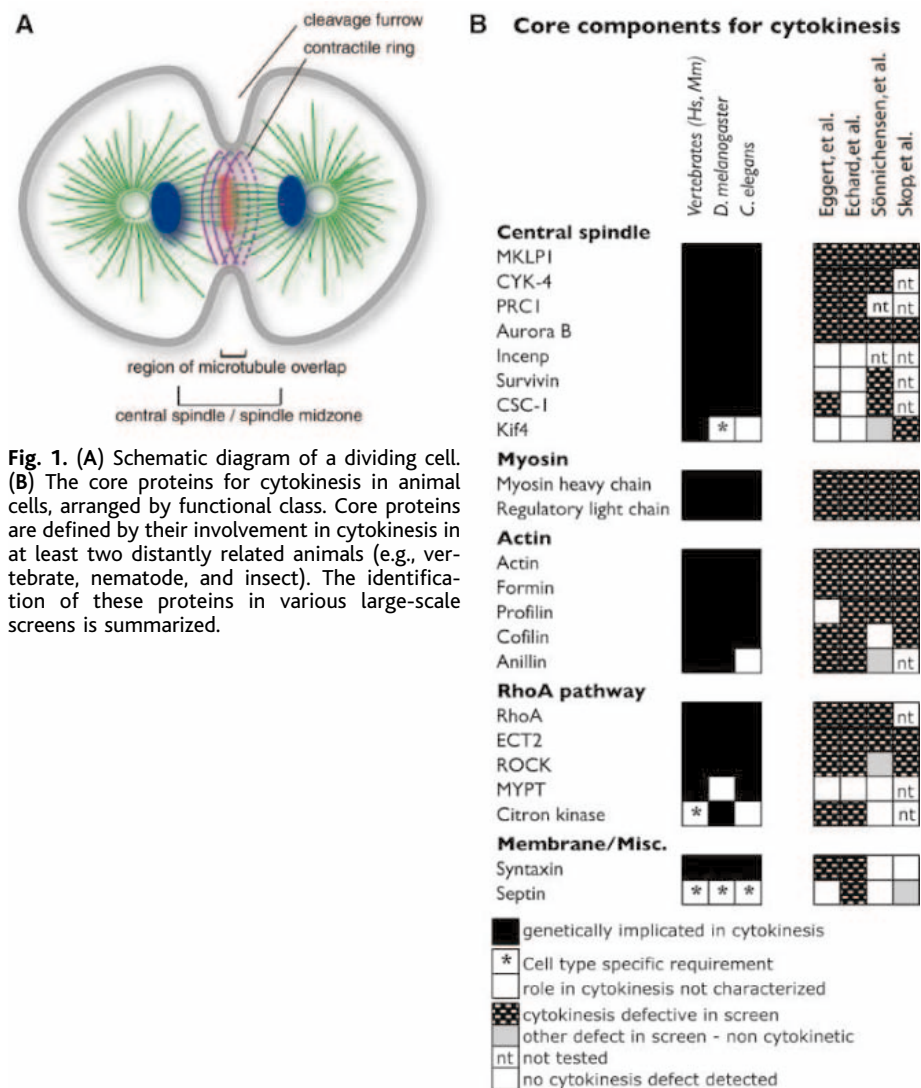
activation apparently occurs in cells depleted of MKLP1 (27–29). Nevertheless, central spindle localization of ECT2 activity could contribute to RhoA activation.

**Myosin: the engine of cytokinesis.** RhoA•GTP activates downstream pathways that lead to actin polymerization and myosin II activation. Nonmuscle myosin II is one of the central machines in cytokinesis, because its activity is required for furrow formation (30–32). This motor consists of a parallel dimer of heavy chains, each bound to an essential light chain and a regulatory light chain (rMlc). These hexamers assemble into filaments that translocate actin filaments and drive constriction of the contractile ring. In animal cells, nonmuscle myosin II is regulated by phosphorylation of the rMlc, which binds between the motor domain and the coiled coil. Phosphorylation of rMlc releases myosin II from an auto-inhibited state, allowing it to assemble into filaments and activating its actin-stimulated adenosine triphosphatase (ATPase) activity (Fig. 3). Phosphorylation of rMlc appears to be critical for

cytokinesis, because a phosphomimetic allele of rMlc can substantially substitute for rMlc in *Drosophila*, whereas a nonphosphorylatable rMlc results in severe cytokinesis defects (33). RhoA regulates the phosphorylation state of rMlc by several mechanisms. RhoA activates Rho kinase (ROCK), which phosphorylates rMlc (34) and regulates cytokinesis (35, 36). In addition, ROCK phosphorylates myosin phosphatase-targeting (MYPT) subunit, thereby inhibiting myosin phosphatase and indirectly promoting rMlc phosphorylation (37). Genetic interactions indicate that rMlc is one of the most important substrates for ROCK (38). However, several additional kinases phosphorylate rMlc, including the RhoA-activated citron kinase (39). However, citron kinase-depleted cells progress to a later stage of cytokinesis than would be expected if it were a major rMlc kinase (39–41).

**Actin assembly: the formin-profilin machine.** The mechanochemical activity of myosin is latent until it interacts with actin filaments, a second major constituent of the contractile ring. Actin filaments in the contractile ring often appear in parallel bundles, as opposed to the dendritic meshwork observed in the leading edge of a migrating cell. The organization of the filaments can be ascribed, at least in part, to the different nucleating complexes that generate these structures. The ARP2/3 complex generates branched filaments and is critical for cell migration but is only weakly involved in contractile ring assembly (42, 43). Rather, formins nucleate unbranched filaments and are essential for contractile ring assembly in animal cells (Fig. 3) (44–46). Formins cap the barbed end of the actin filament but allow filament growth (47–49). Together with profilin, the central region of formin, containing the conserved FH1 (profilin-binding) and FH2 (actin-binding) domains, induces ATP hydrolysis by actin and uses the released free energy to favor processive growth of actin filaments (50). In vivo, however, formin is autoinhibited because of intramolecular binding of the N and C termini. Active RhoA binds the N terminus and relieves this autoinhibition (51). Thus, spatially restricted RhoA activation could induce local activation of myosin activity and actin filament assembly.

Another actin-binding protein that is required for cytokinesis is the actin-severing protein cofilin/ADF (52, 53). In vitro, cofilin can antagonize filament growth by severing and destabilizing filaments as well as promote growth by increasing the number of elongation competent barbed ends. The net effect of cofilin activation depends on the concentration of actin monomers and other factors that regulate filament ends. In cytokinesis, it seems that the primary role of cofilin is to destabilize actin filaments, because in cofilin mutants the contractile ring



contains an overabundance of actin filaments at late stages of cytokinesis.

Lastly, another actin-binding protein, anillin, has been genetically implicated in cytokinesis. This multidomain protein is tightly localized to the cleavage furrow and interacts with myosin and septins, but its biochemical function in the context of cytokinesis is not fully defined (54). Anillin-depleted animal cells have late defects in cytokinesis; contractile ring formation and ingression are not abolished (36, 55, 56).

**The membrane fusion machinery.** The actomyosin system is not sufficient to fully execute cytokinesis. Ultimately, each daughter cell must be surrounded by an independent plasma membrane, and the contractile ring, being linked to the inner cytoplasmic face of the membrane, is not in an appropriate location to promote membrane fusion. The final step of cytokinesis, membrane fusion, requires delivery of membrane vesicles that bridge the space remaining after full ingression of the contractile ring (57). Membrane addition may also be required to provide the membrane surface necessary to surround the two daughter cells. The machinery involved in membrane insertion during cytokinesis includes syntaxins, syntaxin-associated proteins, coatomer complex members, rab family GTPases, and subunits of the exocyst complex (36, 57–59). Conventional kinesin may help to deliver membranes to the midbody region (60).

### Evolutionary Conservation of the Cytokinesis Machinery

In addition to animal cells, cytokinesis has been intensively studied in budding and fission yeast as well as in *Dictyostelium*. There are both similarities and differences in the genetic requirements for the major cytokinetic machines in eukaryotes [see (61) for more details].

Some of the components of the central spindle are widely conserved, whereas others appear to be specific for metazoans. For example, the microtubule-bundling protein PRC1 has a clear ortholog in budding yeast, *Ase1p*, and although it plays role in late mitotic events in budding yeast, it is not required for cytokinesis (62). Genes weakly related to PRC1 also exist in the *S. pombe* and *Dictyostelium* genomes, but their involvement

in cytokinesis have not yet been evaluated. A kinesin-6 exists in the *Dictyostelium* genome and it plays a role in cytokinesis (63), but it does not share all the sequence features characteristic of vertebrate MKLP1 and there is no protein clearly related to CYK-4 in the *Dictyostelium* genome. Neither budding nor fission yeast contain proteins that resemble MKLP1 or CYK-4. On the other hand, aurora B kinase and most of its associated subunits are widely conserved and are found in budding and fission yeast and *Dictyostelium*.

Although actomyosin contractile rings form in budding yeast, fission yeast, and *Dictyostelium*, they are not strictly essential in budding yeast nor in *Dictyostelium*. In both of these systems, redundant pathways mediate

driven division in suspension, but mutations in either of these genes synergize with myosin II mutations and either double mutant fails to divide on a surface. This may reflect a direct role in substrate-mediated division or an indirect one in maintaining the substrate contacts required for myosin-independent division. Two other important factors are the actin-bundling proteins cortexillin I and II, which are highly concentrated in the equatorial region (68). These related proteins regulate cytokinesis in a partially redundant fashion (69). Their concentration to the equatorial region is thought to locally modulate cortical tension, thereby promoting furrow ingression.

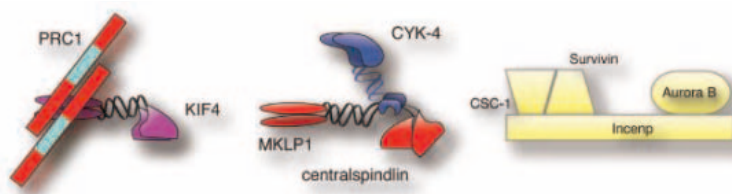
The Rho family of GTPases is ancient. It consists of three major branches—Rho, Rac,

Cdc42—and several members that do not fit into these major groupings. *Dictyostelium* has at least 15 Rho family members. Although none of these genes are closely related to RhoA or Cdc42, there are several Rac-related genes and a large number of outliers not highly related to RhoA, Rac1, or Cdc42. This latter class includes RacE, which is an important regulator of cytokinesis in this system (70). Both *S. pombe* and *S. cerevisiae* contain true Rho orthologs that participate in cytokinesis, primarily by regulating deposition of cell wall material. In addition, *S. pombe* contains the Spg1 GTPase, which is an extremely divergent member of the Ras superfamily and a critical regulator of cytokinesis, being necessary and sufficient for septum formation (71).

The effectors regulated by RhoA in animal cells are not universally required for cytokinesis in other eukaryotes.

Phosphorylation of rMlc is not essential in *S. pombe* or *Dictyostelium* (even in suspension growth) (72, 73). However, formins are essential for cytokinesis in budding and fission yeast, and in the former case they are known to be activated by Rho family GTPases, primarily Rho3p and Rho4p (74). The GAPs and GEFs that regulate cytokinesis in yeast, *Dictyostelium*, and animal cells do not appear to be orthologous.

The *S. pombe* ortholog of the actin-binding protein anillin, Mid1, controls division plane positioning in fission yeast. It is the first protein known to localize to the furrow in *S. pombe*, and mutants have severe ring-positioning defects (75, 76). Although anillin is an early marker of the division plane in



**Nomenclature of the central spindle**

	<i>H. sapiens</i>	<i>D. melanogaster</i>	<i>C. elegans</i>	ref.
<u>Microtubule Associated Protein</u>				
PRC1	PRC1	Fascetto	SPD-1	(1-4)
KIF4	KIF4	KLP3A	KLP-19	
<u>Centralspindlin complex</u>				
CYK-4	MgcRacGAP	RacGAP50C	CYK-4	(6-8)
MKLP1	MKLP1	Pavarotti	ZEN-4	
<u>Aurora kinase complex</u>				
Aurora B	Aurora B	Aurora B	AIR-2	(9-16)
Incenp	Incenp	Incenp	ICP-1	
Survivin	Survivin	Deterin	BIR-1	
CSC-1	Dasra/Borealin	Borealin	CSC-1	
<u>RhoGEF</u>				
ECT2	ECT2	Pebble	LET-21	(23, 24)

**Fig. 2.** Guide to the nomenclature of proteins that organize and concentrate on the central spindle. Also shown are schematic models for the molecular organization of a subset of these complexes: PRC1/KIF4, centralspindlin, and aurora B kinase.

cell division in the absence of myosin. For example, in budding yeast, there is a pathway that can build a septum sufficient to divide the cell in the absence of myosin II (64).

Myosin II is dispensable for cytokinesis in *Dictyostelium* cells cultured on a surface, although it is required for these cells to grow in suspension (65, 66). Remarkably, the division of myosin II-deficient *Dictyostelium* cells on a surface is morphologically similar to that of wild-type cells. If translocation of actin filaments by myosin II normally provides the force for furrow ingression, what substitutes in its absence? Two genes are proposed to act in a parallel, myosin-independent pathway, *amiA* and *coronin* (67). These genes are not required for myosin-

animal cells, anillin-depleted cells form furrows that fail to complete, indicating that anillin is not essential for division plane positioning in animal cells (36, 55, 56).

Some factors required for trafficking and fusion of membrane vesicles appear to have a conserved requirement for cytokinesis in both metazoans and unicellular eukaryotes. These include the exocyst complex and syntaxins (77). Whereas in metazoans microtubules and kinesins appear to play the primary delivery role for membrane deposition during cytokinesis (60), in yeast this function is primarily mediated by actin filaments and myosin (78).

Thus, a number of related molecules mediate cytokinesis in divergent eukaryotes. However, differences do exist, particularly in the regulatory mechanisms and the degree of reliance on particular pathways. Nevertheless, many insights obtained into cytokinesis in unicellular eukaryotes have been transferable to multicellular eukaryotes. The apparent differences in these systems may be obscuring common biochemical mechanisms of cytokinesis.

### Toward a Comprehensive List of Core Cytokinesis Genes

Identification of the proteins required for cytokinesis is a critical step that provides the starting material for the biochemical, biophysical, and structural investigations required to understand the molecular basis of cytokinesis. With the use of forward and/or reverse genetics, ~20 core components required for cytokinesis in vertebrates, insects, and nematodes have been identified. These data can be compared to the results of four large-scale RNAi screens using *Drosophila* or *C. elegans* (Fig. 1B) (36, 58, 79, 80). RNAi allows efficient depletion of individual genes and is a useful method to functionally dissect cytokinesis. Defects in cytokinesis cause a readily recognizable phenotype that is not lethal to cells over short time periods. These data have been tabulated (Fig. 1B). A criterion that can aid the evaluation of these data is whether an individual gene scored positive in multiple independent screens. Of the core cytokinesis genes, 17 of 22 were identified in at least two of the three largely comprehensive screens (36, 79, 80), suggesting that, collectively, these screens did not suffer from a large number of false negatives. Conversely, the genes identified in

multiple screens largely overlaps with those defined by conventional genetics, implying that there exists a relatively small set of core cytokinesis genes that are each essential for cytokinesis.

Genes not previously implicated in cytokinesis scored positive in each of these screens. Of the 40 novel genes identified in one proteomic screen (58), 7 may be explained by other primary defects (such as osmosensitivity, microtubule defects, and chromosome segregation), 13 have been tested in at least two other screens and no phenotypes were observed (80) (www.wormbase.org), and the remaining 20 were previously found to cause a detectable, although noncytokinetic, phenotype. Of the 214 genes identified in a

generally found in multiple screens, factors involved in this process were identified in independent screens, so this class can be considered a robust hit.

Are there additional factors involved in cytokinesis that remain to be identified? The list of actin-binding proteins among the cytokinesis genes is remarkably short: myosin, formin, profilin, cofilin, and anillin. Are no additional actin-bundling proteins required for animal cell cytokinesis? What is responsible for linking the contractile ring to the plasma membrane? Are there structural proteins that stabilize the interaction between the contractile ring and the central spindle? What are the critical molecules through which spindle position directs contractile ring assembly?

Are there myosin-independent pathways that can contribute to cytokinesis in animal cells as in *Dictyostelium* and budding yeast?

Genetic redundancy may have impaired the identification of genes that are critical for cytokinesis. Functionally redundant genes will not be identified in screens in which single genes are inactivated. Although cytokinesis is largely dependent on the same machinery in most animal cells, the molecular requirements for cytokinesis do vary somewhat in different organisms. For example, vertebrates have multiple kinesin-6 family members that are each involved in cytokinesis (81), whereas there is only one such family member in *C. elegans*. Similarly, KIF4 is required for cytokinesis in vertebrate cells and in *Drosophila* spermatocytes; it is not apparently required in somatic cells in *Drosophila*.

More surprising is the case of citron kinase. In cultured human cells, overexpression of a kinase-defective mutant causes cytokinesis defects (82). Likewise, *Drosophila* citron kinase is essential for cytokinesis in cell culture and in the larval brain (26, 36, 40, 41). These data suggest citron kinase is a core part of the cytokinetic machinery. However, the most closely related gene in the *C. elegans* genome has not been implicated in cytokinesis. More strikingly, mice homozygous for a deletion of the citron kinase gene are viable, and tissues other than brain and testis do not show cytokinesis defects (83, 84). Redundancy at the process level as opposed to the molecular level also impedes genetic analysis of cytokinesis. For example, in some organisms, parallel pathways regulate furrow

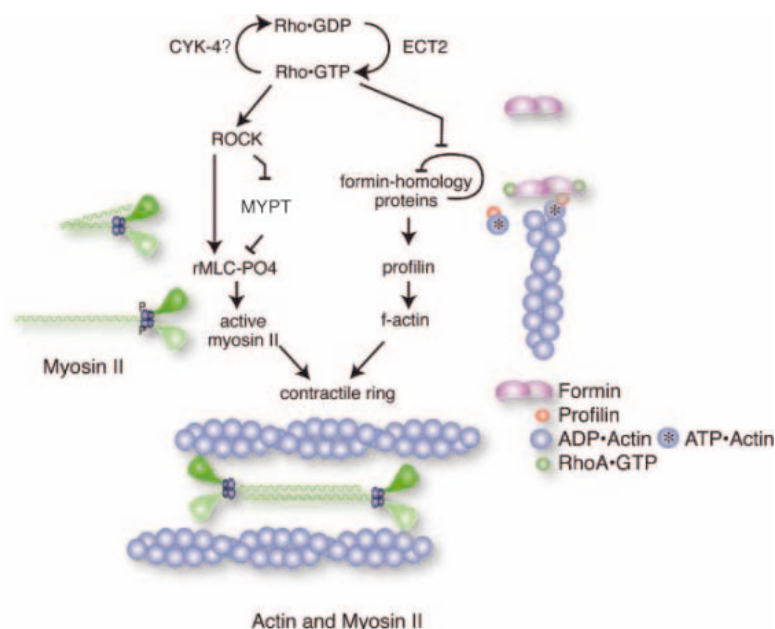


**Fig. 3.** The RhoA GTPase activates myosin and actin filament assembly. RhoA induces phosphorylation of the regulatory light chain of myosin (blue) and induces a conformational change permissive for filament assembly. Formin autoinhibition is relieved by RhoA-GTP and allows the processive elongation of the barbed end of actin filaments, a reaction that is profilin dependent.

*Drosophila* cell culture screen (79), 16 genes are among those listed in Fig. 1B, 12 are involved in membrane trafficking, and 116 have known functions in transcription, translation, chromatin, or cell cycle control. Most of the other genes caused weakly penetrant phenotypes, and there is insufficient information available for these genes to assess whether they are directly involved in cytokinesis. The novel genes from these large-scale screens do not overlap extensively, suggesting that they need to be studied in further detail to verify their direct involvement in cytokinesis.

One exception could be proteins involved in membrane trafficking. This class of proteins was found more frequently in the new screens as compared with previous studies. Even though the same genes were not

positioning. In *Drosophila*, central spindle components are essential for cleavage furrow formation. However, *C. elegans* embryos lacking central spindle components do form furrows (22); similar results have been observed in vertebrate cells (1, 29). Thus, although there is a significant degree of conservation in the mechanism of cytokinesis in animal cells, there is genetic variability in the requirements for cytokinesis. Because our understanding of cytokinesis is emerging from analyses of different experimental systems, these evolutionary changes vex efforts to derive a consensus mechanism. In addition, various kinds of functional redundancy may preclude a full account of the genes required for cytokinesis.

For the sake of comparison, although ~4700 out of ~6000 genes are nonessential in budding yeast, systematic synthetic lethal screens indicate that a sizable fraction (probably >50%) of these nonessential genes have an easily detected phenotype when combined with a second mutation (85). Three general strategies will be useful for teasing apart the underlying mechanisms of cytokinesis. First, by developing more sensitive assays, it is possible to determine whether a gene participates in cytokinesis, even when it is not strictly essential for the process. Second, it is likely that the pattern of genetic redundancy will vary in different systems, and therefore some pathways will be accessible in some systems but not others. Third, sensitized strains in which cytokinesis is less robust may be useful for second-generation screens and for analyzing factors identified by biochemistry and bioinformatics.

The average human consists of about  $10^{14}$  cells. How do cells maintain their integrity through so many multiplication cycles? DNA replication is nearly error-free, producing an average of three mutations each time a human-sized genome is replicated. To ensure equal segregation of the replicated sister chromatids, the spindle checkpoint delays mitotic exit until all sister chromatids are bi-oriented and under tension. It is not clear whether there are mechanisms that prevent or correct errors in cytokinesis. After anaphase onset, mammalian cells have a 1-hour window in which to complete cytokinesis (86). After that time, cells will exit mitosis and either arrest in G1 or continue to cycle. If they fail cytokinesis, the resulting polyploid cells have four possible fates. They can either undergo apoptosis, remain polyploid, rectify the situation by extruding a nucleus, or, if the two sets of chromosomes remain independent until the next mitosis and align on independent mitotic spindles, the cell could then cleave into four karyotypically normal cells. The relative frequencies of these alternate fates are unknown, particularly in vivo. There is evidence that the tumor suppressor p53 can block S-phase entry in cleavage-defective cells

(87, 88). However, multinucleation per se is not sufficient to arrest the cell cycle, and the G1 arrest may be due to general perturbations of the actin cytoskeleton (89, 90). In any case, a G1 arrest after cytokinesis failure would not correct the defect; it would merely reduce its potential to cause harm. Perhaps redundant mechanisms for cytokinesis exist to prevent defects in cytokinesis, because the repair processes may not be sufficiently robust.

The molecular mechanism of cytokinesis is coming into focus, but a number of blind spots persist. Although it will be important to identify additional components, the challenge for the future will be to analyze the underlying biochemistry and cell biology of this dynamic and dramatic event in the life of a cell.

#### References and Notes

1. C. Mollinari et al., *J. Cell Biol.* **157**, 1175 (2002).
2. F. Verni et al., *Curr. Biol.* **14**, 1569 (2004).
3. K. J. Verbrugghe, J. G. White, *Curr. Biol.* **14**, 1755 (2004).
4. Y. Kurasawa, W. C. Earnshaw, Y. Mochizuki, N. Dohmae, K. Todokoro, *EMBO J.* **23**, 3237 (2004).
5. M. Mishima, V. Pavicic, U. Gruneberg, E. A. Nigg, M. Glotzer, *Nature* **430**, 908 (2004).
6. M. Mishima, S. Kaitna, M. Glotzer, *Dev. Cell* **2**, 41 (2002).
7. J. Matulienė, R. Kuriyama, *Mol. Biol. Cell* **13**, 1832 (2002).
8. W. G. Somers, R. Saint, *Dev. Cell* **4**, 29 (2003).
9. J. M. Schumacher, A. Golden, P. J. Donovan, *J. Cell Biol.* **143**, 1635 (1998).
10. A. F. Severson, D. R. Hamill, J. C. Carter, J. Schumacher, B. Bowerman, *Curr. Biol.* **10**, 1162 (2000).
11. S. Kaitna, M. Mendoza, V. Jantsch-Plunger, M. Glotzer, *Curr. Biol.* **10**, 1172 (2000).
12. R. R. Adams et al., *Curr. Biol.* **10**, 1075 (2000).
13. E. K. Speliotes, A. Uren, D. Vaux, H. R. Horvitz, *Mol. Cell* **6**, 211 (2000).
14. A. Romano et al., *J. Cell Biol.* **161**, 229 (2003).
15. S. C. Sampath et al., *Cell* **118**, 187 (2004).
16. R. Gassmann et al., *J. Cell Biol.* **166**, 179 (2004).
17. R. Ban, Y. Irino, K. Fukami, H. Tanaka, *J. Biol. Chem.* **279**, 16394 (2004).
18. T. Raemaekers et al., *J. Cell Biol.* **162**, 1017 (2003).
19. Y. H. Inoue et al., *J. Cell Biol.* **149**, 153 (2000).
20. M. J. Daniels, Y. Wang, M. Lee, A. R. Venkataraman, *Science* **306**, 876 (2004); published online 16 September 2004 (10.1126/science.1102574).
21. R. R. Adams, A. A. Tavares, A. Salzberg, H. J. Bellen, D. M. Glover, *Genes Dev.* **12**, 1483 (1998).
22. R. Dechant, M. Glotzer, *Dev. Cell* **4**, 333 (2003).
23. T. Tatsumoto, X. Xie, R. Blumenthal, I. Okamoto, T. Miki, *J. Cell Biol.* **147**, 921 (1999).
24. S. N. Prokopenko et al., *Genes Dev.* **13**, 2301 (1999).
25. V. Jantsch-Plunger et al., *J. Cell Biol.* **149**, 1391 (2000).
26. P. P. D'Avino, M. S. Savoian, D. M. Glover, *J. Cell Biol.* **166**, 61 (2004).
27. W. B. Raich, A. N. Moran, J. H. Rothman, J. Hardin, *Mol. Biol. Cell* **9**, 2037 (1998).
28. J. Powers, O. Bossinger, D. Rose, S. Strome, W. Saxton, *Curr. Biol.* **8**, 1133 (1998).
29. J. Matulienė, R. Kuriyama, *Mol. Biol. Cell* **15**, 3083 (2004).
30. I. Mabuchi, M. Okuno, *J. Cell Biol.* **74**, 251 (1977).
31. S. Guo, K. J. Kempfues, *Nature* **382**, 455 (1996).
32. A. J. Straight et al., *Science* **299**, 1743 (2003).
33. P. Jordan, R. Karess, *J. Cell Biol.* **139**, 1805 (1997).
34. M. Amano et al., *J. Biol. Chem.* **271**, 20246 (1996).
35. A. J. Piekny, P. E. Mains, *J. Cell Sci.* **115**, 2271 (2002).
36. A. Echard, G. R. Hickson, E. Foley, P. H. O'Farrell, *Curr. Biol.* **14**, 1685 (2004).
37. K. Kimura et al., *Science* **273**, 245 (1996).
38. C. G. Winter et al., *Cell* **105**, 81 (2001).
39. S. Yamashiro et al., *Mol. Biol. Cell* **14**, 1745 (2003).
40. T. Shandala, S. L. Gregory, H. E. Dalton, M. Smallhorn, R. Saint, *Development* **131**, 5053 (2004).
41. V. Naim, S. Imarisio, F. Di Cunto, M. Gatti, S. Bonaccorsi, *Mol. Biol. Cell* **15**, 5053 (2004).
42. J. Withee, B. Galligan, N. Hawkins, G. Garriga, *Genetics* **167**, 1165 (2004).
43. A. F. Severson, D. L. Baillie, B. Bowerman, *Curr. Biol.* **12**, 2066 (2002).
44. K. A. Swan et al., *J. Cell Sci.* **111**, 2017 (1998).
45. F. Chang, D. Drubin, P. Nurse, *J. Cell Biol.* **137**, 169 (1997).
46. D. H. Castrillon, S. A. Wasserman, *Development* **120**, 3367 (1994).
47. D. R. Kovar, J. R. Kuhn, A. L. Tichy, T. D. Pollard, *J. Cell Biol.* **161**, 875 (2003).
48. I. Sagot, A. A. Rodal, J. Moseley, B. L. Goode, D. Pellman, *Nature Cell Biol.* **4**, 626 (2002).
49. D. Pruyne et al., *Science* **297**, 612 (2002); published online 6 June 2002 (10.1126/science.1072309).
50. S. Romero et al., *Cell* **119**, 419 (2004).
51. A. S. Alberts, *J. Biol. Chem.* **276**, 2824 (2001).
52. K. C. Gunsalus et al., *J. Cell Biol.* **131**, 1243 (1995).
53. K. Ono, M. Parast, C. Alberico, G. M. Benian, S. Ono, *J. Cell Sci.* **116**, 2073 (2003).
54. C. M. Field, B. M. Alberts, *J. Cell Biol.* **131**, 165 (1995).
55. M. P. Somma, B. Fasulo, G. Cenci, E. Cundari, M. Gatti, *Mol. Biol. Cell* **13**, 2448 (2002).
56. A. F. Straight, C. M. Field, T. J. Mitchison, *Mol Biol Cell* **16**, 193 (2004).
57. S. H. Low et al., *Dev. Cell* **4**, 753 (2003).
58. A. R. Skop, H. Liu, J. Yates III, B. J. Meyer, R. Heald, *Science* **305**, 61 (2004).
59. M. Murthy, T. L. Schwarz, *Development* **131**, 377 (2004).
60. J. Fan, K. A. Beck, *J. Cell Sci.* **117**, 619 (2004).
61. M. K. Balasubramanian, E. Bi, M. Glotzer, *Curr. Biol.* **14**, R806 (2004).
62. S. C. Schuyler, J. Y. Liu, D. Pellman, *J. Cell Biol.* **160**, 517 (2003).
63. G. S. Lakshmikanth, H. M. Warrick, J. A. Spudich, *Proc. Natl. Acad. Sci. U.S.A.* **101**, 16519 (2004).
64. E. A. Vallen, J. Caviston, E. Bi, *Mol. Biol. Cell* **11**, 593 (2000).
65. R. Neujahr, C. Heizer, G. Gerisch, *J. Cell Sci.* **110**, 123 (1997).
66. A. De Lozanne, J. A. Spudich, *Science* **236**, 1086 (1987).
67. A. Nagasaki, E. L. de Hostos, T. Q. Uyeda, *J. Cell Sci.* **115**, 2241 (2002).
68. I. Weber et al., *EMBO J.* **18**, 586 (1999).
69. J. Faix et al., *Cell* **86**, 631 (1996).
70. D. A. Larochelle, K. K. Vithalani, A. De Lozanne, *J. Cell Biol.* **133**, 1321 (1996).
71. S. Schmidt, M. Sohrmann, K. Hofmann, A. Woollard, V. Simanis, *Genes Dev.* **11**, 1519 (1997).
72. D. McCollum, A. Feoktistova, K. L. Gould, *J. Biol. Chem.* **274**, 17691 (1999).
73. B. D. Ostrow, P. Chen, R. L. Chisholm, *J. Cell Biol.* **127**, 1945 (1994).
74. Y. Dong, D. Pruyne, A. Bretscher, *J. Cell Biol.* **161**, 1081 (2003).
75. A. Paoletti, F. Chang, *Mol. Biol. Cell* **11**, 2757 (2000).
76. J. Q. Wu, J. R. Kuhn, D. R. Kovar, T. D. Pollard, *Dev. Cell* **5**, 723 (2003).
77. H. Wang et al., *Mol. Biol. Cell* **13**, 515 (2002).
78. R. C. Stevens, T. N. Davis, *J. Cell Biol.* **142**, 711 (1998).
79. U. S. Eggert et al., *PLoS Biol.* **2**, e379 (2004).
80. B. Sönnichsen et al., *Nature*, in press.
81. R. Neef et al., *J. Cell Biol.* **162**, 863 (2003).
82. P. Madaule et al., *Nature* **394**, 491 (1998).
83. F. Di Cunto et al., *Neuron* **28**, 115 (2000).
84. F. Di Cunto et al., *J. Cell Sci.* **115**, 4819 (2002).
85. A. H. Y. Tong et al., *Science* **303**, 808 (2004).
86. S. N. Martineau, P. R. Andreassen, R. L. Margolis, *J. Cell Biol.* **131**, 191 (1995).
87. P. R. Andreassen, O. D. Lohez, F. B. Lacroix, R. L. Margolis, *Mol. Biol. Cell* **12**, 1315 (2001).
88. P. Meraldi, R. Honda, E. A. Nigg, *EMBO J.* **21**, 483 (2002).
89. Y. Uetake, G. Sluder, *J. Cell Biol.* **165**, 609 (2004).
90. O. D. Lohez, C. Reynaud, F. Borel, P. R. Andreassen, R. L. Margolis, *J. Cell Biol.* **161**, 67 (2003).
91. M.G. thanks all the members of his research group for comments on this review and acknowledges the support of the Austrian Science Foundation (P15579) and Boehringer Ingelheim.
92. After 1 July 2005, the author will be at the Department of Molecular Genetics and Cell Biology, University of Chicago, Chicago, IL 60637, USA. E-mail: mglotzter@uchicago.edu.

10.1126/science.1096896



## Self-Organized Origami

L. Mahadevan<sup>1\*</sup> and S. Rica<sup>2</sup>

The controlled folding and unfolding of maps, space structures, wings, leaves, petals, and other foldable laminae is potentially complicated by the independence of individual folds; as their number increases, there is a combinatorial explosion in the number of folded possibilities. The artificially constructed Miura-ori (*I*) pattern, with a periodic array of geometrically and elastically coupled mountain and valley folds (Fig. 1A), circumvents this complication by allowing the entire structure to be folded or unfolded simultaneously. Making such a pattern is not easy, so it may be surprising to find an elegant natural counterpart that is a few hundred millennia old. In Fig. 1B, we show the different stages of the opening of a hornbeam leaf that starts life in its bud as a Miura-ori folded pattern (2). Similar structures arise in insect wings (3) and elsewhere in nature (4), suggesting that these origami patterns are a result of convergent design. This raises a question of mechanism: How might this spatial organization of folds be brought about?

In Fig. 1C, we show the realization of a simple physical solution to this question. The biaxial compression of a thin, stiff, elastic film (with Young's modulus  $E$ , Poisson ratio  $\nu$ , thickness  $h$ , and size  $L \gg h$ ) supported on a thick, soft substrate (with Young's modulus  $E_p \ll E$  and thickness  $H \gg h$ ) yields into a Miura-ori pattern without any external guidance other than that induced by relatively benign, isotropic, compressive strains that arise because of the relative expansion and contraction between the film and substrate induced by thermal (5) or desiccating (6) effects. Initially, we get primary buckles with wavelength  $\lambda \sim h(E/E_p)^{1/3}$  (5), which is very small compared to the lateral extent of the system. However, at the onset of the instability, these straight primary buckles do not have any preferred orientation in a large system and instead form large uncorrelated patches. Non-linear deformations of these primary buckles, through global compression or extension parallel or perpendicular to their orientation, lead to modulational instabilities wherein the buckles collectively deform through soft modes, which are energetically cheaper than the local extension or compression of individual buckles (supporting online text). Thus, the Miura-ori pattern is just the natural response of a softly

supported stiff skin to weak compression along the primary buckles (or weak extension perpendicular to them), wherein the buckles tilt into a zigzag pattern separated by kinks.

Quantifying this through a mathematical analysis of the equations of elasticity (supporting online text) away from the onset of the instability leads to the Newell-Whitehead-Segel equation (7, 8) for the complex-valued amplitude  $A(x,y)$

$$\epsilon A + \frac{h^2}{12(1-\nu^2)} \times (\partial_x - \frac{i}{2k_c} \partial_{yy})^2 A - g|A|^2 A = 0 \quad (1)$$

Here  $Re[A(x,y)e^{ik_c x}]$  is the vertical deflection of the skin,  $k_c = 2\pi/\lambda$  is the wave number at onset,  $\epsilon$  characterizes the distance from the instability threshold, and  $g$  characterizes the saturation amplitude. The form of Eq. 1 follows from symmetry considerations (supporting online text) and describes a variety of planform patterns, including the zigzag patterns found in fluid convection, superconductivity, liquid crystals, etc. Our interpretation in the context of folding patterns suggests that Eq. 1 also provides a

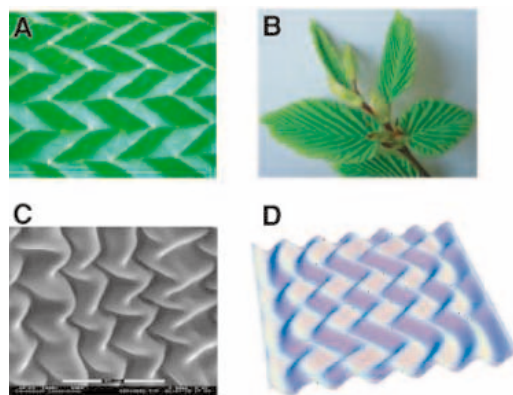


**Fig. 1.** (A) Plan view of a paper Miura-ori pattern (size, 5 cm), showing the periodic mountain-valley folds. The sharp re-entrant creases that come together at kinks allow the whole structure to fold or unfold simultaneously. (B) Hornbeam leaves (length, 5 cm) in the process of blooming show a natural occurrence of Miura-ori. A single row of kinks along the midrib allows a folded leaf to be deployed once the bud opens (2), as seen in the different stages of leaf opening (clockwise from the top). (C) Zigzag Miura-ori patterns in a thin film atop a thick elastic substrate that is compressed biaxially manifest here in a drying slab of gelatin with a thin skin that forms naturally (6), showing the physically driven self-organization of Miura-ori. Scale bar, 35  $\mu\text{m}$ . (D) Simulations of Eq. 1 yield Miura-ori patterns that arise as a modulational instability of the primary (straight) wrinkles (supporting online text).

natural mathematical framework for the self-organization of Miura-ori. Indeed, a numerical simulation of Eq. 1 in a rectangular domain with periodic boundary conditions in one direction and Neumann conditions in an orthogonal direction reproduces the Miura-ori patterns with creases of wavelength  $\lambda$  (Fig. 1D).

Although Eq. (1) is asymptotically valid only in the weakly nonlinear regime, in practice it describes the patterns well even far from the onset of the zigzag folds. Additionally, the strong localization of the creases and kinks follows naturally from the nonlinear evolution of the pattern in light of the small thickness of the skin-like upper film and the softness of the substrate, leading to almost isometric mountain-valley fold patterns (Fig. 1, A and C). The size  $d$  of the kinks is determined by minimizing the sum of the kink-bending energy  $U_k \sim Eh^3 \ln(R/d)$ , due primarily to conical bending of the thin sheet of size  $R$ , and the additional energy of deforming the attached substrate below the kinks,  $U_s \sim E_p d^3$ . This yields  $d \sim h(E/E_p)^{1/3} \sim \lambda$ , consistent with observations (Fig. 1C).

Our observations and analysis provide a mechanism for naturally occurring Miura-ori. Stresses induced by the relative growth of stiff skins on soft supports will spontaneously fold into structures such as those shown in Fig. 1; stress-mediated apoptosis may then separate the skin from the tissue to form deployable laminae such as leaves and insect wings.

### References and Notes

1. K. Miura, *Proceedings of the 31st Congress of the International Astronautical Federation, IAF-80-A 31*, (American Institute for Aeronautics and Astronautics, New York, 1980), pp. 1–10.
2. H. Kobayashi, B. Kresling, J. Vincent, *Proc. R. Soc. London Ser. B*, **265**, 147 (1998).
3. F. Haas, R. W. Wootton, *Proc. R. Soc. London Ser. B*, **263**, 1651 (1996).
4. B. Kresling, *Biomimetics* **3**, 105 (1991).
5. N. Bowden, S. Brittain, A. G. Evans, J. Hutchinson, G. Whitesides, *Nature* **393**, 146 (1998).
6. R. Rizzieri, personal communication.
7. L. A. Segel, *J. Fluid Mech.* **38**, 203 (1969).
8. A. C. Newell, J. Whitehead, *J. Fluid Mech.* **38**, 279 (1969).
9. L.M. acknowledges support from the Harvard Materials Research Science and Engineering Center and the Office of Naval Research Young Investigator Program; S.R. acknowledges support from Fondo de Ciencia y Tecnología (FONDECYT), Chile.

### Supporting Online Material

[www.sciencemag.org/cgi/content/full/307/5716/1740/DC1](http://www.sciencemag.org/cgi/content/full/307/5716/1740/DC1)

SOM Text

Fig. S1

References and Notes

13 September 2004; accepted 2 February 2005  
10.1126/science.1105169

<sup>1</sup>Division of Engineering and Applied Sciences and Department of Organismic and Evolutionary Biology, Harvard University, Cambridge, MA 02138, USA. <sup>2</sup>Departamento de Física, Universidad de Chile, Blanco Encalada 2008, Santiago, Chile.

\*To whom correspondence should be addressed.  
E-mail: lm@deas.harvard.edu

# Southern Hemisphere Water Mass Conversion Linked with North Atlantic Climate Variability

Katharina Pahnke<sup>1\*†</sup> and Rainer Zahn<sup>2†</sup>

Intermediate water variability at multicentennial scales is documented by 340,000-year-long isotope time series from bottom-dwelling foraminifers at a mid-depth core site in the southwest Pacific. Periods of sudden increases in intermediate water production are linked with transient Southern Hemisphere warm episodes, which implies direct control of climate warming on intermediate water conversion at high southern latitudes. Coincidence with episodes of climate cooling and minimum or halted deepwater convection in the North Atlantic provides striking evidence for interdependence of water mass conversion in both hemispheres, with implications for interhemispheric forcing of ocean thermohaline circulation and climate instability.

Water mass formation in the Southern Hemisphere oceans is involved in the global thermohaline circulation (THC) through the convection and interocean exchanges of surface, intermediate, and bottom waters. These water masses transport heat, salt, and freshwater through the world ocean and are relevant for a range of climatic processes. Yet, water mass production in the Southern Hemisphere has long been perceived as a passive player in ocean and climate dynamics, and research into the causes of rapid climate change has focused on the northern North Atlantic as the presumed primary driver of global ocean THC (1, 2). While evidence is accumulating that climatic upheaval occurred within the recent geologic past with substantial forcing from ocean-climate processes (1), numerical and conceptual models are increasingly highlighting an active involvement of water mass conversion in the Southern Hemisphere (3–7). The role of Antarctic Intermediate Water (AAIW) in redistributing heat and freshwater within the upper ocean is particularly recognized as pivotal in these changes (4, 7, 8). However, detailed insight into the linking between AAIW and past ocean-climate change has long been hampered by a lack of observational time series of sufficient length and temporal resolution. Fine-scale paleoceanographic re-

cords are now available from the southwest Pacific that document the history of AAIW variability at multicentennial scales and enable a detailed assessment of Southern Hemisphere water mass conversion and its linking with climate variability in both hemispheres.

**Benthic isotope records.** We have generated benthic foraminiferal oxygen ( $\delta^{18}\text{O}_b$ ) and carbon isotope ( $\delta^{13}\text{C}_b$ ) records along 36-m-long IMAGES (International Marine Past Global Changes Studies) core MD97-2120 from Chatham Rise off New Zealand ( $45^\circ 32.06'\text{S}$ ,  $174^\circ 55.85'\text{E}$ ) (Fig. 1A).  $\delta^{18}\text{O}_b$  and  $\delta^{13}\text{C}_b$  were measured on monospecific samples of the benthic foraminifers *Cibicidoides wuellerstorfi*, *C. cicatricosus*, and *C. kullenbergi*. In intervals lacking *Cibicidoides* spp., the records were complemented by analyses on *Melonis barleeanum* and *Bulimina aculeata* to maintain fine-scale resolution along the entire core (9). The age scale for core MD97-2120 is derived from accelerator mass spectrometry (AMS)  $^{14}\text{C}$  dating, a tephrochronological marker event, and tuning of the benthic and planktonic records to paleoclimatic profiles from the North Atlantic and Antarctica, respectively (9). The core spans the last three climatic cycles and at its base reaches glacial termination IV at 340,000 years (340 ky) before the present (B.P.). High sedimentation rates at the core site permit a mean temporal resolution along the records of  $199 \pm 94$  years (at 2-cm sample spacing). At a water depth of 1210 m, core MD97-2120 lies close to the AAIW core layer (Fig. 1B). The stable isotope records thus provide the first detailed documentation of the history of mid-depth circulation and AAIW renewal at high southern latitudes over the past three glacial-interglacial cycles.

The  $\delta^{18}\text{O}_b$  record (Fig. 2B) displays prominent glacial-interglacial modulation that reflects

the growth and decay of global ice volumes and associated sea-level fluctuations during the last three climatic cycles (10). Glacial-to-interglacial  $\delta^{18}\text{O}_b$  amplitudes of 1.6 to 1.98‰ exceed the coeval mean-ocean  $\delta^{18}\text{O}$  change of 0.8 to 1.1‰ (11, 12), documenting changes of temperature and salinity (*T-S*) at intermediate water depth. Additional variability is seen in fine structure that closely follows the suborbital changes in the Antarctic Vostok ice-core deuterium ( $\delta\text{D}$ ) record (13) that reflects atmospheric temperature changes over Antarctica. Correlation with Vostok  $\delta\text{D}$  has been found for a northeast Atlantic deepwater  $\delta^{18}\text{O}_b$  record and used to infer sea-level variations during Antarctic climatic events (14) with considerable meltwater contributions from Northern and Southern Hemisphere ice sheets (15). Sea-level oscillations on millennial time scales have been confirmed recently by using high-resolution isotope data from a Red Sea sediment core (16) and are estimated on the order of  $30 \pm 5$  m. Close fine-structural similarity of our  $\delta^{18}\text{O}_b$  record to these millennial-scale sea-level changes indicates predominant control of global ice-volume fluctuations on the  $\delta^{18}\text{O}_b$  signature in our core. The residual amplitude, up to 0.35‰, not explained by global sea level, reflects changes in mid-depth *T-S* hydrography that occurred in conjunction with Southern Hemisphere climatic shifts.

Benthic  $\delta^{13}\text{C}_b$  levels along core MD97-2120 are reduced during glacial periods of the past 340 ky (Fig. 2E).  $\delta^{13}\text{C}_b$  is derived from  $\delta^{13}\text{C}$  of total dissolved carbon ( $\delta^{13}\text{C}_{\text{TCO}_2}$ ) in the ocean that is controlled by biological nutrient cycling and water mass chemical “aging” (17). This makes foraminiferal  $\delta^{13}\text{C}_b$  a valuable proxy to reconstruct past water mass variability. Several lines of evidence (9) strongly suggest that  $\delta^{13}\text{C}_b$  variability along our record has not been substantially driven by secondary overprints, for example, from organic debris fluff layers at the sediment-water interface (18), temperature-dependent fractionation during air-sea gas exchange in the convection region (19), and source-water (“preformed”)  $\delta^{13}\text{C}_{\text{TCO}_2}$  changes. Rather, it is suggested that  $\delta^{13}\text{C}_b$  fluctuations at the mid-depth core site are linked directly with changes in the rate of AAIW production.

The substantial glacial  $\delta^{13}\text{C}_b$  depletion in core MD97-2120 is contrasted by  $\delta^{13}\text{C}_b$  levels in glacial sections of North Atlantic and Pacific mid-depth cores that remain similar to or are elevated over interglacial levels, indicating that mid-depth ventilation in these basins remained high over long time scales (20, 21). Full-glacial  $\delta^{13}\text{C}_b$  depletion by 0.8‰ (Fig. 2) is substantially in excess of the mean-ocean  $\delta^{13}\text{C}_{\text{TCO}_2}$  depletion of 0.32‰ (21). It is also in excess of the change of only 0.2‰ recorded at intermedi-

<sup>1</sup>School of Earth, Ocean, and Planetary Sciences, Cardiff University, Park Place, Cardiff CF10 3YE, UK.

<sup>2</sup>Institució Catalana de Recerca i Estudis Avançats, ICREA, i Universitat Autònoma de Barcelona, Institut de Ciència i Tecnologia Ambientals, ICTA, Edifici Cn, Campus UAB, E-08193 Bellaterra, Spain.

\*Present address: Department of Earth, Atmospheric, and Planetary Sciences, Massachusetts Institute of Technology, Cambridge, MA 02139, USA.

†To whom correspondence should be addressed. E-mail: kpahnke@mit.edu, rainer.zahn@icrea.es

ate water sites in the subantarctic East Atlantic [ODP Site 1088 (22), core TN057-20 (23)] but is similar to the  $\delta^{13}\text{C}_b$  found at mid-depth in the Tasman Sea (24). We note that the South Atlantic records do not display typical Holocene levels (Site 1088) or do not reach late Holocene times (TN057-20) at their core tops, whereas amplitudes during previous glacial-interglacial transitions are similar to those in our record (Site 1088) (fig. S5). Although genuine differences may exist between ocean basins, we suggest that the South Atlantic sites do not capture the full amplitude of the last glacial-interglacial change.

Outstanding features of our  $\delta^{13}\text{C}_b$  record are frequent positive excursions in glacial intervals with amplitudes of up to 0.8‰, that is,  $\delta^{13}\text{C}_b$  values during some of these events reach full-interglacial levels (Figs. 2 and 3). The events coincide with Southern Hemisphere warm anomalies seen in Mg/Ca-derived sea surface temperatures ( $\text{SST}_{\text{Mg/Ca}}$ ) (25) and in Antarctic ice-core records (13) (Figs. 2 and 3). Consistent correlation of intermediate water  $\delta^{13}\text{C}_b$  and Southern Hemisphere temperature variability on orbital to millennial time scales suggests direct linking of water mass conversion at high southern latitudes with climatic changes.

**The Southern Ocean meridional overturning cell.** Primary forcing of intermediate water formation at southern latitudes is exerted by air-sea interaction in the Subantarctic Zone (SAZ); cross-frontal northward Ekman transport of cold, fresh Antarctic surface waters; and the southward advection of heat and salt within the subtropical gyre circulation (8, 26). These processes result in surface buoyancy loss in the SAZ and determine the rate and variability of Subantarctic Mode Water (SAMW) formation (Fig. 1A). Wintertime cooling causes SAMW density to further increase until finally the densest classes of SAMW convect and feed AAIW (8, 26, 27). Primary sources for AAIW renewal are in the Southeast Pacific and Southwest Atlantic, with additional sources in the South Pacific and Indian Oceans where Antarctic surface waters are directly transformed into AAIW through air-sea buoyancy fluxes and the southward movement of the circum-Antarctic fronts (8, 28). Increased westerly wind stress has been suggested to contribute to and invigorate shallow overturning in the Southern Hemisphere by enhancing northward Ekman transports and the subduction and convection of AAIW (29).

Environmental conditions were different during glacial periods for an array of ocean and atmospheric parameters with implications for the operation of the Southern Ocean Meridional Overturning Circulation (SOMOC). Substantial atmosphere and surface ocean cooling (13, 25), in conjunction with intensified winds, resulted in a northward displacement of circumpolar ocean fronts and the westerly wind belt by some 5° in latitude (30). Expansion of the sea-ice cover by as much as 70% (30) led to

enhanced seasonal meltwater supply to the Southern Ocean, thereby increasing the stratification of the upper water column (31, 32).

The longer term changes of  $\delta^{13}\text{C}_b$  along our record reflect the response of the SOMOC to glacial boundary conditions. Glacial intensification of the westerlies plausibly intensified northward Ekman freshwater transports, which freshened the surface layer in the SAZ. Whereas today the effect of these low-salinity waters on surface buoyancy in the SAZ is partly offset by their low temperatures (26, 29), increased freshwater transports under glacial conditions plausibly enhanced the salinity anomaly across the SAZ and reduced production of AAIW. This process would then contribute to the large glacial  $\delta^{13}\text{C}_b$  depletion in core MD97-2120. Increased upwelling of UCDW in response to enhanced glacial wind stress and stronger bottom-water formation

(e.g., 33) with upward displacement of the AAIW-UCDW interface are also consistent with low glacial intermediate water  $\delta^{13}\text{C}_b$  values. However, while the operation of such processes cannot be excluded, the direct coupling of high-amplitude  $\delta^{13}\text{C}_b$  changes with Southern Hemisphere warming strongly suggests changes in AAIW production as the dominant factor in causing  $\delta^{13}\text{C}_b$  variability along our record. As we will discuss below, the positive mid-depth  $\delta^{13}\text{C}_b$  anomalies in our record are coeval with pronounced deepwater  $\delta^{13}\text{C}_b$  minima that are linked with reductions in the southward advection of North Atlantic deep water (NADW) (22, 23, 34, 35). Apparent decoupling of Southwest Pacific mid-depth  $\delta^{13}\text{C}_b$  from deepwater  $\delta^{13}\text{C}_b$  variability requires changes in AAIW production so as to maximize  $\delta^{13}\text{C}_b$  in core MD97-2120 and steepen vertical gradients between the mid-depth and deeper water column.

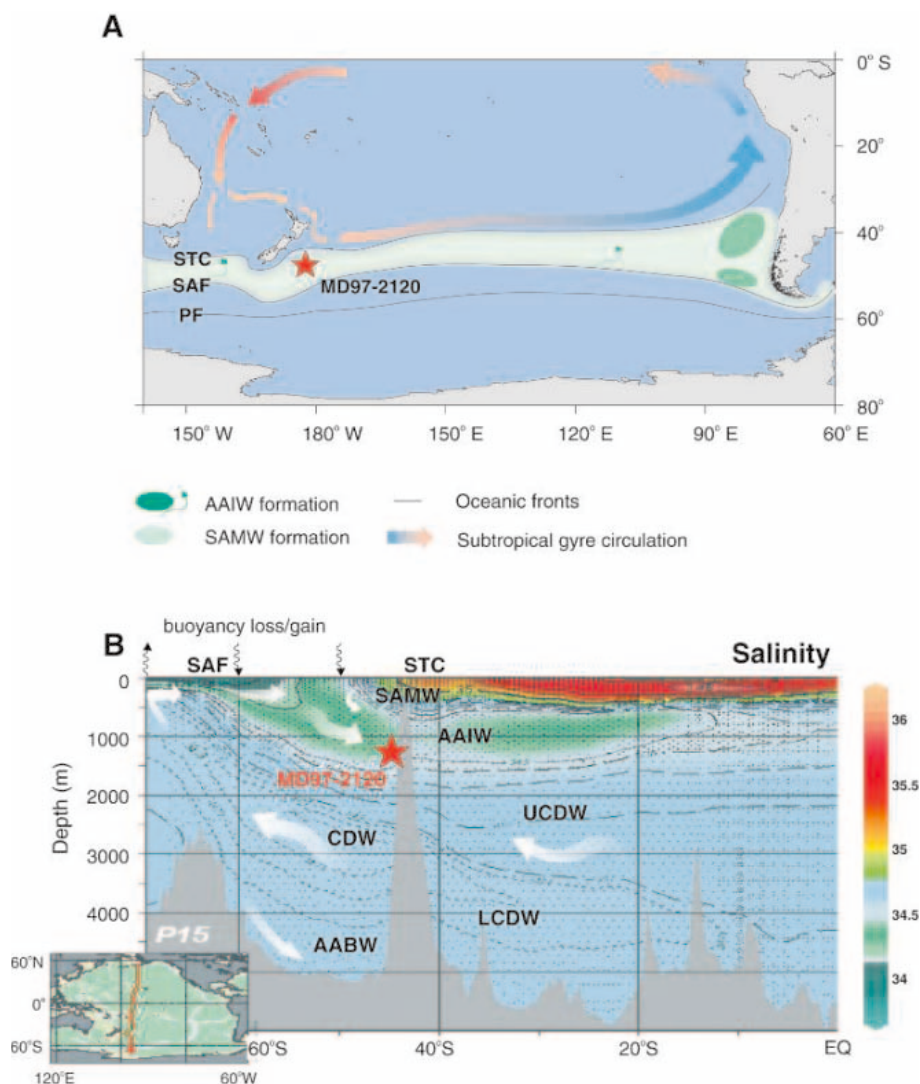


**Fig. 1.** Subtropical gyre circulation in the South Pacific and the Southern Ocean meridional overturning cell. (A) Schematic surface circulation in the South Pacific subtropical gyre with areas of SAMW and AAIW formation (8, 27). PF, polar front; SAF, subantarctic front; STC, subtropical convergence. (B) World Ocean Circulation Experiment (WOCE) meridional salinity transect in the southwest Pacific (44). Superimposed, circulation in the SOMOC (45). AABW, Antarctic Bottom Water; (U/L)CDW, (Upper/Lower) Circumpolar Deep Water. Oceanic fronts as in (A).

Rapid departures from low glacial  $\delta^{13}\text{C}_b$  background levels are closely linked with Southern Hemisphere warming, providing striking evidence that the production of newly ventilated AAIW was tightly coupled with abrupt changes in Southern Hemisphere climate. Relaxation and southward shifting of circumpolar wind trajectories, consistent with hemisphere-wide warming, presumably resulted in a decrease of northward Ekman freshwater transports and thus weakened the freshwater anomaly in the SAZ. Increased surface salinity in the Southwest Pacific (25) further suggests enhanced southward salt transports in the western branch of the subtropical gyre, causing rapid buoyancy loss and preconditioning of the SAZ toward intensified AAIW formation. Weakened easterly winds in the tropics at these times (36) could have aided the process through intermittent releases of saline waters from the western tropical Pacific into the subtropical gyre, thereby enhancing southward salt transports and providing the impetus for AAIW production.

**Interhemispheric linking.** Comparison with a high-resolution deepwater  $\delta^{13}\text{C}_b$  record from the North Atlantic (37) shows that some  $\delta^{13}\text{C}_b$  anomalies in our core are in antiphase with Northern Hemisphere  $\delta^{13}\text{C}_b$ . This is

particularly evident during Heinrich (H) meltwater events H4 and H5 in the northern North Atlantic, when freshwater surges from the Northern Hemisphere ice sheets slowed down NADW convection (9, 14) (Figs. 2 and 3). The ventilation collapses associated with these events are evident in discrete  $\delta^{13}\text{C}_b$  minima along the North Atlantic deepwater record but are directly contrasted by  $\delta^{13}\text{C}_b$  maxima in our core. Positive  $\delta^{13}\text{C}_b$  excursions are also developed in our record during the episodes of the North Atlantic H1, H3, H5a, and H6 events. However, these events are not obviously antiphased with corresponding changes in the North Atlantic, perhaps as a result of insufficient temporal resolution of the northern record. We note, however, that the millennial-scale mid-depth  $\delta^{13}\text{C}_b$  variability along our records is in pace with SST changes in the same core, which in turn are synchronous with the Antarctic temperature history and in antiphase with the Greenland ice-core record (38). This linking therefore supports an out-of-phase correlation of the mid-depth  $\delta^{13}\text{C}_b$  ventilation events with Northern Hemisphere cooling and NADW reduction (38).

The incursion of warm episodes in planktonic records from our core during periods of

convection slowdown and cooling in the Northern Hemisphere is consistent with the concept of a bipolar antiphase response of climatology (39). While the climatic “seesaw” (39) links the interhemispheric temperature history with changes in marine northward heat transport, it does not predict the observed antiphased pattern between water mass conversion in both hemispheres. The apparent NADW-AAIW anticorrelation suggests that anomalous climate and ocean perturbations in one hemisphere force an immediate response of water mass conversion in the other hemisphere. Numerical and conceptual models postulate the existence of such a mechanism (3, 4, 6, 7) and predict interhemispheric THC changes as a result of varying freshwater budgets at high latitudes and concomitant changes of interhemispheric density gradients. Such a scenario particularly holds for periods of North Atlantic meltwater surges during H-events in that the increased freshwater input to the northern North Atlantic reversed the meridional density gradient in favor of increased AAIW formation (6, 7). Intensified production and northward flow of AAIW then forced a compensating southward flow of saline surface and thermocline waters (6, 7), thereby further diminishing

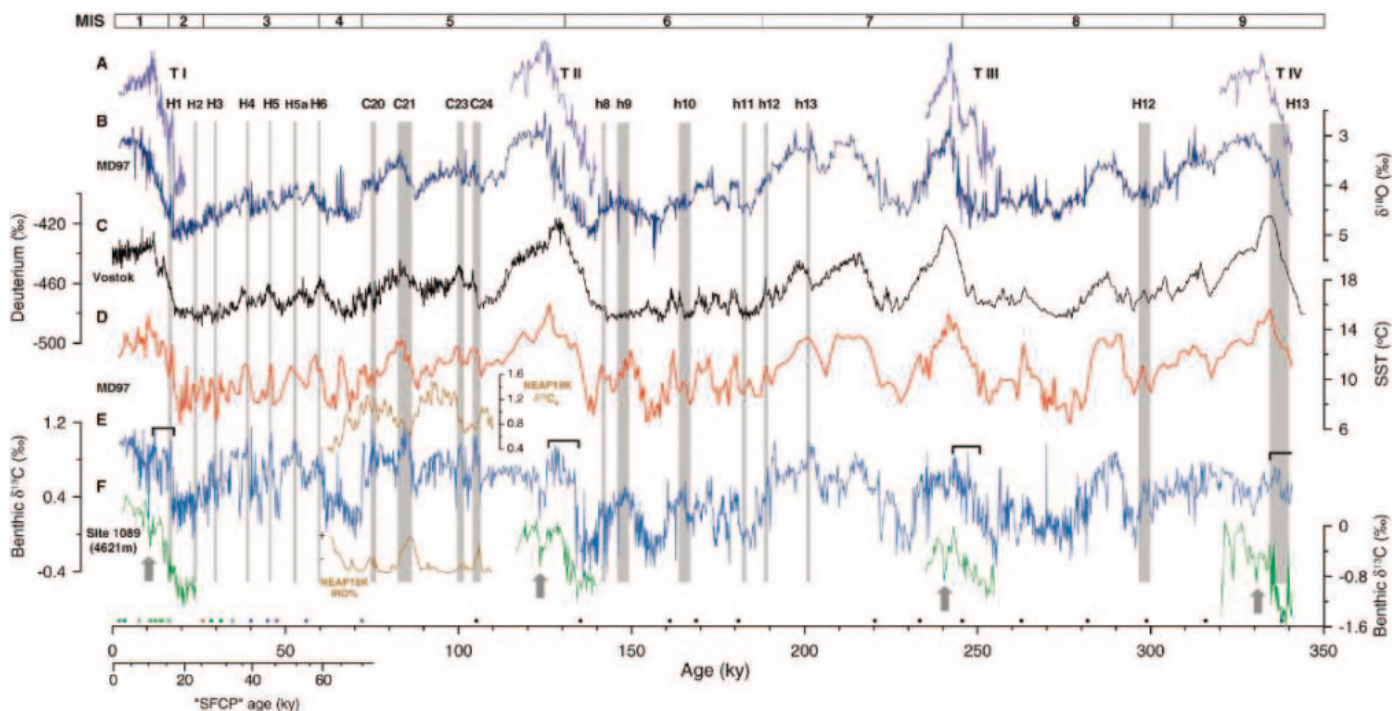


**Fig. 2.** AAIW proxy records along core MD97-2120 compared with surface hydrographic profiles of the same core and the Vostok climate record over the past 340 ky. (A) Glacial terminations of the planktonic foraminiferal (*Globigerina bulloides*)  $\delta^{18}\text{O}$  record of core MD97-2120 (25). (B)  $\delta^{18}\text{O}_b$  record of core MD97-2120 measured on *Cibicides* spp. and supplemented by analyses on *M. barleeanum* and *B. aculeata* (9). (C) Antarctic Vostok deuterium ( $\delta\text{D}$ ) record (13). (D) *G. bulloides* SST<sub>Mg/Ca</sub> (25) and (E)  $\delta^{13}\text{C}_b$  of core MD97-2120. (F) Glacial terminations of the  $\delta^{13}\text{C}_b$  record from South Atlantic Site 1089 (35). Insets during MIS 5 are a  $\delta^{13}\text{C}_b$  section and ice-rafted debris (IRD) record from the deep North Atlantic (NEAP 18K) (46). The NEAP-18K age scale is adjusted to that of core MD97-2120 using benthic  $\delta^{18}\text{O}$ .

Vertical gray bars mark times of reduced North Atlantic deepwater formation associated with increased meltwater influx into the northern North Atlantic [H-events: H1 to H6 (40), h8 to h13 (47), H12 and H13 (48)] and North Atlantic cold events C20 to C24 between 75 and 110 ky B.P. (46). Gray arrows mark negative  $\delta^{13}\text{C}_b$  anomalies at the end of glacial terminations in core MD97-2120 and at Site 1089. Brackets indicate positive  $\delta^{13}\text{C}_b$  excursions during glacial terminations. Age control points are shown along the bottom axis:  $^{14}\text{C}$  AMS dates (green), Kawakawa tephra (red),  $\delta^{18}\text{O}_b$  tie-points to North Atlantic core MD95-2042 (blue), and SST<sub>Mg/Ca</sub> tie-points to the Vostok deuterium record (black) (9, 25). Alternate “SFCP” age scale at bottom is from (49) [see (9)]. Glacial terminations I to IV are labeled T1 to TIV.

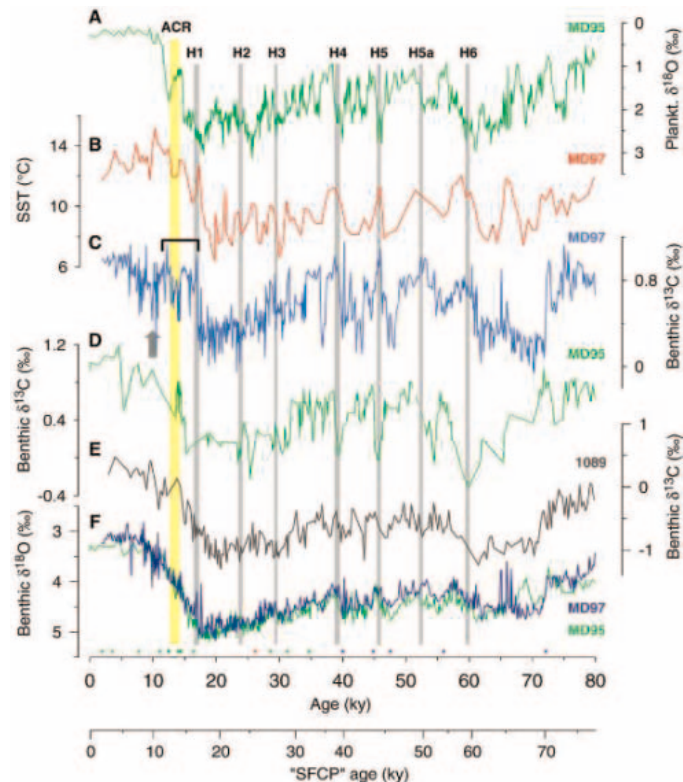
Atlantic salt inventories and, ultimately, stabilizing the NADW “off” mode.

**Glacial terminations.** Abrupt changes also mark the end of glacial periods as climate shifted to its warm mode. Abrupt increases in  $\delta^{13}\text{C}_b$  occur early in the deglacial phase, when values increase by up to 0.8‰ within as little as 200 to 700 years (Fig. 4). These sudden shifts span most of the total glacial-interglacial  $\delta^{13}\text{C}_b$  amplitude, but they lag the likewise abrupt warming seen in the planktonic SST<sub>Mg/Ca</sub> profile by some 1 to 3 ky. The delayed response of initial mid-depth ventilation increase to Southern Hemisphere warming points to transient inertia of buoyancy budgets across the SAZ, plausibly caused by enhanced northward meltwater fluxes and reduced southward salt transports in the subtropical gyre during large-scale deglacial warming.

Once started, AAIW production was closely coupled with rapid climatic rebounds in both hemispheres. The sequence of negative and positive  $\delta^{13}\text{C}_b$  anomalies during TI (labeled 1 to 3 in Fig. 4) is tied to the North Atlantic H-event 1 [H1, <17.6 ky B.P. (40)], the Antarctic cold reversal [ACR, 14.1 ky B.P. (38)], and the subsequent Younger Dryas cold spell (YD, 13 ky B.P.). Within this TI sequence, the Northern Hemisphere cold episodes (H1 and YD) consistently correlate with  $\delta^{13}\text{C}_b$  maxima in our record, whereas the Southern Hemisphere ACR is marked by a salient  $\delta^{13}\text{C}_b$  minimum (Fig. 4A). A similar alternation between positive and negative mid-depth  $\delta^{13}\text{C}_b$  excursions and anticorrelation with North Atlantic deepwater  $\delta^{13}\text{C}_b$  (41) is seen during TII and TIII in association with two-step warmings that are interrupted by midtermination cold events in the Southern Hemisphere (25, 42) (Fig. 4, B and C). Coupling of the  $\delta^{13}\text{C}_b$  swings with temperature in the south confirms the pattern observed along the rest of the records that links positive/negative  $\delta^{13}\text{C}_b$  anomalies with warm/cold climates on orbital and suborbital time scales. The ventilation minimum in the south during the ACR correlates with strengthened NADW formation during the Northern Hemisphere Bølling/Allerød (B/A) warm period (7), whereas the subsequent  $\delta^{13}\text{C}_b$  increase coincides with the YD cold reversal when NADW production was reduced. Such anticorrelation of water mass conversion during deglaciations corroborates similar phasing of NADW and AAIW production observed during glacial and interglacial periods and demonstrates bipolar anticorrelation of THC forcing to be a persistent feature across different climate states.

The final phases of the glacial terminations are marked by brief negative  $\delta^{13}\text{C}_b$  anomalies during or immediately after early-interglacial peak warmth (Fig. 4). These anomalies are exceptional in that they document ventilation minima during Southern Hemisphere warm episodes, whereas along the rest of the record ventilation minima correlate with cold events.

**Fig. 3.** Paleoceanographic records along core MD97-2120 for the past 80 ky compared with benthic and planktonic stable isotope records from deepwater North Atlantic core MD95-2042 (14, 37) and South Atlantic Site 1089 (35). (A) Planktonic  $\delta^{18}\text{O}$  record from core MD95-2042. (B) SST<sub>Mg/Ca</sub> and (C)  $\delta^{13}\text{C}_b$  records of core MD97-2120. (D and E)  $\delta^{13}\text{C}_b$  records of North Atlantic core MD95-2042 and South Atlantic Site 1089, respectively. (F)  $\delta^{18}\text{O}_b$  records from MD97-2120 (blue) and MD95-2042 (green) for stratigraphic control. Gray bars, age control points, and secondary age axis as in Fig. 2. Yellow bar marks the ACR in SST<sub>Mg/Ca</sub> and the concomitant negative  $\delta^{13}\text{C}_b$  anomaly in core MD97-2120. Note correlation of positive  $\delta^{13}\text{C}_b$  excursions during H-events in core MD97-2120 with negative  $\delta^{13}\text{C}_b$  anomalies in core MD95-2042 and at Site 1089. Bracket marks the abrupt increase and positive  $\delta^{13}\text{C}_b$  plateau during the deglaciation; arrow indicates negative post-termination  $\delta^{13}\text{C}_b$  anomaly in core MD97-2120. Alternate “SFCP” age scale at bottom is from (49) [see (9)].



Similar peak-interglacial ventilation minima are indicated at a bottom-water core site in the South Atlantic (ODP 1089, 4621-m water depth) (Fig. 2) (22, 35), which suggests that the events affected the entire water column at high southern latitudes. We are not aware of similar  $\delta^{13}\text{C}_b$  anomalies at core sites upstream along the deep-water flow path in the Atlantic basin (14, 41), which suggests that the anomalies were forced regionally in the Southern Ocean. Teleconnections with coeval maxima in tropical monsoons and reduced southward salt transports may be indicated, plausibly in connection with northward displacements of the intertropical convergence zone that drives precipitation patterns, and thus ocean salt budgets, in the tropics.

The high-amplitude variability seen along our records demonstrates that water mass conversion in the Southern Hemisphere oceans is as sensitive to rapid climate change as in the North Atlantic. Although this does not seem unexpected, it casts new light on the role of Southern Hemisphere ocean THC in climate change. The incursion of abrupt increases of AAIW renewal during periods of thermohaline slowdown in the North Atlantic is intriguing in that it demonstrates synchronicity of changing THC forcing in both hemispheres. The lack of high-resolution records from other sectors of the Southern Ocean does not enable us to unambiguously assess whether the abrupt swings document changes of localized convection in the

South Pacific or whether they are representative of mid-depth ventilation changes in wider SAZ. Yet, antiphased  $\delta^{13}\text{C}_b$  patterns between the hemispheres during some glacial, interglacial, and deglacial periods (Figs. 2, 3, and 4) suggest that the THC seesaw operated across different climate states and is a robust feature of the global THC. This then raises the possibility that decreasing AAIW production that is observed during the past few decades (43), through its influence on basin-wide salt budgets and density gradients (4, 6, 7), will have the potential to stabilize thermohaline overturn in the North Atlantic, with implications for climate stability in the course of increasing atmospheric greenhouse-gas concentrations and global warming.

#### References and Notes

1. G. C. Bond *et al.*, *Nature* **365**, 143 (1993).
2. S. Rahmstorf, *Clim. Dyn.* **12**, 799 (1996).
3. D. Seidov, E. Barron, B. J. Haupt, *Global Planet. Change* **30**, 257 (2001).
4. R. F. Keeling, B. B. Stephens, *Paleoceanography* **16**, 112 (2001).
5. G. Knorr, G. Lohmann, *Nature* **424**, 532 (2003).
6. O. A. Saenko, A. J. Weaver, J. M. Gregory, *J. Clim.* **16**, 2797 (2003).
7. A. J. Weaver, O. A. Saenko, P. U. Clark, J. X. Mitrovica, *Science* **299**, 1709 (2003).
8. B. M. Sloyan, S. R. Rintoul, *J. Phys. Oceanogr.* **31**, 1005 (2001).
9. Supporting material is available on Science Online.
10. J. Imbrie *et al.*, in *Milankovitch and Climate, Part 1*, A. L. Berger, J. Imbrie, J. Hays, G. Kukla, B. Saltzman, Eds. (D. Reidel Publishing Company, Dordrecht, Netherlands, 1984), pp. 269–305.

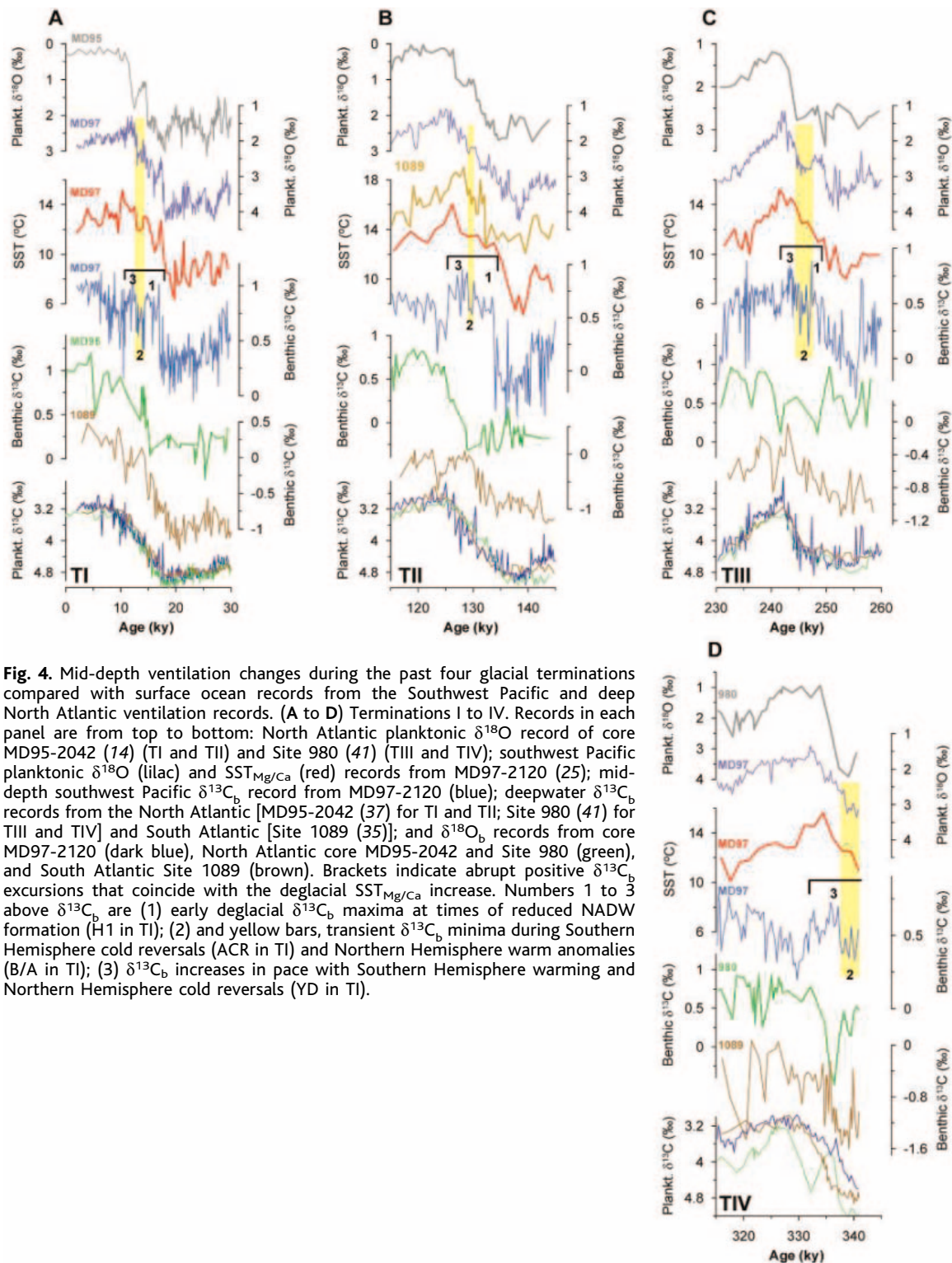


**Fig. 4.** Mid-depth ventilation changes during the past four glacial terminations compared with surface ocean records from the Southwest Pacific and deep North Atlantic ventilation records. (A to D) Terminations I to IV. Records in each panel are from top to bottom: North Atlantic planktonic  $\delta^{18}\text{O}$  record of core MD95-2042 (14) (TI and TII) and Site 980 (41) (TIII and TIV); southwest Pacific planktonic  $\delta^{18}\text{O}$  (lilac) and SST<sub>Mg/Ca</sub> (red) records from MD97-2120 (25); mid-depth southwest Pacific  $\delta^{13}\text{C}_b$  record from MD97-2120 (blue); deepwater  $\delta^{13}\text{C}_b$  records from the North Atlantic [MD95-2042 (37) for TI and TII; Site 980 (41) for TIII and TIV] and South Atlantic [Site 1089 (35)]; and  $\delta^{18}\text{O}_b$  records from core MD97-2120 (dark blue), North Atlantic core MD95-2042 and Site 980 (green), and South Atlantic Site 1089 (brown). Brackets indicate abrupt positive  $\delta^{13}\text{C}_b$  excursions that coincide with the deglacial SST<sub>Mg/Ca</sub> increase. Numbers 1 to 3 above  $\delta^{13}\text{C}_b$  are (1) early deglacial  $\delta^{13}\text{C}_b$  maxima at times of reduced NADW formation (H1 in TI); (2) and yellow bars, transient  $\delta^{13}\text{C}_b$  minima during Southern Hemisphere cold reversals (ACR in TI) and Northern Hemisphere warm anomalies (B/A in TI); (3)  $\delta^{13}\text{C}_b$  increases in pace with Southern Hemisphere warming and Northern Hemisphere cold reversals (YD in TI).

11. D. P. Schrag *et al.*, *Quat. Sci. Rev.* **21**, 331 (2002).
12. C. Waelbroeck *et al.*, *Quat. Sci. Rev.* **21**, 295 (2002).
13. J. R. Petit *et al.*, *Nature* **399**, 429 (1999).
14. N. J. Shackleton, M. A. Hall, E. Vincent, *Paleoceanography* **15**, 565 (2000).
15. E. J. Rohling, R. Marsh, N. C. Wells, M. Siddall, N. R. Edwards, *Nature* **430**, 1016 (2004).
16. M. Siddall *et al.*, *Nature* **423**, 853 (2003).
17. P. M. Kroopnick, *Deep-Sea Res.* **32**, 57 (1985).
18. A. Mackensen, H. W. Hubberten, T. Bickert, G. Fischer, D. K. Fuetterer, *Paleoceanography* **8**, 587 (1993).
19. W. S. Broecker, E. Maier-Reimer, *Global Biogeochem. Cycles* **6**, 315 (1992).
20. R. Zahn *et al.*, *Paleoceanography* **12**, 696 (1997).
21. J. C. Duplessy *et al.*, *Paleoceanography* **3**, 343 (1988).
22. D. A. Hodell, K. A. Venz, C. D. Charles, U. S. Ninnemann, *Geochem. Geophys. Geosyst.* **4**, 1004 (2003).
23. U. S. Ninnemann, C. D. Charles, *Earth Planet. Sci. Lett.* **201**, 383 (2002).
24. H. C. Bostock, B. N. Opdyke, M. K. Gagan, L. K. Fifield, *Paleoceanography* **19**, doi: 10.1029/2004PA001047 (2004).
25. K. Pahnke, R. Zahn, H. Elderfield, M. Schulz, *Science* **301**, 948 (2003).
26. S. R. Rintoul, M. H. England, *J. Phys. Oceanogr.* **32**, 1308 (2002).
27. L. D. Talley, in *Mechanisms of Global Climate Change at Millennial Time Scales*, P. U. Clark, R. S. Webb, L. D. Keigwin, Eds. (American Geophysical Union, Washington, DC, 1999), vol. 112, pp. 1–21.
28. A. R. Piola, D. T. Georgi, *Deep-Sea Res.* **29**, 687 (1982).
29. J. Ribbe, *Geophys. Res. Lett.* **28**, 535 (2001).

30. R. Gersonde *et al.*, *Paleoceanography* **18**, 1061 (2003).  
 31. A. Shemesh, L. H. Burckle, J. D. Hays, *Science* **266**, 1542 (1994).  
 32. D. M. Sigman, E. A. Boyle, *Nature* **407**, 859 (2000).  
 33. I. R. Hall, I. N. McCave, N. J. Shackleton, G. P. Weedon, S. E. Harris, *Nature* **412**, 809 (2001).  
 34. C. D. Charles, S. J. Lynch, U. S. Ninnemann, R. G. Fairbanks, *Earth Planet. Sci. Lett.* **142**, 19 (1996).  
 35. P. G. Mortyn, C. D. Charles, U. S. Ninnemann, K. Ludwig, D. A. Hodell, *Geochem. Geophys. Geosyst.* **4**, 8405 (2003).  
 36. L. D. Stott, C. Poulsen, S. Lund, R. Thunell, *Science* **297**, 222 (2002).  
 37. N. J. Shackleton, *Pangaea*, <http://doi.pangaea.de/10.1594/PANGAEA.58229> (2001).  
 38. T. Blunier, E. J. Brook, *Science* **291**, 109 (2001).  
 39. T. F. Stocker, *Science* **282**, 61 (1998).  
 40. H. Rashid, R. Hesse, D. J. W. Piper, *Paleoceanography* **18**, 1077 (2003).  
 41. J. F. McManus, D. W. Oppo, J. L. Cullen, *Science* **283**, 971 (1999).  
 42. G. Cortese, A. Abelmann, *Palaeogeogr. Palaeoclim. Palaeoecol.* **182**, 259 (2002).  
 43. A. P. S. Wong, N. L. Bindoff, J. A. Church, *Nature* **400**, 440 (1999).  
 44. R. Schlitzter, *Eos Trans. AGU* **81**, 45 (2000).  
 45. K. Speer, S. R. Rintoul, B. Sloyan, *J. Phys. Oceanogr.* **30**, 3212 (2000).  
 46. M. R. Chapman, N. J. Shackleton, *Geology* **27**, 795 (1999).  
 47. S. A. van Kreveld, M. Knappertsbusch, J. Ottens, G. M. Ganssen, J. E. van Hinte, *Mar. Geol.* **131**, 21 (1996).  
 48. R. N. Hiscott, A. E. Aksu, P. J. Mudie, D. F. Parsons, *Global Planet. Change* **28**, 227 (2001).  
 49. N. J. Shackleton, R. G. Fairbanks, T.-C. Chiu, F. Parrenin, *Quat. Sci. Rev.* **23**, 1513 (2004).  
 50. The sediment core for this study was obtained through the International Marine Global Change Studies (IMAGES) project. We thank the Institut Polaire Français Paul Emile Victor (IPEV) for technical support and for making the research vessel *Marion Dufresne* available for core retrieval. We are particularly indebted to Y. Balut and his team for their expert skills in designing

and running the long Calypso piston corer. Financial support from the Deutsche Forschungsgemeinschaft contributed to the coring campaign. Special thanks go to G. Bianchi, Cardiff, for running the mass spectrometer and maintaining the high quality of data output. This work was supported by The Leverhulme Trust (UK) through grant F/407/J to R.Z. The data will be made available on the NOAA Paleoclimatology Web site ([www.ngdc.noaa.gov/paleo/data.html](http://www.ngdc.noaa.gov/paleo/data.html)) and in the PANGAEA database ([www.pangaea.de](http://www.pangaea.de)).

#### Supporting Online Material

[www.sciencemag.org/cgi/content/full/307/5716/1741/DC1](http://www.sciencemag.org/cgi/content/full/307/5716/1741/DC1)

Materials and Methods

SOM Text

Figs. S1 to S5

References

30 June 2004; accepted 24 January 2005

10.1126/science.1102163

## An Acylation Cycle Regulates Localization and Activity of Palmitoylated Ras Isoforms

Oliver Rocks,<sup>1,3</sup> Anna Peyker,<sup>3</sup> Martin Kahms,<sup>1</sup> Peter J. Vermeer,<sup>3</sup> Carolin Koerner,<sup>1</sup> Maria Lumbierres,<sup>2</sup> Jürgen Kuhlmann,<sup>1</sup> Herbert Waldmann,<sup>2</sup> Alfred Wittinghofer,<sup>1\*</sup> Philippe I. H. Bastiaens<sup>3\*</sup>

We show that the specific subcellular distribution of H- and Nras guanosine triphosphate-binding proteins is generated by a constitutive de/reacylation cycle that operates on palmitoylated proteins, driving their rapid exchange between the plasma membrane (PM) and the Golgi apparatus. Depalmitoylation redistributes farnesylated Ras in all membranes, followed by repalmitoylation and trapping of Ras at the Golgi, from where it is redirected to the PM via the secretory pathway. This continuous cycle prevents Ras from nonspecific residence on endomembranes, thereby maintaining the specific intracellular compartmentalization. The de/reacylation cycle also initiates Ras activation at the Golgi by transport of PM-localized Ras guanosine triphosphate. Different de/repalmitoylation kinetics account for isoform-specific activation responses to growth factors.

Signaling networks are spatially organized by the specific localization of their protein constituents to distinct protein scaffolds, membrane systems, or microdomains. The three abundant Ras guanosine triphosphate-binding proteins Hras, Nras, and Kras4B (1, 2) are a paradigm example of this spatial organization of signaling molecules. Although highly homologous and indistinguishable in most in vitro assays, these proteins have been shown to produce isoform-specific biological outputs, attributed to differences in plasma membrane (PM) and subcellular membrane localization. Their distribution is determined by different C-terminal

lipid modifications. Posttranslationally modified Hras and Nras localize to the PM and to Golgi membranes, whereas Kras is apparently confined to the PM. The isoforms take different trafficking routes during posttranslational maturation. All isoforms undergo three steps of modification of the C-terminal CAAX motif (3), including farnesylation of the CAAX cysteine (4) in the cytosol, AAX proteolysis (5), and methylation of the farnesylated cysteine (6) on the endoplasmic reticulum (ER). Farnesylation alone cannot stably anchor proteins to lipid bilayers (7). Nras and Hras are further modified with palmitate moieties that are attached to one or two cysteines, respectively. Both fully posttranslationally modified isoforms access the PM from the surface of the ER via the secretory pathway (8, 9). Kras bypasses the secretory pathway and exits the ER toward the PM without further lipid modification. A polybasic sequence near the C terminus allows stable interaction with anionic

phospholipids at the inner leaflet of the PM. Unlike farnesylation, palmitoylation is reversible. The localization and mechanism of the latter lipid modification reaction in mammals is currently unclear, as both enzymatic and nonenzymatic processes are debated (10).

A long-held view has been that Ras only operates at the PM. Recent publications, however, have pointed out the importance of Ras compartmentalization for signal transduction (11, 12). The Ras Golgi pool might represent a signaling entity separate from the PM, with distinct activation kinetics and signal propagation (12, 13). Growth factor-induced Golgi Hras activation occurs independently of PM Hras and involves a pathway containing Src family kinases, phospholipase C- $\gamma$  (PLC $\gamma$ ), and the Ras exchange factor RasGRP1 (14). A Golgi-resident mitogen-activated protein kinase scaffold (15), Sef, further supports this organelle as a signal platform. Yet it is unclear how cells achieve specific compartmentalized localization and regulate activity of palmitoylated Ras isoforms. Golgi Ras is believed to represent a trafficking intermediate of nascent protein en route to the PM, its ultimate target. However, considering the 1-day half-life of Ras (16) and exocytic transport on the time scale of 10 to 20 min (17), it is unlikely that a cell could uphold high Golgi Ras concentrations by the unidirectional transport model. Likewise, it is not clear how a cell prevents spillover of PM Ras to endomembranes, considering spontaneous intermembrane transfer (18) and continuous fusion and mixing of membranes (19). We show that the reversibility of palmitoylation is essential for maintaining specific localization of palmitoylated Ras isoforms to the PM and Golgi apparatus and has a role in the differential Ras isoform activity responses by regulating the partitioning between these compartments.

**Rapid retrograde trafficking of palmitoylated Ras isoforms from the PM to the Golgi apparatus.** Hras- or Nras-expressing cells were treated with a protein synthesis

<sup>1</sup>Department of Structural Biology, <sup>2</sup>Department of Chemical Biology, Max Planck Institute for Molecular Physiology, Otto-Hahn-Straße 11, 44227 Dortmund, Germany. <sup>3</sup>European Molecular Biology Laboratory, Meyerhofstraße 1, 69117 Heidelberg, Germany.

\*To whom correspondence should be addressed. E-mail: [alfred.wittinghofer@mpi-dortmund.mpg.de](mailto:alfred.wittinghofer@mpi-dortmund.mpg.de) (A.W.) and [bastiaen@embl.de](mailto:bastiaen@embl.de) (P.I.H.B.)

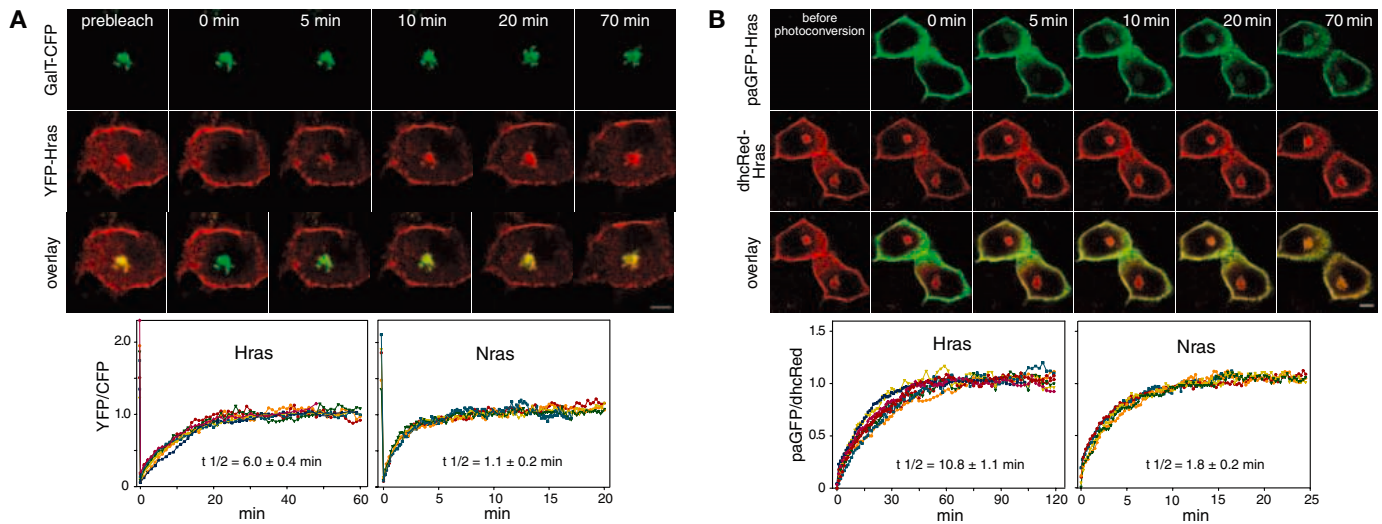


**Fig. 1.** Retrograde PM-Golgi trafficking of palmitoylated Ras. **(A)** (Top) MDCK cells expressing YFP-Hras were treated with 50  $\mu$ g/ml of cycloheximide for at least 2 hours before the experiment and maintained at 37°C. YFP fluorescence was bleached at 514 nm in a polygon comprising the Golgi area, as identified from GalT-CFP staining. Confocal images were obtained at the time points indicated. (Bottom) Binary masks obtained from thresholded GalT-CFP images were used to determine the YFP/CFP fluorescence ratio at the Golgi for Hras ( $n = 6$  cells) and Nras ( $n = 5$  cells) in MDCK cells at every time point after photobleaching. Individual experiments are represented by different colors. Plateau values were normalized to 1. **(B)** (Top) MDCK cells cotransfected with paGFP-Hras and dhcRed-Hras were briefly illuminated with 405-nm laser light in a region of interest comprising the lateral PM for paGFP photoconversion. paGFP and dhcRed fluorescence was imaged at the indicated time points. (Bottom) Ratiometrically determined increase in paGFP fluorescence intensities at the Golgi for Hras ( $n = 7$  cells) and Nras ( $n = 5$  cells) in MDCK cells. **(C)** (Top) MDCK cells coexpressing GalT-CFP and YFP-Hras after incubation with 50  $\mu$ M 2BP for 30 min. (Bottom) FRAP experiments in the presence of 2BP (red,  $n = 5$  cells) were compared to the experiments in (A) (black,  $n = 6$  cells). Results were normalized to prebleach values, because FRAP curves in 2BP-treated cells did not reach a plateau. wt, wild type. Scale bars, 8  $\mu$ m.

inhibitor to chase nascent proteins out of the secretory pathway. In contrast to earlier reports (8, 9), we observed extensive Golgi localization of both isoforms even after 12 hours of incubation with cycloheximide (fig. S1, A and B). Newly synthesized protein en route to the PM therefore does not solely account for Golgi-localized Ras. Fluorescence recovery after photobleaching (FRAP) experiments were performed to investigate if the Golgi Ras pool is a fraction of nascent protein that is temporally arrested at the Golgi during PM transport. Cells were transfected with the cyan fluorescent protein (CFP)-tagged Golgi marker GalT and either yellow fluorescent protein (YFP)-tagged Hras or Nras, then treated with cycloheximide. YFP fluorescence was then bleached at the Golgi, and the fluorescence recovery was determined ratiometrically (Fig. 1A). YFP-Hras Golgi fluorescence rapidly recovered with a half-time ( $t_{1/2}$ ) of  $6.0 \pm 0.4$  min in Madin-Darby canine kidney (MDCK) cells and  $6.3 \pm 0.3$  min in COS-7 cells (fig. S2B). Because a substantial quantity of total Ras fluorescence was irreversibly photo-

bleached at the Golgi, the extent of recovery depended on the relative Golgi volume of the individual cell observed. In COS-7 cells that have a much smaller relative Golgi volume, fluorescence recovery reached near-prebleach intensities, arguing against an immobilized fraction of Golgi Hras and suggesting an unhindered passage through this compartment. Reversibility of fluorescence as a cause of recovery at the Golgi could be ruled out, because YFP fluorescence recovered to not more than 3% of the initial intensity when the whole cell was bleached (20). Fluorescence recovery of monopalmitoylated YFP-Nras was almost six times faster than that of YFP-Hras, with a  $t_{1/2}$  of  $1.1 \pm 0.2$  min (Fig. 1A and fig. S2A). Thus, Golgi Ras is rapidly replenished by a protein pool present in the cell with kinetics that depend on the number of palmitoyl groups on the Ras isoforms.

To show that the Golgi pool is exchanged with protein from the PM, we fused a photoactivatable variant of green fluorescent protein (paGFP) (21) to Hras or Nras. paGFP-Hras or -Nras was selectively photoconverted at the

lateral PM with 405-nm laser light, and accumulation of fluorescence was tracked at the Golgi. Coexpression of Ras fused to a tandem construct of *Heteractis crispata* hcRed (dhcRed-Ras), displaying correct subcellular localization and a minimized tendency to aggregate (22), allowed for ratiometric normalization of the photoproduct signal. Hras appeared at the Golgi with a  $t_{1/2}$  of  $10.8 \pm 1.1$  min (Fig. 1B), which is on the same time scale as that observed in the FRAP experiments. Similarly, retrograde trafficking of Nras occurred six times faster, with a  $t_{1/2}$  of  $1.8 \pm 0.2$  min (Fig. 1B). Palmitoylated Ras thus cycles between the PM and the Golgi, with a retrograde transport of PM-localized protein replenishing the Golgi pool. This transport is constitutive and independent of Ras activation state, because the same Golgi FRAP kinetics are seen in cells expressing oncogenic YFP-Hras G12V or dominant-negative YFP-Hras S17N (fig. S3A) that is no longer capable of interacting with downstream effectors.

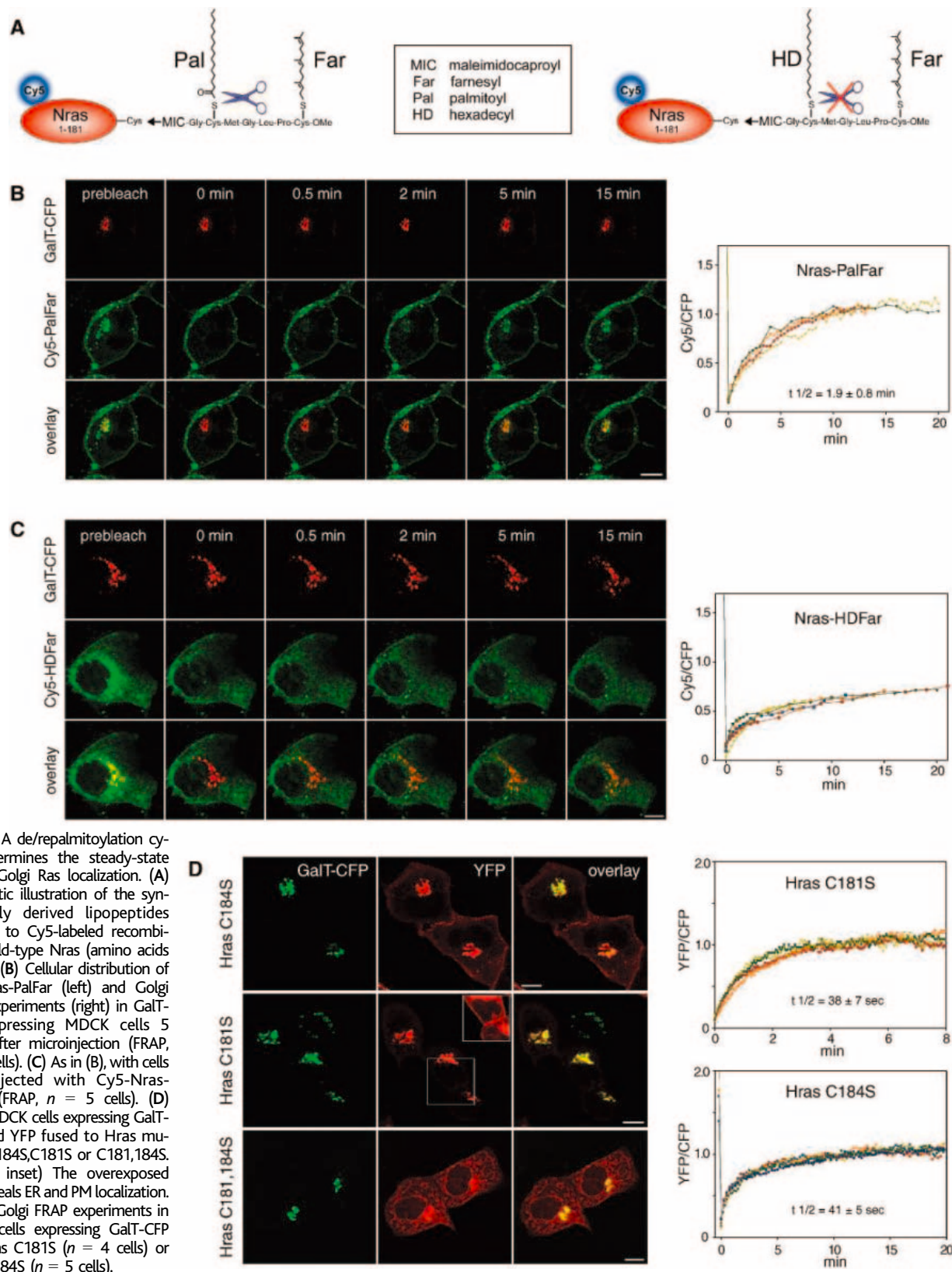
**A de/reacylation cycle is essential for specific PM or Golgi Ras localization.** An



extensive set of experiments revealed that this retrograde trafficking is not mediated by clathrin coat-based endocytosis or by caveolae- or cholesterol-dependent endocytic mechanisms (supporting online text) (fig. S4, A to

E). We therefore investigated if a sequence of depalmitoylation of Ras, redistribution to endomembranes, and repalmitoylation at the Golgi could account for the observed trafficking phenomenon, whereas spontaneous inter-

membrane transfer of dual lipid-anchored Ras peptides occurs on the order of hours (18), depalmitoylated Ras equilibrates in seconds between the aqueous and membrane phases (23), allowing rapid exchange between mem-



branes. A fusion of paGFP to farnesylated but not palmitoylated Hras C181,184S, which was selectively photoactivated in a restricted area of MDCK cells, indeed repartitioned to all membranes in less than a minute (fig. S5A). To inhibit protein palmitoylation, MDCK cells expressing GalT-CFP and YFP-Hras were incubated with 2-bromopalmitate (2BP) (24, 25). The fluorescence recovery kinetic of YFP-Hras at the Golgi under these conditions was greatly reduced and did not reach a plateau on the time scale observed for untreated cells (Fig. 1C). Because trapping at the Golgi did not occur, we observed only a slow increase in Golgi fluorescence in the FRAP curves because of the unspecific accumulation of depalmitoylated but still farnesylated Ras in all membranes. In a control experiment, we verified that 2BP did not block endocytosis under the same conditions (fig. S5B).

To obtain an independent proof for the requirement of de/repalmitoylation for retrograde Ras trafficking, we applied a chemical-biological approach by using two different synthetically lipidated Nras proteins: a palmitoylated control protein (PalFar) and a hexadecylated protein (HDFar) with a noncleavable thioether bond that cannot undergo de/reacylation. The synthesis of these lipidated Nras proteins was achieved by coupling their respective lipopeptides to Cy5-labeled, C-terminally truncated, recombinant Nras (Fig. 2A). The PalFar hybrid protein resembles full-length Nras, except for the nonpeptide maleimidocaproyl linker, and has been shown earlier to interact properly with effector proteins and to have activity in pheochromocytoma cell (PC12) differentiation assays comparable to that of

wild-type Ras (26). Indeed, the microinjected PalFar hybrid protein localized normally to PM and the Golgi and exhibited Golgi FRAP kinetics similar to those of YFP-Nras (Fig. 2B). Under the same conditions, the hexadecylated HDFar protein localized unspecifically to the entire membrane system and did not display restricted Golgi or PM localization, even 20 hours after injection (Fig. 2C). Specific Golgi recovery was not apparent in a FRAP experiment. Instead, the recovery was incomplete and biphasic, with only partial recovery on ER membranes colocalizing with the Golgi through lateral diffusion. These experiments show that retrograde PM-Golgi trafficking of Hras and Nras is mediated by depalmitoylation/repalmitoylation activities that act on Ras in different subcellular localizations. Together with the anterograde transport, which we further verified to occur via the secretory pathway (8) (supporting online text) (fig. S6, A to C), a cycle is generated that determines the specific PM and Golgi localization of Ras. This is in contrast to a model where the physicochemical properties of palmitate per se provide affinity for a particular membrane, allowing thermodynamic equilibrium binding. Without the de/reacylation cycle, palmitoylated Ras would incorrectly localize to any membrane compartment, as shown with the hexadecylated Nras protein.

**Monopalmitoylation results in faster PM-Golgi exchange and increased partitioning to the Golgi apparatus.** Because different kinetics of retrograde trafficking of monopalmitoylated Nras and dually palmitoylated Hras suggest that the speed of PM-Golgi exchange is dictated by the stability of

palmitate attachment, we investigated if monopalmitoylated Hras mutants resemble Nras in their de/reacylation characteristics. Indeed, Hras C184S displayed a pronounced Golgi localization similar to that of Nras and more extensive than that of wild-type Hras (Fig. 2D). Hras C181S nearly exclusively localized to the Golgi, with only a little material at the PM and on the ER. In contrast, nonpalmitoylated Hras C181,184S did not exhibit a preference for specific membrane systems and appeared on all endomembranes including the Golgi. Golgi FRAP experiments revealed that both monopalmitoylated mutants exhibited rapid fluorescence recovery kinetics, with a  $t_{1/2}$  of 38 s for Hras C181S and a  $t_{1/2}$  of 41 s for Hras C184S (Fig. 2D). In agreement, earlier pulse-chase experiments have revealed a palmitate turnover six and four times faster for the respective mutants than for wild-type Hras (27, 28). The nearly exclusive Golgi localization of the least stable palmitoylated Hras C181S suggests that palmitoylation is confined to the Golgi and is rapid relative to depalmitoylation and endomembrane repartitioning, because otherwise the protein would accumulate on endomembranes.

**The de/reacylation cycle acts on N- and C-terminally palmitoylated peptide sequences.** Both the minimal Hras membrane-targeting domain comprising the C-terminal nine amino acids of Hras [YFP-th (9)] and a geranylgeranylated Hras mutant exhibiting the C-terminal CAAX box of Rap1a (YFP-Hras-CLLL) (29) revealed Golgi fluorescence recovery kinetics similar to those of wild-type Hras (fig. S3, B and C). Thus, neither the Ras G domain nor specific farnesylation is required for retrograde Ras trafficking. We

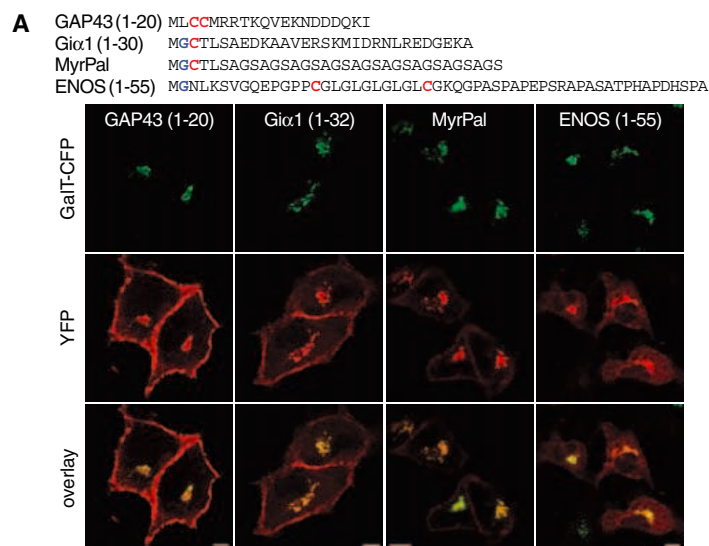
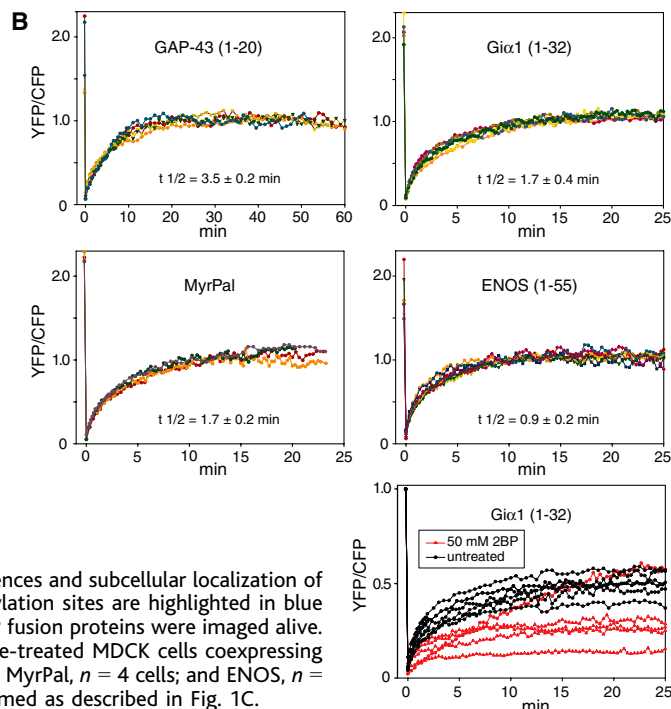


**Fig. 3.** N-terminal palmitoylated peptides cycle by de/reacylation. (A) Sequences and subcellular localization of different N-terminally palmitoylated peptides. Myristoylation and palmitoylation sites are highlighted in blue and red, respectively. MDCK cells expressing GalT-CFP and the indicated YFP fusion proteins were imaged alive. Scale bars, 8  $\mu$ m. (B) Results from Golgi FRAP experiments in cycloheximide-treated MDCK cells coexpressing GalT-CFP and the indicated constructs (GAP43,  $n = 4$  cells; Gi $\alpha$ 1,  $n = 6$  cells; MyrPal,  $n = 4$  cells; and ENOS,  $n = 5$  cells). FRAP experiments in the presence of 2BP ( $n = 5$  cells) were performed as described in Fig. 1C.



then investigated if N-terminal palmitoylated proteins are likewise controlled in their subcellular distribution by dynamic palmitoylation. A variety of these proteins have been

reported to localize to the Golgi and PM, similar to C-terminally palmitoylated Ras (30). Four different palmitoylated N-terminal sequences were probed: GAP43-YFP (amino

acids 1 to 20);  $G_{i\alpha 1}$ -YFP (amino acids 1 to 32); MyrPal-YFP, an artificial myristoylated and palmitoylated sequence of 33 amino acids (31); and eNOS-YFP (endothelial NO-synthase, amino acids 1 to 55). All proteins displayed substantial Golgi staining and a varying extent of PM localization (Fig. 3A). Golgi FRAP experiments in the presence of cycloheximide revealed recovery kinetics similar to those observed with the different Ras isoforms and mutants. Moreover, inhibition of palmitoylation by 2BP resulted in a decreased fluorescence recovery (Fig. 3B). The FRAP kinetics again correlated with the extent of PM localization and thus might reflect the stability of palmitoylation. Dually palmitoylated GAP43, like Hras, was almost equally distributed between the Golgi and PM and recovered slowest ( $t_{1/2} = 3.5 \pm 0.2$  min). Monopalmitoylated  $G_{i\alpha 1}$  and MyrPal, like Nras, recovered faster, and their PM localization was less pronounced than that of GAP43. ENOS displayed only little PM staining and recovered fastest. Although eNOS contains two palmitoylation sites, the fast kinetics might reflect inefficient acylation, because it has been shown earlier that the efficiency of acylation is dependent on the proximity of the reactive thiol to the membrane (31, 32).

From these experiments, we propose a universal role for the de/reacylation cycle in targeting and dynamically distributing palmitoylated proteins to the PM and the Golgi. The lack of any apparent recognition sequences, together with the experiments with hexadecylated Nras and 2BP, strongly argues against the involvement of additional proteins facilitating membrane redistribution.

**The lipid modification cycle initiates Golgi Ras activation.** We investigated if retrograde Ras trafficking also accounts for net transport of PM Ras-GTP and thereby for active Golgi Ras after growth factor stimulation. A quantitative assay was developed to compare Ras activation dynamics in both compartments. In this assay, Ras-GTP is detected by its interaction with the Ras binding domain of Raf (RafRBD) through fluorescence resonance energy transfer (FRET) between YFP on Ras and  $\text{dChcRed}$  on RafRBD (Fig. 4A). Measuring FRET by the change in the fluorescence lifetime of the YFP donor with fluorescence lifetime imaging microscopy (FLIM), we can determine the molar fraction of Ras-GTP at each microscopically resolvable volume element (33). The selective occurrence of FRET between YFP and  $\text{dChcRed}$  upon Ras-RafRBD interaction, as measured by FLIM, has been validated by acceptor photobleaching (34) (fig. S7A). In agreement with previous experiments (12), this assay showed that Hras was rapidly and transiently activated at the plasma membrane after growth factor stimulus, whereas Golgi activation is delayed (by 10 to 20 min) and sustained (Fig. 4B). Importantly, the FLIM experiments demon-

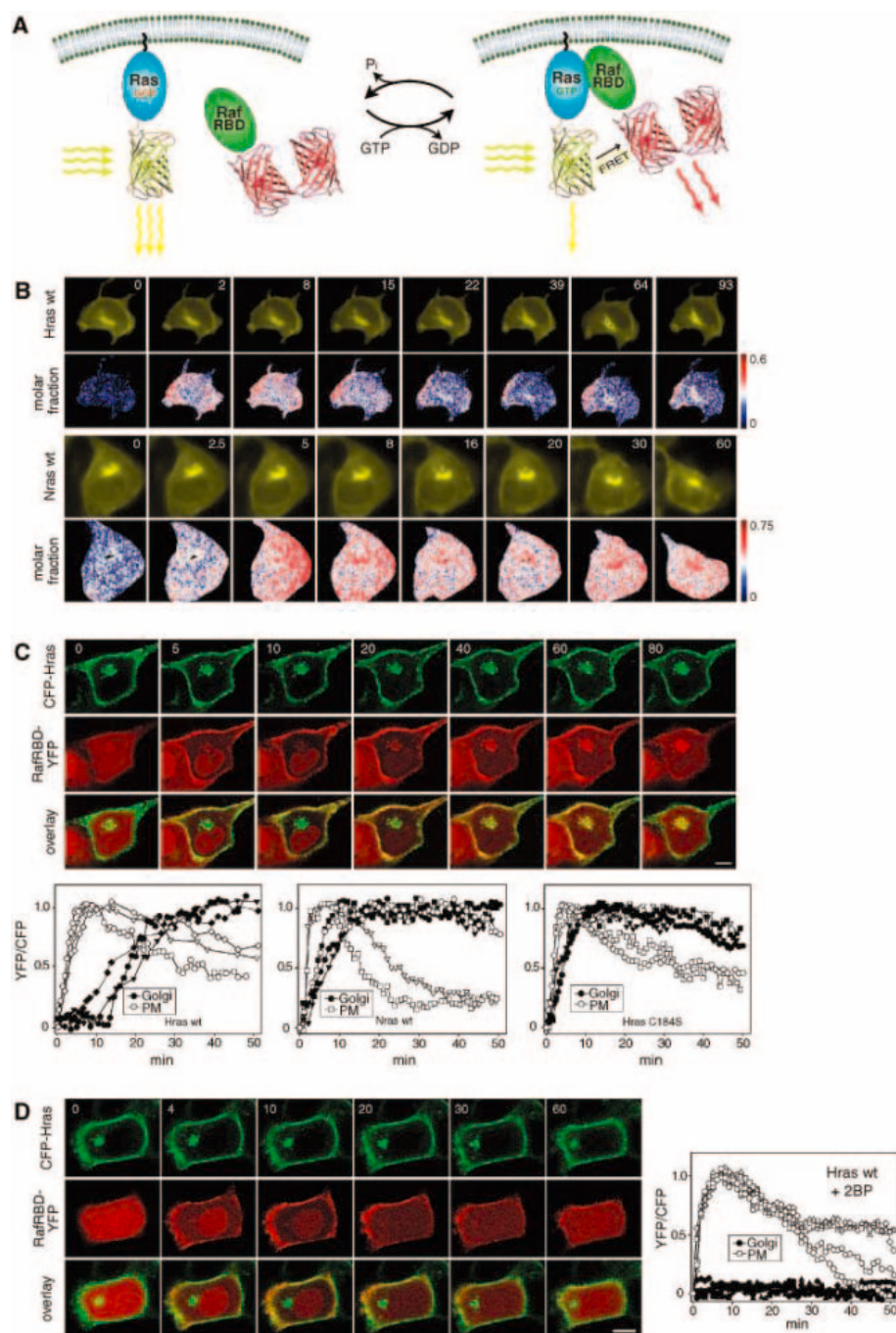


**Fig. 4.** The de/reacylation initiates Golgi Ras activation. (A) Schematic illustration of the FRET-FLIM-based Ras activation sensor. GDP, guanosine diphosphate; RBD, Ras binding domain; GTP, guanosine triphosphate; P<sub>i</sub>, phosphate. (B) FLIM-derived images of molar fractions of active Ras in MDCK cells coexpressing RafRBD-dChcRed and either YFP-Hras or YFP-Nras, after stimulation with 100 ng/ml EGF. Color bars: Calculated molar fraction of Ras-GTP. (C) (Top) EGF-induced membrane translocation of RafRBD-YFP in MDCK cells coexpressing CFP-Hras. (Bottom) Ratiometrical quantification of RafRBD-YFP translocation to the PM or the Golgi in MDCK cells cotransfected with wild-type CFP-Hras, wild-type CFP-Nras, or CFP-Hras C184S ( $n = 3$  cells, represented by triangles, circles, and squares). Solid symbols, Golgi apparatus; open symbols, PM. (D) (Left) EGF-induced membrane translocation of RafRBD-YFP in 2BP-treated MDCK cells coexpressing CFP-Hras. (Right) Ratiometrical quantification of RafRBD-YFP translocation to the PM or the Golgi ( $n = 5$  cells, each represented by different symbols). Solid symbols, Golgi apparatus; open symbols, plasma membrane.

strate that a large fraction of all Golgi Ras is activated after epidermal growth factor (EGF) stimulus. Hras activation kinetics were also monitored by tracking EGF-induced translocation of RafRBD-YFP to the PM or the Golgi in MDCK cells. Coexpression of CFP-Hras allowed ratiometric normalization to account for changes in local Ras concentration over time. PM Hras activation occurred with a  $t_{1/2}$  of  $2.9 \pm 0.6$  min, whereas Golgi Hras activation displayed a  $t_{1/2}$  of  $16.5 \pm 4.0$  min (Fig. 4C), resulting in a substantial delay of Golgi Hras activation ( $\Delta t_{1/2} = 13.6 \pm 4.0$  min).

In contrast, activation of Nras or Hras C184S at the Golgi was detectable at markedly earlier time points and almost paralleled PM Ras activation in the FLIM assay (Fig. 4B and fig. S7C). Likewise, Golgi translocation of RafRBD-YFP occurred with a  $\Delta t_{1/2}$  of only  $2.3 \pm 1.0$  min or  $1.9 \pm 1.2$  min in cells coexpressing the CFP fusions of Nras or Hras C184S, respectively (Fig. 4C and fig. S7B). Thus, the different time scales of retrograde PM to Golgi trafficking for the different palmitoylated Ras proteins correlate with their respective Golgi activation kinetics. We therefore investigated if inhibition of protein palmitoylation blocks Golgi Ras activation. Upon EGF stimulus, exclusive PM but no Golgi translocation of RafRBD-YFP was observed in cells coexpressing CFP-Hras that were pretreated with 2BP (Fig. 4D). Likewise, the fraction of active Golgi Ras was markedly reduced in the FLIM assay (fig. S7D). Taking together the findings that the faster retrograde Golgi trafficking of Nras or monopalmitylated Hras correlates with their faster Golgi activation kinetics and that inhibition of retrograde trafficking blocks Golgi Ras activation, we conclude that a de/reacylation-driven transport of Ras-GTP from the PM accounts for initiation of Golgi Ras activity upon growth factor stimulation.

**Discussion.** A continuous cycle of de- and reacylation reactions accounts for the specific localization of palmitoylated Ras isoforms to the PM and Golgi apparatus and drives the rapid exchange of both protein pools. After depalmitoylation of fully lipid modified Ras, the still-farnesylated protein equilibrates between membranes and cytosol, allowing rapid redistribution to any cellular membrane. Stable membrane anchorage by repalmitoylation then occurs at the Golgi, where Ras is captured in the bulk-flow exocytic pathway redirecting the protein to the PM. This mechanism confers high accuracy in protein localization, because any spillover into other membrane compartments is prevented by the de/reacylation cycle that continuously resets the system. The precise localization is lost when the palmitate thioester is changed to a thioether bond that cannot undergo dynamic palmitoylation. The de/reacylation cycle not only occurs on Ras but acts on both N- and C-terminal palmitoylated

peptide sequences. We therefore propose that the localization of peripheral membrane proteins is universally regulated by the de/reacylation cycle, provided that no other subcellular targeting mechanisms prevent access to this lipidation cycle. This mechanism could allow proper targeting of other palmitoylated proteins to distinct PM sites in polarized cells. These proteins will continuously have access to the sorting compartment and subsequently enter distinct post-Golgi trafficking pathways that could be specified by additional protein interactions (35). This localized bilayer trapping and release in different subcellular membrane compartments, governed by kinetic rather than thermodynamic factors (36), is a mechanism to generate compartmentalization of peripheral membrane proteins. Although these proteins are targeted into two separated membrane systems, the mechanism allows communication between both protein pools.

The lack of any apparent recognition signature for de/reacylation argues against the involvement of mammalian palmitoyltransferases (PATs) with unique sets of substrates, such as the recently reported yeast PATs Akrl and Erf2/Erf4 (37, 38). Alternatively, a very large family of similar specific PATs must exist. In a different scenario, palmitoylation might require a cysteine residue in membrane proximity, an environment that favors the formation of a thiolate ion in the cysteine to be acylated (39), and locally accessible acyl-coenzyme A (CoA). Transfer of the latter may be facilitated by acyl donor proteins (40) or by release of palmitoyl-CoA from acyl-CoA binding proteins, both on Golgi membranes.

A constitutive de/reacylation cycle accounts for transport of PM Ras-GTP to the Golgi after growth factor stimulation, and this is essential for initiation of Golgi Ras activation. This is distinct from but does not exclude a Golgi Ras activation mechanism involving the receptor tyrosine kinase (RTK)/Src/PLC $\gamma$ /Ca $^{2+}$ /RasGRP1 pathway that was postulated to be separate from PM Ras activation through RTK/SOS (14). Because activation at the Golgi is prolonged in contrast to transient activation at the PM and because both compartments continuously exchange Ras through the de/reacylation cycle, an amplification through a positive feedback loop at the Golgi is likely to maintain local Ras activity after the initial triggering signal has vanished. A feedback mechanism for Ras activity involving Ras-GTP-induced exchange factor activation has been described (41).

By net transport of PM Ras-GTP, a cell can generate acute signaling at the PM in the context of receptor activation and initiate sustained signaling at the Golgi in a topologically separated membrane environment using the same signaling molecule. The stability of palmitate attachment, i.e., dual versus monopalmitylation, thereby dictates the steady-state

distribution and the speed of exchange of the PM and Golgi pools. This in turn allows fine-tuning of both the amplitude and the duration of signaling from each of the two compartments and thus determines which of the two protein pools will generate a stronger signaling output. Monopalmitylated Nras displays a more pronounced Golgi localization, a faster retrograde PM-to-Golgi trafficking, and a several-fold shorter PM dwell time as compared to dually palmitoylated Hras. As a consequence, a larger fraction of Nras will exhibit prolonged activation patterns at the Golgi relative to Hras. This might cause Nras to couple more efficiently into Golgi-specific signaling pathways, as was recently shown for Erk1/2 activation in T cells (13). In addition, because of its fast palmitate turnover, Nras might have no access to the endosomal compartment, thereby adding another aspect of putative isoform-specific, compartmentalized signaling.

## References and Notes

1. J. R. Silvius, *J. Membr. Biol.* **190**, 83 (2002).
2. J. F. Hancock, *Nature Rev. Mol. Cell Biol.* **4**, 373 (2003).
3. D. R. Lowy, B. M. Willumsen, *Nature* **341**, 384 (1989).
4. J. F. Hancock, A. I. Magee, J. E. Childs, C. J. Marshall, *Cell* **57**, 1167 (1989).
5. W. K. Schmidt, A. Tam, K. Fujimura-Kamada, S. Michaelis, *Proc. Natl. Acad. Sci. U.S.A.* **95**, 11175 (1998).
6. Q. Dai et al., *J. Biol. Chem.* **273**, 15030 (1998).
7. J. F. Hancock, H. Paterson, C. J. Marshall, *Cell* **63**, 133 (1990).
8. E. Choy et al., *Cell* **98**, 69 (1999).
9. A. Apolloni, I. A. Prior, M. Lindsay, R. G. Parton, J. F. Hancock, *Mol. Cell. Biol.* **20**, 2475 (2000).
10. J. E. Smotrys, M. E. Linder, *Annu. Rev. Biochem.* **73**, 559 (2004).
11. S. Roy, B. Wyse, J. F. Hancock, *Mol. Cell. Biol.* **22**, 5128 (2002).
12. V. K. Chiu et al., *Nature Cell Biol.* **4**, 343 (2002).
13. I. Perez de Castro, T. G. Bivona, M. R. Philips, A. Pellicer, *Mol. Cell. Biol.* **24**, 3485 (2004).
14. T. G. Bivona et al., *Nature* **424**, 694 (2003).
15. S. Torii, M. Kusakabe, T. Yamamoto, M. Maekawa, E. Nishida, *Dev. Cell* **7**, 33 (2004).
16. A. I. Magee, L. Gutierrez, I. A. McKay, C. J. Marshall, A. Hall, *EMBO J.* **6**, 3353 (1987).
17. K. Hirschberg et al., *J. Cell Biol.* **143**, 1485 (1998).
18. H. Schroeder et al., *Biochemistry* **36**, 13102 (1997).
19. R. G. Parton, K. Prydz, M. Bomsel, K. Simons, G. Griffiths, *J. Cell Biol.* **109**, 3259 (1989).
20. O. Rocks et al., unpublished data.
21. G. H. Patterson, J. Lippincott-Schwartz, *Science* **297**, 1873 (2002).
22. D. Gerlich et al., *Cell* **112**, 751 (2003).
23. J. R. Silvius, F. l'Heureux, *Biochemistry* **33**, 3014 (1994).
24. Y. Webb, L. Hermida-Matsumoto, M. D. Resh, *J. Biol. Chem.* **275**, 261 (2000).
25. D. Michaelson et al., *J. Cell Biol.* **152**, 111 (2001).
26. B. Bader et al., *Nature* **403**, 223 (2000).
27. J. Y. Lu, S. L. Hofmann, *J. Biol. Chem.* **270**, 7251 (1995).
28. Our FRAP experiments reveal a palmitate turnover 15 to 20 times faster than previously found in pulse-chase experiments. This discrepancy is most likely due to incomplete removal of radioactive material from the cell on the time scale of lipid turnover, resulting in substantial reincorporation of tritiated palmitate.
29. B. T. Kinsella, R. A. Erdman, W. A. Maltese, *Proc. Natl. Acad. Sci. U.S.A.* **88**, 8934 (1991).
30. M. J. Bijlmakers, M. Marsh, *Trends Cell Biol.* **13**, 32 (2003).
31. I. Navarro-Lerida, A. Alvarez-Barrientos, F. Gavilanes, I. Rodriguez-Crespo, *J. Cell Sci.* **115**, 3119 (2002).
32. A. ten Brinke et al., *Biochem. J.* **361**, 663 (2002).
33. P. J. Verwee, F. S. Wouters, A. R. Reynolds, P. I. Bastiaens, *Science* **290**, 1567 (2000).

34. P. I. Bastiaens, I. V. Majoul, P. J. Verwee, H. D. Soling, T. M. Jovin, *EMBO J.* **15**, 4246 (1996).
35. A. D. el Husseini, D. S. Bredt, *Nature Rev. Neurosci.* **3**, 791 (2002).
36. S. Shahinian, J. R. Silviu, *Biochemistry* **34**, 3813 (1995).
37. A. F. Roth, Y. Feng, L. Chen, N. G. Davis, *J. Cell Biol.* **159**, 23 (2002).
38. L. Zhao, S. Lobo, X. Dong, A. D. Ault, R. J. Deschenes, *J. Biol. Chem.* **277**, 49352 (2002).
39. O. A. Bizzozero, H. A. Bixler, A. Pastuszyn, *Biochim. Biophys. Acta* **1545**, 278 (2001).
40. L. Xue, D. R. Gollapalli, P. Maiti, W. J. Jahng, R. R. Rando, *Cell* **117**, 761 (2004).
41. S. M. Margarit et al., *Cell* **112**, 685 (2003).
42. We thank J. Ellenberg, J. Lippincott-Schwartz, I. Rodriguez-Crespo, M. R. Phillips, J. Hancock, and H. T. McMahon for generously providing plasmids and A. Squire for technical help in microscopy. M.K. was supported by a fellowship of the Boehringer Ingelheim Fonds.

## Supporting Online Material

www.sciencemag.org/cgi/content/full/1105654/DC1  
Materials and Methods  
SOM Text  
Figs. S1 to S7  
References and Notes

24 September 2004; accepted 10 December 2004  
Published online 11 February 2005;  
10.1126/science.1105654  
Include this information when citing this paper.

# Evolution of Oxygen Secretion in Fishes and the Emergence of a Complex Physiological System

Michael Berenbrink,<sup>1,2\*</sup> Pia Koldkjær,<sup>1</sup> Oliver Kepp,<sup>2,†</sup>  
Andrew R. Cossins<sup>1</sup>

We have reconstructed the events that led to the evolution of a key physiological innovation underpinning the large adaptive radiation of fishes, namely their unique ability to secrete molecular oxygen (O<sub>2</sub>). We show that O<sub>2</sub> secretion into the swimbladder evolved some 100 million years after another O<sub>2</sub>-secreting system in the eye. We unravel the likely sequence in which the functional components of both systems evolved. These components include ocular and swimbladder countercurrent exchangers, the Bohr and Root effects, the buffering power and surface histidine content of hemoglobins, and red blood cell Na<sup>+</sup>/H<sup>+</sup> exchange activity. Our synthesis reveals the dynamics of gains and losses of these multiple traits over time, accounting for part of the huge diversity of form and function in living fishes.

Teleost fishes achieve neutral buoyancy by means of a gas-inflated swimbladder (1). This innovation removed constraints on pectoral and caudal fin structure (2), allowing the adaptive radiation of the life-styles, habitats, and morphologies in modern fishes. The subsequent evolution of an O<sub>2</sub> secretion mechanism to inflate the swimbladder removed the need to take in air through the esophagus at the surface, allowing colonization of new habitats such as the deep sea. The underlying physiology of O<sub>2</sub> secretion involves pH-sensitive "Root-effect" hemoglobins and an elaborate vascular arrangement known as the *rete mirabile* (Latin: wonderful network; plural, *retia mirabilia*).

Arterial blood passing through the capillaries of the gas gland in the swimbladder wall is acidified by release of lactic acid and carbon dioxide from gas gland cells (3). Low pH then causes a strong decrease in the O<sub>2</sub> binding capacity of Root-effect hemoglobins (Hbs) despite high oxygen tensions (4). The concomitant increase in physically dissolved O<sub>2</sub> is amplified by the *rete mirabile*, a tight bundle

of arterial and venous capillaries running closely together in opposite directions, which provides a countercurrent exchange allowing diffusion of O<sub>2</sub> unloaded from Hb in the venous capillaries back into the arterial supply to the swimbladder. The ensuing buildup of high O<sub>2</sub> tensions then fills the swimbladder by diffusion, even against high hydrostatic pressures (3). The (alkaline or normal) Bohr effect of mammalian Hbs describes the acid-induced decrease in Hb O<sub>2</sub> affinity at alkaline to neutral pH. The Root effect differs from the Bohr effect in that acidification unloads O<sub>2</sub> from Root-effect Hbs even at O<sub>2</sub> tensions above atmospheric levels (3, 4).

Teleosts deviate in two other important ways from the general pattern of vertebrate blood gas transport: They have Hbs with unusually low specific buffer values such that less acid is needed to elicit the Root effect (5), and they can use an isoform of the vertebrate Na<sup>+</sup>/H<sup>+</sup> exchanger family (βNHE) to regulate the intracellular pH of red blood cells (6, 7). Low Hb buffer values also mean that less acid need be shifted by the βNHE to modify red blood cell pH. Teleost Hbs also display some of the greatest (alkaline or normal) Bohr effects among jawed vertebrates (5).

There is currently no coherent explanation for the many advanced teleost groups that lack one or several of these various physiological traits. This picture is further complicated by the presence of elevated O<sub>2</sub> tensions in the eyes of

many fishes (8). An ocular mechanism comprising a choroid *rete* works similarly to the swimbladder *rete* to increase physically dissolved O<sub>2</sub> and thereby supports the vigorous O<sub>2</sub> demand of the often avascular fish retina (9).

By taking advantage of the wide divergence of fishes and by integrating data from all levels of organization, we reconstruct on a vertebrate phylogeny the likely sequence of evolutionary events leading to the ability to secrete O<sub>2</sub>. We support this analysis by identifying consistent patterns of secondary losses of several of these components in specific clades of advanced fishes, thereby characterizing factors that affect their maintenance.

**Evolution of the Root effect and *rete mirabile*.** In the absence of the acid-induced elevation of venous O<sub>2</sub> tension by the Root effect, the *rete* would shunt O<sub>2</sub> from the arterial supply directly to the venous drainage, bypassing the tissue. Thus, evolution of an O<sub>2</sub>-permeable *rete* before the Root effect may conceivably be physiologically constrained (*retia*-only-with-Root hypothesis). We tested this hypothesis by first establishing the presence or absence of choroid and swimbladder *retia* in more than 50 selected vertebrate species and then reconstructing the evolution of these structures on a composite vertebrate phylogeny (10) (Fig. 1). The choroid *rete* evolved only once, some 250 million years ago. By contrast, swimbladder *retia* evolved independently in four major teleost groups (A, B, C, and D in Fig. 1) and were secondarily lost several times. The two earliest origins of swimbladder *retia* are found among the Elopomorpha (C) and Euteleostei (A) and can be dated back to 130 to 140 million years ago. Evolution of swimbladder O<sub>2</sub> secretion was followed by the invasion of a deep-sea habitat in Elopomorpha (C) and can be associated with modifications of the swimbladder for increased auditory sensitivity in Osteoglossomorpha (D) (10). In both groups, this was paralleled by significant adaptive radiations, as is evident from a substantial increase in extant species numbers relative to the respective sister groups without swimbladder O<sub>2</sub> secretion [771 versus 8 species for Albuliformes + Notacanthiformes + Anguilliformes versus Elopiformes, and 198 versus 8 species for Mormyroidea versus Notopteroidea; *P* < 0.05 in both cases (amplified diversification test) (10)].

Next, we measured the Root effect in 49 of the species used for reconstruction of *rete*

<sup>1</sup>School of Biological Sciences, University of Liverpool, Crown Street, Liverpool L69 7ZB, UK. <sup>2</sup>Department of Animal Physiology, Humboldt Universität zu Berlin, Philippstraße 13, D-10115 Berlin, Germany.

\*To whom correspondence should be addressed. E-mail: michaelb@liv.ac.uk

†Present address: Molecular Biology, Max Planck Institute for Infection Biology, Schumannstr. 21/22, D-10117 Berlin, Germany.

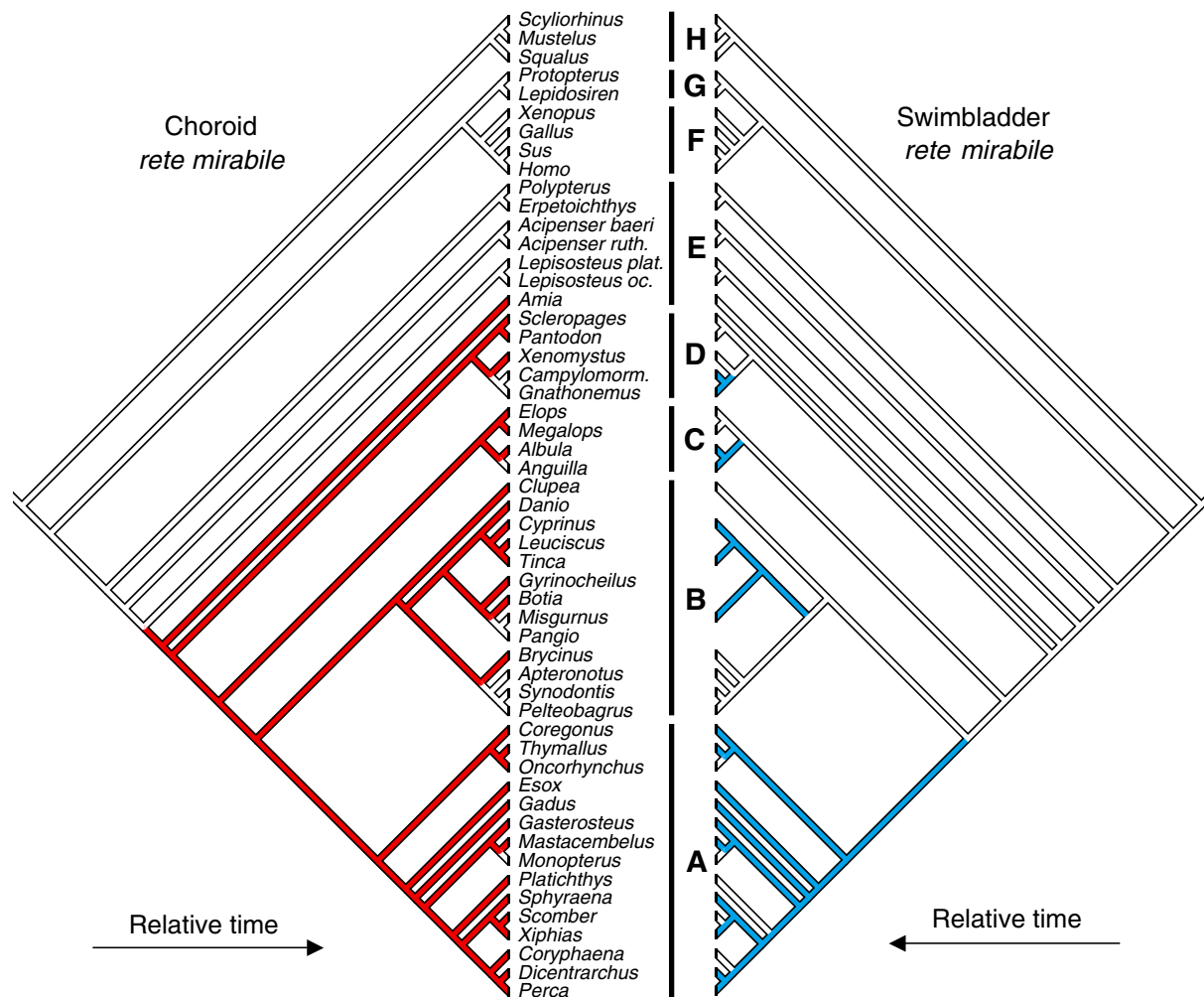


**Fig. 1.** Evolution of choroid and swimbladder *retia*. Presence of the choroid and swimbladder *retia* is marked with red and blue lines, respectively; absence is marked by white lines. Cladograms represent mirror images of each other and are based on literature sources (10). Some branches where

information on the swimbladder *rete* is missing are omitted. Ancestral states were reconstructed by parsimony (10). A, Euteleostei; B, Otocephala; C, Elopomorpha; D, Osteoglossomorpha; E, early ray-finned fish lineages; F, Tetrapods; G, Dipnoi; H, Chondrichthyes.

evolution. In sharks, lungfishes, and tetrapods, the Root effect caused reductions in Hb O<sub>2</sub> saturation by less than 10% (H, G, and F in Fig. 2A). Only the amphibian *Xenopus* showed a somewhat higher Root effect of 15%. A similar-sized Root effect occurs in *Polypterus* and *Erpetoichthys*, the two sole genera of the most basal lineage of living ray-finned fishes. The surviving members of other ancient ray-finned fish lineages (E) show successively higher Root effects increasing from just above 20% to around 60% in *Amia*. Most teleosts (A to D) have Root effects above 40%, but there is considerable variation, from 80% in the cod *Gadus* to 2% in the catfish *Silurus*. A substantial Root effect of 20 to 40% evolved only once among these vertebrates, in the ray-finned fishes (Fig. 2B). This occurred before the divergence of *Lepisosteus* from the *Amia* + Teleostei clade and establishes the evolution of a pronounced Root effect well before the first appearance of the choroid *rete* and long before swimbladder *retia*.

**Secondary reduction of the Root effect.** Analysis of Root-effect evolution recon-

structs five independent secondary decreases below 40% within teleosts. These are located on the branches leading to *Gnathonemus*, *Anguilla*, the loaches *Misgurnus* and *Pangio*, the catfishes *Silurus* and *Pelteobagrus*, and on the branch leading to *Monopterus* (Fig. 2A). The *retia*-only-with-Root hypothesis predicts that after the choroid *rete* had evolved in *Amia* and teleosts, large secondary decreases of the Root effect were only viable in the absence of the *rete*. The corresponding reconstruction of choroid *rete* evolution has also identified five independent cases in which this structure has been secondarily lost. Most important, all five reductions of the Root effect to below 40% are located on branches where the choroid *rete* has been lost (Fig. 2A). The probability of observing this pattern by chance on the *Amia* + Teleostei clade is  $P < 0.001$  (concentrated changes test).

As long as a choroid *rete* is present, loss of swimbladder O<sub>2</sub> secretion has no impact on the magnitude of the Root effect as seen in Euteleostei (A), in which the swimbladder *rete*

or the whole swimbladder were lost several times independently (Figs. 1 and 2). However, once the essential anatomical structure for ocular O<sub>2</sub> secretion has vanished, the maximal extent of Root-effect reduction appears to depend on whether swimbladder O<sub>2</sub> secretion is present. Thus, *Gnathonemus* + *Campylomormyrus*, *Anguilla*, and *Misgurnus* have all independently lost the choroid *rete* but still maintain Root effects above 20%, which is in line with the presence of a swimbladder *rete* in these groups. By contrast, secondary reductions of the Root effect to values below 10% are only observed in groups that have lost not only ocular but also swimbladder O<sub>2</sub> secretion. This is illustrated by the two catfishes *Silurus* and *Pelteobagrus*, which lack a *rete* in their swimbladder, and by *Monopterus*, which has lost the swimbladder altogether (Figs. 1 and 2) (10).

It is highly unlikely by chance that three separate reductions of the Root effect to values below 40%, but still above 20%, would be observed only in those three groups that have lost the choroid *rete* but still retain a swimbladder

rete ( $P < 0.001$ , concentrated changes test). Similarly, observing two separate reductions of the Root effect to below 10% in precisely those two groups that have lost both *retia* carries a probability of  $P < 0.01$ . This suggests that, although originally not an adaptation for  $O_2$  secretion, the Root effect is maintained in modern teleosts by its role in  $O_2$  secretion. It also shows that the minimally required Root effect for the ocular system is distinctly higher than for the swimbladder system and that the magnitude of the Root effect is under dynamic, selective control in teleosts.

The virtual disappearance of the Root effect in modern teleosts without either *rete* may be explained by its negative side effects. As a result of low plasma bicarbonate and Hb buffer values (5, 11), lactic acid production during severe exercise or environmental hypoxia may cause venous pH values in the general circulation that are too low for full oxygenation of Root-effect Hbs at the respiratory surface, compromising  $O_2$  supply to the tissues. Early ray-finned fishes, which lacked a *rete* yet possessed a sizable Root effect, may have been protected from these

negative side effects under general acidosis if the Root effect had evolved in the presence of high Hb buffer values.

**The role of Hb buffer values.** We have determined Hb buffer values across a wide range of vertebrates, including teleosts and basal ray-finned fishes. Our reconstruction of Hb buffer value evolution in 23 selected vertebrates suggests that a high Hb buffer value was the ancestral state for all jawed vertebrates (Fig. 3, node 1). Following the trajectory of the Percomorpha lineage, one of the most advanced groups among teleosts, further suggests that Hb buffer values were indeed still high when the Root effect first started to increase (node 3). After divergence of the Polypteriformes, Hb buffer values decreased only gradually within ray-finned fishes (nodes 4 and 5) until they reached a lower plateau in the last common ancestor of *Amia* and teleosts (node 6). This was at a time when the Root effect had reached a distinct upper plateau and when the choroid *rete* and ocular  $O_2$  secretion first appeared (between nodes 5 and 6, Fig. 3).

What underlies the evolutionary decrease in Hb buffer value? The  $C_\alpha$ -imidazole side chain of the amino acid histidine is largely responsible for hydrogen ion buffering at physiological pH (5, 12). Analysis of histidine substitution in Fig. 4 indicates that, of the five histidine sites that are conserved in the  $\alpha$ -globins of most jawed vertebrates, only one is titratable in human Hb A; similarly, of the four histidine sites that are conserved in their  $\beta$ -globins, only two are titratable in human Hb A. Nonteleosts among jawed vertebrates (F, G, and H) have up to eight additional, nonconserved histidines per  $\alpha$ - and  $\beta$ -globin, most of which are titratable or external in human Hb A. Teleosts (A, B, and C) typically have just one and two additional nonconserved histidine substitutions in their  $\alpha$ - and  $\beta$ -globins, respectively. We suggest that this, together with acetylation of the normally titratable N-terminal  $C_\alpha$ - $NH_2$  groups in their  $\alpha$ -globins (5) (Fig. 4A), accounts for their greatly diminished Hb buffer values. This conclusion is supported by a highly significant correlation ( $P < 0.01$ , PDTREE) between the sum of these physiological buffer groups from the predicted protein structure and the measured buffer value across major vertebrate groups (Fig. 5).

The evolution of the Root effect in early ray-finned fishes before this reduction in Hb buffer value and before any *rete* suggests that it may initially have been neutral.

**Correlated evolution of Bohr and Root effects.** If the Root effect is a feature of a specific molecular mechanism for the Bohr effect in Hbs of ray-finned fishes, its evolution may have been driven indirectly by the selective advantage of the Bohr effect. Our evolutionary reconstruction of the Bohr effect in Fig. 6 suggests that a low Bohr effect of no

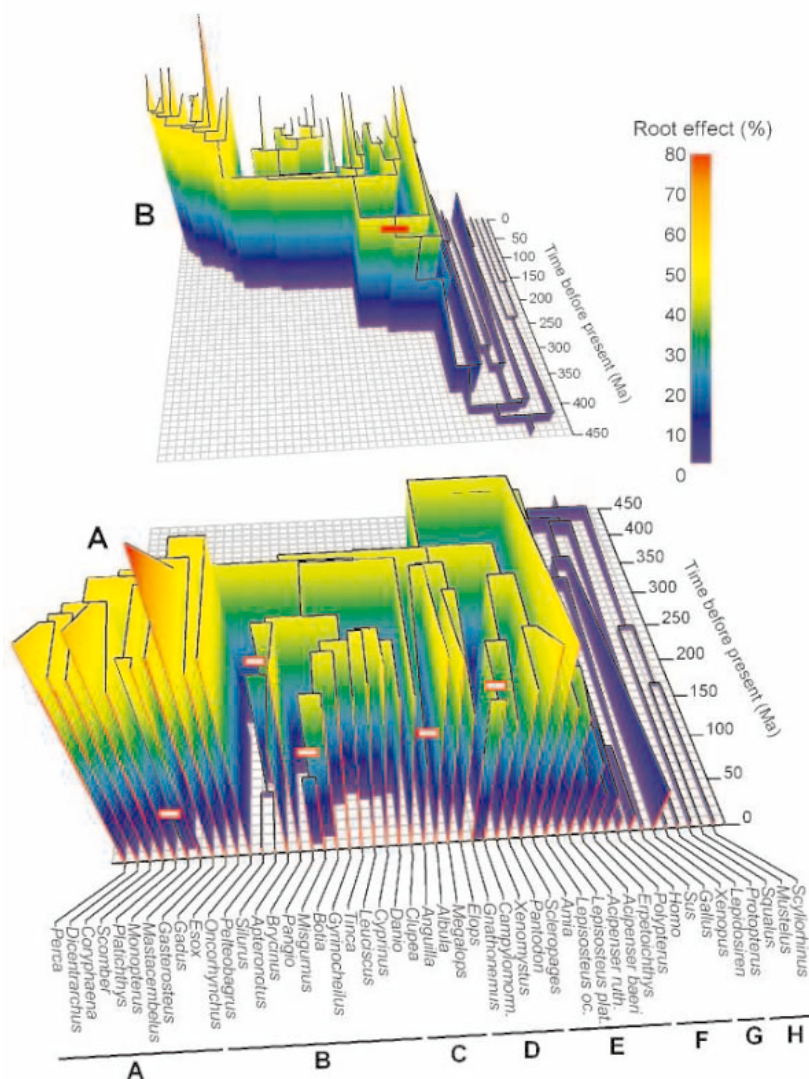


**Fig. 2.** Evolution of the Root effect in jawed vertebrates. The underlying phylogeny in the x, y plane is based on the cladogram in Fig. 1, with branch lengths estimated from minimal divergence times mapped onto an axis representing evolutionary time (10) (Ma, million years ago). The vertical z axis describes measured and reconstructed values of the Root effect, which have been color coded. (A) and (B) are mirror images of each other to allow both sides of the structure to be viewed. Major living gnathostome groups are labeled A to H as in Fig. 1. Values for the Root effect represent the maximal percentage decrease in  $O_2$  saturation of functional Hb in air-equilibrated hemolysates in citrate buffer (pH 5.5) relative to Tris buffer (pH  $\geq 8.0$ ). Hemolysates were prepared in physiological salines whose pH ranged from 7.4 to 7.9, depending on the respective physiological temperature of the animal (41° to 15°C, respectively). The Root effect was treated as a continuously varying character; ancestral values at nodes of the tree were estimated by linear parsimony. Equivocal nodes were resolved with the maxstate option (10). For comparison, red and white bars indicate branches along which the choroid *rete* was gained or secondarily lost, respectively (from Fig. 1).

more than one oxyliable proton was the ancestral state for jawed vertebrates. An increase of the Bohr effect evolved independently by convergent evolution in amniotes (reptiles, birds, and mammals) and early ray-finned fishes, which is in line with distinct differences in the molecular mechanism of the Bohr effect in mammalian and teleost Hb (13, 14). The Bohr effect increased further during the evolution of ray-finned fishes, reaching values of three Bohr protons in the last common ancestor of *Amia* and teleosts and four Bohr protons in some modern teleosts (Fig. 6). In many Hbs of both ray-finned fishes and amniotes, the presence of the naturally occurring, species-specific organic phosphate modulators uncovers even further Bohr protons (15, 16), although in vivo this effect would at least be partially counteracted in Hbs of air-breathing vertebrates, where elevated CO<sub>2</sub> tensions decrease the Bohr effect (16, 17).

Thus, our Bohr effect measurements may slightly underestimate its value under physiological conditions of organic phosphates and CO<sub>2</sub>, especially in water-breathers. On the other hand, conditions for the determination of the Root effect were chosen to yield close to physiological values. But even so, phylogenetic independent contrast analysis of our data set still reveals a highly significant correlation between the magnitudes of the Bohr and the Root effects in ray-finned fishes ( $P < 0.001$ , PDTREE program) (fig. S2). This correlation suggests that the first occurrence of the Root effect may indeed have been linked to the increased Bohr effect in early ray-finned fishes. It is noteworthy that both independent reductions of the Bohr effect in ray-finned fishes down to the ancestral values of jawed vertebrates (*Silurus* and *Monopterus*, Fig. 6) co-occur with a loss of the Root effect (Fig. 2;  $P < 0.01$ , concentrated changes test).

**Regulation of red blood cell pH.** The  $\beta$ -adrenergically activated Na<sup>+</sup>/H<sup>+</sup> exchanger ( $\beta$ NHE) protects intracellular pH against acidosis, and thereby safeguards O<sub>2</sub> loading of Root-effect Hbs under exercise- or hypoxia-induced blood acidification (6). The unusual O<sub>2</sub> dependence of the transporter allows considerable  $\beta$ NHE modulation even above atmospheric O<sub>2</sub> levels (18). This is in striking contrast to O<sub>2</sub>-sensitive ion transport in red blood cells of other vertebrate groups (19), and we suggest here that the  $\beta$ NHE evolved specifically to protect O<sub>2</sub> secretion. Swimbladder O<sub>2</sub> secretion is slow, lasting from several hours to days (20). In contrast, impairing O<sub>2</sub> secretion in the eye causes deterioration of the normal electroretinogram and blindness within minutes (21, 22). Therefore, the  $\beta$ NHE should be primarily associated with highly visual teleosts relying on ocular O<sub>2</sub> secretion.

We have measured the activity of the  $\beta$ NHE and reconstructed its evolution in 38

selected jawed vertebrates (fig. S1). The  $\beta$ NHE appears to be absent in all groups except teleosts. It is also absent in Osteoglossomorpha, the most basal group of living teleosts. Thus, following the trajectory of the Percomorpha lineage in Fig. 3, high  $\beta$ NHE activities evolved in higher teleosts only after the divergence of the Osteoglossomorpha some 150 million years ago (between nodes 7 and 8 in Fig. 3). This was at a time when Hb histidine contents and buffer values had already approached the low values characteristic of recent teleosts and about 100 million years after the substantial increase of the Root effect.

Evolutionary reconstruction also reveals four separate secondary reductions of  $\beta$ NHE activities in higher teleosts. These occurred in *Anguilla*, the *Botia* + *Misgurnus* clade, the *Apteronotus* + Siluriformes clade, and *Monopterus*. Most strikingly, the choroid *rete* has also been lost independently four times, in exactly those groups. The probability of observing this pattern by chance is  $P < 0.01$  (concentrated changes test). The presence of swimbladder O<sub>2</sub> secretion in *Anguilla* and *Misgurnus* is obviously not enough to sustain elevated  $\beta$ NHE activities, which suggests that the primary selection pressure acting on  $\beta$ NHE evolution is the safeguarding of ocular O<sub>2</sub> secretion.

**Discussion.** We propose that the ancestral condition for all jawed vertebrates was the possession of Hbs with high histidine

contents and buffer values but with low Root and alkaline Bohr effects (fig. S3). They lacked a  $\beta$ NHE but had a red blood cell anion exchanger to equilibrate bicarbonate across the cell membrane, which allowed changes in plasma pH to be translated directly to Hb inside the cell (23). This condition is still evident in contemporary elasmobranchs (H, fig. S3), lungfishes (G), and amphibians (F, in part).

Early ray-finned fishes (E) and amniotes within the tetrapods (F) then independently evolved an increased Bohr effect. In ray-finned fishes, this mechanism was associated with an increase in the Root effect, as already found in Polypteriformes. Thus, the Root effect initially did not evolve as an adaptation for O<sub>2</sub> secretion but may merely have been a by-product of a specific mechanism by which ray-finned fishes increased their Bohr effect. Hb buffer values then started to progressively decrease, as still evident in *Acipenser*, *Lepisosteus*, and *Amia*. This may have allowed a more efficient exploitation of the Bohr effect. In contrast to the classical view, which rationalizes major changes in Hb function by only a few amino acid substitutions in key positions, we demonstrate a mechanism by which the magnitude of Hb buffer values is determined by a varying number of additive histidine substitutions that can be more or less randomly distributed across the whole surface of the Hb tetramer.

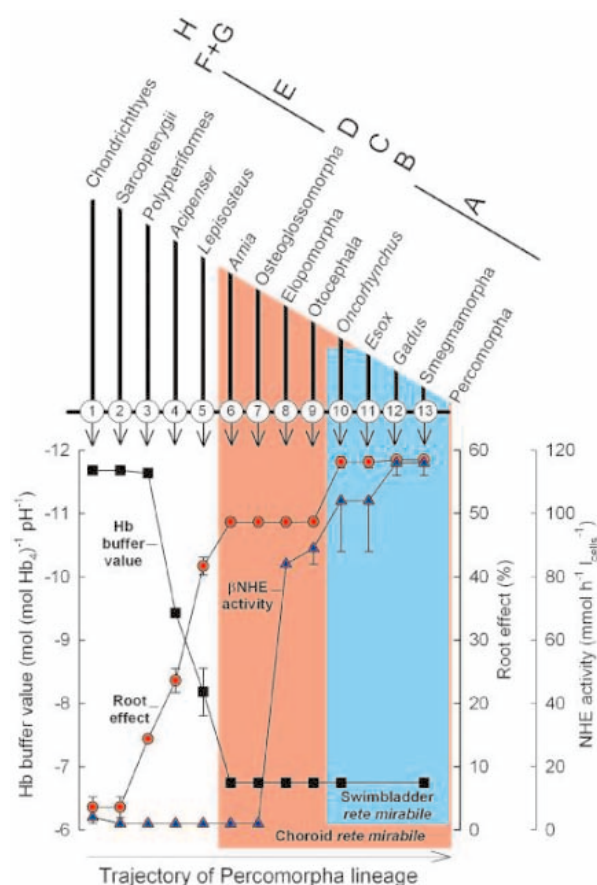


**Fig. 3.** Timing the evolutionary changes in specific Hb buffer value, Root effect, and  $\beta$ NHE. Values have been reconstructed by linear parsimony from information in living vertebrates as in Fig. 2. Only values for nodes in the trajectory of the Percomorpha lineage are shown (labeled 1 to 13), as indicated by the respective arrows from the cladogram above. The means of the minimal and maximal reconstructed values and their range (error bars) were plotted at nodes for which the reconstruction was ambiguous. Red and blue fields indicate the presence of a choroid or swimbladder *rete*, respectively (the latter has been secondarily lost in the *Oncorhynchus* lineage). Hb buffer values refer to deoxygenated and organic phosphate-free hemolysates in 0.1 M KCl at physiological temperature and approximate red blood cell intracellular pH.  $\beta$ NHE activities were measured on deoxygenated red blood cells in physiological salines at arterial pH and physiological temperature according to the isoproterenol-activated rate of <sup>22</sup>Na uptake (10). Maximal Root-effect values are taken from Fig. 2.



Unlike in ray-finned fishes, buffer values and surface histidine contents of Hb in amniotes remained unchanged after the Bohr effect had independently increased. Perhaps the importance of reduced Hb buffer values for the Bohr effect is greatly reduced in the presence of the higher bicarbonate buffer values found in terrestrial air-breathers (11). In addition, the molecular mechanism of the Bohr effect in amniotes may depend on more histidine residues than in teleosts. Thus, histidines  $\alpha 50$ ,  $\alpha 72$ , and  $\alpha 89$ , which contribute to the alkaline Bohr effect in human Hb A (12), are conserved in the major Hbs of amniotes but are substituted in most teleost Hbs (Fig. 4A). The proposed independent, qualitatively different molecular mechanism for the Bohr effect in mammals and ray-finned fishes challenges the classical view of Perutz and Brunori (24) but should come as less of a surprise in view of the lamprey, which has evolved a strong Bohr-effect Hb by yet another, entirely different mechanism (25, 26).

The Root effect increased in parallel with the Bohr effect in early ray-finned fishes, allowing for effective ocular  $O_2$  secretion once the choroid *rete* evolved in the ancestor of *Amia* and teleosts. This innovation may have been crucial for improving aerobic metabolism in an avascular retina where the low-pressure circulatory system of fishes resulted in limited rates of blood flow to the choroid capillaries.

Our reconstruction further indicates that swimbladder  $O_2$  secretion first evolved ~100 million years after  $O_2$  secretion in the ocular system. This occurred several times independently and suggests that the evolution of the Root effect released a functional constraint on the evolution of the *retia*, which subsequently evolved numerous times and at different body locations. Finally, we suggest that the  $\beta$ NHE of fish red blood cells evolved as a paralog of the other members of the vertebrate family of  $Na^+/H^+$  exchangers to safeguard ocular  $O_2$  secretion from conditions of general circulatory acidosis.

Our reconstruction is critically supported first by the identification of intermediate stages in the form of the living members of ancient fish lineages, particularly Polypteriformes, *Acipenser*, *Lepisosteus*, and *Amia*. Second, it is rational and can be justified mechanistically. For example, evolution of a *rete* before the Root effect is liable to short-circuit tissue  $O_2$  supply. Third, the proposed evolutionary sequence is robust against alternative phylogenetic hypotheses currently discussed. Thus, accepting a clade composed of *Acipenser*, *Lepisosteus*, and *Amia* together as the sister group of teleosts (27, 28) merely reconstructs a second, independent instance in which the proposed evolutionary scenario is partially repeated. Fourth, our identification of the selective forces and constraints acting on the mechanisms of ocular  $O_2$  secretion is supported by the analysis of multiple independent

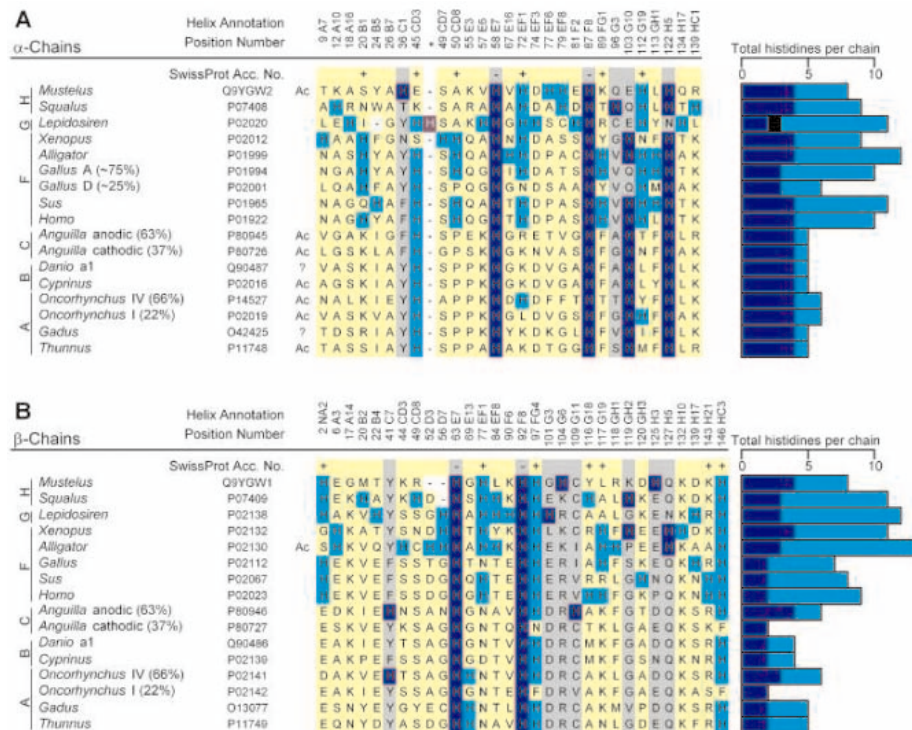
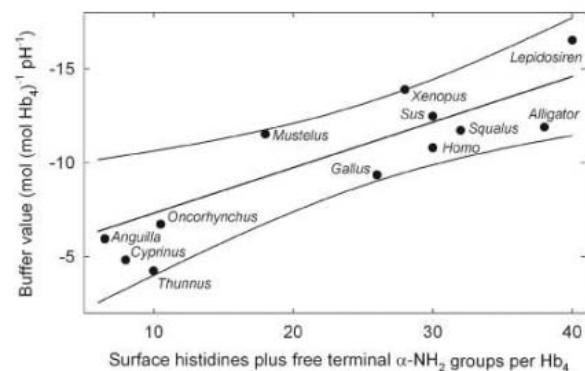


**Fig. 4.** Position and number of histidine residues in selected vertebrate Hbs. Aligned sequences are given with SwissProt database accession numbers. All sites occupied by histidine in at least one of the globins are shown together with their helix annotation and positional number in human  $\alpha$ -globin (A) and  $\beta$ -globin (B). In the case of multiple globins, the relative abundance of major chain types is given in brackets. Light and dark blue positions indicate titratable and nontitratable histidine positions, respectively. Yellow background indicates positions that contain titratable histidines (+) or are considered external at homologous positions in human Hb A. Gray background indicates positions that contain nontitratable histidines (–) or are internal and inaccessible to solvent at homologous positions in human Hb A (10). Asterisk indicates insertion of a histidine between positions 46 and 47 of human  $\alpha$ -globin in *Lepidosiren* of unknown titratability (black). Ac indicates an acetyl group chemically blocking terminal  $C_\alpha$ - $NH_2$  groups (10); question mark indicates unknown titratability of N terminus. Letters next to species names indicate major gnathostome groups as in Fig. 1. Single-letter abbreviations for amino acid residues: A, Ala; C, Cys; D, Asp; E, Glu; F, Phe; G, Gly; H, His; I, Ile; K, Lys; L, Leu; M, Met; N, Asn; P, Pro; Q, Gln; R, Arg; S, Ser; T, Thr; V, Val; W, Trp; Y, Tyr.

**Fig. 5.** Correlation between measured specific buffer value and the sum of predicted physiological buffer groups. The latter was obtained by the number of unblocked N-terminal  $C_\alpha$ - $NH_2$  groups plus surface histidine residues per Hb tetramer from Fig. 4. In cases of multiple Hbs, the sum of predicted physiological buffer groups is the weighted average of all major Hbs (>10% of total Hb). Specific Hb buffer values were measured as in Fig. 3. The regression line and 95% confidence intervals were obtained by the phylogenetic independent contrast method and are mapped onto the original data space (10).



versals to the ancestral condition. This provides statistical support in asserting causal relationships between, for example, the maintenance of the Root effect and the presence of a choroid or swimbladder *rete*, or between the maintenance of the  $\beta$ NHE and ocular  $O_2$  secretion.

The respiratory system of half of all living vertebrates has thus been shaped by the evo-

lution of ocular  $O_2$  secretion, and this set the stage for subsequent and multiple evolutions of swimbladder  $O_2$  secretion. Our demonstration of convergent evolution of the Bohr effect in amniotes and of the Bohr-Root effect in ray-finned fishes, by different molecular mechanisms and in Hbs whose evolutionary paths separated about 400 million years ago, may explain why all attempts to transfer the

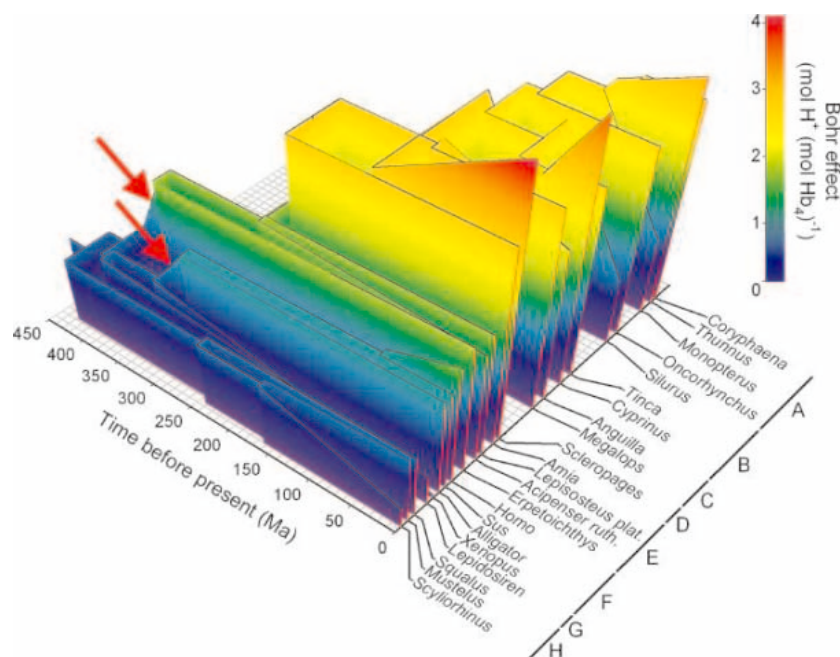


**Fig. 6.** Evolution of the Bohr effect. Values refer to the maximal alkaline Bohr effect of organic phosphate-free hemolysates in 0.1 M KCl at physiological temperature. They were determined by titration of hemolysates equilibrated under  $N_2$  and  $O_2$  atmospheres and calculated as the number of additional protons bound upon deoxygenation of Hb at constant pH. Values at ancestral nodes were calculated by linear parsimony under the maxstate resolving option for equivocal nodes (10). Arrows indicate the two independent increases of the Bohr effect during evolution of tetrapods (F) and early ray-finned fishes (E). See Figs. 1 and 2 for further details.

Root effect onto human Hb A by site-directed mutagenesis of a few key amino acid positions have so far failed (29).

Our study emphasizes the importance of phylogenies in disentangling the origins of complex physiological systems. Indeed, understanding how multiple contributing components arose or were subsequently lost depends critically on combining this historical view with a detailed mechanistic understanding. Integrating molecu-

lar, cellular, anatomical, and physiological data provides the foundation for this task.

#### References and Notes

1. R. McN. Alexander, *Biol. Rev.* **41**, 141 (1966).
2. G. V. Lauder, K. F. Liem, *Bull. Mus. Comp. Zool.* **150**, 95 (1983).
3. B. Pelster, D. J. Randall, in *Fish Respiration*, S. F. Perry, B. L. Tufts, Eds. (Academic Press, San Diego, CA, 1998), pp. 113–139.
4. R. W. Root, *Biol. Bull.* **61**, 427 (1931).
5. F. B. Jensen, *J. Exp. Biol.* **143**, 225 (1989).

6. M. Nikinmaa, *Physiol. Rev.* **72**, 301 (1992).
7. F. Borgese, C. Sardet, M. Cappadoro, J. Pouyssegur, R. Motais, *Proc. Natl. Acad. Sci. U.S.A.* **89**, 6765 (1992).
8. J. B. Wittenberg, B. A. Wittenberg, *Nature* **194**, 106 (1962).
9. J. B. Wittenberg, B. A. Wittenberg, *Biol. Bull.* **146**, 116 (1974).
10. See supporting data on Science Online.
11. N. Heisler, in *Acid-Base Regulation in Animals*, N. Heisler, Ed. (Elsevier, Amsterdam, 1986), pp. 397–450.
12. T.-Y. Fang, M. Zou, V. Simplaceanu, N. T. Ho, C. Ho, *Biochemistry* **38**, 13423 (1999).
13. N. Ito, N. H. Komiyama, G. Fermi, *J. Mol. Biol.* **250**, 648 (1995).
14. T. Yokoyama et al., *J. Biol. Chem.* **279**, 28632 (2004).
15. R. G. Gillen, A. Riggs, *Arch. Biochem. Biophys.* **183**, 678 (1977).
16. J. V. Kilmartin, *Br. Med. Bull.* **32**, 209 (1976).
17. M. Farmer, *Comp. Biochem. Physiol. A* **62**, 109 (1979).
18. R. Motais, F. Garcia-Romeu, F. Borgese, *J. Gen. Physiol.* **90**, 197 (1987).
19. M. Berenbrink, S. Völkel, N. Heisler, M. Nikinmaa, *J. Physiol.* **526**, 69 (2000).
20. C. Bohr, *J. Physiol.* **15**, 494 (1894).
21. D. B. Fanner, J. R. Hoffert, P. O. Fromm, *Comp. Biochem. Physiol. A* **46**, 559 (1973).
22. M. B. Fairbanks, J. R. Hoffert, P. O. Fromm, *J. Gen. Physiol.* **64**, 263 (1974).
23. M. Nikinmaa, *J. Exp. Biol.* **200**, 369 (1997).
24. M. F. Perutz, M. Brunori, *Nature* **299**, 421 (1982).
25. H. A. Heaslet, W. E. Royer, *Structure* **7**, 517 (1999).
26. Y. Qiu, D. H. Mailliet, J. Knapp, J. S. Olson, A. F. Riggs, *J. Biol. Chem.* **275**, 13517 (2000).
27. B. Venkatesh, M. V. Erdmann, S. Brenner, *Proc. Natl. Acad. Sci. U.S.A.* **98**, 11382 (2001).
28. J. G. Inoue, M. Miya, K. Tsukamoto, M. Nishida, *Mol. Phylogenet. Evol.* **26**, 110 (2003).
29. M. F. Perutz, *Nature Struct. Biol.* **3**, 211 (1996).
30. We thank K. R. Olson, H. Tuurala, T. G. Pottinger, and P. J. Walsh for specimens, T. M. Beaumont for performing some early experiments, and A. F. Bennett for critically reading an earlier version of the manuscript. Supported by a grant from the Biotechnology and Biological Sciences Research Council, UK (M.B.).

#### Supporting Online Material

www.sciencemag.org/cgi/content/full/307/5716/1752/DC1  
Materials and Methods  
SOM Text  
Figs. S1 to S3  
Table S1  
References

22 November 2004; accepted 25 January 2005  
10.1126/science.1107793

## REPORTS

### Microwave Manipulation of an Atomic Electron in a Classical Orbit

H. Maeda,\* D. V. L. Norum, T. F. Gallagher

Although an atom is a manifestly quantum mechanical system, the electron in an atom can be made to move in a classical orbit almost indefinitely if it is exposed to a weak microwave field oscillating at its orbital frequency. The field effectively tethers the electron, phase-locking its motion to the oscillating microwave field. By exploiting this phase-locking, we have sped up or slowed down the orbital motion of the electron in excited lithium atoms by increasing or decreasing the microwave frequency between 13 and 19 gigahertz; the binding energy and orbital size change concurrently.

Atoms are inherently quantum mechanical, and attempts to explain their behavior provided the impetus to develop quantum mechanics. None-

theless, our intuitive picture of an atom is an electron moving in a Kepler orbit about an ionic core. As pointed out by Schrödinger, classical

motion can be recovered from time-independent quantum wave functions by constructing coherent superpositions of these wave functions. The result is a localized wave packet that moves as a classical particle does (1). The degree of localization increases with the number of states in the wave packet, and the orbital frequency is equal to the frequency separating the adjacent quantum states that constitute the wave packet (i.e., the energy separating them divided by Planck's constant  $h$ ).

Using picosecond or femtosecond laser pulses, it is now straightforward to create

Department of Physics, University of Virginia, 382 McCormick Road, Charlottesville, VA 22904, USA.

\*To whom correspondence should be addressed.  
E-mail: hm3c@virginia.edu.

wave packets of atoms of high principal quantum number  $n$ , in which the electrons move in Kepler orbits (2, 3). With the binding energies given by  $Ry/n^2$  (where  $Ry$  is the Rydberg constant), the energy spacing between adjacent levels is  $2 Ry/n^3$ , which is almost constant over a band of states  $\Delta n$  wide if  $\Delta n \ll n$ . Typically  $\Delta n \approx 5$  (2, 3). In a wave packet comprising a superposition of  $\Delta n$  states, the electrons have an orbital or Kepler frequency of  $f_K = (2 Ry/h)n^3$ , where  $2 Ry/h = 6.6 \times 10^{15}$  Hz. For  $n = 70$ ,  $f_K = 19.2$  GHz, in the microwave region.

If the electron is left to move freely in the Coulomb field of the atomic nucleus, the dispersion in  $f_K$  over the constituent states (4), as well as dephasing due to experimental imperfections such as stray fields, results in delocalization of the radial wave packets after only tens of orbits. However, adding a small oscillating field at the orbital frequency can phase-lock the motion of the electron to the oscillatory field (5–11), such that the localization of the electron persists at least for thousands of orbits (11)—perhaps long enough to

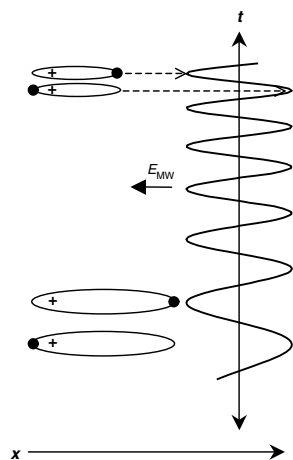
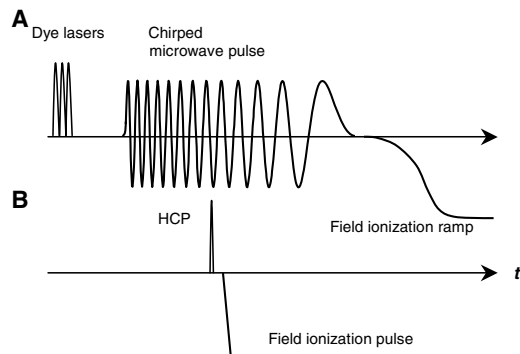


**Fig. 1.** Position of the electron in its highly elliptical orbit, aligned in the  $x$  direction at four times during the chirped microwave pulse. Time  $t$  increases in the downward direction for chirp to lower frequency and in the upward direction for chirp to higher frequency. The electron motion is synchronized to the field as shown, and the size of the orbit is larger at the low-frequency end of the chirp.

**Fig. 2.** Timing diagram for the experiment. Three dye-laser pulses excite the Li atoms, which are then exposed to the chirped microwave pulse. (A) The final states of the atoms are analyzed by a selective field ionization ramp subsequent to the microwave pulse. Alternatively, (B) the synchronization of the Rydberg electron with the chirped microwave field is probed by a HCP and electron-collection pulse during the microwave pulse.



actually use these classical atoms in applications such as information processing (12). From Ehrenfest's theorem we expect long-lived, highly localized wave packets only for the ideal harmonic oscillator (13), but the addition of the microwave field allows them to be realized in other systems, such as this Coulomb system, as well. In a microwave field linearly polarized in the  $x$  direction, the most localized wave packet is one in which the electron moves synchronously with the field, on a highly eccentric orbit aligned along the  $x$  axis (Fig. 1) (11). The motion is approximately one-dimensional and can be described with a one-dimensional model using only the principal quantum number  $n$ . We use a one-dimensional description throughout this report.

Here we report the manipulation of such a classical electron orbit. We use the alkali atom lithium, which has one valence electron outside a closed-shell ionic core. Atoms in which the valence electron has been excited are exposed to a microwave pulse tuned initially to the electron's Kepler frequency, and are then chirped to higher or lower frequency, as suggested by Kalinski and Eberly (14). The microwave field first phase-locks the electron's motion and then increases or decreases the electron's orbital frequency during the chirp, leading simultaneously to an increased orbital size and reduced binding energy (Fig. 1). We have verified the change in quantum number  $n$  induced by the chirped pulse, as well as the persistent phase-locking of the electron to the microwave field throughout the chirp. In quantum mechanical terms, this process can be thought of as a multilevel adiabatic rapid passage (14, 15). At the halfway point in the adiabatic passage between two atomic levels, the electron is phase-locked to the applied oscillating field (16). In simple physical terms, adding the oscillating microwave field produces a potential well that oscillates in position. The electron is localized in the well, forcing it to oscillate in phase with the microwave field. As we chirp the frequency, we are cranking up or down the oscillation frequency of the electron.

Although we have also used pulses chirped up in frequency from 13 to 19 GHz, for

brevery we present here the results obtained when chirping the frequency down from 19 to 13 GHz. With this chirped pulse, an atom initially in  $n = 70$  is converted to an  $n = 79$  atom. A similar process, increasing the rotational frequency of a diatomic chlorine molecule by a chirped laser pulse, has been reported by Villeneuve *et al.* (17).

The timing sequences of the two types of measurements we have done are shown in Fig. 2 (18). Lithium atoms are excited by three 5-ns pulses of a dye laser via the sequence  $2s \rightarrow 2p \rightarrow 3s \rightarrow np$  states of  $65 < n < 90$ . The atoms are then exposed to a 500-ns microwave pulse. If the initial frequency of the microwave pulse matches the Kepler frequency of the  $np$  state excited by the lasers, the microwave field converts the  $np$  state into a phase-locked wave packet. Quantum mechanically, it is a periodically varying Floquet state, which is a superposition of several  $n$  ( $\Delta n \approx 6$ ) states. In our one-dimensional description the Floquet states are superpositions of  $n$  states, but in a real atom they are superpositions of  $n$  and  $l$  states of  $m = 0$ , where  $l$  and  $m$  are the orbital and azimuthal angular-momentum quantum numbers.

After applying the microwave pulse, we analyzed the final states by selective field ionization (Fig. 2A) (19). We exposed the atoms to a field ramp rising from 0 to 40 V/cm in 1  $\mu$ s. Ionization occurs when the field lowers the potential on one side of the atom sufficiently that the electron can escape over the saddle point in the potential. The ionization field is given approximately by  $F = (5.8 \times 10^8)/n^4$  V/cm (19), so as the field ramps up, higher  $n$  levels lose their electrons before lower  $n$  levels do. The electrons resulting from field ionization are detected with negligible time delay, and the time-resolved field ionization signal is used to infer the final-state distribution.

In Fig. 3A we show a false-color rendition of the 26 oscilloscope traces obtained when atoms initially excited to  $n = 70$  are exposed to unchirped 500-ns, 19-GHz microwave pulses, for values of microwave field amplitude  $E_{MW}$  ranging from 0.01 to 7.1 V/cm. The width of the signal, from  $F = 20$  to 37 V/cm at  $E_{MW} = 0.01$  V/cm, reflects the distribution of ionization fields for  $n = 70$  atoms. The strongest signal (red) remains near  $F = 27$  V/cm, where  $n = 70$  atoms are field-ionized, until  $E_{MW}$  reaches 4 V/cm, where it begins to disappear as a result of microwave ionization. In short, the atoms stay in  $n = 70$  or are ionized by the microwaves if they are intense enough. When atoms prepared in  $n = 79$  are exposed to the same amplitude range of 500-ns, 19-GHz pulses, the strongest signal occurs earlier in the field ramp, at  $F = 18$  V/cm (Fig. 3B), because  $n = 79$  atoms are easier to ionize. Otherwise the result is the same; the atoms

either remain in  $n = 79$  or are ionized. A frequency of 19 GHz is too far from the  $n = 79$  Kepler frequency to substantially redistribute the atoms before ionization occurs. Similar results are obtained when atoms are excited to  $n = 70$  or  $n = 79$  states and then exposed to 500-ns, 13-GHz pulses.

If we start with atoms initially in  $n = 70$ , which have a Kepler frequency  $f_K$  of 19.2 GHz, and expose them to a 500-ns microwave pulse chirped from 19 to 13 GHz, we obtain the very different result shown in Fig. 3C. Starting at fields of  $E_{MW} = 0.03$  V/cm, the electrons leave  $n = 70$ , becoming dispersed over many states. For fields  $0.5$  V/cm  $< E_{MW} < 1.4$  V/cm, the electrons are very efficiently transferred to  $n = 79$  ( $f_K = 13.4$  GHz), and at higher fields microwave ionization begins to occur. From Fig. 3C we estimate that for  $E_{MW} = 1$  V/cm, more than 80% of the  $n = 70$  atoms are transferred to  $n = 79$ . A 19 GHz  $\rightarrow$  13 GHz chirped microwave field phase-locks the electron's motion of an atom in  $n = 70$  and reduces its orbital frequency from 19 to 13 GHz, increasing  $n$  from 70 to 79. The field strength  $E_{MW} = 0.5$  V/cm is the threshold to phase-lock the electron's motion in  $n = 70$  (11). Depending on the strength of the microwave field, we can observe efficient transfer from other initial states near  $n = 70$ . For example, with a field of 1 V/cm, we observe transfer to  $n = 79$  for initial  $np$  states of  $67 \leq n \leq 72$ . Analogous results were also seen when electrons initially excited to  $n = 79$  were exposed to a positively chirped (13 GHz  $\rightarrow$  19 GHz) microwave pulse.

We verified that the electron's motion remained phase-locked to the microwave field by momentum-selective ionization with a subpicosecond half-cycle pulse (HCP) (Fig. 2B) (20, 21). The electron's motion follows a very eccentric elliptical orbit aligned along the  $x$  axis, the polarization axis of the microwave and HCP fields (Fig. 1). The HCP gives the electron a momentum kick  $\Delta p$  in the  $+x$  direction. If the electron is moving in the  $+x$  direction, it gains enough energy from the HCP to escape from the atom; if it is moving in the  $-x$  direction, it loses energy, and ionization does not occur (21).

We exposed the atoms to the HCP at several times during the chirped microwave pulse to verify that the electron's momentum remained synchronized to the microwave field. Because the HCP is not synchronized with the microwave field, we also sampled the microwave field coincident with the application of the HCP to determine the time-dependent phase  $\phi$  of the microwave field  $E_{MW} \cos \phi$ . Using the rapidly rising field ionization pulse shown in Fig. 2B, 10 ns after the HCP, we field-ionized those atoms not ionized by the HCP and detected the electrons produced. The observed ionization signal  $S(\phi)$  is thus 1 minus the probability of ionization by the HCP and

reveals the electron's momentum  $p(\phi)$  at the same phase. Our measurements were made for 4095 shots of the laser, and in Fig. 4A we show the resulting, apparently random, signals obtained when the HCP appears roughly 25% of the way through the chirp (i.e., when the instantaneous frequency of the microwave field is 17.5 GHz).

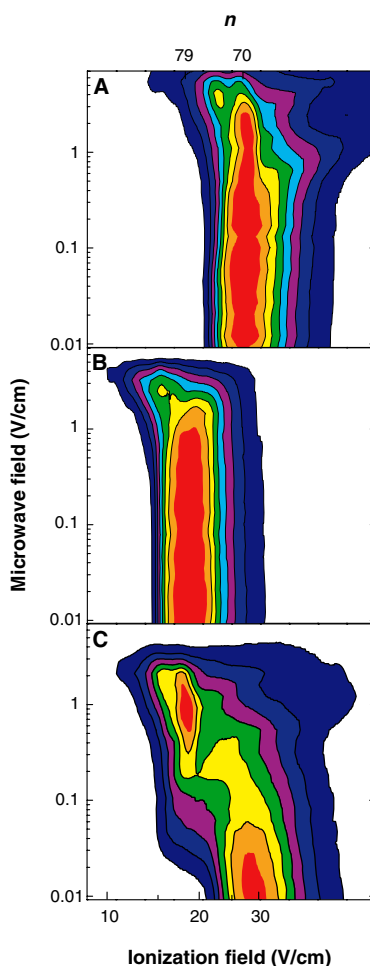


**Fig. 3.** Plots showing the final-state distributions after exposure to the microwave pulses. The field strength  $F$  of the field ionization ramp is indicated on the bottom horizontal axis, the corresponding  $n$  on the top horizontal axis, and the microwave field amplitude  $E_{MW}$  on the vertical axis. The signal intensity is shown using eight colors and white. Red is 8.75 to 10, green is 5.00 to 6.25, and white is 0. (A) When  $n = 70$  atoms are exposed to a 19-GHz pulse, they remain predominantly in the  $n = 70$  state, ionizing at  $F = 27$  V/cm, until  $E_{MW} = 4$  V/cm when microwave ionization occurs. (B) When  $n = 79$  atoms are exposed to a 19-GHz pulse, they remain in  $n = 79$ , ionizing at  $F = 18$  V/cm, until they are microwave-ionized at  $E_{MW} = 2.5$  V/cm. (C) When  $n = 70$  atoms are exposed to a pulse chirped from 19 to 13 GHz for field amplitudes  $0.5 \leq E_{MW} \leq 1.4$  V/cm, they are largely transferred from  $n = 70$  to  $n = 79$ . The plots are constructed from the time-resolved oscilloscope signals taken at microwave amplitudes of 0.01 to 7.1 V/cm. The horizontal axis is linear in time, with the entire figure corresponding to 270 to 940 ns, slightly longer than the rise time of the ionization pulse.

If the signals are plotted versus  $\phi$ , we observe, after averaging, the clear phase dependence in Fig. 4B; thus, the electron's motion appears to be phase-locked to the microwave field. In particular, at  $\phi = 0$ , the electron's momentum is in the same direction as  $\Delta p$ , whereas at  $\phi = \pm\pi$  it is in the opposite direction. Repeating this process with the HCP applied at later times in the frequency chirp shows that the electron's motion remains phase-locked during the entire chirped pulse. In Fig. 4, C and D, we show the signals obtained at instantaneous frequencies of 15.5 and 13.5 GHz, respectively. To observe the same phase of the signal to within  $20^\circ$  in Fig. 4, B to D, requires that we sample the

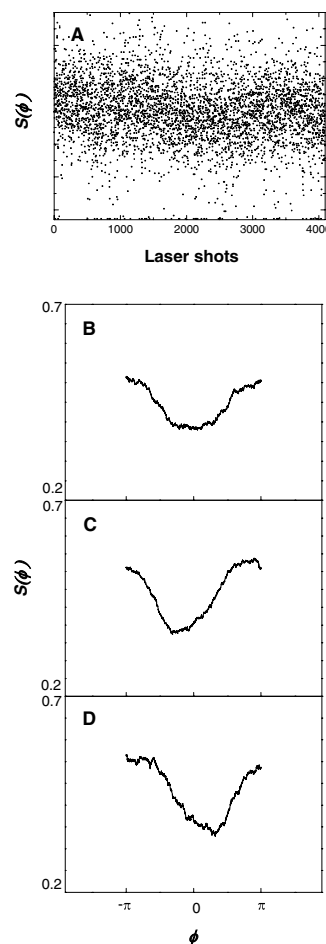


**Fig. 4.** Ionization signals produced by the HCP at three different points in the 19 GHz  $\rightarrow$  13 GHz chirp. The atoms are initially in  $n = 70$ , and the microwave field amplitude is  $\sim 1$  V/cm. (A) Apparently random signal  $S(\phi)$  obtained at 17.5 GHz as a function of laser shot. (B) Signal of (A) taken at 17.5 GHz but sorted by the instantaneous phase  $\phi$  of the microwave field obtained from the sampling oscilloscope. The Rydberg electron is clearly phase-locked to the microwave field. (C and D) Signal at 15.5 GHz (C) and 13.5 GHz (D) sorted by the instantaneous phase  $\phi$  of the microwave field. The electron evidently remains phase-locked throughout the chirped microwave pulse.

microwave field within 10 ps of when the HCP strikes the atom.

It is informative to contrast the high population transfer efficiency shown in Fig. 3C (80%) with the relatively low variation of the HCP ionization signal (~15%) shown in Fig. 4, B to D. The former suggests that 80% of the atoms are in phase-locked wave packets in which the electron's orbital frequency is reduced as the microwave frequency is chirped. If the atoms are all in the wave packet corresponding to the orbit shown in Fig. 1, we would expect nearly 100% variation in Fig. 4. The apparent discrepancy is resolved by the realization that the orbit of Fig. 1 represents one quantum wave packet (or Floquet state). There are others that do not yield as much contrast in Fig. 4 yet are still wave packets. It appears that we produce several different wave packets, all of which are phase-locked to the microwave field. The possibility of several wave packet states may contribute to the robustness of the process.

Microwave control of electron orbits could be improved by tailoring the variation of frequency and field amplitude during the pulse. Extension of the frequency chirp should be quite useful. With a factor of 10 chirp to lower frequency, the pulse would transfer population to states of higher  $n$  and reduce the ionization field by a factor of 20; this

would constitute a useful method of labeling Rydberg states for molecular spectroscopy (22). Chirping the frequency up can move unstable populations (23, 24) to lower, less fragile configurations. For example, anti-hydrogen atoms are currently produced in high- $n$  Rydberg states (25). Although the strong magnetic field and the accompanying possibility of a large population in high- $m$  states may preclude an efficient transfer, exposing the antihydrogen atoms to a chirped pulse might be a way to move them to lower lying, more stable states.

#### References and Notes

1. E. Schrödinger, in *Collected Papers on Wave Mechanics* (Blackie, London, ed. 1, 1928), p. 41.
2. J. A. Yeazell, C. R. Stroud Jr., *Phys. Rev. Lett.* **60**, 1494 (1988).
3. A. ten Wolde, L. D. Noordam, A. Lagendijk, H. B. van Linden van den Heuvell, *Phys. Rev. Lett.* **61**, 2099 (1988).
4. J. Mehra, H. Rechenberg, *The Historical Development of Quantum Theory* (Springer-Verlag, New York, 1987), vol. 5, pp. 633ff.
5. I. Bialynicki-Birula, M. Kalfinski, J. H. Eberly, *Phys. Rev. Lett.* **73**, 1777 (1994).
6. D. Farrelly, E. Lee, T. Uzer, *Phys. Rev. Lett.* **75**, 972 (1995).
7. D. Farrelly, E. Lee, T. Uzer, *Phys. Lett. A* **204**, 359 (1995).
8. A. Buchleitner, thesis, Université Pierre et Marie Curie (1993).
9. A. Buchleitner, D. Delande, *Phys. Rev. Lett.* **75**, 1487 (1995).

10. M. Kalfinski, J. H. Eberly, J. A. West, C. R. Stroud Jr., *Phys. Rev. A* **67**, 032503 (2003).
11. H. Maeda, T. F. Gallagher, *Phys. Rev. Lett.* **92**, 133004 (2004).
12. J. Ahn, T. C. Weinacht, P. H. Bucksbaum, *Science* **287**, 463 (2000).
13. A. Messiah, *Quantum Mechanics* (Wiley, New York, ed. 1, 1962), pp. 216–218.
14. M. Kalfinski, J. H. Eberly, *Opt. Express* **1**, 216 (1997).
15. C. P. Slichter, *Principles of Magnetic Resonance* (Springer-Verlag, Berlin, ed. 2, 1980), pp. 25–26.
16. C. P. Slichter, D. Ailion, *Phys. Rev.* **135**, A1099 (1964).
17. D. M. Villeneuve et al., *Phys. Rev. Lett.* **85**, 542 (2000).
18. See supporting data on Science Online.
19. T. F. Gallagher, *Rydberg Atoms* (Cambridge Univ. Press, Cambridge, ed. 1, 1994), pp. 103–119.
20. D. You, R. R. Jones, P. H. Bucksbaum, D. R. Dykaar, *Opt. Lett.* **18**, 290 (1993).
21. R. R. Jones, *Phys. Rev. Lett.* **76**, 3927 (1996).
22. K. Müller-Dethlefs, E. W. Schlag, *Annu. Rev. Phys. Chem.* **42**, 109 (1991).
23. T. J. Bensch, M. B. Campbell, R. R. Jones, *Phys. Rev. Lett.* **81**, 3112 (1998).
24. C. Wesdorp, F. Robicheaux, L. D. Noordam, *Phys. Rev. Lett.* **84**, 3799 (2000).
25. G. Gabrielse et al., *Phys. Rev. Lett.* **89**, 213401 (2002).
26. We thank R. G. Bryant, R. R. Jones, and B. C. Gallagher for helpful comments. Supported by NSF grants DHY-0244320 and CHE-0215957.

#### Supporting Online Material

[www.sciencemag.org/cgi/content/full/1108470/DC1](http://www.sciencemag.org/cgi/content/full/1108470/DC1)

Materials and Methods

Fig. S1

References

8 December 2004; accepted 1 February 2005

Published online 10 February 2005;

10.1126/science.1108470

Include this information when citing this paper.

## Rheological Measurements of the Thermoviscoelastic Response of Ultrathin Polymer Films

P. A. O'Connell and G. B. McKenna\*

Measurement of the thermoviscoelastic behavior of glass-forming liquids in the nanometer size range offers the possibility of increased understanding of the fundamental nature of the glass-transition phenomenon itself. We present results from use of a previously unknown method for characterizing the rheological response of nanometer-thick polymer films. The method relies on the imaging capabilities of the atomic force microscope and the reduction in size of the classical bubble inflation method of measuring the biaxial creep response of ultrathin polymer films. Creep compliance as a function of time and temperature was measured in the linear viscoelastic regime for films of poly(vinyl acetate) at a thickness of 27.5 nanometers. Although little evidence for a change in the glass temperature is found, the material exhibits previously unobserved stiffening in the rubbery response regime.

Full understanding of the fundamentals of glass formation and glassy behavior remains one of the major unsolved problems of condensed matter physics (1, 2). One potential source of improved understanding comes from the observation of important changes in the behavior of glass-forming materials at the nanometer size scale (3–10). Polymeric materials in particular make excellent model systems, because they can be made

into ultrathin films that maintain their integrity.

Past work in thin polymer films has been performed primarily in a pseudothermodynamic mode, where a change in the slope of a property with temperature is interpreted as the glass transition temperature ( $T_g$ ). In particular, thin polymer films have been characterized with often-conflicting results (11, 12) by x-ray reflectivity (13), Brillouin scatter-

ing (14), neutron reflectivity (15), etc. in an attempt to determine the impact of film thickness and constraint on the glass transition behavior of the materials. Other methods, such as lateral force atomic force microscopy (AFM) (16) and hole growth in thin films (17, 18), have also been used to examine the problem but with less clearly defined results. The aim of the current work is to develop and apply a previously unknown nanorheological measurement method that allows the determination of the viscoelastic response of thin films in which the film thickness and lateral constraints can be varied systematically. The approach is to take the bubble inflation of thin membranes biaxial test method (19–22) and scale it so that films of nanometer thickness can be tested. This paper presents details of the preparation, measurement, and analysis of such nanobubbles and shows the validity of such an approach. Initial results on the creep compliance of a poly(vinyl acetate) (PVAc) are presented, which show that there is no significant change (<3°C) in the  $T_g$  for this material at an effective film thickness of 27.5 nm. The results do show, however, surprising stiffening in the

Department of Chemical Engineering, Texas Tech University, Lubbock, TX 79409–3121, USA.

\*To whom correspondence should be addressed. E-mail: greg.mckenna@ttu.edu

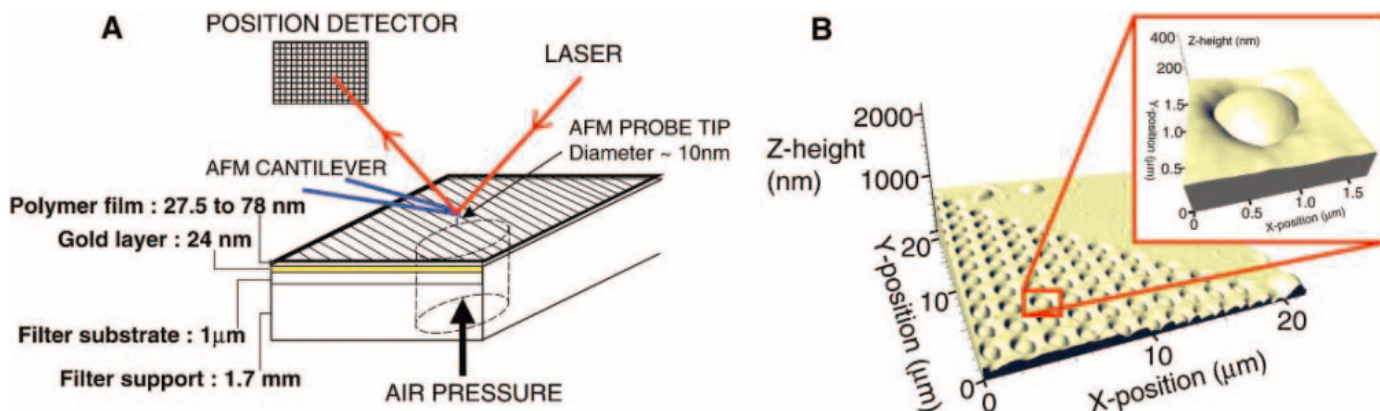


**Fig. 1.** (A) Schematic of the nanobubble inflation technique for a single bubble. (B) Three-dimensional image of a 22- $\mu\text{m}$  square scan. The image shows the regular array of inflated bubbles. (Inset) Enlarged view of a single bubble.

rubbery response regime that remains to be explained.

The material used in this study was a PVAc [molecular mass = 157,000 daltons, polydispersity index (PDI) = 2.73, Scientific Polymer Products, Incorporated (Ontario, NY), lot 08] having a measured  $T_g$  of 30.6°C. Thin films of the PVAc were made by spin coating 2% to 3.5% w/w solutions of the polymer in toluene onto glass slides (23). After drying, the films were floated off the glass slides onto water and transferred to the filter substrate. The substrate (24) consists of a silicon nitride layer about 1  $\mu\text{m}$  thick on a silicon support layer into which an array of 1.2- $\mu\text{m}$  holes has been etched. A 24-nm gold coating was sputtered onto the filter to promote PVAc adhesion. The film was then annealed at 50.6°C (20°C above the nominal  $T_g$ ) for 1 hour to get good adhesion to the filter surface. Before testing, score marks were made on the filter edge to remove the polymer film, and the film thickness was measured by looking at the step height change with the AFM. The filter was loaded into the temperature-controlled pressure cell, pressurized air was applied below the filter, and the AFM imaged the filter surface.

The bubble inflation experiment is shown schematically (Fig. 1A). Placing a pressure gradient across a constrained membrane results in the inflation of the bubble, and, in the domain for which the membrane remains hemispherical in shape, the stress ( $\sigma$ ) is related to the pressure,  $P$ ; the film thickness,  $t_0$ ; and the radius of curvature,  $R$ , of the membrane as (19):

$$\sigma_{11} = \sigma_{22} = \frac{PR}{2t_0} \quad (1)$$

The biaxial deformation or strain,  $\epsilon_{11} = \epsilon_{22}$ , at the pole of the bubble is related to the bubble geometry by the following expression (19):

$$\epsilon_{11} = \epsilon_{22} = \frac{s}{2R_0} - 1 \quad (2)$$

where  $s$  is the segment length of the bubble and  $R_0$  is the radius of the membrane before

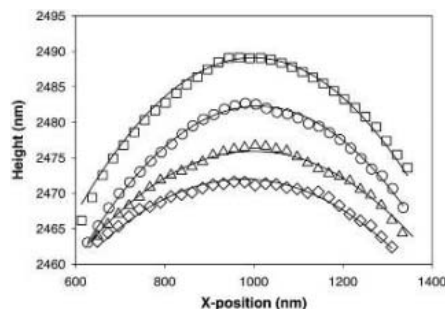


**Fig. 2.** Bubble center-line profiles as a function of time for a PVAc film of 43-nm thickness at 30°C and a pressure of 0.7 MPa. Diamonds indicate position at 288 s; triangles, at 853 s; circles, at 3868 s; and squares, at 7636 s. The solid lines are fits of the respective data to Eq. 3 for a segment of a circle.

inflation (the hole radius). An important aspect of this technique is that it uses the imaging capability of the AFM to perform the deformation measurements; this removes the problems associated with contact mechanics that come into play when the AFM is used as a nanolevel mechanical testing or indentation machine (25–27).

We show an example of a three-dimensional image of a 22- $\mu\text{m}$  square scan of the PVAc film under pressure (Fig. 1B). The lower left section shows the regular array of bubbles that form under pressure, with the dome-like structure of the bubbles clearly visible. An expanded view of a single bubble is also shown (Fig. 1B, inset). The bubbles sit somewhat below the filter surface because of capillary effects pulling the film down about 150 nm into the hole during the annealing stage of the film deposition process. This leads to a pre-strain in the material of about 25% ( $\lambda = 1.25$ ), which in turn leads to a reduction in the original film thickness (43 nm) of about 0.64. Hence, the film thickness as tested is about 27.5 nm.

Center-line profile plots of a typical bubble as a function of time are shown in Fig. 2. The main feature is the observation that the

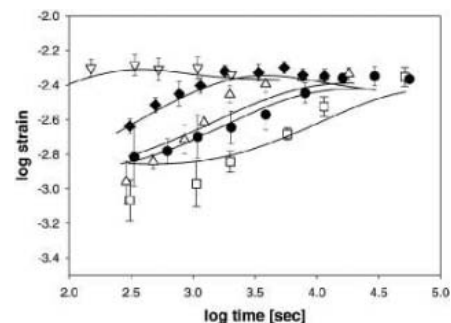


**Fig. 3.** Log-log plot of the strain as a function of time for a range of temperatures for PVAc film. Open squares at 25.5°C, solid circles at 27°C, open up triangles at 30°C, solid diamonds at 32°C, and open down triangles at 35°C. The solid lines are results from fits to Eq. 5. The data represent averages of four to six bubbles per data point. Error bars indicate a single standard deviation of the average of the strain measurements on four to six bubbles in a single test.

material at the base of the hole has formed a bubble under the applied pressure, which grows (creeps) with time up to a height of about 35 nm after 7600 s.

From Eqs. 1 and 2, it can be seen that the only measurement required for the calculation of the stress and strain in the inflated bubble is the radius of curvature ( $R$ ) of the bubble.  $R$  is calculated by taking the bubble profile and fitting it to the equation of a circle:

$$R^2 = (x - a)^2 + (y - b)^2 \quad (3)$$

where  $R$  is the radius of curvature,  $x$  and  $y$  are the  $x$  position and height data for the bubble profile, respectively, and  $a$  and  $b$  are offset constants for a circle not centered on the coordinate axes.

The time-dependent creep compliance of the PVAc films is measured by following the growth of the bubble as a function of time and temperature. Coated filters are loaded into the pressure cell, heated to the test temperature, and allowed to equilibrate for 30 min. The air pressure is then ramped in about 15 s

to the required value. The AFM is then set to continuously scan a 6- $\mu\text{m}$  square area of the surface. This allows up to nine bubbles to be imaged per scan, though, due to a slight drift on the sample stage, typically four to six complete bubbles are available on each scan.

Tests were carried out at temperatures of 25.5°C, 27°C, 30°C, 32°C, and 35°C at a fixed pressure of 10 psi ( $\sim 0.07$  MPa, corresponding to  $\sim 0.7$  MPa of stress on the polymer film). Figure 2 shows a set of bubble profiles for a single bubble as a function of time for data collected at 30°C. (In practice, a single profile scan is taken on each bubble in the scan field, and the results are averaged. A profile scan is determined by taking the scan that has the maximum height on the bubble.) Each curve is fitted to Eq. 3, and the fitted data, with radii of curvature varying from about 600 nm to 3300 nm, are also shown in Fig. 2. Using Eqs. 1 and 2 and the profile data, the stress,  $\sigma_{11}(t)$ , and strain,  $\epsilon_{11}(t)$ , were determined.

A double logarithmic plot of the strain as a function of time is shown (Fig. 3) for the range of data covering the temperatures quoted. Although there is a degree of scatter in the data, the general trend with temperature is clear: i.e., as the temperature increases the strain curves shift to shorter time scales, indicating increased molecular mobility. The uncertainty in the temperature at the filter surface is  $\pm 0.5^\circ\text{C}$ , and this leads to an error on the time scale of the material response of about  $\pm 0.3$  of a decade.

The creep compliance,  $D(t)$ , is given by the ratio of  $\epsilon_{11}(t)$  to  $\sigma_{11}(t)$ :

$$D(t) = \epsilon_{11}(t)/\sigma_{11}(t) \quad (4)$$

However, because of the varying stress on the bubble as it expands and the fact that the response of a viscoelastic material is a function of the entire stress history, the measured creep compliance curves are apparent compliances and cannot be directly compared to bulk data from standard (constant stress) creep experiments. In order to directly compare the present data with bulk data on PVAc from Plazek (28), we used Boltzmann superposition (29) to model the growth of a bubble by using the known stress history,  $\sigma(t)$ , and a material function incorporating the glassy and rubbery compliances and the retardation time (a measure of the dynamics of the system), the parameters of which are adjusted to give a best fit to the data (also, the original shear compliance data was converted to uniaxial compliance assuming the material is incompressible). Importantly, the material function parameters should be fixed for all the data sets, the only variable being the retardation time, which is expected to vary with temperature. The model can be expressed as

$$\epsilon(t) = \int_0^t D(t - \zeta) \left( \frac{d\sigma}{d\zeta} \right) d\zeta \quad (5)$$

where  $D(t - \zeta)$  is the material function given by

$$D(t) = D_G + (D_R - D_G)(1 - e^{-(t/\tau)^\beta}) \quad (6)$$

where  $D_G$  is the glassy compliance,  $D_R$  the rubbery compliance,  $\tau$  the retardation time, and  $\beta$  the shape parameter for the creep function. Acceptable fits to the data were obtained by using the following parameters:  $D_G = 1.6 \times 10^{-10} \pm 0.4 \times 10^{-10} \text{ Pa}^{-1}$ ,  $D_R = 15.0 \times 10^{-10} \pm 4.0 \times 10^{-10} \text{ Pa}^{-1}$ ,  $\beta = 0.84$ , and  $\tau$  values of 20,000, 4500, 2000, 750 and 120 s at, respec-

tively, 25.5°C, 27°C, 30°C, 32°C, and 35°C. The error in the  $\tau$  values is estimated at  $\pm 50\%$  and reflects the scatter in the data and the error in the temperature at the filter surface. The  $\beta$  parameter was the same value used in fitting the bulk data of Plazek (28).

The calculated true creep compliance data at temperatures of 25.5°C, 30°C, and 35°C are compared with the bulk data of Plazek (28) in Fig. 4A. The three main features of the data follow.

1) The experimental data at 25.5°C and 30°C show the glassy response at short times, with a glassy compliance comparable to that of the bulk data ( $2.0 \times 10^{-10} \text{ Pa}^{-1}$  compared to  $1.6 \times 10^{-10} \text{ Pa}^{-1}$ ).

2) The longer time data at 25.5°C and 30°C and the data at 35°C show a leveling off, indicating the approach to the rubbery plateau. The rubbery compliance for the thin film is smaller by a factor of about 320 compared with the bulk material ( $1.5 \times 10^{-9} \text{ Pa}^{-1}$  compared with  $4.8 \times 10^{-7} \text{ Pa}^{-1}$ ). We note that tests conducted on thicker samples (56 nm and 78 nm) at 35°C showed (Fig. 4A, insert) increasing rubbery plateau values ( $9.8 \times 10^{-9} \text{ Pa}^{-1}$  and  $1.4 \times 10^{-8} \text{ Pa}^{-1}$ , respectively). Extrapolation to the bulk value is estimated to occur at about 150 nm.

3) The temperature shift factors,  $a_T$  (a measure of the relative change in the dynamics of the system with temperature), from the current study agree closely with the bulk data (Fig. 4B). Importantly, if the glass transition were substantially depressed, we would expect that the temperature shift factors would show much less temperature sensitivity than the bulk data.

Thus, we observe that the glassy compliance and dynamics of the thin film are com-

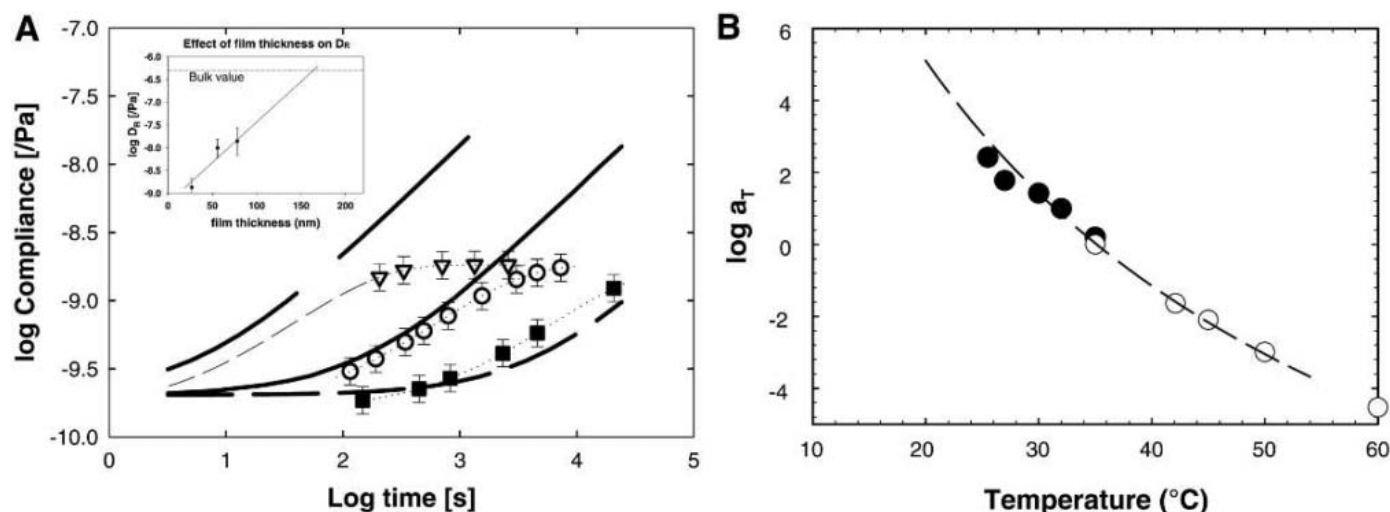


**Fig. 4.** (A) Experimental creep compliance data for PVAc film (symbols) compared to the bulk data of Plazek (28) (lines). Solid squares, open circles, and open down triangles represent the data from this study at, respectively, 25.5°C, 30°C, and 35°C. The heavy short dashed, solid, and long dashed lines represent the bulk data of Plazek at, respectively, 25.5°C, 30°C, and 35°C. (Inset) Log of the rubbery plateau compliance ( $D_R$ ) as a function of film

thickness, with the bulk value indicated by the dashed line. Error bars indicate a standard error of estimate from the curve fit to the data of Fig. 3. For insert, error bars have same meaning as in Fig. 3. (B) Log of the temperature shift factors,  $a_T$ , as a function of temperature from the current study (solid circles) and from the Plazek data (open circles), both referenced to 35°C. The dashed line is a Williams, Landel, Ferry (35) fit to the data of Plazek.

parable to the bulk material, and, in the regime where segmental motions are dominant (i.e., in the glassy and early transition regions), the glass transition temperature of the thin films is unchanged within an estimated error of  $\pm 3^\circ\text{C}$ . Calculations using a three-layer viscoelastic model in which the outer two layers have substantially reduced glass transition ( $15^\circ\text{C}$ ) show that the method is sensitive to such layers or gradients when the layer is about 10% or more of the film thickness. The rubbery compliance shows a much reduced value at 27.5 nm, although this is seen to increase as the film thickness increases. It is possible that at this thickness (27.5 nm) the material responds in a different manner to the bulk, perhaps because of a change in the chain conformation (30) or because the entanglement density is affected by the constraint imposed by the thickness. However, recent work (31) suggests that the entanglement density is reduced in thin films, which would increase the compliance. As such, the observation of a reduced rubbery plateau is surprising and cannot be reconciled within our current understanding of the behavior of ultrathin films. We do not think that it is an artifact of the experiment, e.g., due to surface tension effects or prestrain on the sample caused by the drawing of the film into the hole. At the nanoscale, surface tension effects could become important, but our calculations suggest these effects would be less than 15% for a film of 27.5-nm thickness at the pressure used here.

The effect of prestrain on the sample was estimated by using classical rubber elasticity theory (32). Such an analysis implies that a prestrain of about 760% ( $\lambda = 7.6$ ) would be needed to account for the apparent decrease in compliance for the bubble growth data. This is much less than the 25% prestrain estimated because of the capillary draw that occurs during the annealing step in the film preparation.

Comparison of our results to bulk data indicates that there is no significant change in the glass transition temperature down to a thickness of 27.5 nm. This is contrary to results reported for free-standing polystyrene (PS) films, where decreases of up to  $70^\circ\text{C}$  for such a thickness have been reported (23). However, recent results for poly(methyl methacrylate) (PMMA) (33) show a much smaller effect of film thickness on  $T_g$ . In this context, the current results would support the possibility that the effect of film thickness on  $T_g$  is not universal (34). Unexpectedly, whereas the material exhibits a glassy compliance comparable to the bulk data, the rubbery plateau compliance is seen to decrease with decreasing film thickness, indicating stiffening of the rubbery response in the ultrathin film. Future investigations of PS and other polymer films will further explore how the difference in results varies with material chemical structure and

how the measurement type (pseudothermodynamic versus dynamic) may impact the interpretation of results.

#### References and Notes

- P. W. Anderson, *Science* **267**, 1615 (1995).
- C. A. Angell, K. L. Ngai, G. B. McKenna, P. F. McMillan, S. W. Martin, *J. Appl. Phys.* **88**, 3113 (2000).
- C. L. Jackson, G. B. McKenna, *J. Non-Cryst. Solids* **131-133**, 221 (1991).
- J. A. Forrest, *Eur. Phys. J. E* **8**, 261 (2002).
- D. Johannsmann, *Eur. Phys. J. E* **8**, 257 (2002).
- S. L. Simon, J. Y. Park, G. B. McKenna, *Eur. Phys. J. E* **8**, 209 (2002).
- S. D. Kim, J. M. Torkelson, *Macromolecules* **35**, 5943 (2002).
- I. Raptis, C. D. Diakoumakos, *Microelectron. Eng.* **61-2**, 829 (2002).
- R. Kugler, W. Knoll, *Macromol. Chem. Phys.* **203**, 923 (2002).
- T. S. Chow, *J. Phys. Condens. Matter* **14**, 1333 (2002).
- G. B. McKenna, *J. Phys. IV (Paris)* **10(P7)**, 53 (2000).
- J. Y. Park, G. B. McKenna, *Phys. Rev. B* **61**, 6667 (2000).
- W. E. Wallace, J. H. van Zanten, W. L. Wu, *Phys. Rev. E* **52**, R3329 (1995).
- J. L. Keddie, R. A. L. Jones, R. A. Cory, *Faraday Discuss. Chem. Soc.* **98**, 219 (1994).
- W. J. Orts, J. H. van Zanten, W. L. Wu, S. K. Satija, *Phys. Rev. Lett.* **71**, 867 (1993).
- C. K. Buenviaje, S.-R. Ge, M. H. Rafailovich, R. M. Overney, in *Fundamentals of Nanondentation and Nanotribology Symposium* (Materials Research Society, Warrendale, PA, 1998), p. 187.
- K. Dalnoki-Veress, B. G. Nickel, C. Roth, J. R. Dutcher, *Phys. Rev. E* **59**, 2153 (1999).
- C. G. Yuan, O. Y. Meng, J. T. Koberstein, *Macromolecules* **32**, 2329 (1999).
- A. E. Green, J. E. Adkins, *Large Elastic Deformations* (Oxford Univ. Press, London, 1970).
- A. S. Wineman, *Trans. Soc. Rheol.* **20**, 203 (1976).
- D. D. Joye, G. W. Poehlein, C. D. Denson, *Trans. Soc. Rheol.* **16**, 421 (1972).
- O. Hassager, S. B. Kristensen, J. R. Larsen, J. Neergaard, *J. Non-Newtonian Fluid Mech.* **88**, 185 (1999).
- J. Mattson, J. A. Forrest, L. Börjesson, *Phys. Rev. E* **62**, 5187 (2000).
- Aquamarijn Micro Filtration B.V., Berkelkade 11, 7201 JE Zutphen, Netherlands.
- M. R. VanLandingham, J. S. Villarrubia, W. F. Guthrie, G. F. Meyers, *Macromol. Symp.* **167**, 15 (2001).
- K. L. Johnson, *Contact Mechanics* (Cambridge Univ. Press, Cambridge, 1985).
- H. Lu, B. Wang, J. Ma, G. Huang, H. Viswanathan, *Mech. Time Dependent Mater.* **7**, 189 (2003).
- D. J. Plazek, *Polym. J.* **12**, 43 (1980).
- L. Boltzmann, *Sitzungsber. Akad. Wiss. Wien Math. Naturwiss. Kl.* **70(2)**, 275 (1874).
- R. L. Jones, S. K. Kumar, D. L. Ho, R. M. Briber, T. P. Russell, *Macromolecules* **34**, 559 (2001).
- S. Lun, M. V. Massa, K. Dalnoki-Veress, H. R. Brown, R. A. L. Jones, *Phys. Rev. Lett.*, in press.
- L. R. G. Treloar, *The Physics of Rubber Elasticity* (Clarendon, Oxford, ed. 3, 1975).
- C. B. Roth, J. R. Dutcher, *Eur. Phys. J. E* **12(suppl. 1)**, S103 (2003).
- G. B. McKenna, *Eur. Phys. J. E* **12(1)**, 191 (2003).
- M. L. Williams, R. F. Landel, J. D. Ferry, *J. Am. Chem. Soc.* **77**, 3701 (1955).
- Thanks to the John R. Bradford Endowment at Texas Tech, the National Science Foundation (grant DMR-0304640), and the U.S. Army Research Office (grant W911NF-04-1-0207) for partial support of this project.

24 September 2004; accepted 3 February 2005  
10.1126/science.1105658

## The Controlled Evolution of a Polymer Single Crystal

Xiaogang Liu,<sup>1\*</sup> Yi Zhang,<sup>1\*</sup> Dipak K. Goswami,<sup>2</sup>  
John S. Okasinski,<sup>2</sup> Khalid Salaita,<sup>1</sup> Peng Sun,<sup>1</sup>  
Michael J. Bedzyk,<sup>2†</sup> Chad A. Mirkin<sup>1‡</sup>

We present a method for controlling the initiation and kinetics of polymer crystal growth using dip-pen nanolithography and an atomic force microscope tip coated with poly-DL-lysine hydrobromide. Triangular prisms of the polymer epitaxially grow on freshly cleaved mica substrates, and their in-plane and out-of-plane growth rates can be controlled by raster scanning the coated tip across the substrate. Atomic force microscope images were concomitantly recorded, providing a set of photographic images of the process as it spans the nanometer- to micrometer-length scales as a function of environmental conditions.

Crystallization is an integral part of many processes and essential for the characterization of many materials, including small molecules, nanoclusters, and biological macromolecules (1–5). For most crystallization

processes, the ability to study the process is limited until the crystal reaches a critical size that allows one to observe it with spectroscopic or x-ray diffraction tools. For single-crystal x-ray diffraction (XRD) techniques, the lower limit is on the order of  $100\ \mu\text{m}^3$ , depending on composition and x-ray beam conditions (6). For spectroscopic tools, the length scale is even larger. Scanning probe microscopy has been used to visualize crystallization processes in situ, but typically in the context of structures growing randomly on a surface from a bulk solution saturated with a feedstock of the molecule involved in crystallization (7–14). There are no tools that allow

<sup>1</sup>Department of Chemistry and Institute for Nanotechnology, <sup>2</sup>Department of Materials Science and Engineering and Nanoscale Science and Engineering Center, Northwestern University, Evanston, IL 60208, USA.

\*These authors contributed equally to this work.

†To whom inquiries pertaining to crystallography should be addressed. E-mail: bedzyk@northwestern.edu

‡To whom all other correspondence should be addressed. E-mail: camirkin@chem.northwestern.edu



one to site-specifically initiate crystal nucleation, control the growth process in a serial manner, and monitor its progress from the nanometer to micrometer scale.

Dip-pen nanolithography (DPN) allows an atomic force microscope (AFM) tip to transport adsorbates to a surface in a controlled manner (15–19). This technique has allowed researchers to control the nanoscale architecture of a surface and is compatible with both hard and soft materials (16). DPN coupled with AFM also can be used as a serial deposition tool to study monolayer formation (16). Polylysine, commonly used as a coating on inorganic substrates for the surface attach-

ment of biomolecules and cells in molecular biology studies, is also regarded as a simple model for protein aggregation studies (20, 21). We show how DPN initiates the crystallization of poly-DL-lysine hydrobromide (PLH) on mica [KAl<sub>2</sub>(AlSi<sub>3</sub>)O<sub>10</sub>(OH)<sub>2</sub>, 2M<sub>1</sub>-muscovite] and study and record the growth process from nanometer-sized seeds to larger crystalline structures as a function of environmental conditions.

In a typical experiment, a PLH-coated silicon AFM tip is used as a deposition tool on a freshly cleaved mica substrate in an AFM raster scanning experiment. The AFM was operated in tapping mode, during which the tip is oscillated at a frequency just below its

resonant frequency (300 kHz). Tapping-mode AFM is more suitable than contact mode for imaging delicate polymer samples because it is less damaging to the sample (19, 22). A single scan over an 8-by-8- $\mu$ m region of the mica surface results in the formation of two equilateral triangular prisms (a and b) that are substantially different in size (Fig. 1, panel 1) (23). The smaller triangular feature (b) has a 320-nm edge length and is 21.8 nm thick, whereas the larger one (a) has a 1.62- $\mu$ m edge length and is 16.5 nm thick. The chemical composition of the nanometer- and micrometer-scale triangular islands was confirmed by time-of-flight secondary ion mass spectroscopy, which exhibits the characteristic fragments for PLH (fig. S1). As the tip was scanned across the same area in tapping mode (scan rate, 2 Hz), one could observe the growth of seed crystals and the formation of new ones (compare panels 1 to 6 in Fig. 1). The growth process is very similar from crystal to crystal under these conditions. All observed structures were equilateral triangles, and crystals that were initiated at approximately the same time had nearly identical dimensions after the same number of raster scans. We found that the crystal thickness and edge length increase with the number of scans or tip-substrate contact time (Fig. 2, A and B).

Control experiments indicate that it is difficult to grow the well-defined triangular prisms through direct exposure of the mica substrate to a solution containing the PLH. In such control experiments, freshly cleaved mica substrates were either soaked in PLH solutions that varied in concentration (2 to 20 mg/ml) for 3 hours or immersed in the solutions and immediately removed and then stored in a humidity chamber (30% relative humidity) at 20°C for 1 to 2 hours, during which time the solvent evaporated. Many types of microstructures could be observed on the mica surfaces, including amorphous materials and truncated triangles of varying dimensions. Conditions that allowed us to visualize the nucleation process on the nanoscale could not be identified (fig. S2). Similar results were observed when microcontact printing with a polydimethylsiloxane (PDMS) stamp was used to crystallize PLH on mica (24).

The data strongly suggest a tip-modulated crystallization process that controls the delivery of the molecules and subsequently the kinetics of crystal growth. The primary role of the tip is in controlling the location of crystallization and a heavy concentration of the crystallizing PLH. The scan direction does not substantially affect the growth process or the orientation of the crystals. Furthermore, the rate of increase for the edge length is substantially faster than that for the thickness. This can be attributed, in part, to the strong electrostatic PLH molecule-substrate interaction (vide infra) that accelerates the growth of the crystal

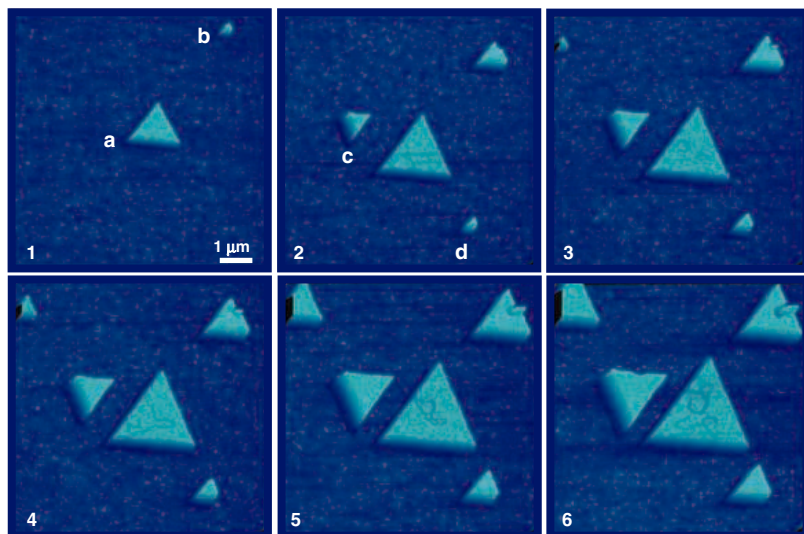
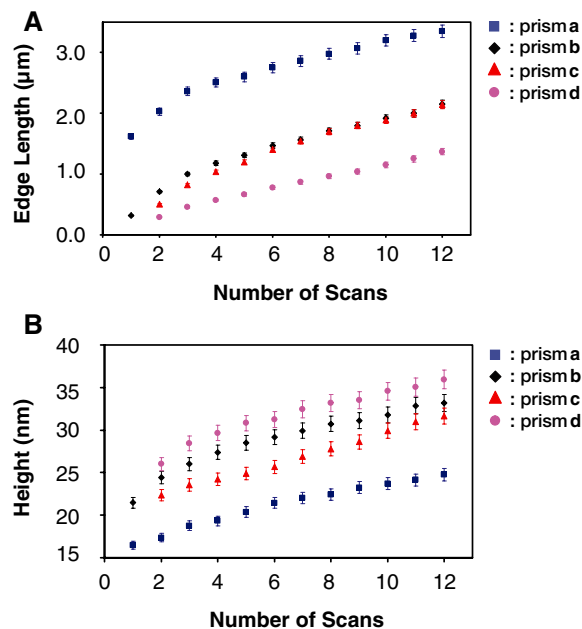


**Fig. 1.** Panels 1 to 6 show a series of 8-by-8- $\mu$ m 3D topographic AFM images of mica taken at 256-s intervals (relative humidity, 30%; temperature, 20°C), obtained by continuously scanning an AFM tip coated with PLH molecules in tapping mode (scan rate, 2 Hz). Crystals (labeled as a, b, c, and d) were chosen for kinetic studies. PLH triangles with edge lengths ranging from 100 nm to 10  $\mu$ m and with heights from 5 to 50 nm were generated. The size of the crystals can be controlled by varying the relative humidity. Lower humidities favor the formation of smaller triangles.

**Fig. 2.** (A) The edge length and (B) the height of PLH prisms a to d shown in Fig. 1 plotted as a function of number of raster scans. Error bars show mean  $\pm$  SD.



along its edges. In addition, because of the thin nature of these structures, the number of molecules required to increase the height of a triangle is larger than the number required to extend their edge lengths. This area effect on growth rate is exacerbated as the crystals grow. Another notable feature of this process is that all of the prisms grow in one of two orientations that differ by a  $180^\circ$  rotation, which indicates oriented epitaxial growth of the PLH crystals with respect to the underlying pseudo-hexagonal two-dimensional (2D) lattice of the mica surface (25). Indeed, control experiments involving the deposition of PLH on silicon, silicon oxide, highly ordered pyrolytic graphite, and amine-terminated mica substrates do not yield triangular-shaped structures (figs. S3 and S4).

Optical microscopy and single-crystal XRD of the mica substrate with back-reflection Laue and single-crystal diffraction methods were employed to determine the crystallographic orientations of the prisms relative to the substrate. These experiments revealed that the two opposing prism orientations aligned with the mica [100] direction as shown in Fig. 3, A and B, and matched the 2D symmetry of the mica surface (26). Consistent with the characterization of the triangular structures as crystals of PLH, drying them results in substantial water loss and morphological change. After drying in air at  $20^\circ\text{C}$  for 20 min, the triangular features transformed into uniform triangular frames that maintained an epitaxial relationship with the underlying mica lattice (Fig. 3C). An analysis of the volumes of filled triangles and their corresponding frame structures shows that water makes up about 60% of their volume.

To show that the triangular structures are indeed crystals and to gain a better understanding of their structure and relationship with the underlying mica substrate, single-crystal oscillation XRD patterns were collected in a grazing-incidence geometry at the Advanced Photon Source 5ID-C undulator beamline with the use of a five-circle Huber diffractometer and a MAR 2D charge-coupled device (CCD) area detector (27). The PLH  $1\text{-by-}1\text{-mm}^2$  area on the mica surface was aligned with the x-ray beam and diffractometer center by observing the  $\text{Br K}\alpha$  fluorescence signal from the PLH with an energy-dispersive solid-state x-ray detector. Two separate sets of oscillation patterns were collected from the same sample under identical conditions: one set from the bare mica (i.e., no  $\text{Br K}\alpha$  fluorescence) and the other set from the PLH-covered mica. The  $\phi$  rotational axis of the diffractometer was laser aligned with the mica  $c^*$  axis [i.e., perpendicular to (001) cleavage face]. The total contiguous and identical rotational range used for each of the two data sets shown in Fig. 3D is  $50^\circ$ . This is the sum of 50 separate 20-s exposures, each

taken over a  $1^\circ$  range in  $\phi$ . The directly measured reciprocal-space coordinates in terms of scattering vector vertical component ( $Q_V$ ) versus horizontal ( $Q_H$ ) for the 2D diffraction pattern in Fig. 3D were produced by converting the  $(x, z)$  pixel coordinate of each peak that appeared in the set of CCD frames. The circles in Fig. 3D were observed diffraction spots in both sets (bare and PLH-covered mica) of data and are (hkl) indexed consistent with the monoclinic  $2M_1$ -muscovite reciprocal

lattice. The triangles in Fig. 3D, which were diffraction spots only observed within the PLH set of oscillation patterns, have (hkl) indices that are noninteger, inconsistent with muscovite, and therefore originating from the PLH triangular prisms (table S1). Typical diffraction spots for a particular  $\phi$  collected in the CCD camera are shown in the inset of Fig. 3D. Each diffraction spot occurs only at a particular  $1^\circ$  interval of  $\phi$ . This indicates that the prisms grown on mica are single crystal

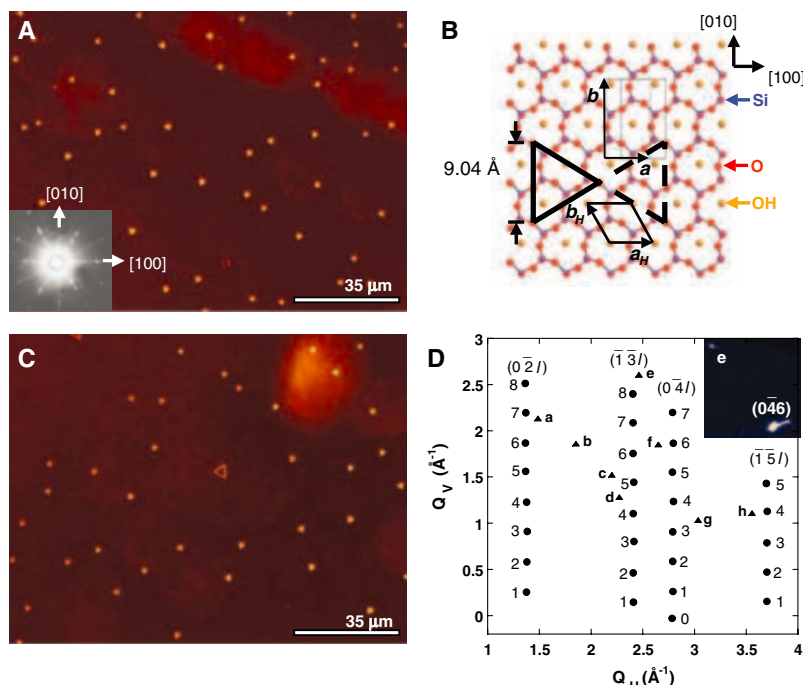


**Fig. 3.** (A) Dark-field light-scattering image of triangular crystals grown by means of the DPN method. (Inset) Laue pattern of the mica substrate. (B) Surface arrangement of the uppermost oxygen layer for cleaved mica. Triangles with edge lengths of 9.04 Å show the proposed arrangements of the prisms on the oxygen layer with solid or dashed lines indicating two possible orientations for the PLH prisms. (C) Dark-field light-scattering image of prisms upon drying in air for 20 min. (D) Single-crystal XRD data from mica (circles) and PLH prisms (triangles labeled a through h).  $Q_H$  and  $Q_V$  are the horizontal and vertical components of the scattering vector, respectively. Each column of mica diffraction spots has the same  $(h, k)$  indices. Each individual spot is marked with the corresponding  $l$  index. (Inset) A typical CCD image. In this frame, the mica  $(0\ 4\ 6)$  diffraction spot and the PLH prism diffraction spot labeled e appear.

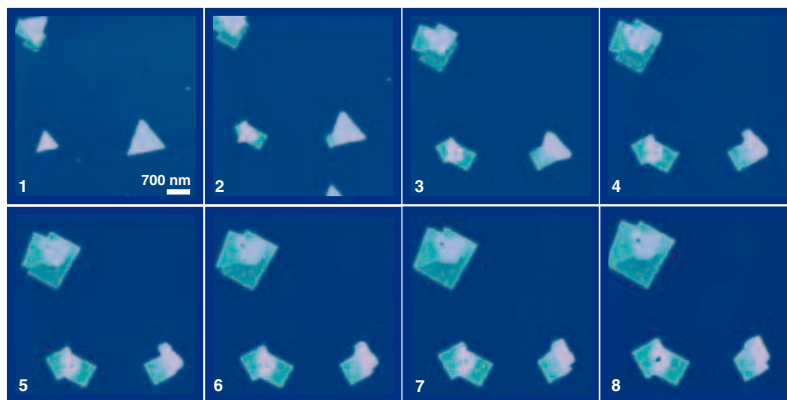


**Fig. 4.** Panels 1 to 8 show the AFM observed phase transformation of triangular prisms into cubes on mica. Images were taken at 256-s intervals by continuously scanning an AFM tip coated with PLH molecules in tapping mode (scan rate, 2 Hz). The relative humidity was 15% and the temperature was  $35^\circ\text{C}$ . The field of panel 2 is slightly offset because of thermal drift.

with a lattice that has an in-plane orientational epitaxy with the underlying mica lattice. The only reason x-ray analysis can be carried out on these structures is because we are able to signal average over a large collection of prisms that are aligned with one another and epitaxially arranged on the mica support.

This approach to controlling and monitoring the kinetics of crystal growth can be used to study environment-imposed changes in crystal morphology (28). Subtle changes in temperature markedly affect the growth of the crystals and the observed morphology of the crystals ultimately formed. Indeed, when the temperature is increased to 35°C, cubic-shaped features emerge at the edges of the prisms while scanning the crystals that were preformed at lower temperature with the PLH-coated AFM tip (Fig. 4). This morphological change is very reproducible and always was induced at the corners or edges of the starting triangular crystals.

This study provides an approach for site-specifically initiating crystal growth on the nanometer-length scale in a way that allows one to monitor growth from crystal seed to more mature structures as a function of environmental conditions (fig. S5). The size of the smallest crystal observed and studied in these experiments (d in Fig. 1) is five orders of magnitude smaller than what could be studied by single-crystal XRD techniques, allowing one to observe morphological changes that would typically go undetected in an x-ray study that

focuses on larger structures. Finally, growing crystals of macromolecules is not a trivial process. DPN is now a massively parallel tool (16, 29, 30), suggesting that this study may open the door for creating combinatorial approaches to identifying the proper conditions to initiate a particular type of crystal growth for a given set of target molecules.

#### References and Notes

- E. M. Landau, M. Levanon, L. Leiserowitz, M. Lahav, J. Sagiv, *Nature* **318**, 353 (1985).
- Y. Yin et al., *Science* **304**, 711 (2004).
- S. Mann, G. A. Ozin, *Nature* **382**, 313 (1996).
- J. L. Fransaer, R. M. Penner, *J. Phys. Chem. B* **103**, 7643 (1999).
- S. A. Empedocles, M. G. Bawendi, *Science* **278**, 2114 (1997).
- J. J. Pluth et al., *Proc. Natl. Acad. Sci. U.S.A.* **94**, 12263 (1997).
- A. C. Hillier, M. D. Ward, *Science* **263**, 1261 (1994).
- M. D. Ward, *Chem. Rev.* **101**, 1697 (2001).
- D. E. Hooks, C. M. Yip, M. D. Ward, *J. Phys. Chem. B* **102**, 9958 (1998).
- T. A. Land, A. J. Malkin, Y. G. Kuznetsov, A. McPherson, J. J. De Yoreo, *Phys. Rev. Lett.* **75**, 2774 (1995).
- H. H. Teng, P. M. Dove, C. A. Orme, J. J. De Yoreo, *Science* **282**, 724 (1998).
- J. K. Hobbs, M. J. Miles, *Macromolecules* **34**, 353 (2001).
- N. Sanz, J. K. Hobbs, M. J. Miles, *Langmuir* **20**, 5989 (2004).
- J. K. H. Hörber, M. J. Miles, *Science* **302**, 1002 (2003).
- R. D. Piner, J. Zhu, F. Xu, S. Hong, C. A. Mirkin, *Science* **283**, 661 (1999).
- D. S. Ginger, H. Zhang, C. A. Mirkin, *Angew. Chem. Int. Ed. Engl.* **43**, 30 (2004).
- B. W. Maynor, J. Li, C. Lu, J. Liu, *J. Am. Chem. Soc.* **126**, 6409 (2004).
- R. J. Barsotti, M. S. O'Connell, F. Stellacci, *Langmuir* **20**, 4795 (2004).

- G. Agarwal, L. A. Sowards, R. R. Naik, M. O. Stone, *J. Am. Chem. Soc.* **125**, 580 (2003).
- B. S. Jacobson, D. Branton, *Science* **195**, 302 (1977).
- W. Dzwolak, R. Ravindra, C. Nicolini, R. Jansen, R. Winter, *J. Am. Chem. Soc.* **126**, 3762 (2004).
- B. Ratner, V. V. Tsukruk, *Scanning Probe Microscopy in Polymers* (ACS Symposium Series, American Chemical Society, Washington, DC, 1998).
- The orientation is not related to the tip scanning direction. Change of the orientation of the mica substrate does not change the growth of the prisms or their orientation with respect to each other and the mica.
- X. Liu et al., data not shown.
- R. Kern, in *Crystal Growth in Science and Technology*, H. Arend, J. Hulliger, Eds. (Plenum Press, New York, 1989), pp. 143–165.
- Materials and methods are available as supporting material on Science Online.
- D. A. Walko et al., *AIP Conf. Proc.* **705**, 1166 (2004).
- W. C. McCrone, in *Physics and Chemistry of Organic Solid State*, D. Fox, M. M. Labes, A. Weissberger, Eds. (Interscience, New York, 1965), pp. 726–767.
- S. Hong, C. A. Mirkin, *Science* **288**, 1808 (2000).
- D. Bullen, S. W. Chung, X. Wang, J. Zou, C. A. Mirkin, *Appl. Phys. Lett.* **84**, 789 (2004).
- Supported by the Nanoscale Science and Engineering Initiative of the NSF under NSF Award No. EEC-0118025, the NIH through Award No. GM62109-02, and a Director's Pioneer Award to C.A.M., the Institute for BioNanotechnology in Medicine, Baxter Healthcare Corp, and the Air Force Office of Scientific Research (AFOSR) through a Multidisciplinary University Research Initiative (MURI) Award.

#### Supporting Online Material

www.sciencemag.org/cgi/content/full/307/5716/1763/DC1

Materials and Methods

Figs. S1 to S5

Table S1

References

6 January 2005; accepted 3 February 2005  
10.1126/science.1109487

## The Climate Change Commitment

T. M. L. Wigley

Even if atmospheric composition were fixed today, global-mean temperature and sea level rise would continue due to oceanic thermal inertia. These constant-composition (CC) commitments and their uncertainties are quantified. Constant-emissions (CE) commitments are also considered. The CC warming commitment could exceed 1°C. The CE warming commitment is 2° to 6°C by the year 2400. For sea level rise, the CC commitment is 10 centimeters per century (extreme range approximately 1 to 30 centimeters per century) and the CE commitment is 25 centimeters per century (7 to 50 centimeters per century). Avoiding these changes requires, eventually, a reduction in emissions to substantially below present levels. For sea level rise, a substantial long-term commitment may be impossible to avoid.

Oceanic thermal inertia causes climate change to lag behind any changes in external forcing and causes the response to be damped relative to the asymptotic equilibrium response (1–3). Because of this lag or damping effect, and because of the changes in atmospheric composition (and radiative forcing) that have already occurred, the climate system will continue to change for many decades (centuries for sea level) even in the absence of future changes in

atmospheric composition. For global-mean temperature, this is referred to as the “unrealized warming” (2), “residual warming” (4), or “committed warming” (5). Here, I use the term “warming commitment” or, to include sea level rise (6, 7), “climate change commitment.”

The assumption of constant atmospheric composition on which the warming commitment idea is based is clearly unrealistic, even as an extreme case of what might happen in the future. An alternative indicator of the commitment to climate change is to assume that the emissions (rather than concentrations)

of radiatively important species will remain constant. This Report investigates the constant-composition (CC) warming and sea level commitments, the constant-emissions (CE) commitments, and the uncertainties in each. Uncertainties arise from uncertainties in the climate sensitivity (2, 4), the rate of ocean heat uptake (2), the magnitude of past forcing, and the ice melt contribution to sea level change.

The usual (or “equilibrium”) CC warming commitment at time  $t$  is the difference between the equilibrium warming for forcing at this time ( $\Delta T_e$ ) and the corresponding realized warming ( $\Delta T_r$ ),  $\Delta T_e - \Delta T_r$ . This is related to the “radiation-imbalance” concept (8, 9). If  $\Delta Q$  is the forcing to date, and if  $\Delta Q_r$  is the forcing that gives an equilibrium warming of  $\Delta T_r$ , then the radiation imbalance is  $\Delta Q - \Delta Q_r$  [ $\Delta Q - \Delta Q_r$  is approximately equal to the flux of heat into the ocean (9)]. Hence

$$\Delta T_e - \Delta T_r = (\Delta Q - \Delta Q_r)(\Delta T_2 \times / \Delta Q_2 \times)$$

where  $\Delta Q_2 \times$  is the radiative forcing for a CO<sub>2</sub> doubling (about 3.7 W/m<sup>2</sup>) and  $\Delta T_2 \times$  is the corresponding equilibrium global-mean warming. A central estimate of  $\Delta Q$  (accounting for both natural and anthropogenic forcings) is about 1.7 W/m<sup>2</sup>, whereas  $\Delta T_r$  is about

National Center for Atmospheric Research, Boulder, CO 80307, USA. E-mail: wigley@cgd.ucar.edu

0.7°C. Given  $\Delta T2\times = 2.6^\circ\text{C}$  (10), a central value for the current equilibrium warming commitment is about 0.5°C, with a corresponding radiation-imbalance estimate of 0.7 W/m<sup>2</sup>. These results are in accord with other estimates in the literature, but uncertainties are large.

Because it would take an infinite time for the unrealized warming to appear, a more useful definition makes the unrealized warming a time-dependent quantity, namely, the evolving changes in global-mean temperature that would result if atmospheric composition were kept constant at its present state (4). This is the definition I use here. Temperatures under this new definition tend asymptotically to the previous equilibrium commitment definition. The new definition can be applied equally to the CC and CE commitments and can be used for both temperature and sea level.

To quantify the changes in global-mean temperature and sea level that would occur if either atmospheric composition or the emissions of radiatively important gases were kept constant at today's levels (the year 2000 is used to define "today"), I used the simple coupled gas-cycle/climate model MAGICC (10–12). MAGICC has been calibrated against a range of coupled atmosphere/ocean general-circulation models (13, 14) and was used in the Intergovernmental Panel on Climate Change (IPCC) Third Assessment Report (TAR) and earlier IPCC reports to produce the standard projections of global-mean temperature and sea level change. For access to MAGICC, see (15).

For sea level rise commitments, a change has been made in the way the melt contribution from land-based Glaciers and Small Ice Caps (GSICs) is calculated. In the TAR, the GSIC formula was only meant to be applied through the year 2100 (I project to the year 2400 here). Because of an empirical area-correction term used in the TAR (16), GSIC results are unrealistic beyond 2100, and the correction term imposes an artificial melt maximum (17). The modified formulation (17) matches the TAR results well through the year 2100 and then tends asymptotically to the initially available GSIC ice mass (taken as 40-cm sea level equivalent).

The other TAR sea level rise terms are (16) thermal expansion (a direct output of the climate model), mass-balance changes for the Greenland and Antarctic ice sheets, long-time-scale changes in these ice masses due to past climate change, deposition of sediments on the ocean floor, and runoff from the thawing of permafrost. In the TAR formulation, the last three components (referred to here as "unforced contributions") are independent of past forcings. To quantify nonexpansion uncertainties, I used methods employed in the TAR.

For the CC and CE temperature commitments, the primary sources of uncertainty are past radiative forcing, the climate sensitivity, and the rate of ocean heat uptake. For past

forcing, I considered the effect of natural forcings from solar irradiance changes (18) and volcanic eruptions (19), and uncertainties in aerosol forcing. For climate sensitivity, I used a central value of  $\Delta T2\times = 2.6^\circ\text{C}$  and a range of 1.5° to 4.5°C, approximately equal to the 90% confidence interval (CI) (10). For ocean mixing, I used vertical diffusivities ( $K_z$ ) of 1.3, 2.3, and 4.1 cm<sup>2</sup>/s, also representing the 90% CI and median values (10).

A breakdown of the natural and anthropogenic components of the CC commitment, together with uncertainties arising from ocean mixing ( $K_z$ ) uncertainties, is given in table S1. Past natural forcing (inclusion of which is the default case here) has a marked effect. The natural forcing component is surprisingly large, 64% of the total commitment in 2050, reducing to 52% by 2400. The effect of ocean mixing uncertainties is small, at most 7%.

Overall results and uncertainties associated with aerosol forcing and the climate sensitivity are shown in Fig. 1 (CC case) and Fig. 2 (CE case). Aerosol forcing is characterized by the forcing in 1990. The central values (and uncertainty ranges) are those used for global-mean warming projections in the TAR

(10, 13):  $-0.4\text{W/m}^2$  ( $-0.3\text{W/m}^2$  to  $-0.5\text{W/m}^2$ ) and  $-0.8\text{W/m}^2$  ( $-0.4\text{W/m}^2$  to  $-1.2\text{W/m}^2$ ) for direct and indirect sulfate forcing, and  $-0.1\text{W/m}^2$  ( $-0.2\text{W/m}^2$  to  $+0.1\text{W/m}^2$ ) for the sum of biomass and fossil and organic carbonaceous aerosols. The central value for total aerosol forcing is  $-1.3\text{W/m}^2$  (range,  $-0.6\text{W/m}^2$  to  $-1.9\text{W/m}^2$ ). Results depend primarily on the total aerosol forcing rather than the specific breakdown into different forcing categories. Extreme combinations, such as high climate sensitivity with low aerosol forcing, have very low probability (20).

In the CC case (Fig. 1), both climate sensitivity and aerosol forcing uncertainties are of similar importance. The eventual (equilibrium) commitment could be larger than 1°C (for high sensitivity and low aerosol forcing; low aerosol forcing means a higher value for past total forcing). This result is consistent with Wetherald *et al.* (5) because the Geophysical Fluid Dynamics Laboratory (GFDL) model used by these authors has a high sensitivity (4°C) (14). At the other extreme, the eventual commitment could be less than 0.2°C (for low sensitivity, virtually independent of the magnitude of aerosol forcing).

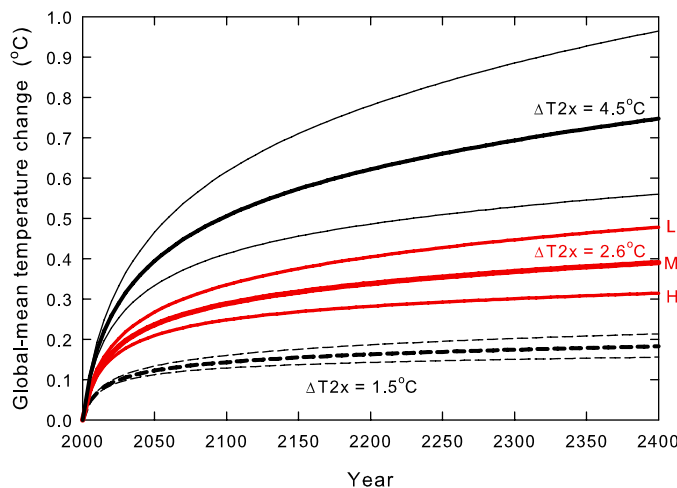


**Fig. 1.** CC warming commitment (constant concentrations after 2000) for different climate sensitivities and aerosol forcing levels (L, M, and H on the right of the figure indicate low, mid-, and high magnitudes for aerosol forcing, respectively). Values for the central sensitivity value (2.6°C equilibrium warming for a CO<sub>2</sub> doubling) are shown in red.

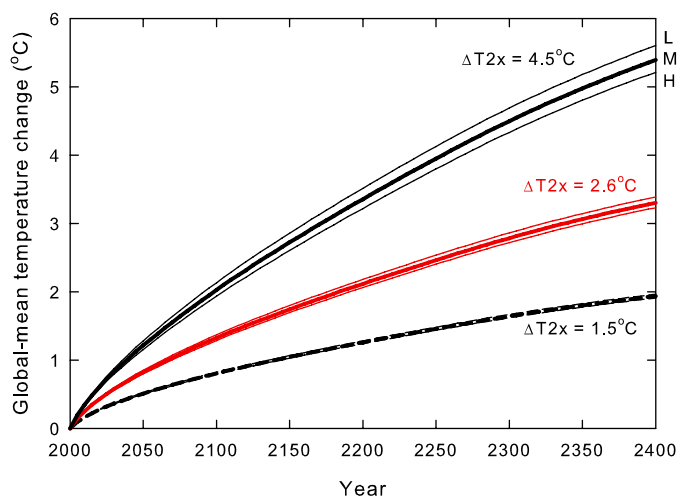


**Fig. 2.** CE warming commitment (CEs after 2000) for different climate sensitivities and aerosol forcing levels (L, M, and H on the right of the figure indicate low, mid-, and high magnitudes for aerosol forcing, respectively). Values for the central sensitivity value (2.6°C equilibrium warming for a CO<sub>2</sub> doubling) are shown in red.

Warming commitments for the CE case are much higher and do not tend to any asymptotic limit even on a time scale of millennia (largely because, at CE,  $\text{CO}_2$  concentrations continue to grow for many centuries). Climate sensitivity uncertainties are the dominant source of commitment uncertainty. By 2400, the warming ranges from about  $2^\circ\text{C}$  (for low sensitivity) to almost  $6^\circ\text{C}$  (high sensitivity). The clear message here is that, if we are to avoid future warming of this magnitude, emissions of radiatively active gases will have to be reduced to substantially below present levels.

For the sea level rise commitment results, we have an additional source of uncertainty in the ice melt and unforced contributions to sea level rise. Table S2 shows uncertainties in the CC commitment arising from ocean mixing uncertainties and gives a breakdown of the sea level rise commitment into contributions due to past natural forcing, past anthropogenic forcing, and unforced contributions.

Uncertainties in the CC sea level commitment resulting from uncertainties in ocean

heat uptake arise in two ways. First, the rate of ocean heat uptake affects the rate of atmospheric warming, which affects the rate of melt of land-based ice. Second, the rate of ocean heat uptake directly affects oceanic thermal expansion. For the temperature/melt effect, larger  $K_z$  leads to a larger warming commitment, which increases sea level rise. For expansion, larger  $K_z$  leads to a greater expansion commitment, also increasing sea level rise. For the commitment, both effects act in concert, in contrast to absolute changes that have compensating effects that reduce overall sensitivity to ocean mixing uncertainties. However, the overall commitment uncertainties arising from  $K_z$  uncertainties are small at 7 to 9%.

The breakdown into natural forcing, anthropogenic forcing, and unforced effects shows that unforced effects make a substantial contribution (for the CC case, less so for the CE case). For sea level changes arising from past forcings, anthropogenic forcing dominates.

Climate sensitivity and sulfate aerosol forcing uncertainties for the sea level com-

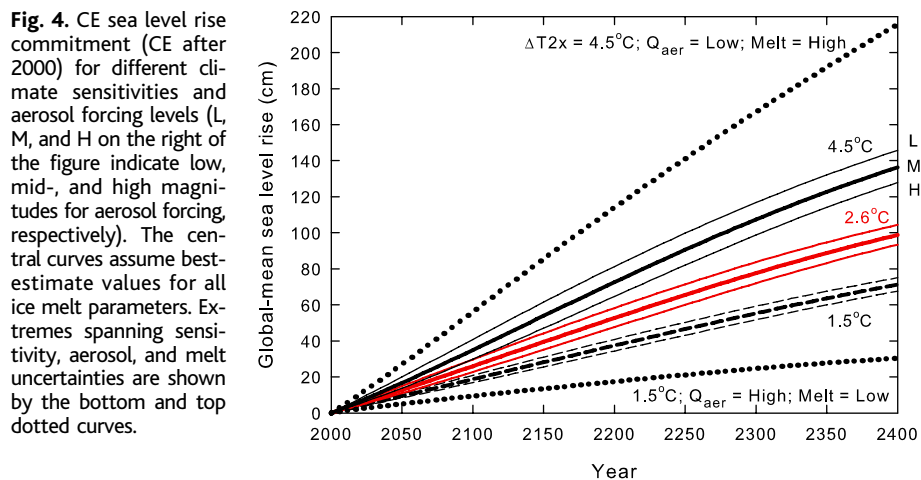
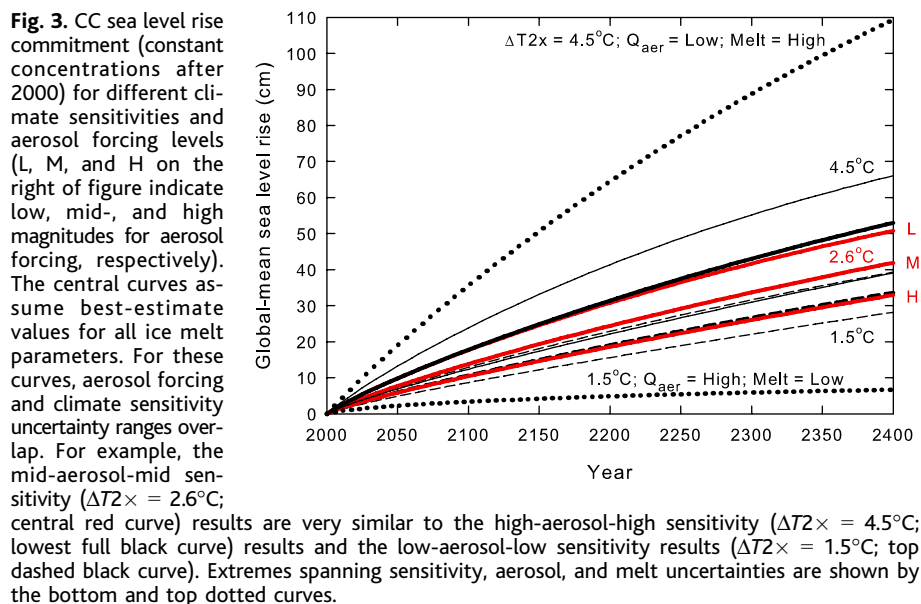
mitment are shown in Figs. 3 and 4. The CC case, constant concentrations from 2000, is shown in Fig. 3. The central commitment estimate (mid-aerosol forcing,  $\Delta T2\times = 2.6^\circ\text{C}$ , mid-melt) is a continuing rise of around 10 cm/century, of which about 40% is due to unforced effects (table S2) (15). Aerosol uncertainty effects (low, middle, and high values for 1990 forcing) are indicated by the letters to the right of the figure. Results are also shown for sensitivities of  $\Delta T2\times = 1.5^\circ$  and  $4.5^\circ\text{C}$  (mid-melt assumed). Climate sensitivity and aerosol forcing uncertainties are equally important, as shown by the overlapping ranges for different sensitivities. At the extreme high end (high sensitivity, low aerosol forcing, high melt), the rate of rise is almost 30 cm/century (26% due to unforced effects). At the extreme low end, the rate of rise is negligible (with zero unforced changes).

For the CE case (Fig. 4), CE from 2000, the central commitment estimate is a continuing rise of almost 25 cm/century. Approximately 15% of this is due to unforced effects. The lower and upper bounds are around 7 cm/century and more than 50 cm/century. These projections do not include the more catastrophic possibilities of accelerated melt in Greenland or the collapse of the West Antarctic ice sheet, as discussed in the TAR (16).

I considered the conventional (CC) commitment of changes that occur if atmospheric composition is held fixed at present (2000) levels, and the CE commitment for which emissions are fixed at their present levels. These commitments have been quantified for both global-mean temperature and sea level rise. Time-dependent changes are considered rather than just the usual asymptotic or equilibrium commitment.

The CC warming commitment rises steadily to an eventual warming of about  $0.2^\circ$  to more than  $1^\circ\text{C}$ . The contribution from past natural forcings exceeds that from past anthropogenic forcing. The corresponding CE warming commitment has no limit even on a time scale of many centuries, primarily because, at CE,  $\text{CO}_2$  concentrations continue to rise for a millennium or more. The CE warming commitment in 2400 ranges from  $2^\circ$  to almost  $6^\circ\text{C}$ , with most of the commitment due to past anthropogenic forcing. Both climate sensitivity and past aerosol forcing uncertainties are important in determining the CC commitment, whereas climate sensitivity is the main source of uncertainty for the CE commitment.

For sea level rise, both the CC and CE commitments lead to almost linear increases in sea level out to at least 2400 and probably much longer. For the CC commitment, sea level rises at about 10 cm/century (uncertainty range, near zero to about 30 cm/century). Except at the low end of the range, a substantial fraction of this increase arises from unforced contributions to sea level rise (40% in the cen-



tral case). For the CE commitment, sea level rises at about 25 cm/century (uncertainty range, 7 to more than 50 cm/century). The fractions arising from unforced contributions to sea level rise are less than those in the CC case.

The CE results reinforce the common knowledge that, in order to stabilize global-mean temperatures, we eventually need to reduce emissions of greenhouse gases to well below present levels (21). The CC results are potentially more alarming, because they are based on a future scenario that is clearly impossible to achieve and so represent an extreme lower bound to climate change over the next few centuries. For temperature, they show that the inertia of the climate system alone will guarantee continued warming and that this warming may eventually exceed 1°C. For sea level, a continued rise of about 10 cm/century for many centuries is the best estimate. Although such a slow rate may allow many coastal communities to adapt, profound long-term impacts on low-lying island communities and on vulnerable ecosystems (such as coral reefs) seem inevitable.

#### References and Notes

- M. L. Hoffert, A. J. Callegari, C.-T. Hsieh, *J. Geophys. Res.* **86**, 6667 (1980).
- J. Hansen et al., *Science* **229**, 857 (1985).
- T. M. L. Wigley, M. E. Schlesinger, *Nature* **315**, 649 (1985).
- T. M. L. Wigley, *Climate Monitor* **13**, 133 (1984).
- R. T. Wetherald, R. J. Stouffer, K. W. Dixon, *Geophys. Res. Lett.* **28**, 1535 (2001).
- T. M. L. Wigley, S. C. B. Raper, in *Climate and Sea Level Change: Observations, Projections and Implications*, R. A. Warrick, E. M. Barrow, T. M. L. Wigley, Eds. (Cambridge Univ. Press, Cambridge, 1993), pp. 111–133.
- R. J. Stouffer, S. Manabe, *J. Clim.* **12**, 2224 (1999).
- J. Hansen et al., *J. Geophys. Res.* **107**, 4347, 10.1029/2001JD001143 (2002).
- R. A. Pielke Sr., *Bull. Am. Met. Soc.* **84**, 331 (2003).
- T. M. L. Wigley, S. C. B. Raper, *Science* **293**, 451 (2001).
- S. C. B. Raper, T. M. L. Wigley, R. A. Warrick, in *Sea-Level Rise and Coastal Subsidence: Causes, Consequences and Strategies*, J. Milliman, B. U. Haq, Eds. (Kluwer Academic Publishers, Dordrecht, Netherlands, 1996), pp. 11–45.
- T. M. L. Wigley, S. C. B. Raper, *J. Clim.* **15**, 2945 (2002).
- U. Cubasch, G. A. Meehl, in *Climate Change 2001: The Scientific Basis*, J. T. Houghton et al., Eds. (Cambridge Univ. Press, Cambridge, 2001), pp. 525–582.
- S. C. B. Raper, J. M. Gregory, T. J. Osborn, *Clim. Dyn.* **17**, 601 (2001).
- Materials and methods are available as supporting material on Science Online.
- J. A. Church, J. M. Gregory, in *Climate Change 2001: The Scientific Basis*, J. T. Houghton et al., Eds. (Cambridge Univ. Press, Cambridge, 2001), pp. 639–693.

- T. M. L. Wigley, S. C. B. Raper, *Geophys. Res. Lett.*, in press.
- J. Lean, J. Beer, R. Bradley, *Geophys. Res. Lett.* **22**, 3195 (1995).
- C. M. Ammann, G. A. Meehl, W. M. Washington, C. S. Zender, *Geophys. Res. Lett.* **30**, 1657, 10.1029/2003GL016875 (2003).
- This is a sensitivity study and not a probabilistic analysis. Simplistically, if the high climate sensitivity and low forcing extremes are independent and each has a probability of exceedance of 0.05, the probability of both being exceeded is 0.0025. Further constraints may be placed by comparing model simulations with observed climate changes over the past century (22).
- T. M. L. Wigley, R. Richels, J. A. Edmonds, *Nature* **379**, 240 (1996).
- C. E. Forest, P. H. Stone, A. P. Sokolov, M. R. Allen, M. D. Webster, *Science* **295**, 113 (2002).
- Supported in part by the U.S. Environmental Protection Agency under contract no. GS-10F-0299K to Stratus Consulting and by NOAA under grant NA87GP0105. Opinions, findings, or conclusions expressed are those of the author and do not necessarily reflect the views of the funding organization. The National Center for Atmospheric Research is supported by the NSF.

#### Supporting Online Material

[www.sciencemag.org/cgi/content/full/307/5716/1766/DC1](http://www.sciencemag.org/cgi/content/full/307/5716/1766/DC1)  
Materials and Methods  
Tables S1 and S2

11 August 2004; accepted 10 January 2005  
10.1126/science.1103934

## How Much More Global Warming and Sea Level Rise?

Gerald A. Meehl,\* Warren M. Washington, William D. Collins,  
Julie M. Arblaster, Aixue Hu, Lawrence E. Buja,  
Warren G. Strand, Haiyan Teng

Two global coupled climate models show that even if the concentrations of greenhouse gases in the atmosphere had been stabilized in the year 2000, we are already committed to further global warming of about another half degree and an additional 320% sea level rise caused by thermal expansion by the end of the 21st century. Projected weakening of the meridional overturning circulation in the North Atlantic Ocean does not lead to a net cooling in Europe. At any given point in time, even if concentrations are stabilized, there is a commitment to future climate changes that will be greater than those we have already observed.

Increases of greenhouse gases (GHGs) in the atmosphere produce a positive radiative forcing of the climate system and a consequent warming of surface temperatures and rising sea level caused by thermal expansion of the warmer seawater, in addition to the contribution from melting glaciers and ice sheets (1, 2). If concentrations of GHGs could be stabilized at some level, the thermal inertia of the climate system would still result in further increases in temperatures, and sea level would continue to rise (2–9). We performed multimember ensemble simulations with two global coupled three-dimensional climate models to quantify

how much more global warming and sea level rise (from thermal expansion) we could experience under several different scenarios.

The Parallel Climate Model (PCM) has been used extensively for climate change experiments (10–15). This model has a relatively low climate sensitivity as compared to other models, with an equilibrium climate sensitivity of 2.1°C and a transient climate response (TCR) (the globally averaged surface air temperature change at the time of CO<sub>2</sub> doubling in a 1% CO<sub>2</sub> increase experiment) of 1.3°C. The former is indicative of likely atmospheric feedbacks in the model, and the latter includes ocean heat uptake and provides an indication of the transient response of the coupled climate system (6, 12). A second global coupled climate model is the newly developed Com-

munity Climate System Model version 3 (CCSM3), with higher horizontal resolution (atmospheric gridpoints roughly every 1.4° as compared to the PCM, with gridpoints about every 2.8°) and improved parameterizations in all components of atmosphere, ocean, sea ice, and land surface (16). The CCSM3 has somewhat higher sensitivity, with an equilibrium climate sensitivity of 2.7°C and TCR of 1.5°C. Both models have about 1° ocean resolution (0.5° in the equatorial tropics), with dynamical sea ice and land surface schemes. These models were run for four- and eight-member ensembles for the PCM and CCSM3, respectively, for each scenario (except for five members for A2 in CCSM3).

The 20th-century simulations for both models include time-evolving changes in forcing from solar, volcanoes, GHGs, tropospheric and stratospheric ozone, and the direct effect of sulfate aerosols (14, 17). Additionally, the CCSM3 includes black carbon distributions scaled by population over the 20th century, with those values scaled by sulfur dioxide emissions for the rest of the future climate simulations. The CCSM3 also uses a different solar forcing data set for the 20th century (18). These 20th-century forcing differences between CCSM3 and PCM are not thought to cause large differences in response in the climate change simulations beyond the year 2000.

The warming in both the PCM and CCSM3 is close to the observed value of about 0.6°C for the 20th century (19), with PCM warming 0.6°C and CCSM3 warming 0.7° (averaged over the period 1980–1999 in relation to 1890–1919). Sea level rises are 3 to 5 cm, respectively, over the 20th century as com-

National Center for Atmospheric Research, Post Office Box 3000, Boulder, CO 80307, USA.

\*To whom correspondence should be addressed.  
E-mail: meehl@ncar.ucar.edu

pared to the observed estimate of 15 to 20 cm. This lower value from the models is consistent with the part of 20th-century sea level rise

thought to be caused by thermal expansion (20, 21), because as the ocean warms, seawater expands and sea level rises. Neither model

includes contributions to sea level rise due to ice sheet or glacier melting. Partly because of this, the sea level rise calculations for the 20th century from the models are probably at least a factor of 3 too small (20, 21). Therefore, the results here should be considered to be the minimum values of sea level rise. Contributions from future ice sheet and glacier melting could perhaps at least double the projected sea level rise produced by thermal expansion (1).

Atmospheric CO<sub>2</sub> is the dominant anthropogenic GHG (22), and its time evolution can be used to illustrate the various scenarios (Fig. 1A). The three Special Report for Emissions Scenarios (SRES) show low (B1), medium (A1B), and high (A2) increases of CO<sub>2</sub> over the course of the 21st century. Three stabilization experiments were performed: one with concentrations of all constituents held constant at year 2000 values and two (B1 and A1B) with concentrations held constant at year 2100 values. Although these are idealized stabilization experiments, it would take a significant reduction of emissions below 1990 values within a few decades and within about a century to achieve stabilized concentrations in B1 and A1B, respectively (23).

Even if we could have stopped any further increases in all atmospheric constituents as of the year 2000, the PCM and CCSM3 indicate that we are already committed to 0.4° and 0.6°C, respectively, more global warming by the year 2100 as compared to the 0.6°C of warming observed at the end of the 20th century (Table 1 and Fig. 1B). (The range of the ensembles for the climate model temperature anomalies here and to follow is about ±0.1°C.) But we are already committed to proportionately much more sea level rise from thermal expansion (Fig. 1C).

At the end of the 21st century, as compared to the end of the 20th century (1980–1999 base period), warming in the low-estimate climate change scenario (SRES B1) is 1.1° and 1.5°C in the two models (Table 1 and Fig. 1B), with sea level rising to 13 and 18 cm above year 1999 levels. The spread among the ensembles for sea level in all cases amounts to less than ±0.3 cm. A medium-range scenario (SRES A1B) produces a warming at the end of the 21st century of 1.9° and 2.6°C, with about 18 and 25 cm of sea level rise in the two models. For the high-estimate scenario (A2), warming at 2100 is about 2.2° and 3.5°C, and sea level rise is 19 and 30 cm. The range of transient temperature response in the two models for the 20th century through the mid-21st century is considerably less than the range in their equilibrium climate sensitivities (Table 1) due in part to less than doubled CO<sub>2</sub> forcing as well as ocean heat uptake characteristics (24). Thus, our confidence in model simulations of 20th-century climate change and projections for much of the 21st century (as represented by the range

**Fig. 1.** (A) Time series of CO<sub>2</sub> concentrations for the various scenarios. (B) Time series of globally averaged surface air temperatures from the PCM and CCSM3. (C) Same as (B), except that sea level rise comes from thermal expansion only. In (C), the control drift is first subtracted from each experiment, and then in (B) and (C), the base period for calculating anomalies is 1980–1999. Solid lines are ensemble means, and shading indicates the range of ensemble members. Line identifiers for the various scenarios and the two models are given in each panel.

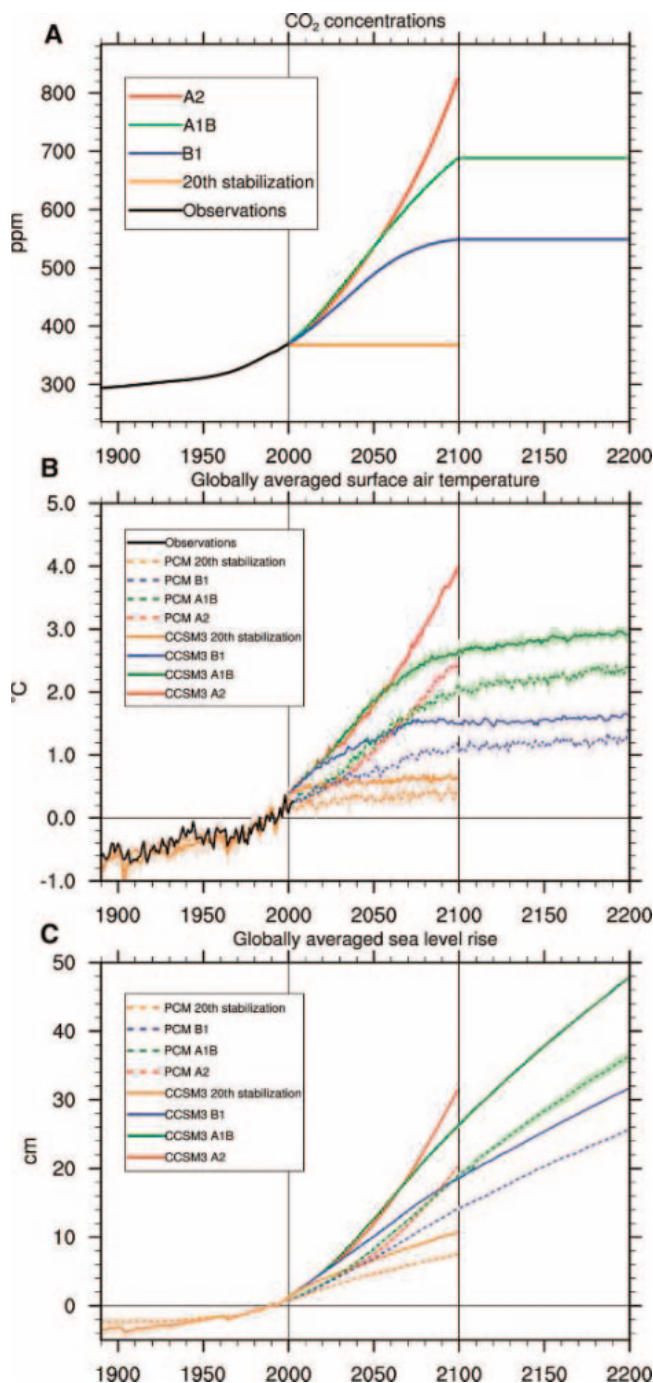


**Table 1.** Globally averaged surface temperature differences (in °C) comparing equilibrium climate sensitivity from the two models with simulated warming for the 20th century, mid-21st century, and late 21st century for the different experiments. Midcentury differences are calculated for 2041–2060 minus 1980–1999, and late century differences are for 2080–2099 minus 1980–1999. A2 at 2100 has more than double present-day CO<sub>2</sub> amounts (Fig. 1A).

Model	Equilibrium sensitivity	20th century	2050 stabilized	2050 B1	2050 A1B	2050 A2	2100 stabilized	2100 B1	2100 A1B	2100 A2
PCM	2.1	0.6	0.3	0.7	1.2	1.1	0.4	1.1	1.9	2.2
CCSM3	2.7	0.7	0.6	1.2	1.9	1.8	0.6	1.5	2.6	3.5

in the transient response of the models) is considerably better than that represented by the larger uncertainty range of the equilibrium climate sensitivity among the models.

If concentrations of all GHGs and other atmospheric constituents in these simulations are held fixed at year 2100 values, we would be committed to an additional warming by the year 2200 for B1 of about 0.1° to 0.3°C for the models (Fig. 1B). This small warming commitment is related to the fact that CO<sub>2</sub> concentrations had already started to stabilize at about 2050 in this scenario (Fig. 1A). But even for this small warming commitment in B1, there is almost double the sea level rise seen over the course of the 21st century by 2200, or an additional 12 and 13 cm (Fig. 1C). For A1B, about 0.3°C of additional warming occurs by 2200, but again there is roughly a doubling of 21st-century sea level rise by the year 2200, or an additional 17 and 21 cm. By 2300 (not shown), with concentrations still held at year 2100 values, there would be less than another 0.1°C of warming in either scenario, but yet again about another doubling of the committed sea level rise that occurred during the 22nd century, with additional increases of 10 and 18 cm from thermal expansion for the two models for the stabilized B1 experiment, and 14 and 21 cm for A1B as compared to year 2200 values. Sea level rise would continue for at least two more centuries beyond 2300, even with these stabilized concentrations of GHGs (2).

The meridional overturning maximum in the North Atlantic, indicative of the thermohaline circulation in the ocean, is stronger in the preindustrial simulation in the PCM (32.1 sverdrups) compared to the CCSM3 (21.9 sverdrups), with the latter closer to observed estimates that range from 13 to 20 sverdrups (25–27). The mean strength of the meridional overturning and its changes are an indication of ocean ventilation, and they contribute to ocean heat uptake and consequent time scales of temperature response in the climate system (12, 24, 28).

The model with the higher sensitivity (CCSM3) has the greater temperature and sea level rise response at the year 2100 for the B1, A1B, and A2 scenarios (Fig. 1, B and C) and also the larger decrease in meridional overturning in the North Atlantic (−4.0, −5.3, and −6.2 sverdrups or −18, −24, and −28%, respectively) as compared to the model that is less sensitive (PCM), with the lower forced response for B1, A1B, and A2 with decreases of meridional overturning in the Atlantic that are about a factor of 2 less (−1.0, −3.5, and −4.5 sverdrups, or −3, −11, and −14%, respectively). This is consistent with the idea that a larger percentage decrease in meridional overturning would be associated with greater ocean heat uptake and greater surface temperature warming (12, 24).

The warming commitment for 20th-century forcing held fixed at year 2000 values is larger

in the CCSM3 than in the PCM (0.6° versus 0.4°C). This is also consistent with the recovery of the meridional overturning in the 21st century after concentrations are stabilized in the PCM (net recovery of +0.2 sverdrups) compared to the CCSM3 (meridional overturning continues to weaken by −0.3 sverdrups before a modest recovery).

Therefore, the PCM, with less climate sensitivity and lower TCR but with greater mean meridional overturning in the Atlantic, has less reduction of North Atlantic meridional overturning and less forced response. The meridional overturning recovers more quickly in the PCM, contributing to even less warming commitment after concentrations are stabilized at year 2000 values. On the other hand, the CCSM3, with higher sensitivity and weaker

mean meridional overturning, has a larger reduction of meridional overturning due to global warming (and particularly a larger percent decrease of meridional overturning) than the PCM and contributes to more warming commitment for GHG concentrations stabilized at year 2000 values.

The processes that contribute to these different warming commitments involve small radiative flux imbalances at the surface (on the order of several tenths of a watt per square meter) after atmospheric GHG concentrations are stabilized. This small net heat flux into the ocean is transferred to the deeper layers through mixing, convection, and ventilation processes such as the meridional overturning circulation that connects the Northern and Southern Hemisphere high-latitude deep

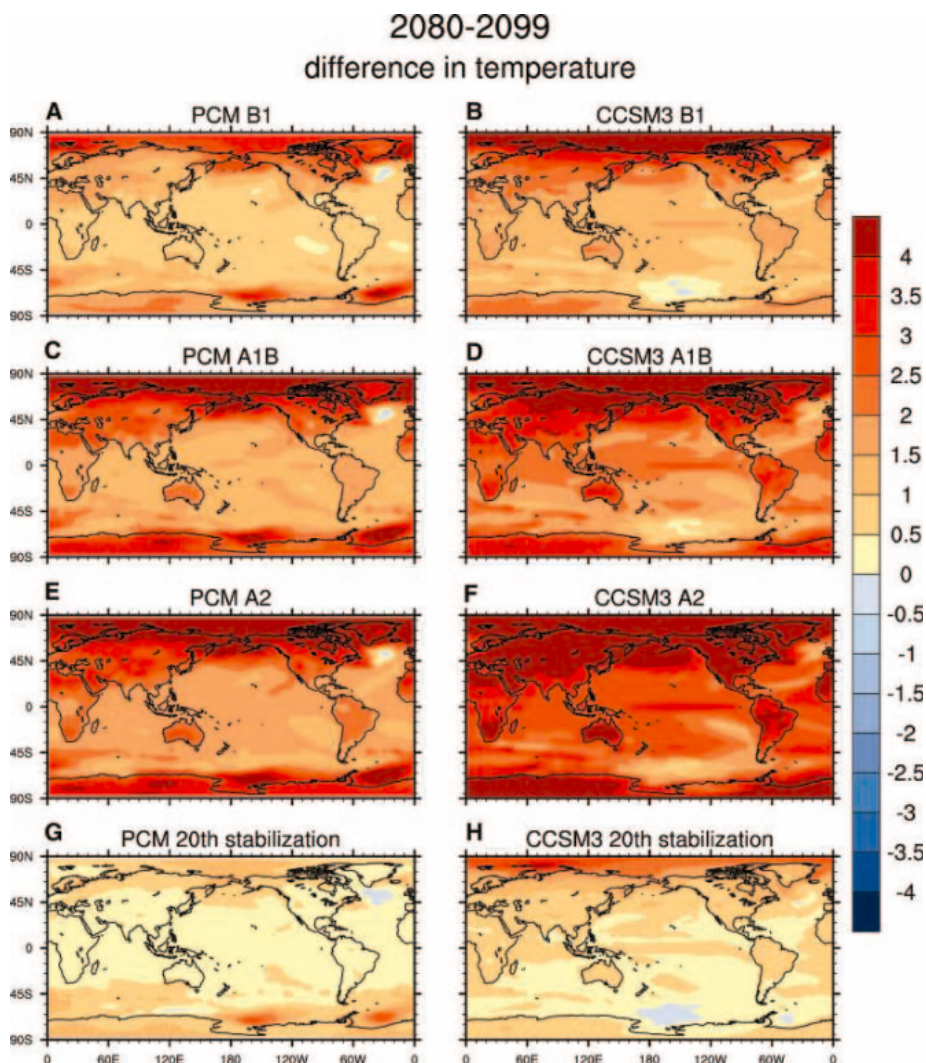
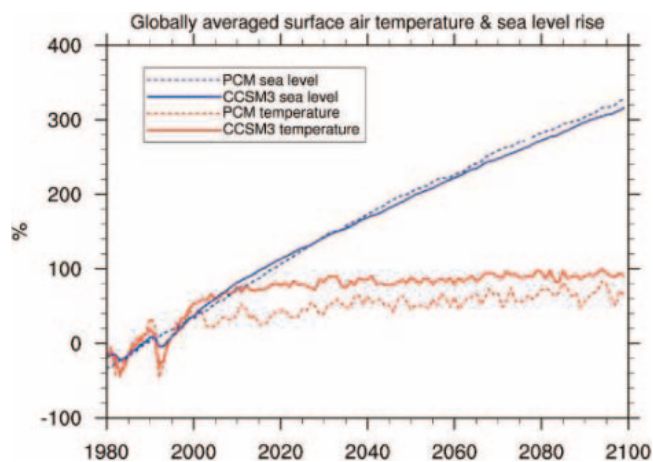


**Fig. 2.** Surface temperature change for the end of the 21st century (ensemble average for years 2080–2099) minus a reference period at the end of the 20th century (ensemble average for years 1980–1999) from 20th-century simulations with natural and anthropogenic forcings. (A) The PCM for the B1 scenario. (B) The CCSM3 for the B1 scenario. (C) The PCM for the A1B scenario. (D) The CCSM3 for the A1B scenario. (E) The PCM for the A2 scenario. (F) The CCSM3 for the A2 scenario. (G and H) Temperature commitment for GHG concentrations stabilized at year 2000 values; ensemble average for years 2080–2099 minus a reference period ensemble average for years 1980–1999 from 20th-century simulations. More than 95% of the values in each panel are significant at the 10% level from a Student's *t* test, and a similar proportion exceed 1 SD of the intraensemble standard deviations.



**Fig. 3.** Ensemble mean percent increase of globally averaged surface air temperature and sea level rise from the two models computed relative to values for the base period 1980–1999 for the experiment in which GHG concentrations and all other atmospheric constituents were stabilized at the end of the 20th century.



ocean circulations (29). Thus, in addition to changes in the meridional overturning circulation, the strength of the mean circulation also plays a role (12, 24, 28). The temperature difference between the upper and lower branches of the Atlantic meridional overturning circulation is smaller in the PCM than in the CCSM3 because of the stronger rate of mean meridional overturning in the PCM that induces a greater heat exchange or ventilation between the upper and deeper ocean. In the PCM, recovery of the meridional overturning is more rapid in the 21st century, thus producing even greater mixing and less warming commitment, whereas the CCSM3 recovers more slowly, with greater warming commitment by the year 2200 and on to 2300.

Geographic patterns of warming (Fig. 2) show more warming at high northern latitudes and over land, generally larger-amplitude warming in the CCSM3 as compared to the PCM, and geographic temperature increases roughly proportional to the amplitude of the globally averaged temperature increases in the different scenarios (Fig. 1B). Slowdowns in meridional overturning in the respective models (which are greater percentage-wise in the CCSM3 than the PCM) are not characterized by less warming over northern Europe in either model. The warming produced by increases in GHGs overwhelms any tendency toward decreased high-latitude warming from less northward heat transport by the weakened meridional overturning circulation in the Atlantic. There is more regional detail in the higher-resolution CCSM3 as compared to the PCM, with an El Niño-like response (30) in the equatorial Pacific (greater warming in the equatorial central and eastern Pacific than in the western Pacific) in the CCSM3 as compared to the PCM. This is related to cloud feedbacks in the CCSM3 involving the improved prognostic cloud liquid water scheme, as compared to the diagnostic cloud liquid water formulation in the PCM (31).

The warming commitment from the 20th-century stabilization experiments (Fig. 2, bottom) shows the same type of pattern in the

forced experiments, with greater warming over high latitudes and land areas. For regions such as much of North America, even after stabilizing GHG concentrations, we are already committed to more than an additional half a degree of warming in the two models. The pattern of the 20th-century stabilization experiments is similar to those produced in the 21st-century stabilization experiments with A1B and B1 (not shown).

Though temperature increase shows signs of leveling off 100 years after stabilization, sea level continues to rise unabated with proportionately much greater increases compared to temperature, with these committed increases over the 21st century more than a factor of 3 greater, percentage-wise, for sea level rise (32) than for temperature change (Fig. 3). Thus, even if we could stabilize concentrations of GHGs, we are already committed to significant warming and sea level rise no matter what scenario we follow. These results confirm and quantify earlier studies with simple and global models in that the sea level rise commitment is considerably more than the temperature change commitment.

#### References and Notes

1. J. A. Church *et al.*, in *Climate Change 2001: The Scientific Basis*, J. T. Houghton *et al.*, Eds. (Cambridge Univ. Press, Cambridge, 2001), pp. 639–693.
2. T. M. L. Wigley, *Science* **307**, 1766 (2005).
3. J. F. B. Mitchell *et al.*, *Geophys. Res. Lett.* **27**, 2977 (2000).
4. F. P. Bretherton *et al.*, in *Climate Change: The IPCC Scientific Assessment*, J. T. Houghton *et al.*, Eds. (Cambridge Univ. Press, Cambridge, 1990), pp. 173–194.
5. A. Kattenberg *et al.*, in *Climate Change 1995: The Science of Climate Change*, J. T. Houghton *et al.*, Eds. (Cambridge Univ. Press, Cambridge, 1995), pp. 285–357.
6. U. Cubasch *et al.*, in *Climate Change 2001: The Scientific Basis*, J. T. Houghton *et al.*, Eds. (Cambridge Univ. Press, Cambridge, 2001), pp. 525–582.
7. R. T. Wetherald *et al.*, *Geophys. Res. Lett.* **28**, 1535 (2001).
8. T. M. L. Wigley, S. Raper, in *Climate and Sea Level Change: Observations, Projections and Implications*, R. A. Warrick *et al.*, Eds. (Cambridge Univ. Press, Cambridge, 2003), pp. 111–133.
9. R. J. Stouffer, S. Manabe, *J. Clim.* **12**, 2224 (1999).
10. W. M. Washington *et al.*, *Clim. Dyn.* **16**, 755 (2000).
11. G. A. Meehl *et al.*, *Clim. Dyn.* **17**, 515 (2001).
12. G. A. Meehl *et al.*, *J. Clim.* **17**, 1584 (2004).
13. G. A. Meehl *et al.*, *Clim. Dyn.* **23**, 495 (2004).

14. G. A. Meehl *et al.*, *J. Clim.* **17**, 3721 (2004).
15. G. A. Meehl, C. Tebaldi, *Science* **305**, 994 (2004).
16. For a description of the CCSM3, see [www.cesm.ucar.edu](http://www.cesm.ucar.edu).
17. B. D. Santer *et al.*, *Science* **301**, 479 (2003).
18. The 20th-century solar forcing in the PCM is from (33). The 20th-century solar forcing in the CCSM3 is from (34).
19. C. K. Folland *et al.*, in *Climate Change 2001: The Scientific Basis*, J. T. Houghton *et al.*, Eds. (Cambridge Univ. Press, Cambridge, 2001), pp. 99–181.
20. L. Miller, B. C. Douglas, *Nature* **428**, 406 (2004).
21. J. A. Church *et al.*, *J. Clim.* **17**, 2609 (2004).
22. V. Ramaswamy, in *Climate Change 2001: The Scientific Basis*, J. T. Houghton *et al.*, Eds. (Cambridge Univ. Press, Cambridge, 2001), pp. 349–416.
23. I. C. Prentice *et al.*, in *Climate Change 2001: The Scientific Basis*, J. T. Houghton *et al.*, Eds. (Cambridge Univ. Press, Cambridge, 2001), pp. 183–237.
24. S. C. B. Raper *et al.*, *J. Clim.* **15**, 124 (2002).
25. M. M. Hall, H. L. Bryden, *Deep Sea Res.* **29**, 150 (1982).
26. D. Roemmich, C. Wunsch, *Deep Sea Res.* **32**, 619 (1985).
27. M. S. McCartney, L. D. Talley, *J. Phys. Oceanogr.* **14**, 922 (1984).
28. P. R. Gent, G. Danabasoglu, *J. Clim.* **17**, 4058 (2004).
29. A. Hu *et al.*, *J. Clim.* **17**, 4267 (2004).
30. G. A. Meehl, W. M. Washington, *Nature* **382**, 56 (1996).
31. G. A. Meehl *et al.*, *J. Clim.* **13**, 1879 (2000).
32. The sea level rise at the year 2100 in the 20th-century stabilization experiment is greater in the CCSM3 than in the PCM in Fig. 1C relative to the 1980–1999 base period, but they both have about the same percentage increase as compared to the total sea level rise that occurred during the 20th century in the respective models as depicted in Fig. 3. This is because the CCSM3 has greater total sea level rise during the 20th century than does the PCM (4.5 cm compared to 3.0 cm, respectively), partly due to the higher sensitivity of the CCSM3 as well as the comparative meridional overturning circulation processes discussed in the text.
33. D. V. Hoyt, K. H. Schatten, *J. Geophys. Res.* **98**, 18895 (1993).
34. J. Lean *et al.*, *Geophys. Res. Lett.* **107**, 10.1029/2001JD001143 (1995).
35. We acknowledge the efforts of a large group of scientists at the National Center for Atmospheric Research (NCAR), at several U.S. Department of Energy (DOE) and National Oceanic and Atmospheric Administration labs, and at universities across the United States who contributed to the development of the CCSM3 and who participated in formulating the 20th-century and future climate change simulations through the CCSM working groups on atmosphere, ocean, land surface, polar climate, climate change, climate variability, paleoclimate, biogeochemistry, and software engineering. In particular, we thank A. Middleton and V. Wayland from NCAR and M. Wehner at the National Energy Research Scientific Computing Center (NERSC) for their work in either running the model experiments or managing the massive amount of model data. The formidable quantity of supercomputer resources required for this ambitious modeling effort was made available at NCAR through the Initiative Nodes and the Climate System Laboratory and through DOE as part of its Advanced Scientific Research (ASCR). ASCR provides computing facilities at NERSC, Los Alamos National Laboratory (LANL), and the Oak Ridge National Laboratory (ORNL) Center for Computational Science. Additional simulations with the CCSM3 were performed by the Central Research Institute for the Electric Power Industry (CRIEPI), using the Earth Simulator in Japan through the international research consortium of CRIEPI, NCAR, and LANL under the Project for Sustainable Coexistence of Human Nature and the Earth of the Japanese Ministry of Education, Culture, Sports, Science and Technology. Portions of this study were supported by the Office of Biological and Environmental Research, DOE, as part of its Climate Change Prediction Program; and by the National Center for Atmospheric Research. This work was also supported in part by the Weather and Climate Impact Assessment Initiative at NCAR. NCAR is sponsored by NSF.

22 October 2004; accepted 24 January 2005  
10.1126/science.1106663

# Type VII Collagen Is Required for Ras-Driven Human Epidermal Tumorigenesis

Susana Ortiz-Urda,<sup>1,2</sup> John Garcia,<sup>1,2</sup> Cheryl L. Green,<sup>1,2</sup> Lei Chen,<sup>1,2</sup> Qun Lin,<sup>1,2</sup> Dallas P. Veitch,<sup>1,2</sup> Lynn Y. Sakai,<sup>3</sup> Hyangkyu Lee,<sup>1,2</sup> M. Peter Marinkovich,<sup>1,2</sup> Paul A. Khavari<sup>1,2\*</sup>

Type VII collagen defects cause recessive dystrophic epidermolysis bullosa (RDEB), a blistering skin disorder often accompanied by epidermal cancers. To study the role of collagen VII in these cancers, we examined Ras-driven tumorigenesis in RDEB keratinocytes. Cells devoid of collagen VII did not form tumors in mice, whereas those retaining a specific collagen VII fragment (the amino-terminal noncollagenous domain NC1) were tumorigenic. Forced NC1 expression restored tumorigenicity to collagen VII-null epidermis in a non-cell-autonomous fashion. Fibronectin-like sequences within NC1 (FNC1) promoted tumor cell invasion in a laminin 5-dependent manner and were required for tumorigenesis. Tumor-stroma interactions mediated by collagen VII thus promote neoplasia, and retention of NC1 sequences in a subset of RDEB patients may contribute to their increased susceptibility to squamous cell carcinoma.

Epidermal squamous cell carcinoma (SCC) is the second most common cancer in the United States, with approximately 250,000 new cases yearly (1). Early-onset, invasive SCCs characterize RDEB, a blistering skin disorder caused by mutations in the *COL7A1* gene that encodes the keratinocyte-secreted type VII collagen epidermal basement membrane zone (BMZ) protein (2–4). More than 55% of RDEB patients die from SCC by age 40 (5). A subset of RDEB patients, how-

ever, does not develop SCCs (5). Whether this phenotypic difference correlates with specific functional defects in collagen VII is unknown. Furthermore, there is no compelling evidence that other inherited chronic blistering diseases are associated with a substantially increased incidence of SCC (5, 6), which indicates that skin fragility alone is insufficient to induce cancer. Collagen VII is expressed in sporadic SCCs arising in a variety of epithelial tissues (7), which in-

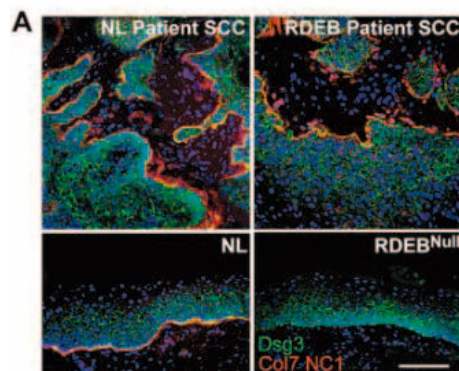
dicates that collagen VII loss is not required for tumorigenesis; however, it is unclear whether collagen VII expression in non-RDEB SCCs limits tumor invasion or facilitates tumor growth.

To investigate the role of collagen VII in tumorigenesis, we studied SCCs obtained from 10 consecutive, unrelated RDEB patients. All of these tumors displayed collagen VII expression, which indicates that collagen VII loss is not characteristic of SCC in RDEB. In contrast, 4 out of 10 skin tissue biopsies from a different group of RDEB patients without SCC lacked detectable collagen VII (Fig. 1A). To explore collagen VII function in this setting, we examined the oncogenic potential of primary epidermal cells from 12 additional unrelated RDEB patients. Tumorigenesis was examined by coexpressing oncogenic Ras and the NF- $\kappa$ B inhibitor I $\kappa$ B $\alpha$  in primary keratinocytes by retroviral transduction to produce cells that generate human epidermal tumors indistinguishable from SCC upon engraftment to immunodeficient mice (8). Cells from four RDEB patients formed no tumors after subcutaneous injection, whereas cells from the remaining eight patients generated tumors that were all collagen VII-positive (Fig. 1, B and

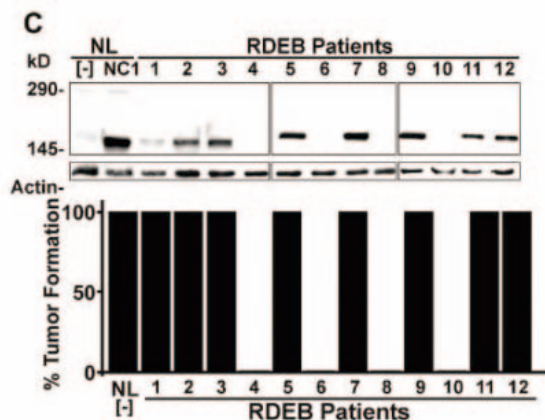
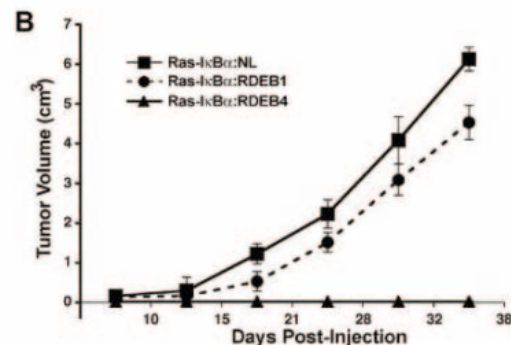
<sup>1</sup>VA Palo Alto Healthcare System, Palo Alto, CA 94304, USA. <sup>2</sup>Program in Epithelial Biology, 269 Campus Drive, Stanford University School of Medicine, Stanford, CA 94305, USA. <sup>3</sup>Department of Biochemistry and Molecular Biology, Oregon Health and Science University, Portland, OR 97201, USA

\*To whom correspondence should be addressed. E-mail: khavari@cmgm.stanford.edu

**Fig. 1.** Relationship of epidermal tumorigenesis in RDEB to type VII collagen expression. (A) Immunostaining with antibodies to the collagen VII NC1 domain in dermally invasive sporadic SCCs from both non-RDEB and RDEB patients. Data are representative of strong NC1 detection observed in SCCs from 10 unrelated RDEB patients and 10 otherwise normal non-RDEB patients (NL). Note the complete absence of NC1 at the dermal-epidermal junction in noncancerous RDEB skin (RDEB<sup>Null</sup>) as a negative staining control (scale bar, 100  $\mu$ m). (B) Tumor growth kinetics in nude mice



after subcutaneous injection of primary RDEB keratinocytes coexpressing oncogenic Ras and I $\kappa$ B $\alpha$ . NL, keratinocytes from normal patients without SCC; RDEB1 and RDEB4 correspond to patients studied below;  $n = 5$  mice per patient; error bars,  $\pm$  SD. (C) Collagen VII immunoblots and tumorigenicity of keratinocytes from 12 unrelated consecutive RDEB patients. Patients 4, 6, 8, and 10 lack collagen VII protein fragments, as detected by pAbs, and are denoted as RDEB<sup>Null</sup>. The bar graph depicts the percentage of mice forming Ras-I $\kappa$ B $\alpha$ -driven tumors for each of the 12 RDEB patients ( $n = 5$  mice per group).



C, and fig. S1), which indicates the existence of tumorigenic and nontumorigenic RDEB subsets.

Collagen VII, as detected by polyclonal antibodies, was entirely absent in the nontumorigenic subset (termed RDEB<sup>Null</sup>) (Fig. 1C). In contrast, cells from all eight tumorigenic RDEB patients retained expression of the 145-kD amino-terminal noncollagenous domain (NC1, denoted RDEB<sup>NC1</sup>) (Fig. 1C). This was unexpected, because mutations in these eight patients generate a variety of premature termination codons that are C terminal to NC1 (table S1). Forced expression of three collagen VII mutants truncated at amino acids 1260 (NC1), 1726 (M1), and 2199 (M2) in RDEB<sup>Null</sup> cells, however, also produced a 145-kD band in each case (fig. S1), which is consistent with the observed stability of NC1 protein fragments (9).

Keratinocytes from RDEB patients thus fall into two distinct phenotypes, a tumorigenic subset retaining expression of a collagen VII fragment and a nontumorigenic subset devoid of collagen VII.

To determine whether RDEB<sup>Null</sup> cells regained tumorigenicity upon collagen VII restoration, we first reintroduced full-length collagen VII directly into keratinocytes using an integrating plasmid approach (10). Collagen VII re-expression restored Ras-driven tumorigenicity in mice to primary RDEB<sup>Null</sup> keratinocytes (Fig. 2A). We next determined whether collagen VII could act in *trans* to rescue Ras-driven tumorigenesis by RDEB<sup>Null</sup> keratinocytes. Coinjection of normal fibroblasts, which also secrete small amounts of collagen VII, restored tumor formation, but RDEB<sup>Null</sup> fibroblasts did not (Fig. 2B). Collagen VII therefore restores tumor formation

to RDEB<sup>Null</sup> keratinocytes in a non-cell-autonomous manner.

We next expressed a series of collagen VII fragments in RDEB<sup>Null</sup> keratinocytes to identify the collagen VII sequences responsible for tumor formation in mice (Fig. 3, A and B). The 1260 amino acid NC1 domain restored tumorigenicity to RDEB<sup>Null</sup> cells, whereas more C-terminal sequences did not (Fig. 3C), which is consistent with NC1 retention in the tumorigenic RDEB subset. A region of NC1 that spans amino acids 761 to 1050 and that encompasses fibronectin III-like repeats (FNC1) was chosen for further study because it contains sequences that bind laminin 5 (9), another extracellular protein expressed in SCC. Deletion of FNC1 sequences from NC1 ( $\Delta$ NC1) abolished tumorigenesis; conversely, introduction of FNC1 sequences alone, which led to secretion of an FNC1-containing protein fragment, restored tumorigenicity to RDEB<sup>Null</sup> cells (Fig. 3C). Thus, FNC1 sequences are both necessary and sufficient for Ras-driven epidermal tumorigenesis.

These findings raised the possibility that FNC1 sequences may be an important determinant of the tumorigenic potential of non-RDEB epidermal cells. Accordingly, we tested whether antibody-mediated inhibition of FNC1 would inhibit subcutaneous tumor formation by normal human keratinocytes. Polyclonal antibodies (pAbs) to NC1 were raised, and their specificity was tested with other available NC1 antibodies (11, 12) by using recombinant NC1,  $\Delta$ NC1, and FNC1 protein (Fig. 3D). A monoclonal antibody (mAb) to NC1, mAb 32, bound FNC1 sequences, whereas mAb 161 and control pAb  $\Delta$ NC1 bound NC1 outside FNC1 (Fig. 3D). Intraperitoneal injection of either pAb or mAb targeting FNC1 at the time of subcutaneous

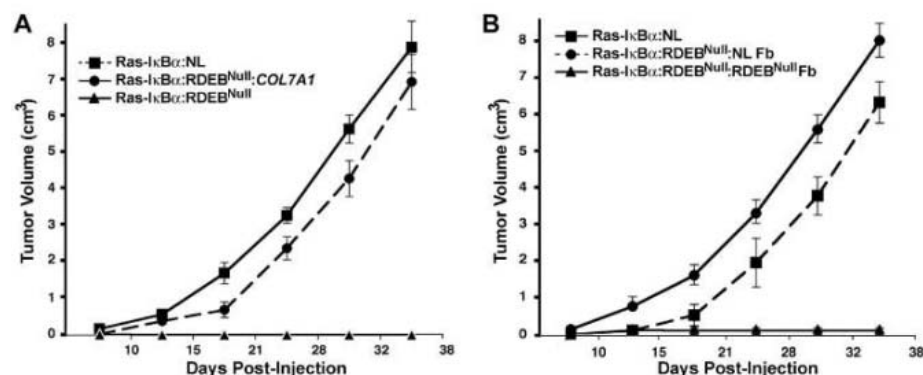
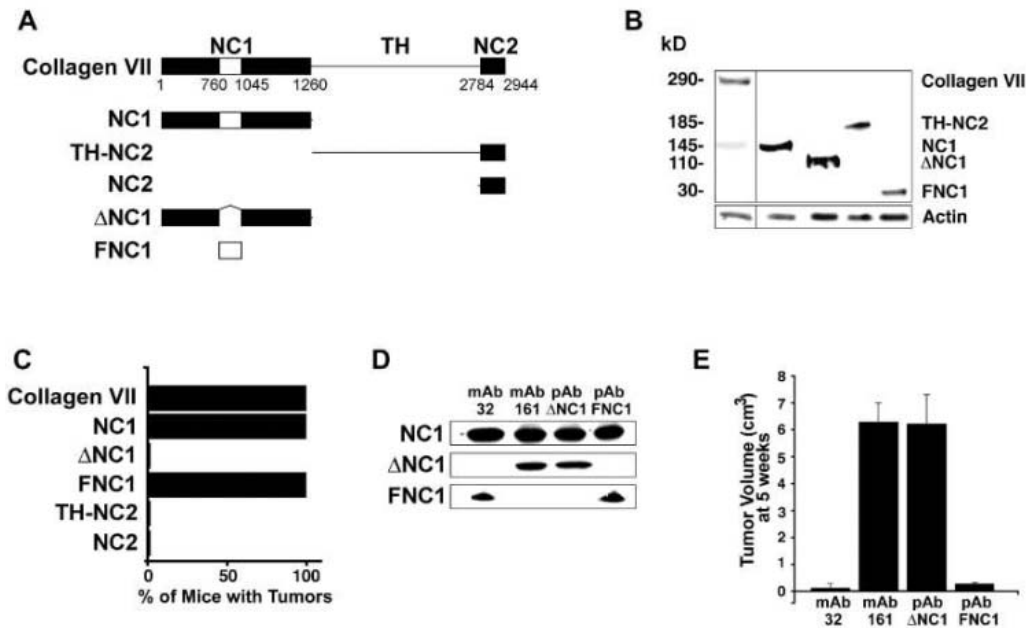


**Fig. 2.** Type VII collagen effects on the tumorigenic potential of RDEB<sup>Null</sup> keratinocytes in mice. (A) Tumor growth kinetics of RDEB<sup>Null</sup> keratinocytes expressing Ras and  $\text{IkB}\alpha$  in which full-length collagen VII has been restored (RDEB<sup>Null</sup>;COL7A1) ( $n = 5$  mice per group  $\pm$  SD). (B) Fibroblasts either from normal individuals confirmed to secrete full-length collagen VII (NL Fb) or from RDEB<sup>Null</sup> patients (RDEB<sup>Null</sup> Fb) were coinjected with Ras- $\text{IkB}\alpha$ -expressing primary RDEB<sup>Null</sup> keratinocytes ( $n = 5$  mice per group  $\pm$  SD).

**Fig. 3.** Type VII collagen sequences in epidermal tumorigenesis. (A) Collagen VII domain constructs. Numbers denote amino acid positions. NC1, noncollagenous domain 1; TH, triple helical domain; NC2, noncollagenous domain 2. (B) Verification of collagen VII domain expression in RDEB<sup>Null</sup> keratinocytes by immunoblotting using pAbs to collagen VII. (C) Tumor formation in nude mice 5 weeks after subcutaneous injection of Ras- $\text{IkB}\alpha$ -expressing RDEB<sup>Null</sup> keratinocytes engineered to express either full-length collagen VII or the sequences noted ( $n = 5$  mice per group). (D) mAbs and pAbs to collagen VII NC1 sequences. Recombinant proteins blotted are noted at left, and antibodies are noted above each lane. (E) Volumes of tumors formed by Ras- $\text{IkB}\alpha$ -expressing normal primary keratinocytes treated with the antibodies noted  $\pm$  SD ( $n = 5$  mice per group).



injection of tumorigenic normal cells prevented tumor formation, whereas  $\Delta$ NC1 antibodies did not (Fig. 3E). These results indicate that FNC1 sequences may be important in common epidermal tumorigenesis and may represent a potential therapeutic target.

In principle, FNC1 could affect a variety of neoplastic processes, such as tumor cell proliferation, survival, and/or invasion. Defects in any of these processes are likely to abolish subcutaneous tumor formation. To distinguish among these potential mechanisms, we used a surface skin regeneration approach on severe combined immunodeficient (SCID) mice (13), which requires that neoplastic cells penetrate through human BMZ and dermal matrix to form tumors. As observed previously (8), epidermal cells in skin regenerated from normal primary human keratinocytes coexpressing Ras and I $\kappa$ B $\alpha$  penetrated the dermal-epidermal junction and aggressively invaded the underlying mesenchyma in vivo (Fig. 4A). Tumor cell invasion was unaffected by intraperitoneal injection of laminin 10–blocking antibodies (14) but was entirely blocked by FNC1 antibodies (Fig. 4A). FNC1 antibodies did not inhibit tumor cell proliferation or trigger apoptosis, as assessed by mitotic index, histology, and terminal deoxynucleotidyl transferase–mediated deoxyuridine triphosphate nick end labeling

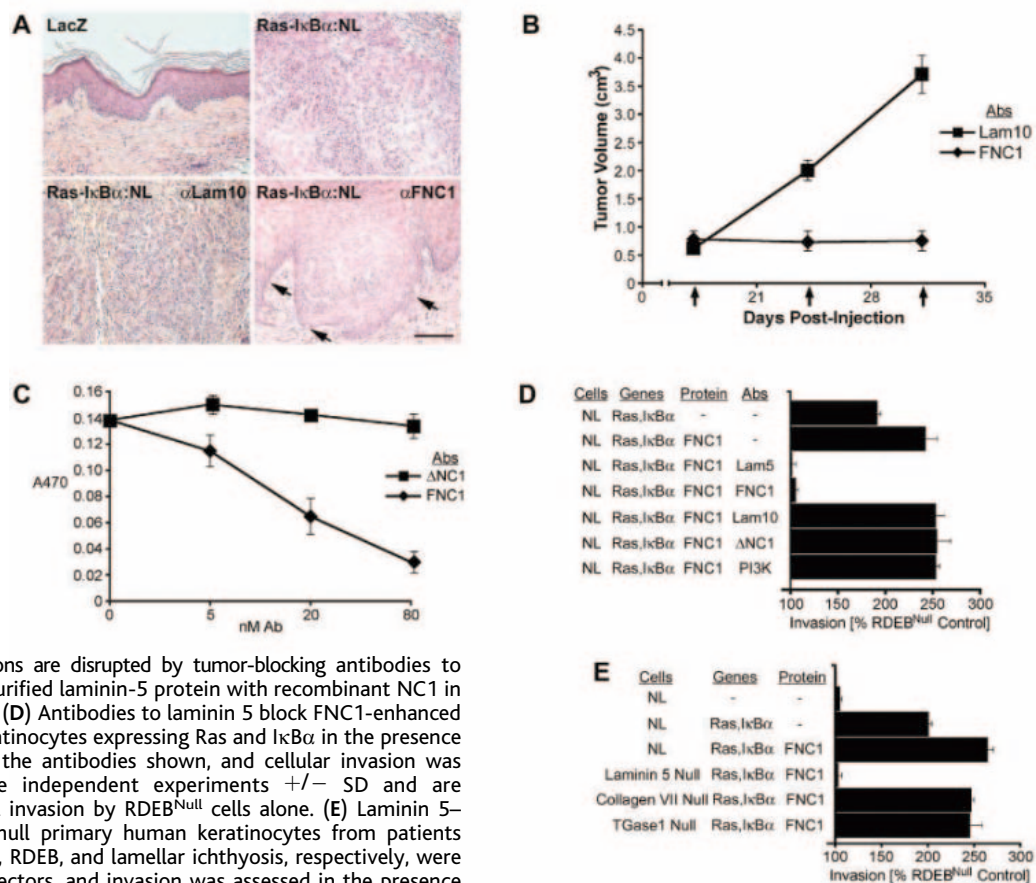
(TUNEL) staining. In vitro invasion assays confirmed that antibodies to FNC1, but not  $\Delta$ NC1, blocked enhanced invasion of normal cells coexpressing Ras and I $\kappa$ B $\alpha$  and that invasiveness of RDEB<sup>Null</sup> cells was restored by FNC1 (figs. S2 and S3). These data indicate that FNC1 sequences act primarily by facilitating invasion rather than by altering other processes important in neoplasia. Consistent with this, injection of FNC1 antibodies arrested expansion of established subcutaneous tumors (Fig. 4B).

FNC1 sequences encompass a region of collagen VII that was previously demonstrated to bind to laminin 5 (9, 15), another extracellular adhesion protein expressed in human epidermal neoplasia (7, 16, 17). To study whether laminin 5 plays a role in FNC1-mediated invasion, we examined interactions between FNC1 and purified laminin 5 using a solid-phase ligand-binding assay. Consistent with previous studies (18), recombinant FNC1 bound laminin 5, but not laminin 1, in a dose-dependent manner (fig. S4). Moreover, tumor-blocking FNC1 antibodies disrupted physical interactions between the entire NC1 domain and laminin 5. In contrast,  $\Delta$ NC1 antibodies, which had no effect on tumor formation, also had no effect on this protein-protein interaction (Fig. 4C). Moreover, antibodies to laminin 5, but not to laminin 10, inhibited the stimu-

latory effect of FNC1 on tumor cell invasion (Fig. 4D). In addition, FNC1 protein enhanced invasiveness in lamellar ichthyosis keratinocytes lacking transglutaminase 1 (TGase1), but it had no effect on laminin 5–null keratinocytes from patients with junctional epidermolysis bullosa, which indicates that FNC1-mediated invasion requires laminin 5 (Fig. 4E).

In summary, we have demonstrated that collagen VII is required for Ras-driven human epidermal tumorigenesis, specifically by enhancing tumor cell invasion in a laminin 5–dependent manner. We propose a model in which physical interactions between laminin 5 and collagen VII that occur outside the cell facilitate cellular invasion. Given this extracellular mode of action, FNC1 would theoretically be accessible to therapeutics such as humanized mAbs. Our preliminary data also suggest that RDEB patients retaining NC1 might be at higher risk of SCC. Of interest, the single RDEB<sup>Null</sup> patient in our series who was over age 30 had not developed SCC by age 45, whereas all three of the RDEB<sup>NC1</sup> patients who were over age 30 had experienced early-onset SCCs by their thirties (table S1). However, whether NC1 retention is a reliable prognostic marker for epidermal cancer in RDEB is a question that can only be addressed through large prospective studies. The present work may have possible safety-monitoring im-

**Fig. 4.** FNC1 sequences enhance tumor cell invasion. (A) FNC1 antibodies block dermal invasion in vivo. Ras-I $\kappa$ B $\alpha$ -expressing and LacZ control-expressing human skin was regenerated on SCID mice using devitalized human dermis, with mice receiving FNC1 mAb 32 or mAb to laminin 10 (Lam10) (14) by weekly intraperitoneal injection starting 1 week after grafting. Representative micrographs are shown at 5 weeks ( $n = 5$  mice per group). Note widespread dermal invasion of keratinocytes in controls in contrast to FNC1 antibody-treated mice, where epidermal tissue is hyperplastic but where cells do not penetrate the dermal-epidermal junction (arrows) (scale bar, 100  $\mu$ m). (B) FNC1 antibodies block expansion of established tumors. Mice growing tumors established by subcutaneous injection of Ras-I $\kappa$ B $\alpha$ -expressing normal keratinocytes were injected intraperitoneally at weekly intervals (arrows) with antibodies to either FNC1 or laminin-10 control. (C) Laminin 5–NC1 interactions are disrupted by tumor-blocking antibodies to FNC1. Solid-phase binding assay of purified laminin-5 protein with recombinant NC1 in the presence of the antibodies noted. (D) Antibodies to laminin 5 block FNC1-enhanced invasion. Normal primary human keratinocytes expressing Ras and I $\kappa$ B $\alpha$  in the presence of FNC1 protein were treated with the antibodies shown, and cellular invasion was assessed. Data represents triplicate independent experiments  $\pm$  SD and are quantitated as a percentage of basal invasion by RDEB<sup>Null</sup> cells alone. (E) Laminin 5–null, collagen VII–null, and TGase1–null primary human keratinocytes from patients with junctional epidermolysis bullosa, RDEB, and lamellar ichthyosis, respectively, were transduced with Ras and I $\kappa$ B $\alpha$  retrovectors, and invasion was assessed in the presence of FNC1. Error bars in all panels represent SD.



plications for collagen VII gene- and protein-therapy studies planned in RDEB.

#### References and Notes

1. M. Alam, D. Ratner, *N. Engl. J. Med.* **344**, 975 (2001).
2. L. Y. Sakai, D. R. Keene, N. P. Morris, R. E. Burgeson, *J. Cell Biol.* **103**, 1577 (1986).
3. L. Bruckner-Tuderman, B. Hopfner, N. Hammami-Hauasli, *Matrix Biol.* **18**, 43 (1999).
4. L. Pulkkinen, J. Uitto, *Matrix Biol.* **18**, 29 (1999).
5. R. Mallipeddi, *Clin. Exp. Dermatol.* **27**, 616 (2002).
6. M. P. Marinkovich, P. A. Khavari, G. S. Herron, E. A. Bauer, in *Dermatology in General Medicine*, I. M. Freedberg *et al.*, Eds. (McGraw-Hill, New York, 2003), vol. 1, pp. 596–608.
7. R. H. Wetzels *et al.*, *Am. J. Pathol.* **139**, 451 (1991).
8. M. Dajee *et al.*, *Nature* **421**, 639 (2003).
9. M. Chen *et al.*, *J. Invest. Dermatol.* **112**, 177 (1999).
10. S. Ortiz-Urda *et al.*, *J. Clin. Invest.* **111**, 251 (2003).
11. H. Hesse, L. Y. Sakai, D. W. Hollister, R. E. Burgeson, E. Engvall, *Differentiation* **26**, 49 (1984).
12. G. P. Lunstrum, L. Y. Sakai, D. R. Keene, N. P. Morris, R. E. Burgeson, *J. Biol. Chem.* **261**, 9042 (1986).
13. M. Lazarov *et al.*, *Nature Med.* **8**, 1105 (2002).
14. J. Li *et al.*, *EMBO J.* **22**, 2400 (2003).
15. P. Roussele *et al.*, *J. Cell Biol.* **138**, 719 (1997).
16. P. Savoia, L. Trusolino, E. Pepino, P. C. Marchisio, *J. Invest. Dermatol.* **101**, 352 (1993).
17. T. Kainulainen *et al.*, *Br. J. Dermatol.* **136**, 331 (1997).
18. M. Chen *et al.*, *J. Biol. Chem.* **272**, 14516 (1997).
19. Supported by the U.S. Veterans Affairs Office of Research and Development, by National Institutes of Arthritis and Musculoskeletal and Skin Diseases, NIH (AR43799 and AR44012), by the Epidermolysis Bullosa Medical Research Foundation, and by a grant from the FWF Austrian Science Foundation (S.O.-U.). We thank A. E. Oro, H. Y. Chang, D. W. Felsner, E. Bauer, J. Reuter, T. Ridky, P. Dumesic, Z. Siprashvili, and R. Kimmel for pre-submission review and helpful discussions; K. Wolff and K. Rappersberger for support; T. Cai for PI3K reagents; L. Nall for help with donor information; N. L. Charbonneau for antibody preparation; and E. Pfendner for mutation detection.

#### Supporting Online Material

www.sciencemag.org/cgi/content/full/307/5716/1773/DC1

Materials and Methods

Figs. S1 to S4

Table S1

References

8 October 2004; accepted 18 January 2005

10.1126/science.1106209

## Uncharged tRNA and Sensing of Amino Acid Deficiency in Mammalian Piriform Cortex

Shuzhen Hao,<sup>1</sup> James W. Sharp,<sup>1</sup> Catherine M. Ross-Inta,<sup>1</sup> Brent J. McDaniel,<sup>2</sup> Tracy G. Anthony,<sup>2</sup> Ronald C. Wek,<sup>3</sup> Douglas R. Cavener,<sup>4</sup> Barbara C. McGrath,<sup>4</sup> John B. Rudell,<sup>1</sup> Thomas J. Koehnle,<sup>5</sup> Dorothy W. Gietzen<sup>1\*</sup>

Recognizing a deficiency of indispensable amino acids (IAAs) for protein synthesis is vital for dietary selection in metazoans, including humans. Cells in the brain's anterior piriform cortex (APC) are sensitive to IAA deficiency, signaling diet rejection and foraging for complementary IAA sources, but the mechanism is unknown. Here we report that the mechanism for recognizing IAA-deficient foods follows the conserved general control (GC) system, wherein uncharged transfer RNA induces phosphorylation of eukaryotic initiation factor 2 (eIF2) via the GC nonderepressing 2 (GCN2) kinase. Thus, a basic mechanism of nutritional stress management functions in mammalian brain to guide food selection for survival.

When supplies of high-quality plant protein or animal source foods are scarce, omnivores are at risk for IAA deficiency. Selection of such high-quality foods played an important role in human evolution (1); scarcity is a worldwide problem still common today. In disease or trauma, inadequate protein intake further compromises recovery, as found with gelatin in the 1800s (2). Combining vegetable protein sources with complementary IAA patterns (e.g., beans and rice) to maintain appropriate IAA balance is a longstanding cultural practice that predates knowledge of IAA and implies exis-

tence of innate detection of IAA deficiency in humans. Moreover, similar IAA complementation occurs in mammals and birds (3–5).

Sensing of IAA deficiency is seen in animals including invertebrates within minutes after diet introduction (3–6). Such sensing does not depend on olfactory, taste, or other peripheral systems (7–9). In the rat, the pyramidal output neurons of the APC are activated by intracellular IAA deficiency, without selective extracellular IAA receptors. These cells project to appropriate feeding control circuits (10). In rats and birds, lesions of the APC (11, 12), abolish the rejection of IAA-deficient foods. Microinjections of 1 to 2 nmol of the limiting IAA into APC selectively increase intake of the deficient diet (13–15) within 20 min (15), without other behavioral changes. Replacement of the limiting IAA into the APC has behavioral, anatomical, and biochemical specificity in the restoration of feeding on an IAA-deficient diet (13, 15). Similar injections into hypothalamic areas known to affect food intake increase deficient diet intake (16) or decrease feeding of a stock diet (17), but the

behavioral/feeding effects are too late to implicate the hypothalamus in the rapid sensing that we report. Injections of nonlimiting amino acids have no effect (13).

In yeast, amino acid deprivation leads to accumulation of uncharged tRNA, inducing GCN2-mediated phosphorylation to form the phospho-protein eukaryotic initiation factor 2 $\alpha$  (p-eIF2 $\alpha$ ). Subsequent cellular adaptation to amino acid deprivation is marked by decreases in global protein synthesis complemented by increased transcription of genes related to amino acid biosynthesis (18). For animals unable to synthesize IAAs, sensing a deficiency and neural signaling necessarily precede appropriate diet selection, which must occur before the remaining amino acids are metabolized and lost (3). Here we report a homologous pathway in the APC that acts 20 min after introduction of an IAA-deficient meal (19).

Diets devoid of an IAA deplete the APC of the limiting IAA by 56% within 21 min (20). We hypothesized that if uncharged tRNA provides the initial signal for IAA depletion in the APC, inhibition of tRNA charging should decrease food intake. We directly inhibited tRNA acylation in the APC using alcohol derivatives of amino acids (amino alcohols) microinjected into the APC as for IAAs in (13). Injections of 0.5  $\mu$ l were made bilaterally over 5 min. Doses (per side) of L-threoninol, D-threoninol, or L-prolinol (each, 4 nmol) and D,L-serinol (150 nmol) were dissolved in saline. L-Leucinol (3 nmol) was dissolved in 0.5 ml ethanol and then diluted 1:100; control rats were given vehicle injections. Animals with misplaced cannulas determined by histology were omitted from the data set, but the lack of effect of L-leucinol or L-threoninol in these animals provides an additional anatomical control. Subsequent food intake of diets, threonine basal (BAS), leucine BAS, or threonine BAS-devoid of threonine (TD) (6), was measured at 20 min, 40 min, 1 hour, 3 hours, 6 hours, and 21 hours after food presentation (21) (Fig. 1). The amino alcohols, such as threoninol, are potent, reversible inhibitors of the ATP exchange reaction in activating amino acids for acylation of their respective

<sup>1</sup>School of Veterinary Medicine, Department of Anatomy, Physiology and Cell Biology, University of California, Davis, CA 95616, USA. <sup>2</sup>Department of Biochemistry and Molecular Biology, Indiana University School of Medicine, Evansville, IN 47712, USA. <sup>3</sup>Department of Biochemistry and Molecular Biology, Indiana University School of Medicine, Indianapolis, IN 46202, USA. <sup>4</sup>Department of Biology, The Pennsylvania State University, University Park, PA, 16802, USA. <sup>5</sup>Department of Neuroscience, University of Pittsburgh, Pittsburgh, PA 15260, USA.

\*To whom correspondence should be addressed. E-mail: dwgietzen@ucdavis.edu

tRNA synthetases (22). After injection of L-threoninol, threonine BAS (6) intake was decreased (Fig. 1A) as if the rats were eating TD. To learn if this effect is seen with another IAA, L-leucinol was injected; it decreased intake of leucine BAS similarly (Fig. 1B). The stereoisomer, D-threoninol, did not affect threonine BAS intake (Fig. 1C). As with D-threoninol, the amino alcohol derivatives of the dispensable amino acids serine and proline, D,L-serinol and L-prolinol, were without effect. These results show that inhibition of the tRNA synthetase is stereospecific and selective for the limiting IAA in this in vivo model.

To evaluate competition for tRNA acylation, rats were preloaded with threonine using

a "corrected" diet (6). High dietary L-threonine competed with injected L-threoninol (Fig. 1D), preventing the food intake depression by the amino alcohol. The effects were reversible when the corrected diet was fed during the postinjection test period, which showed that there were no nonspecific effects of amino alcohols on neural tissue or other short-term processes. These results suggest that dietary IAA depletion is recognized at the level of uncharged tRNA in APC.

In the yeast GC response, uncharged tRNA binds to a regulatory site in GCN2 that is homologous to histidyl-tRNA synthetases, which increases p-eIF2 $\alpha$  (18). Although some cellular stressors activate multiple eIF2 kinases, dietary IAA deprivation increases p-

eIF2 $\alpha$  in a strictly GCN2-dependent manner (18, 23). To test the roles of GCN2 and eIF2 $\alpha$  in mammalian brain, we used GCN2 null (*GCN2*<sup>-/-</sup>; C57BL/6J background 8 to 10 generations) mice (23, 24) and their BL/6J controls (*GCN2*<sup>+/+</sup>). The mouse homolog, mGCN2, is highly expressed in brain (25), and when activated, directly phosphorylates eIF2 $\alpha$  (26). Both L-histidine limitation in the presence of L-histidinol in liver and L-leucine deprivation in embryonic stem cells and mouse liver, increase p-eIF2 $\alpha$  in *GCN2*<sup>+/+</sup> mice, with no effect in *GCN2*<sup>-/-</sup> mice (23, 24). In Western blots (19) of APCs dissected as in (27), there was more p-eIF2 $\alpha$  protein in *GCN2*<sup>+/+</sup> than in *GCN2*<sup>-/-</sup> mice (Fig. 2A). This was not due to the absence of total eIF2 $\alpha$  protein in the APC of the *GCN2*<sup>-/-</sup> mice, as there were equal amounts of total eIF2 $\alpha$  in APCs from both genotypes (Fig. 2B). Intake of TD was correlated ( $P < 0.001$ ) with p-eIF2 $\alpha$  only in the *GCN2*<sup>+/+</sup> mice (Fig. 2C). The percent of phosphoprotein to total eIF2 $\alpha$  in APCs taken from *GCN2*<sup>-/-</sup> mice after 20 min of eating either threonine BAS or TD was the same as that seen in mice that failed to eat. Therefore, GCN2 is required for the TD effect in eIF2 $\alpha$  phosphorylation. After prefeeding threonine BAS (6), *GCN2*<sup>+/+</sup> mice ate significantly less TD ( $P = 0.015$ ), whereas *GCN2*<sup>-/-</sup> mice ate the same amounts of both threonine BAS and TD diets over 40 min (Fig. 2D). Because the *GCN2*<sup>-/-</sup> mice failed to recognize the deficient diet, we suggest that the GCN2 kinase is also essential for early recognition of IAA deficiency in the mouse.

Levels of p-eIF2 $\alpha$  in immunoblots from rat APCs taken after L-threoninol versus saline injections were similar to those after feeding TD versus threonine BAS (19) (Fig. 3). Four eIF2 kinases exist in mammals; each is activated in response to specific environmental

**Fig. 1.** Food intake responses after amino alcohol injection into APC of rats (13, 15). Food intake seen at 40 min remained the same at 1 hour, but did not differ between groups after 3 hours in any experiment. Controls, vehicle-injected groups, are indicated by white bars; experimental groups are represented by black bars. Values are means  $\pm$  SEM; \* $P < 0.05$ , \*\* $P < 0.01$  for differences between treated and control groups. (A) L-Threoninol decreased threonine BAS intake starting at 20 min (left), reaching significance at 40 min (right;  $P < 0.01$ ) ( $n = 11$ /group). (B) Effects of L-leucinol injections and leucine BAS diet. L-Leucinol ( $n = 11$ ) decreased food intake at 20 min ( $P = 0.05$ ) and 40 min ( $P < 0.05$ ) (controls,  $n = 13$ ). (C) Injection of D-threoninol had no effect on threonine BAS intake at any time ( $n = 7$ /group). This indicates a stereospecific effect of L-threoninol. (D) Rats ( $n = 7$ /group) that were preloaded with threonine via the corrected diet for 3 days did not respond to L-threoninol, when eating BAS, as did those prefed threonine BAS (Fig. 1A). Reciprocally, those prefed threonine BAS but offered corrected after injection also did not respond (data similar to Fig. 1C); this shows competitive inhibition of L-threoninol by dietary threonine.

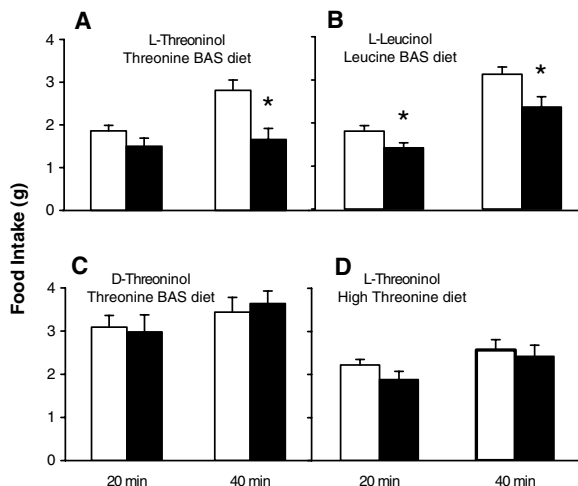
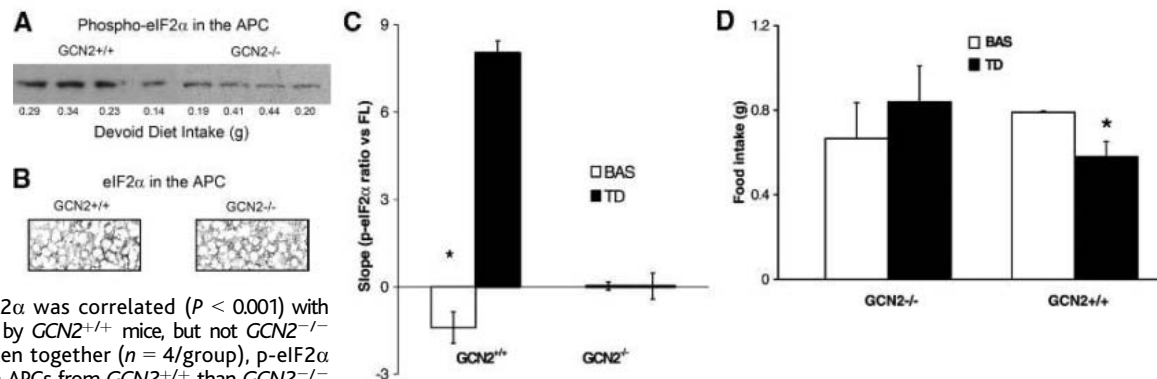


**Fig. 2.** Phospho- and total eIF2 $\alpha$  in mouse APC; feeding responses of wild-type and GCN2 null mice. (A) Phospho-eIF2 $\alpha$  in tissue from individual 42-day-old mice after 40-min access to TD. Grams of TD eaten by each mouse are given below the protein band for that mouse. Phosphorylation of eIF2 $\alpha$  was correlated ( $P < 0.001$ ) with the amount of TD eaten by *GCN2*<sup>+/+</sup> mice, but not *GCN2*<sup>-/-</sup> mice [see also (C)]. Taken together ( $n = 4$ /group), p-eIF2 $\alpha$  was greater ( $P < 0.04$ ) in APCs from *GCN2*<sup>+/+</sup> than *GCN2*<sup>-/-</sup> mice, calculated as density units (U) [*GCN2*<sup>+/+</sup> 19.1  $\pm$  6.2 U (mean  $\pm$  SD) versus *GCN2*<sup>-/-</sup> 9.8  $\pm$  2.0 U]. (B) Cell body layers in APC of both genotypes contained ample and equal amounts of total eIF2 $\alpha$  protein (black punctate areas surrounding white nuclei.) Immunoblot values for total eIF2 $\alpha$  protein, as density units (U), also did not differ (means  $\pm$  SEM: *GCN2*<sup>+/+</sup> 66.2  $\pm$  6.6 U versus *GCN2*<sup>-/-</sup> 71.0  $\pm$  4.8 U,  $P =$  NS). (C) Slopes of the phospho/total eIF2 $\alpha$  ratio in APC are correlated with 40-min intake of TD in *GCN2*<sup>+/+</sup> (left), but not *GCN2*<sup>-/-</sup> mice (right), and not in either genotype fed threonine BAS. With increased



ingestion of TD in *GCN2*<sup>+/+</sup> mice, the phosphorylation ratio of eIF2 $\alpha$  (19) was increased (slope 8.03,  $R^2 = 0.99$ ,  $P = 0.001$ ). With ingestion of BAS by these mice, p-eIF2 $\alpha$  decreased slightly (slope -0.25,  $R^2 = 0.02$ ,  $P =$  NS). (D) Food intake of *GCN2*<sup>+/+</sup> and *GCN2*<sup>-/-</sup> mice (42 to 78 days of age,  $n = 7$  or 8 per group) eating threonine BAS or TD for 40 min. The control *GCN2*<sup>+/+</sup> mice decreased their intake of the TD ( $P = 0.015$ ) whereas the *GCN2*<sup>-/-</sup> did not. Values are means  $\pm$  SEM for grams eaten.

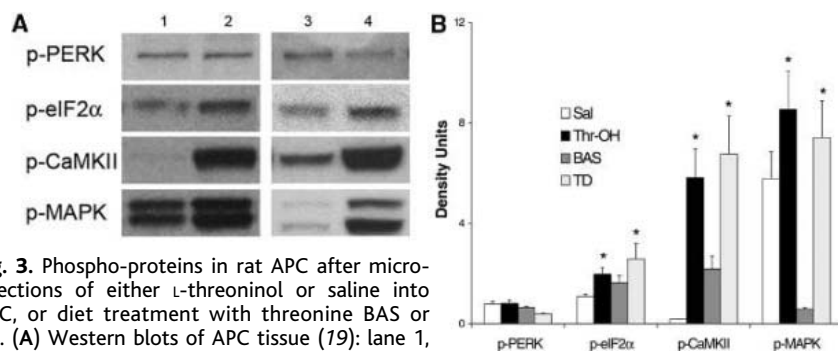


**Fig. 3.** Phospho-proteins in rat APC after micro-injections of either L-threoninol or saline into APC, or diet treatment with threonine BAS or TD. (A) Western blots of APC tissue (19); lane 1, saline; lane 2, L-threoninol; both offered BAS for 20 min; lane 3, un.injected rats that ate threonine BAS; lane 4, un.injected rats offered TD, both for 20 min. Animals that failed to eat > 0.8 g of diet were excluded. Phospho- (p-) proteins (defined in the text) are indicated at the left of each band. (B) Western blot data from (A); Values are U (means ± SEM) for each protein. Stars indicate significant differences for the experimental groups compared with their respective controls ( $P < 0.05$ ).

stressors. Double-stranded RNA-activated protein kinase (PKR) is not involved in IAA starvation (28), and heme-related inhibitor (HRI) is not found in brain (18). Pancreatic endoplasmic reticulum-resident kinase (PERK), is associated with misfolded proteins in the ER, and it is found in brain. We found no increase in phospho-PERK (p-PERK) in Western blots of APC taken 20 min after either L-threoninol injection or eating TD (Fig. 3). This supports GCN2 as the eIF2 $\alpha$  kinase in this system. Downstream signaling (29, 30) was also seen similarly in animals fed TD or injected with L-threoninol, including increased phosphorylation of calcium calmodulin kinase II (p-CAMKII) (29) and mitogen-activated protein kinase (p-MAPK) (30) (Fig. 3).

We conclude that the tRNA/GCN2/p-eIF2 $\alpha$  system signals IAA deficiency in the output neurons of the brain area essential for the adaptive rejection of an IAA-deficient diet within the 20-min time frame of the behavioral response (6). These unique neurons of the APC, the vertebrate IAA chemosensors, respond to IAA starvation as do yeast: one by feeding behavior, the other by biosynthesis. The responses in both systems lead to restoration of IAA homeostasis and show conservation of this crucial nutrient sensor across evolution, from yeast to mammals.

**References and Notes**

1. K. Milton, *J. Nutr.* **133** (11 Suppl. 2), 3886S (2003).
2. K. J. Carpenter, *J. Nutr.* **133**, 638 (2003).
3. D. W. Gietzen, in *Neural and Metabolic Control of Macronutrient Intake*, H. R. Berthoud, R. J. Seeley, Eds. (CRC, New York, 2000), chap. 23.
4. M. E. Murphy, S. D. Percy, *Physiol. Behav.* **53**, 689 (1993).
5. K. Delaney, A. Gelperin, *J. Comp. Physiol. A Sens. Neural Behav. Psychol.* **159**, 281 (1986).
6. T. J. Koehnle, M. C. Russell, D. W. Gietzen, *J. Nutr.* **133**, 2331 (2003).
7. P. M. B. Leung, D. M. Larson, Q. R. Rogers, *Physiol. Behav.* **9**, 553 (1972).
8. S. Markison, D. W. Gietzen, A. C. Spector, *J. Nutr.* **129**, 1604 (1999).
9. B. S. Washburn, J. C. Jiang, S. L. Cummings, K. Dixon, D. W. Gietzen, *Am. J. Physiol.* **266**, R1922 (1994).

10. L. B. Haberly, J. L. Price, *J. Comp. Neurol.* **178**, 711 (1978).
11. P. M. B. Leung, Q. R. Rogers, *Am. J. Physiol.* **221**, 929 (1971).
12. J. D. Firman, W. J. Kuenzel, *Brain Res. Bull.* **21**, 637 (1988).
13. J. L. Beverly, D. W. Gietzen, Q. R. Rogers, *Am. J. Physiol.* **259**, R709 (1990).
14. M. Monda, A. Sullo, V. DeLuca, M. P. Pellicano, A. Viggiano, *Am. J. Physiol.* **273**, R554 (1997).
15. M. C. Russell, T. J. Koehnle, J. A. Barrett, J. E. Blevins, D. W. Gietzen, *Nutr. Neurosci.* **6**, 247 (2003).

16. J. E. Blevins, K. D. Dixon, E. J. Hernandez, J. A. Barrett, D. W. Gietzen, *Brain Res.* **879**, 65 (2000).
17. J. Panksepp, D. A. Booth, *Nature* **233**, 341 (1971).
18. S. A. Wek, S. Zhu, R. Wek, *Mol. Cell. Biol.* **15**, 4497 (1995).
19. D. W. Gietzen, C. M. Ross, S. Hao, J. W. Sharp, *J. Nutr.* **134**, 717 (2004).
20. T. J. Koehnle, M. C. Russell, A. S. Morin, L. F. Erecius, D. W. Gietzen, *J. Nutr.* **134**, 2365 (2004).
21. The procedures used in these experiments were approved by our institutional Animal Care and Use committees.
22. B. S. Hansen, M. H. Vaughan, L. J. Wang, *J. Biol. Chem.* **247**, 3854 (1972).
23. T. G. Anthony et al., *J. Biol. Chem.* **279**, 36553 (2004).
24. P. Zhang et al., *Mol. Cell. Biol.* **22**, 6681 (2002).
25. R. Sood, A. C. Porter, D. A. Olsen, D. R. Cavener, R. C. Wek, *Genetics* **154**, 787 (2000).
26. S. R. Kimball, D. A. Antonetti, R. M. Brawley, L. S. Jefferson, *J. Biol. Chem.* **266**, 1969 (1991).
27. D. W. Gietzen, P. M. B. Leung, Q. R. Rogers, *Physiol. Behav.* **36**, 1071 (1986).
28. S. R. Kimball et al., *Biochem. Biophys. Res. Commun.* **280**, 293 (2001).
29. J. W. Sharp, C. M. Ross, T. J. Koehnle, D. W. Gietzen, *Neuroscience* **126**, 1053 (2004).
30. J. W. Sharp, L. J. Magrum, D. W. Gietzen, *Brain Res. Mol. Brain Res.* **105**, 11 (2002).
31. The authors acknowledge support from NIH, NS043231 and NS33347, and U.S. Department of Agriculture, 2000 1049 (D.W.G.) and NIH, GM49164 (R.C.W.).

7 September 2004; accepted 20 January 2005  
10.1126/science.1104882

# Human Symbionts Use a Host-Like Pathway for Surface Fucosylation

Michael J. Coyne, Barbara Reinap, Martin M. Lee, Laurie E. Comstock\*

The mammalian intestine harbors a beneficial microbiota numbering approximately 10<sup>12</sup> organisms per gram of colonic content. The host tolerates this tremendous bacterial load while maintaining the ability to efficiently respond to pathogenic organisms. In this study, we show that the *Bacteroides* use a mammalian-like pathway to decorate numerous surface capsular polysaccharides and glycoproteins with L-fucose, an abundant surface molecule of intestinal epithelial cells, resulting in the coordinated expression of this surface molecule by host and symbiont. A *Bacteroides* mutant deficient in the ability to cover its surface with L-fucose is defective in colonizing the mammalian intestine under competitive conditions.

The ability of humans to tolerate a complex microbiota despite their exquisite ability to distinguish self from nonself has been called an “immunological paradox” (1). One mechanism that may contribute to the tolerance of these resident microorganisms is molecular mimicry, whereby the bacteria display surface molecules resembling those of the host’s surface to render them immuno-

logically inert. Immunologic similarities between the abundant colonic microorganisms *Bacteroides* and tissues of the host are known (2, 3).

The surfaces of intestinal epithelial cells are covered with an abundance of terminally fucosylated glycoproteins and glycolipids (4, 5), which are induced by the intestinal microbiota and specifically by *Bacteroides* (6), which in turn cleave L-fucose moieties from the host’s surface and internalize them for use as an energy source (7). Here we show that *Bacteroides* convert exogenously acquired L-fucose to guanosine diphosphate (GDP)-L-fucose to incorporate it into multiple

Channing Laboratory, Department of Medicine, Brigham and Women’s Hospital, Harvard Medical School, Boston, MA 02115, USA.

\*To whom correspondence should be addressed. E-mail: lcomstock@channing.harvard.edu

surface capsular polysaccharides and glycoproteins. This study suggests a basis for molecular mimicry by these indigenous microorganisms and demonstrates that the synthesis of fucosylated surface molecules gives these symbionts a competitive colonization advantage.

*Bacteroides fragilis* 9343 is covered with multiple capsular polysaccharides whose expression is regulated by DNA inversions (8, 9). Of the eight capsular polysaccharides (termed PSA to PSH) known to be synthesized by this organism, the structures of only two, PSA and PSB, have been elucidated (10). The repeating unit of PSB contains a terminal  $\alpha$ 1,2-linked L-fucose moiety, and its biosynthesis locus encodes an  $\alpha$ 1,2 fucosyltransferase (11), which incorporates L-fucose into the PSB repeating unit. We found that three other capsular polysaccharide biosynthesis loci of *B. fragilis* 9343 (PSC, PSD, and PSH) also contain fucosyltransferase homologs.

The donor for the incorporation of fucose into eukaryotic glycoproteins, glycolipids, and bacterial polysaccharides is GDP-L-fucose [recently reviewed in (12)]. In bacteria, GDP-L-fucose is formed from GDP-D-mannose by GDP-mannose dehydratase (Gmd) and fucose synthetase (Fcl) (Fig. 1A) (13). Mammalian organisms also convert L-fucose to GDP-L-fucose through an L-fucose-1-phosphate intermediate (Fig. 2A). In *B. fragilis* 9343, *gmd* and *fcl* reside approximately 4 kb upstream of the oppositely transcribed PSB locus (Fig. 1A). Polymerase chain reaction (PCR) analysis (Fig. 1B) of 50 *B. fragilis* strains demonstrated that these genes are always present in tandem upstream of the PSB locus (14). Analysis of the completed genome sequence of *B. fragilis* 9343 confirmed that these are the only *gmd-fcl* genes in the genome.

Deletion of *gmd* and *fcl* from *B. fragilis* was expected to render the organism unable to synthesize the four polysaccharides predicted to contain L-fucose. However, when  $\Delta$ *gmd-fcl* was grown in standard medium, all eight polysaccharides were synthesized (Fig. 1C, lanes 1 and 2). When this mutant was grown in minimal glucose or minimal mannose medium, the synthesis of PSB, PSC, PSD, and PSE was abrogated (Fig. 1C, lanes 3 to 6). The PSE-null and PSH-positive phenotypes were not predicted on the basis of genetics; however, because *B. fragilis* synthesizes a large number of polysaccharides, it is likely that various gene products are not exclusive to the synthesis of their respective polysaccharide. When *gmd-fcl* genes were restored in trans (plasmid pMJC20),  $\Delta$ *gmd-fcl* recovered full polysaccharide synthesis (Fig. 1D, lane 3). The *Escherichia coli* K-12 *gmd-fcl* genes, involved in colanic acid biosynthesis (13), also restored capsule expression to near wild-type levels in minimal glucose medium (Fig. 1D, lane 4).

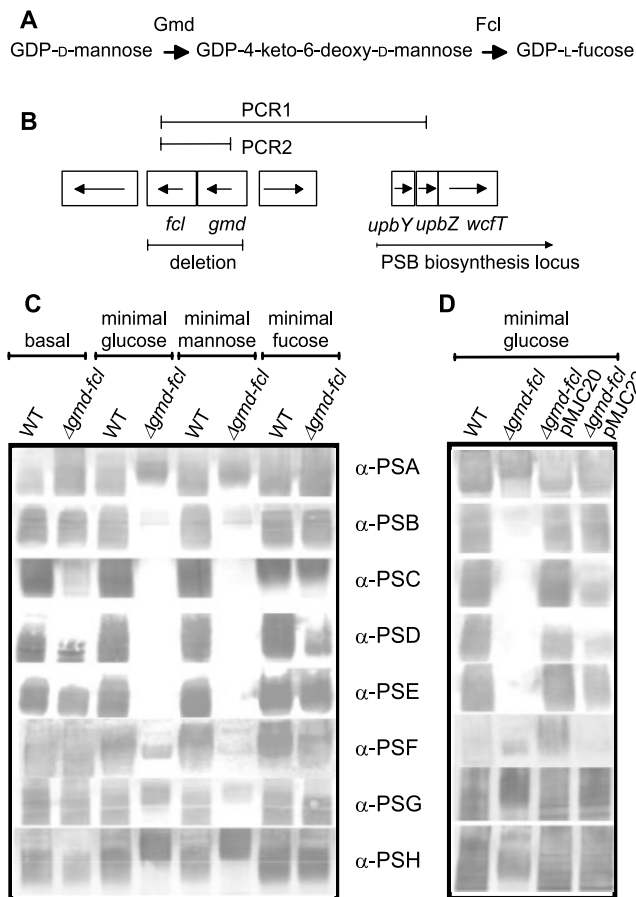


**Fig. 1.** Gmd and Fcl are essential for the synthesis of four of the capsular polysaccharides of *B. fragilis* 9343 when grown in media lacking fucose. (A) Biosynthesis pathway leading to the formation of GDP-L-fucose from GDP-D-mannose. Gmd represents GDP-mannose dehydratase and Fcl represents fucose synthetase. (B) Open reading frame (ORF) map of the chromosomal region containing *gmd-fcl*. A product was amplified by PCR1 and PCR2 for all 50 *B. fragilis* strains analyzed. The region deleted in  $\Delta$ *gmd-fcl* is shown. (C) Western blot analysis demonstrating the eight capsular phenotypes from organisms grown in rich medium or in defined media with glucose, mannose, or fucose.  $\alpha$ -, antiserum. (D) Western blot analysis demonstrating that the capsular phenotypes of the  $\Delta$ *gmd-fcl* mutant grown in minimal glucose medium are restored when *gmd-fcl* from *B. fragilis* (pMJC20) or *E. coli* (pMJC22) is supplied in trans.

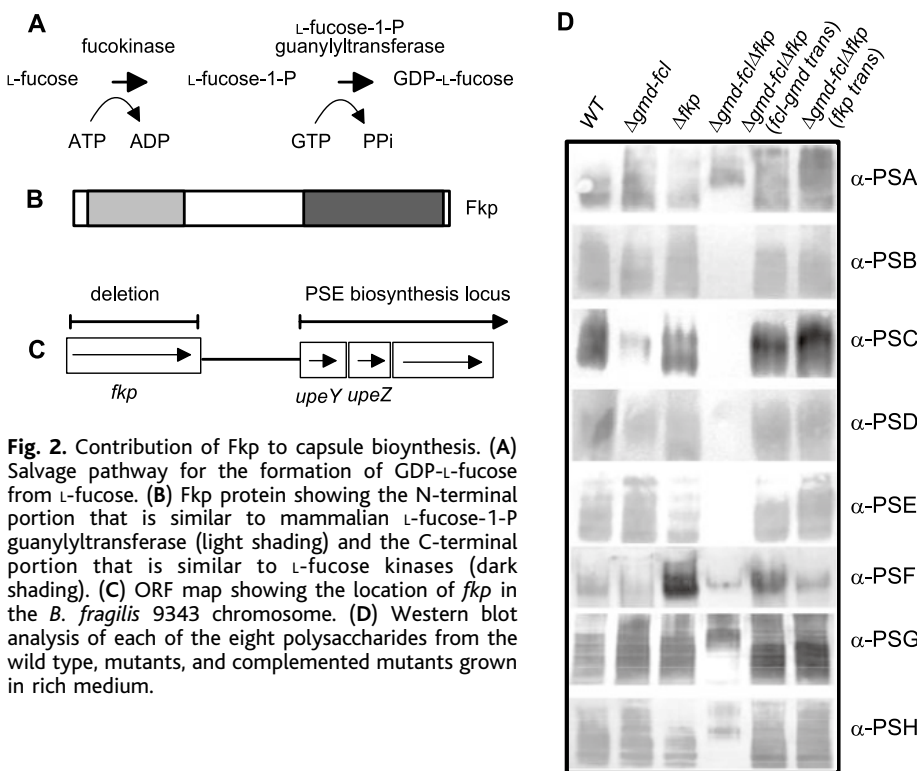


**Fig. 2.** Contribution of Fkp to capsule bioynthesis. (A) Salvage pathway for the formation of GDP-L-fucose from L-fucose. (B) Fkp protein showing the N-terminal portion that is similar to mammalian L-fucose-1-P guanylyltransferase (light shading) and the C-terminal portion that is similar to L-fucose kinases (dark shading). (C) ORF map showing the location of *fkp* in the *B. fragilis* 9343 chromosome. (D) Western blot analysis of each of the eight polysaccharides from the wild type, mutants, and complemented mutants grown in rich medium.

By contrast, when  $\Delta$ *gmd-fcl* was grown in minimal medium supplemented with L-fucose, the polysaccharide phenotypes resembled the

wild type (Fig. 1C, lanes 7 and 8), suggesting that the organism directly uses L-fucose from the medium for incorporation into its capsu-



lar polysaccharides, a previously undescribed phenomenon in the prokaryotic superkingdom. Surface expression of a distinct monosaccharide, sialic acid, after acquisition from host molecules has been described for other microbes (15, 16). The use of exogenous fucose in this manner would require a mammalian-like pathway containing L-fucose-1-P guanylyltransferase, which converts L-fucose-1-phosphate to

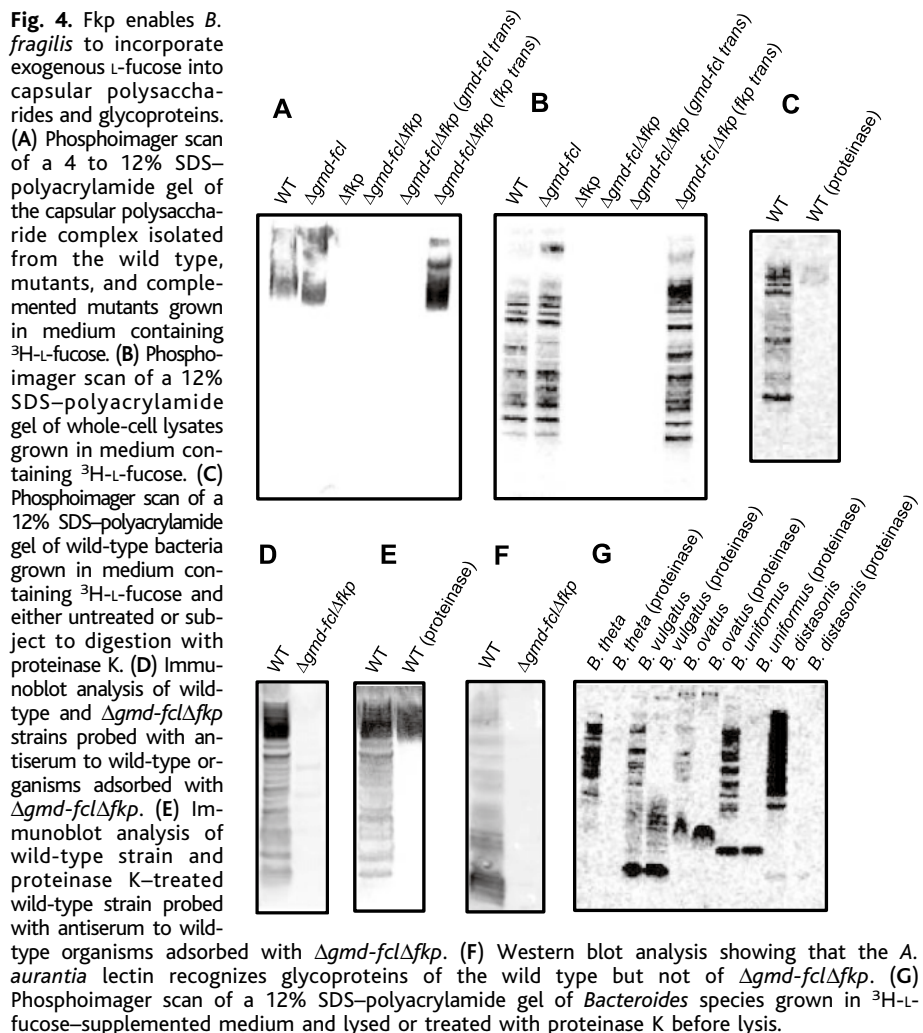
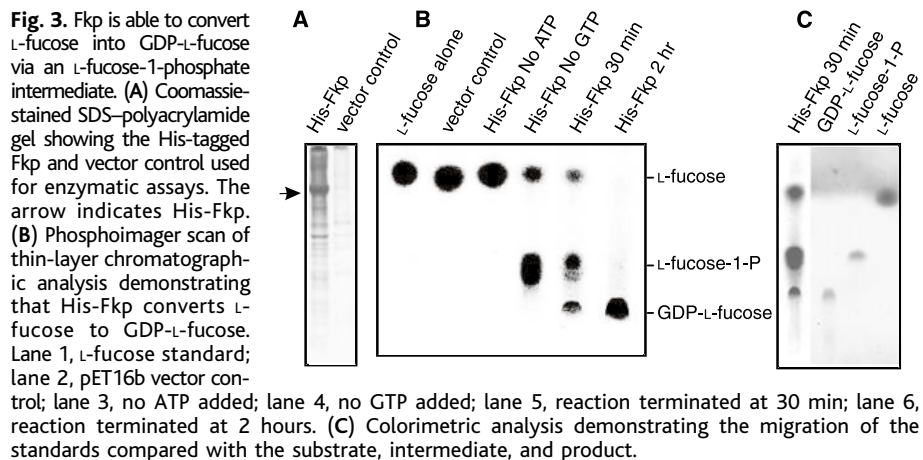
GDP-L-fucose (Fig. 2A). We detected a protein in the *B. fragilis* proteome with N-terminal similarity to the human L-fucose-1-P guanylyltransferase (Fig. 2B). Further analysis of this *B. fragilis* protein revealed C-terminal similarity to mammalian L-fucokinases, which convert L-fucose to L-fucose-1-phosphate. These findings suggested that this protein catalyzes both steps in the conversion of L-fucose to

GDP-L-fucose. The gene encoding this hybrid protein, which we designate Fkp, is in a conserved genetic region upstream of the PSE capsule locus (Fig. 2C).

We deleted *fkp* from both wild-type and  $\Delta gmd-fcl$  backgrounds. Mutational analysis revealed that  $\Delta fkp$  expressed all capsular polysaccharides (Fig. 2D, lane 3), whereas the  $\Delta gmd-fcl\Delta fkp$  mutant was unable to synthesize PSB, PSC, PSD, or PSE, even when grown in rich medium (Fig. 2D, lane 4). The four polysaccharides synthesized by this mutant are more homogeneous in size in the higher molecular-weight range as compared to the wild type, which is possibly attributable to less competition for nucleotide-activated monosaccharide precursors. When the  $\Delta gmd-fcl\Delta fkp$  mutant is complemented with either *gmd-fcl* or *fkp*, polysaccharide synthesis is restored (Fig. 2D, lanes 5 and 6). These results demonstrate the involvement of Fkp in capsular polysaccharide biosynthesis and strongly suggest that this enzyme converts L-fucose to GDP-L-fucose.

To confirm the activity of Fkp, a His-tagged fusion protein was used in enzymatic assays (14). Tritiated L-fucose (Fig. 3B, lane 1) was fully converted to GDP-L-fucose by His-Fkp (lane 6) but not by a control lysate purified in the same way (lane 2). When adenosine triphosphate (ATP) was omitted, no conversion occurred, because ATP is required to convert L-fucose to L-fucose-1-phosphate (lane 3). When guanosine triphosphate (GTP) was omitted, the reaction produced only L-fucose-1-phosphate (lane 4), because GTP is necessary to convert this intermediate to GDP-L-fucose. High-performance anion-exchange chromatography analysis of the enzymatic reaction confirmed the identity of all reaction products (fig. S1).

When grown in rich medium supplemented with  $^3H$ -L-fucose, *B. fragilis* incorporates this radiolabeled sugar into its capsular polysaccharides in an Fkp-dependent manner (Fig. 4A). Moreover, Fkp also enables the  $^3H$ -L-fucose to associate with numerous proteins (Fig. 4B), which are sensitive to digestion by proteinase K (Fig. 4C). Antiserum raised to wild-type organisms and adsorbed with  $\Delta gmd-fcl\Delta fkp$  detected numerous noncapsular polysaccharide molecules synthesized by the wild type but not by  $\Delta gmd-fcl\Delta fkp$  (Fig. 4D), which were destroyed by proteinase K treatment (Fig. 4E). The presence of L-fucose in these proteinacious molecules was confirmed by their binding of the *Aleuria aurantia* lectin, which is specific to fucose in  $\alpha$ -1,3 or  $\alpha$ -1,6 linkages (Fig. 4F). Therefore, *B. fragilis* synthesizes multiple fucosylated capsular polysaccharides and numerous fucosylated glycoproteins and is able to use an external source of L-fucose in an Fkp-dependent manner for their synthesis. Because dietary forms of L-fucose are absorbed with other simple monosaccharides in the small intestine, the *Bacteroides* must acquire exog-



enous L-fucose from the host (7). This is the first report of glycoprotein synthesis by an intestinal *Bacteroides* species and, to our knowledge, of bacterial glycoproteins containing L-fucose.

*B. thetaiotaomicron* is the only other sequenced bacterial genome containing an *fkp* homolog. Southern blot analysis using the L-fucose-1-P guanylyltransferase portion of *fkp* as a probe revealed homologs in all 20 *B. fragilis* strains tested and in all *Bacteroides* species analyzed (fig. S2). *Porphyromonas gingivalis* and *Tannerella forsythensis*, both members of the Bacteroidales order that colonize the oral cavity, do not contain *fkp*, suggesting acquisition after the Bacteroidales diverged into separate genera but before *Bacteroides* speciation. When representative *Bacteroides* species were grown in medium containing <sup>3</sup>H-L-fucose, they also incorporated L-fucose into multiple glycoproteins, whereas *Enterococcus faecalis* and *E. coli*, used as controls, did not (Fig. 4G and fig. S3).

Full-length homologs of *fkp* were also detected in the genomes of *Arabidopsis thaliana* and *Oryza sativa*. This may explain why the *A. thaliana mur1* mutant (17), which is deficient in the synthesis of GMD2 (GDP-mannose 4,6-dehydratase), synthesizes fucosylated glycoconjugates when grown on media containing fucose (17, 18).

We performed colonization experiments to determine whether the synthesis of fucosylated molecules confers an advantage on *B. fragilis* in the mammalian intestine by inoculating Swiss Webster germ-free mice with either the wild-type strain or  $\Delta gmd-fcl\Delta fkp$ . Two days after inoculation, mice colonized with either strain showed similar numbers of bacteria in their feces ( $1.7 \times 10^{10}$  to  $3.1 \times 10^{10}$  bacteria per gram of feces, table S1) and maintained this level for the duration of the experiment (6 weeks). Thus,  $\Delta gmd-fcl\Delta fkp$  is as fit as the wild-type strain to colonize the mouse intestine in the absence of competition. Next, a competitive colonization assay was performed, in which a bacterial mixture containing 50% wild-type and 50%  $\Delta gmd-fcl\Delta fkp$  was used for inoculation. PCR analysis of the bacterial colonies from feces collected 24 hours after inoculation demonstrated that only 5% of the fecal bacteria were  $\Delta gmd-fcl\Delta fkp$ . Three days after inoculation, no mutant bacteria were detected in the feces of any mice. This experiment was repeated, with the percentage of  $\Delta gmd-fcl\Delta fkp$  in the inoculum increased to 60%. Twenty-four hours after bacterial inoculation, 3.2% of the fecal bacteria from mice in cage 1 and 8.6% of the fecal bacteria from mice in cage 2 were  $\Delta gmd-fcl\Delta fkp$ . By day 3, the percentages of  $\Delta gmd-fcl\Delta fkp$  in the feces of mice were reduced to 0% and 1.2% in cages 1 and 2, respectively.

Therefore, the synthesis of fucosylated surface molecules by *B. fragilis* gives these

organisms a survival advantage in the competitive mammalian intestinal ecosystem; an ecosystem in which the synthesis of fucosylated host surface molecules is induced by the *Bacteroides* themselves (6). Because L-fucose is involved in *Bacteroides*' signaling of the synthesis of host fucosylated glycan production (7), it will be interesting to determine whether  $\Delta gmd-fcl\Delta fkp$  is able to induce this symbiotic signal.

#### References and Notes

- H. R. Gaskins, in *Gastrointestinal Microbes and Host Interactions*, R. I. Mackie, B. A. White, R. E. Isaacson, Eds. (Chapman & Hall, New York, 1997), vol. 2, pp. 537–587.
- M. C. Foo, A. Lee, *Infect. Immun.* **9**, 1066 (1974).
- R. D. Berg, D. C. Savage, *Infect. Immun.* **11**, 320 (1975).
- S. Bjork, M. E. Breimer, G. C. Hansson, K. A. Karlsson, H. Leffler, *J. Biol. Chem.* **262**, 6758 (1987).
- J. Finne et al., *J. Biol. Chem.* **264**, 5720 (1989).
- L. Bry, P. G. Falk, T. Midtvedt, J. I. Gordon, *Science* **273**, 1380 (1996).
- L. V. Hooper, J. Xu, P. G. Falk, T. Midtvedt, J. Gordon, *Proc. Natl. Acad. Sci. U.S.A.* **96**, 9833 (1999).
- C. M. Krinos et al., *Nature* **414**, 555 (2001).
- M. J. Coyne, K. G. Weinacht, C. M. Krinos, L. E. Comstock, *Proc. Natl. Acad. Sci. U.S.A.* **100**, 10446 (2003).
- H. Baumann, A. O. Tzianabos, J. R. Brisson, D. L. Kasper, H. J. Jennings, *Biochemistry* **31**, 4081 (1992).
- M. J. Coyne, W. Kalka-Moll, A. O. Tzianabos, D. L. Kasper, L. E. Comstock, *Infect. Immun.* **68**, 6176 (2000).

- D. J. Becker, J. B. Lowe, *Glycobiology* **13**, 41R (2003).
- K. Andrianopoulos, L. Wang, P. R. Reeves, *J. Bacteriol.* **180**, 998 (1998).
- Methods are provided in supporting material on Science Online.
- V. Bouchet et al., *Proc. Natl. Acad. Sci. U.S.A.* **100**, 8898 (2003).
- J. O. Previato, A. F. Andrade, M. C. Pessolani, L. Mendonca-Previato, *Mol. Biochem. Parasitol.* **16**, 85 (1985).
- C. P. Bonin, I. Potter, G. F. Vanzin, W. D. Reiter, *Proc. Natl. Acad. Sci. U.S.A.* **94**, 2085 (1997).
- G. Freshour et al., *Plant Physiol.* **131**, 1602 (2003).
- We thank A. Watts for PCR analysis, A. Nichols for Southern blot analysis, J. Wang for thin-layer chromatography advice, and D. Kasper and S. Mazmanian for helpful discussions. Sequence data for *B. fragilis* strain NCTC 9343 were generated by the Pathogen Sequencing Unit of the Sanger Institute and are available from [http://www.sanger.ac.uk/Projects/B\\_fragilis/](http://www.sanger.ac.uk/Projects/B_fragilis/). The GenBank accession no. for *B. fragilis* Gmd and Fcl is AF285774 and for *B. fragilis* Fkp is AY849806. This work was supported by grants AI44193 and AI53694 from NIH (National Institute of Allergy and Infectious Diseases).

#### Supporting Online Material

[www.sciencemag.org/cgi/content/full/307/5716/1778/DC1](http://www.sciencemag.org/cgi/content/full/307/5716/1778/DC1)

Materials and Methods

Figs. S1 to S3

Table S1

References

18 October 2004; accepted 26 January 2005  
10.1126/science.1106469

## A Mitotic Septin Scaffold Required for Mammalian Chromosome Congression and Segregation

Elias T. Spiliotis,<sup>1</sup> Makoto Kinoshita,<sup>2</sup> W. James Nelson<sup>1\*</sup>

Coordination of cytokinesis with chromosome congression and segregation is critical for proper cell division, but the mechanism is unknown. Here, septins, a conserved family of polymerizing guanosine triphosphate-binding proteins, localized to the metaphase plate during mitosis. Septin depletion resulted in chromosome loss from the metaphase plate, lack of chromosome segregation and spindle elongation, and incomplete cytokinesis upon delayed mitotic exit. These defects correlated with loss of the mitotic motor and the checkpoint regulator centromere-associated protein E (CENP-E) from the kinetochores of congressing chromosomes. Mammalian septins may thus form a mitotic scaffold for CENP-E and other effectors to coordinate cytokinesis with chromosome congression and segregation.

In eukaryotic cells, genetic inheritance requires replicated chromosomes to congress within the mitotic spindle at the midplane of the dividing cell and segregate equally into two daughter cells (1). Fidelity in chromosome segregation is achieved by the spindle-assembly checkpoint that signals anaphase

when all proper attachments have been made between chromosomes and spindle microtubules (2). Though many molecular details of these events are described, it is unknown how chromosome congression and segregation, anaphase, and the final separation of daughter cells (cytokinesis) are coordinated.

In fungi and animals, septins are a conserved family of guanosine triphosphate (GTP)-binding proteins required for cell division (3). In the budding yeast *Saccharomyces cerevisiae*, spindle assembly and chromosome-microtubule attachments are enclosed within the nuclear envelope; septins assemble into filaments at the cortex of mother-daughter cell neck (4, 5) and regulate cortical localization of proteins

<sup>1</sup>Department of Molecular and Cellular Physiology, Beckman Center for Molecular and Genetic Medicine, Stanford University School of Medicine, Stanford, CA 94305–5435, USA. <sup>2</sup>Biochemistry and Cell Biology Unit, Horizontal Medical Research Organization, Kyoto University Graduate School of Medicine, Yoshida Konoe, Sakyo, Kyoto 606–8501, Japan.

\*To whom correspondence should be addressed.  
E-mail: [wjnelson@stanford.edu](mailto:wjnelson@stanford.edu)

involved in cell cycle progression and cytokinesis (6–11).

In mammalian cells, there are at least 12 septin genes (12). Mammalian septins are found at the plasma membrane and in the cytosol, and during cytokinesis, they colocalize with actin in the cleavage furrow and with microtubules in the midbody and central spindle (13–15). Interference with septin expression results in binucleate cells (13–15), but the septin functions that are disrupted are unknown.

We reassessed the distribution of mammalian septins during mitosis by staining Madin Darby canine kidney (MDCK) and HeLa cells with antibodies against septin 2 (Sept2) and septin 6 (Sept6). Sept2 localized to the midbody, the ingressing cleavage furrow, and the central spindle of cells undergoing cytokinesis (Fig. 1, A to C). However, in metaphase cells, Sept2 and Sept6 localized within the microtubule spindle (Fig. 1, D to I, and fig. S1, A to F). At the metaphase plate, a network of short interwoven Sept2 filaments was observed in close apposition to the kinetochores of the congressed chromosomes and kinetochore mi-

crofibules (Fig. 1, G to I). Similar distribution of septin filaments was observed within the spindle apparatus of living cells (fig. S2). When spindle microtubules were depolymerized, septins remained throughout the metaphase plate (Fig. 1, J to L, and fig. S1, G to I).

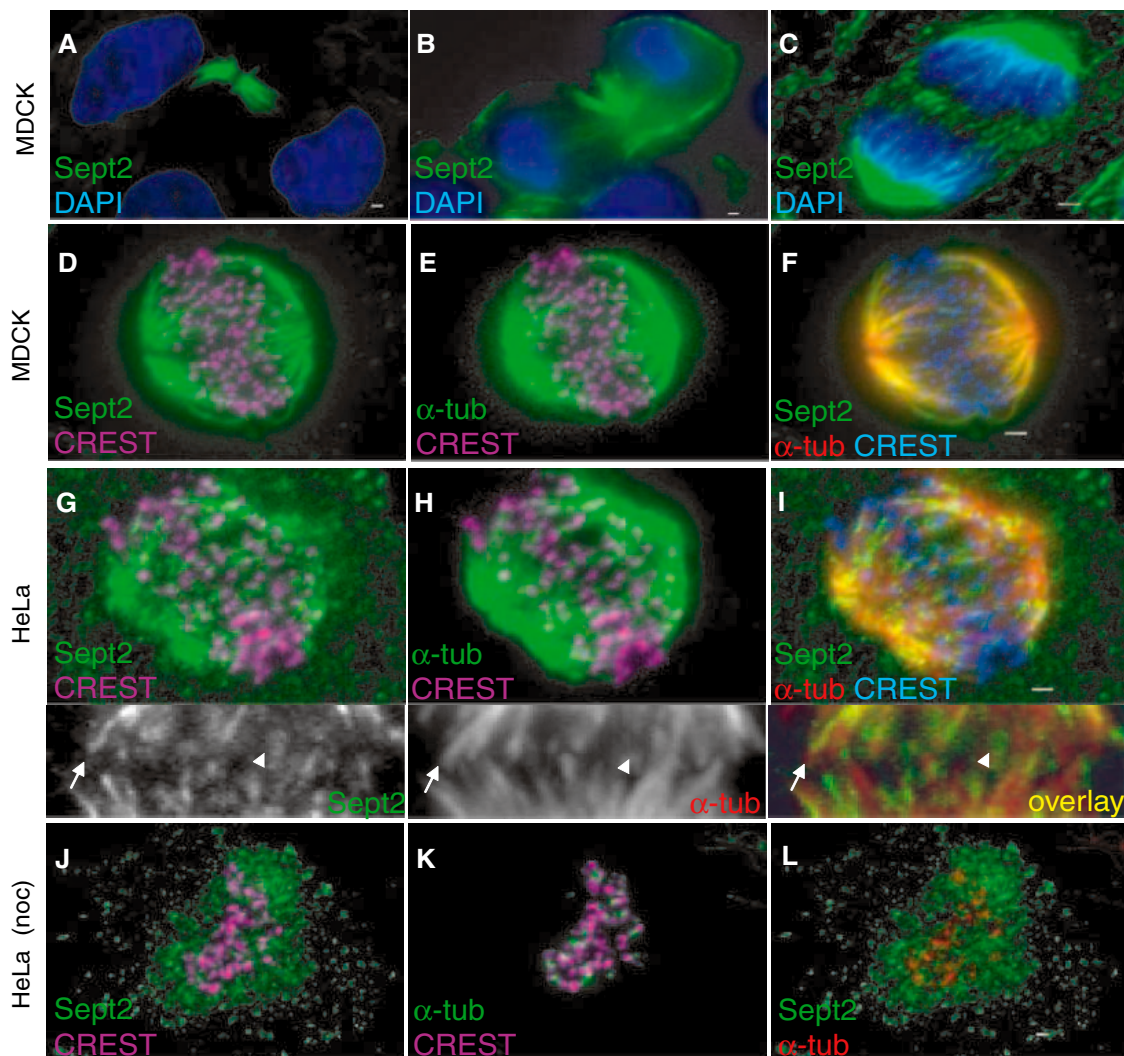
To probe for septin function during mitosis, we used RNA interference (RNAi) to deplete septins. High amounts of septin depletion over long periods have pleiotropic effects on microtubule and actin cytoskeleton organization (15, 16). To avoid cell death and the cumulative effects of chronic septin depletion (14), we transfected cells with Sept2 small interfering RNAs (siRNAs) for 18 to 48 hours, yielding a 10 to 65% reduction in Sept2 expression in the cell population whereas  $\alpha$ -tubulin expression was unaffected (Fig. 2A). Reduction of Sept6 and Sept7 also occurred upon Sept2 knockdown (16).

After 18 hours, the percentage of mitotic cells in Sept2 siRNA-treated cells was higher than in the control (14% versus 5%) (Fig. 2B). Half of Sept2 siRNA-treated cells accumulated in prometaphase (Fig. 2B), with some chromo-

somes aligned at the metaphase plate and some near the spindle poles (Fig. 2D). The same phenotype was observed in cells transfected with plasmid DNAs encoding hairpin siRNAs to Sept2 and Sept7 (fig. S3). In Sept2 siRNA-treated cells, Sept2 was depleted from the metaphase plate, and the nocodazole-resistant septin network was not detected (Fig. 2, D and E). The overall spindle length and bipolarity and formation of stable kinetochore microtubules remained unaffected (Fig. 2C and fig. S4). However, real-time imaging of histone B–green fluorescent protein (GFP)–labeled chromosomes showed failure in chromosome congression during early prometaphase (movie S1) (17) and loss of chromosome maintenance at the metaphase plate in later stages of prometaphase; chromosomes gradually dislocated from the metaphase plate and accumulated near the spindle poles (Fig. 2, F to H, and movies S2 and S3).

Treatment of cells with Sept2 siRNAs for 36 hours resulted in binucleate cells (14% versus 5% in controls) (Fig. 3, A to C). Because 18 hours earlier there was only a high

**Fig. 1.** (A to I) Fixed MDCK and HeLa cells stained (77) with Sept2, Sept6,  $\alpha$ -tubulin, CREST (kinetochores) antibodies and 4',6'-diamidino-2-phenylindole (DAPI) (nuclei). Insets show magnified images of the metaphase plate. Arrows indicate Sept2 filaments coaligning with kinetochore microtubules; arrowheads, tubulin-free Sept2 structures. (J to L) Cells treated with 35  $\mu$ M nocodazole (noc) for 20 min at room temperature. Scale bars indicate  $\sim$ 1  $\mu$ m.



percentage of prometaphase cells with no difference in the percentage of binucleate cells (5% versus 5%) (Fig. 3C), we reasoned that chronically arrested prometaphase cells had

exited mitosis and progressed straight to binucleate cells. Indeed, misaligned HisB-GFP-tagged chromosomes decondensed into two attached nuclei (Fig. 3D). Nuclear enve-

lope formation (Fig. 3A) and kinetochore distribution into two, albeit attached to each other, nuclear masses (fig. S5, J to L) indicated that these cells had entered anaphase. However, chromosome segregation remained incomplete because of lack of spindle elongation (Fig. 3, E and F); the spindle apparatus maintained the same length for at least twice as long as control cells before forming an interphase-like network (Fig. 3G). This abnormal transition in microtubule morphology was accompanied by defective cytokinesis (cleavage furrow regression) (movie S6). Cytokinetic defects have been seen in septin-depleted cells (13–15), but our data identify an earlier defect involving chromosome congression and segregation.

In yeast, septins are required for the maintenance of several proteins at the site of cell cleavage (4). To examine whether mammalian septins have a similar function within the mitotic spindle apparatus, we probed for the localization of CENP-E (centromere-associated protein E) and MCAK (mitotic centromere-associated kinesin) motor proteins. CENP-E, a protein without an apparent homolog in yeast, is a mitotic kinesin required for stable kinetochore binding to spindle microtubules (18–20). CENP-E deletion results in chromosome misalignment and loss of a sustainable mitotic checkpoint (20–22). Similarly, depletion of MCAK, a protein of the KinI family of microtubule depolymerases, leads to defects in chromosome congression and segregation (23, 24).

In Sept2 siRNA-treated prometaphase cells, the percentage of CENP-E-containing kinetochores was significantly reduced (23% ± 3% versus 45% ± 3%) (Fig. 4, A and E), and large CENP-E aggregates were often observed near the spindle poles (Fig. 4A). In contrast, no significant change in MCAK-containing kinetochores was observed (39% ± 3% versus 41% ± 3%) (Fig. 4, B and E). To test whether septins are required for CENP-E localization in the absence of microtubule-kinetochore attachments, we incubated mock and Sept2 siRNA-treated cells with nocodazole for 2 hours (Fig. 4D). In siRNA-treated cells, large CENP-E aggregates overlapped with a few kinetochores (20% ± 5%) (Fig. 4, D and E), whereas in mock-treated cells, where the septin network remained intact, CENP-E was enriched on many individual kinetochores (51% ± 4%) (Fig. 4, D and E). Thus, septins are required for proper CENP-E localization at kinetochores in the absence of microtubule-kinetochore attachments.

Septins may thus be required at the metaphase plate for CENP-E maintenance at the kinetochore ends of disassembling microtubules during chromosome congression. Indeed, loss of CENP-E from kinetochores resulted in chromosome dislocation from the metaphase plate and in a high number of mono-oriented, unattached chromosomes (Fig. 2, F to H). In addition, an increased number of kinetochores contained the mitotic checkpoint protein Mad2

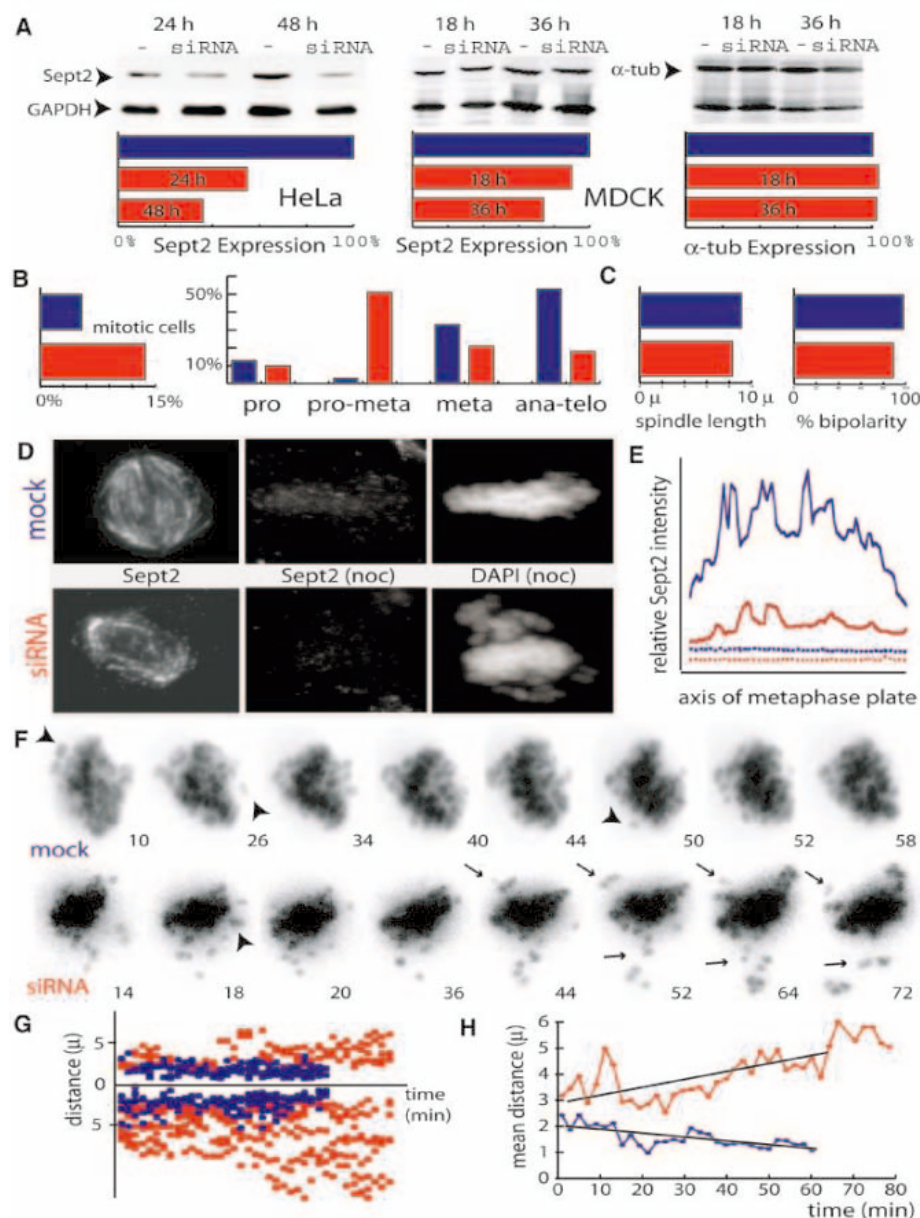


**Fig. 2.** (A) HeLa and MDCK cells treated with mock (blue) and Sept2 siRNAs (red). Cell extracts were immunoblotted with  $\alpha$ -tubulin, Sept2, and glyceraldehyde-3-phosphate dehydrogenase (GAPDH, loading control) antibodies. Histograms show percent change in protein expression after normalization to 100% for the control. (B) Percentage of mitotic MDCK cells from mock ( $n = 1409$ ) and Sept2 siRNA-treated ( $n = 1124$ ) samples and percentage of prophase, prometaphase, metaphase, and anaphase/telophase cells within their respective mitotic populations. (C) Mean distance between the two  $\gamma$ -tubulin-labeled spindle poles of metaphase (mock,  $n = 36$ ) and prometaphase (Sept2 siRNA,  $n = 49$ ) MDCK cells and percentage of cells (mock,  $n = 83$ ; Sept2 siRNA,  $n = 83$ ) with a bipolar spindle. (D and E) Untreated and nocodazole-treated MDCK cells stained with Sept2 antibodies and DAPI. Sept2 fluorescence intensities were measured along the axis of the metaphase plate of untreated mock (solid blue) and Sept2 siRNA (solid red) cells. Dotted lines represent background fluorescence in the respective cells. Mean relative fluorescence intensity was  $69 \pm 10$  in mock ( $n = 19$ ) and  $34 \pm 9$  in Sept2 siRNA ( $n = 12$ ) cells. (F) MDCK cells transfected with His2B-GFP and mock/Sept2 siRNAs for 20 hours and imaged every 2 min. Arrows, mono-oriented chromosomes dislocated from the metaphase plate; arrowheads, mono-oriented chromosomes that move toward the metaphase plate. (G and H) The distance of individual HisB-GFP spots was measured from the long axis of the metaphase plate and plotted as a function of time, and mean distances were calculated and plotted versus time.

[46% ± 4% compared with 36% ± 3% (Fig. 4, C and E)], which accumulates on unattached kinetochores (25).

In CENP-E-depleted cells where recruitment of CENP-E is affected, chromosomes did not dislocate from the metaphase plate (fig. S6) (26). Moreover, when both septins and CENP-E were depleted by siRNA, an additive phenotype was observed (fig. S7). Thus, septin depletion appears to affect not only maintenance of CENP-E localization but also some of the redundant mechanisms responsible for partial chromosome congression in the absence of CENP-E (26).

We suggest that mammalian septins form a novel scaffold at the midplane of the mitotic spindle that coordinates several key steps in mammalian mitosis. First, at metaphase, the septin scaffold is required to maintain CENP-E at kinetochores and consequently chromosome congression. Second, the septin scaffold may be involved indirectly in the timing of chromosome segregation, because maintenance of CENP-E localization at kinetochores is critical for activation of the mitotic checkpoint. Third, during anaphase, the septin scaffold remains within the central spindle, where it is required for chromosome segregation and spindle elongation. Indeed, CENP-E also redistributes to the central spindle of anaphase cells (18), and in septin-depleted cells, chromosomal passenger proteins failed to redistribute to the central spindle or the midbody (fig. S5). Thus, the septin scaffold may be involved in integrating molecular information necessary to coordinate chromosome congression and segregation with positioning and activation of the division plane and the site of cytokinesis.

These functions of mammalian septins are similar to those of yeast septins, which are required for proper positioning of the spindle apparatus (27), spatial coordination of cytokinesis (11), and proper activation of the mitotic exit network (9). Hence, septin functions may have been conserved during transition from a closed (yeast) to open (mammals) mitosis by adapting roles within the mitotic spindle apparatus. Septin abnormalities have been found in human tumors (28). Disruption of septin function in different stages of mitosis could potentially lead to chromosome instability and changes in ploidy common to cancers.

References and Notes

1. J. M. Scholey, I. Brust-Mascher, A. Mogilner, *Nature* **422**, 746 (2003).  
 2. D. W. Cleveland, Y. Mao, K. F. Sullivan, *Cell* **112**, 407 (2003).  
 3. M. S. Longtine et al., *Curr. Opin. Cell Biol.* **8**, 106 (1996).  
 4. A. S. Gladfelter, J. R. Pringle, D. Lew, *Curr. Opin. Microbiol.* **4**, 681 (2001).  
 5. M. S. Longtine, E. Bi, *Trends Cell Biol.* **13**, 403 (2003).  
 6. C. W. Carroll, R. Altman, D. Shieltz, J. R. Yates III, D. Kellogg, *J. Cell Biol.* **143**, 709 (1998).  
 7. Y. Barral, M. Parra, S. Bidlingmaier, M. Snyder, *Genes Dev.* **13**, 176 (1999).  
 8. M. S. Longtine et al., *Mol. Cell Biol.* **20**, 4049 (2000).  
 9. G. A. Castillon et al., *Curr. Biol.* **13**, 654 (2003).

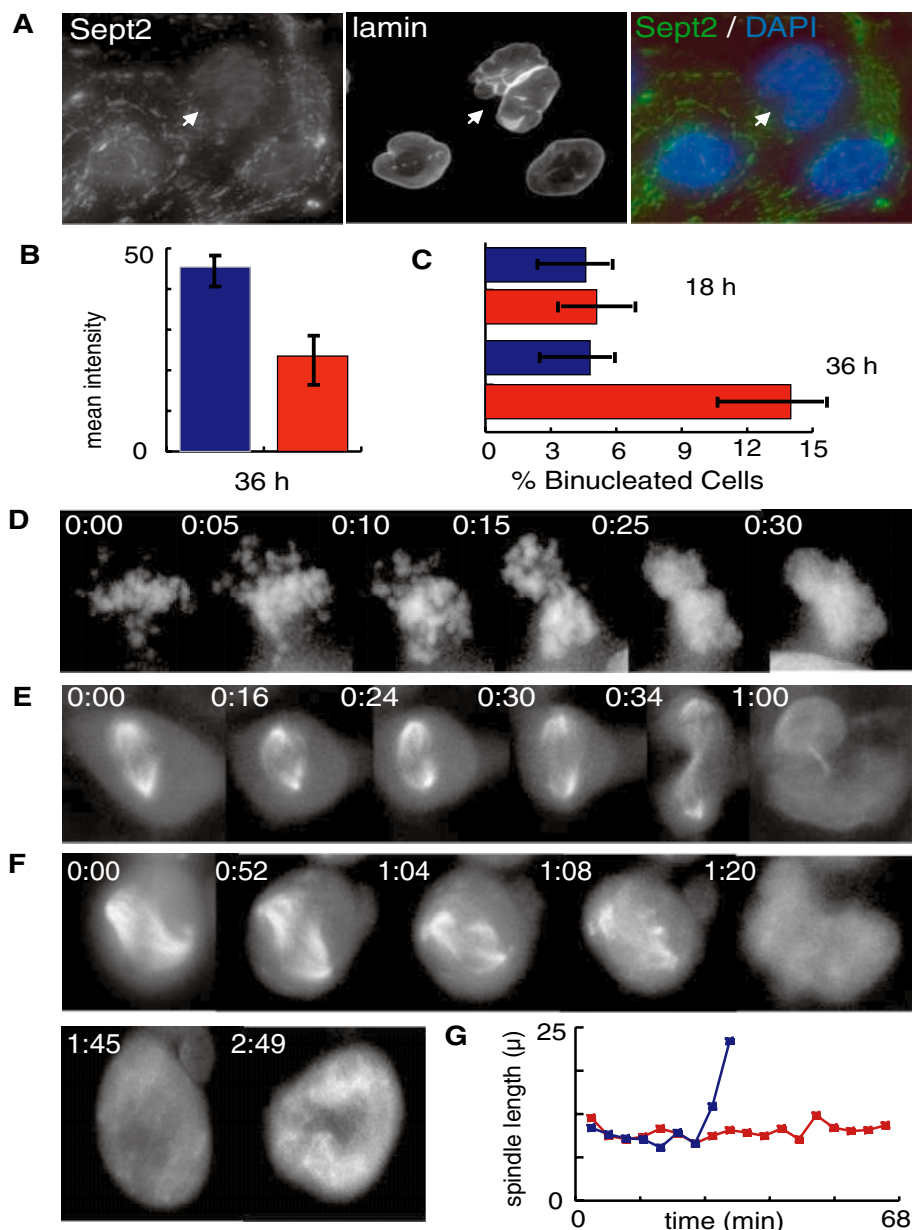


**Fig. 3.** (A) MDCK cells transfected with Sept2 siRNAs for 36 hours and stained with Sept2 and lamin A/C antibodies. Arrows, Sept2-depleted cell with two attached nuclei. (B and C) Histograms show mean Sept2 fluorescence intensities in cells with one (blue,  $n = 32$ ) and two (red,  $n = 13$ ) attached nuclei and the percentage of binucleate cells within a random population of cells ( $n = 500$ ) treated with mock (blue) and Sept2 (red) siRNAs. (D) MDCK cells transfected with His2B-GFP and Sept2 siRNAs and imaged every 5 min. (E to G) MDCK- $\alpha$ -tub-GFP cells transfected with mock (E) and Sept2 siRNAs (F) for 20 hours and imaged every 4 min. Spindle pole distances were measured for each time point and plotted as a function of time (movies S1 to S6).

10. J. Lippincott, R. Li, *J. Cell Biol.* **140**, 355 (1998).  
 11. J. Dobbelaere, Y. Barral, *Science* **305**, 393 (2004).  
 12. M. Kinoshita, *Genome Biol.* **4**, 236 (2003).  
 13. M. Kinoshita et al., *Genes Dev.* **11**, 1535 (1997).  
 14. M. C. Surka, C. W. Tsang, W. S. Trimble, *Mol. Biol. Cell* **13**, 3532 (2002).  
 15. K. Nagata et al., *J. Biol. Chem.* **278**, 18538 (2003).  
 16. M. Kinoshita, C. M. Field, M. L. Coughlin, A. F. Straight, T. J. Mitchison, *Dev. Cell* **3**, 791 (2002).  
 17. Materials and methods are available as supporting material on Science Online.  
 18. T. J. Yen, G. Li, B. T. Schaar, I. Szilak, D. W. Cleveland, *Nature* **359**, 536 (1992).  
 19. X. Yao, K. L. Anderson, D. W. Cleveland, *J. Cell Biol.* **139**, 435 (1997).  
 20. F. R. Putkey et al., *Dev. Cell* **3**, 351 (2002).  
 21. B. A. Weaver et al., *J. Cell Biol.* **162**, 551 (2003).  
 22. Y. Mao, A. Abrieu, D. W. Cleveland, *Cell* **114**, 87 (2003).  
 23. T. Maney, A. W. Hunter, M. Wagenbach, L. Wordeman, *J. Cell Biol.* **142**, 787 (1998).  
 24. S. L. Kline-Smith, A. Khodjakov, P. Hergert, C. E. Walczak, *Mol. Biol. Cell* **15**, 1146 (2004).  
 25. R. H. Chen, J. C. Waters, E. D. Salmon, A. W. Murray, *Science* **274**, 242 (1996).  
 26. B. F. McEwen et al., *Mol. Biol. Cell* **12**, 2776 (2001).  
 27. J. Kusch, A. Meyer, M. P. Snyder, Y. Barral, *Genes Dev.* **16**, 1627 (2002).  
 28. P. A. Hall, S. E. Russell, *J. Pathol.* **204**, 489 (2004).  
 29. We thank V. Varenika, S. Bahmanyar, and S. Yamada for technical help and W. Brinkley, G. Fang, A. Hoyt, E. Salmon, B. Schaar, C. Walczak, L. Wordeman, J.

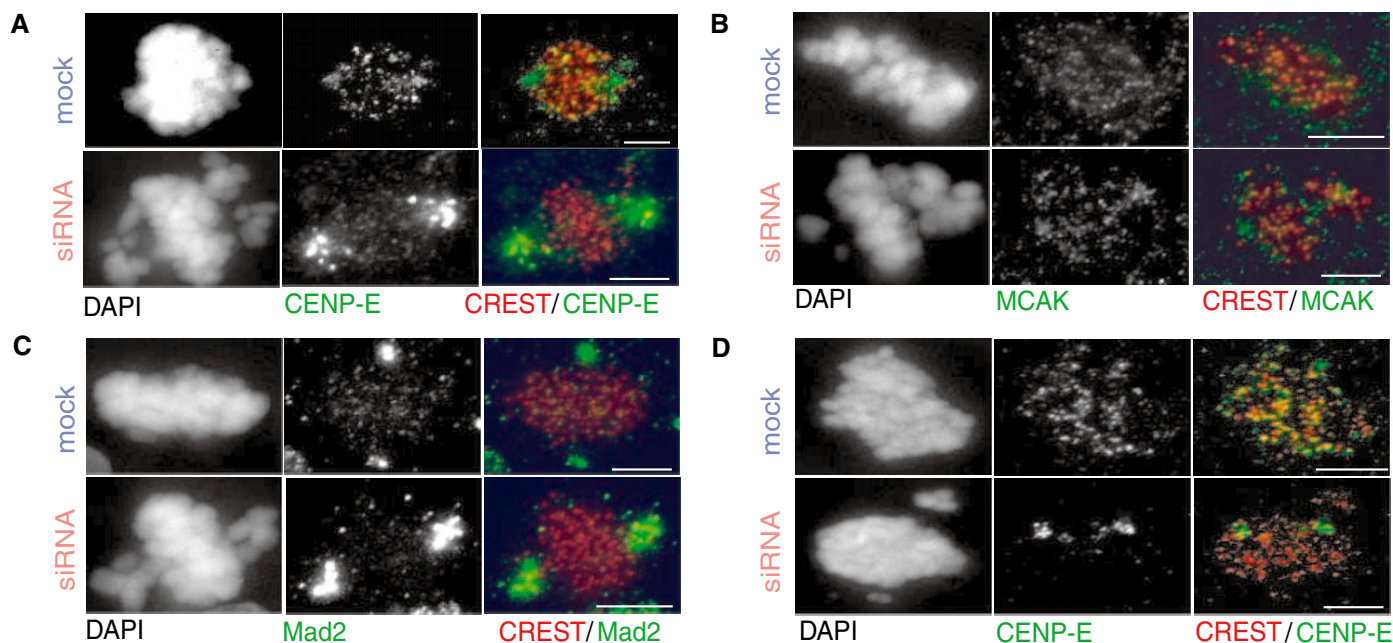
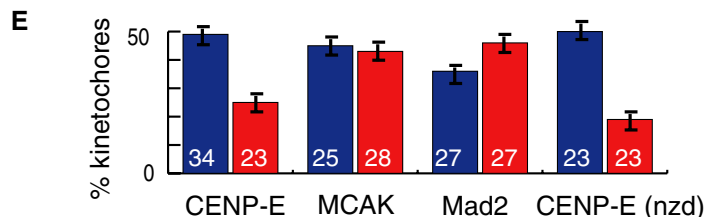


**Fig. 4.** MDCK cells transfected with mock (blue) and Sept2 siRNAs (red) for 18 hours. Scale bars,  $\sim 5 \mu\text{m}$ . (A to C) Cells were stained with DAPI and CREST, CENP-E, MCAK, and Mad2 antibodies. (D) Cells were incubated with  $35 \mu\text{M}$  nocodazole (nzd) for 2 hours at  $37^\circ\text{C}$ . (E) Percentages of CENP-E-, MCAK-, and Mad2-positive kinetochores per cell. An average of 110 kinetochores were counted per cell (17); the number of cells counted is shown within each bar. Error bars represent the 95% confidence interval of the mean value according to the unpaired Student's *t* test.



Wong, and T. Yen for helpful advice and reagents. Supported by NIH grant GM35527 (W.J.N.) and by a research grant PRESTO from Japan Science and Technology Agency (M.K.). E.S. is a Jane Coffin Childs Memorial Fund postdoctoral fellow.

**Supporting Online Material**  
www.sciencemag.org/cgi/content/full/307/5716/1781/DC1  
Materials and Methods  
Figs. S1 to S7

References  
Movies S1 to S6

27 October 2004; accepted 26 January 2005  
10.1126/science.1106823

## Extrusion and Death of DPP/BMP-Compromised Epithelial Cells in the Developing *Drosophila* Wing

Matthew C. Gibson and Norbert Perrimon\*

During animal development, epithelial cell fates are specified according to spatial position by extracellular signaling pathways. Among these, the transforming growth factor  $\beta$ /bone morphogenetic protein (TGF- $\beta$ /BMP) pathways are evolutionarily conserved and play crucial roles in the development and homeostasis of a wide range of multicellular tissues. Here we show that in the developing *Drosophila* wing imaginal epithelium, cell clones deprived of the BMP-like ligand Decapentaplegic (DPP) do not die as previously thought but rather extrude from the cell layer as viable cysts exhibiting marked abnormalities in cell shape and cytoskeletal organization. We propose that in addition to assigning cell fates, a crucial developmental function of DPP/BMP signaling is the position-specific control of epithelial architecture.

The *Drosophila* wing primordium (imaginal disc) is a cellular monolayer that has invaginated and flattened to form a two-sided epithelial sac. During larval development, one side of this sac forms a thin squamous sheet,

whereas the apposed epithelial surface adopts a pseudostratified columnar morphology (1, 2). Although such range in epithelial form is common among metazoans and central to the morphogenesis of complex organ and appendage

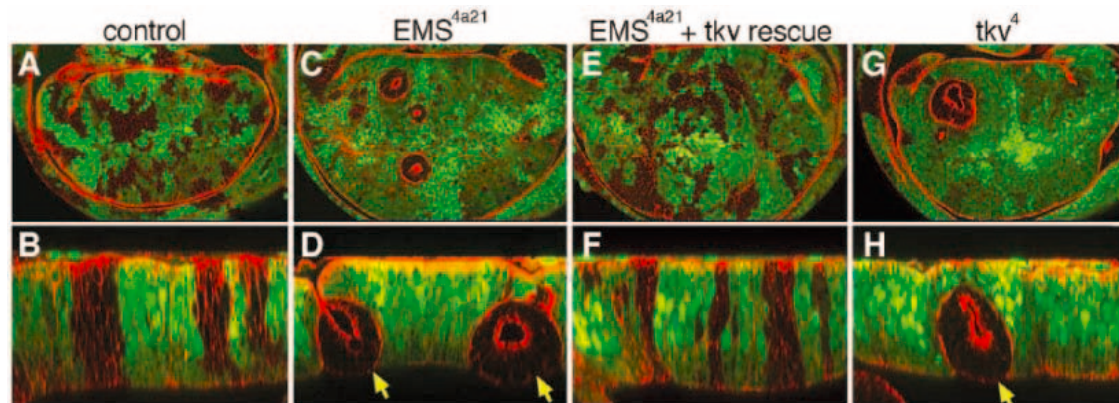
structures, very little is known about the molecular mechanisms that drive epithelia into their distinctive squamous, cuboidal, and columnar morphologies. To address this issue, we initiated a genetic screen for factors that control epithelial cell shape during *Drosophila* imaginal disc development.

To circumvent the embryonic lethality associated with many mutant alleles, we used the directed mosaic FLP/FRT system (3) to screen somatic cell clones homozygous for a collection of ethylmethane sulfonate (EMS)-induced lethal mutations. This approach uses a tissue-specific Gal4 driver (*T155-Gal4*) to direct expression of the *flipase* (*flp*) enzyme in developing epithelia, thus catalyzing a low frequency of mitotic recombination between an EMS-mutagenized FRT chromatid and its green fluorescent protein (GFP)-marked homolog. Within the disc epithelium, mitotic re-

Department of Genetics and Howard Hughes Medical Institute, Harvard Medical School, Boston, MA 02115, USA.

\*To whom correspondence should be addressed.  
E-mail: perrimon@receptor.med.harvard.edu

**Fig. 1.** Extrusion of *tkv* mutant clones from the wing disc. Clones lacking GFP (green) were stained for F-actin (ACT, red) to delineate cell outlines. Upper panels are standard confocal XY sections; the lower panels are XZ optical cross sections. Individual channel images of ACT and GFP are available in fig. S1. (A and B) Control clones lacking GFP expression. Note that GFP-negative cells integrate normally into the epithelial layer. (C) *EMS*<sup>4a21</sup> mutant clones change shape and segregate from control cells, disrupting the continuity of the epithelial layer. Also note the reduced number of GFP-negative clones [compare (C) with (A)], indicative of intermittent clone cell death. (D) In XZ sections, *EMS*<sup>4a21</sup> homozygous clones extrude basally as inverted epithelial



cysts (yellow arrows). (E and F) Confirming *EMS*<sup>4a21</sup> as an allele of *tkv*, *EMS*<sup>4a21</sup> clone lethality and extrusion are rescued by expression of *UAS-tkv*. (G and H) *T155>flp*-induced *tkv*<sup>4</sup> clones also extrude from the wing epithelium (yellow arrow), indicating that this phenotype is not allele specific.

combination events produce a GFP-negative cell clone homozygous for the mutation of interest as well as a corresponding “twin spot” identifiable by the presence of two copies of GFP. In this study, GFP-negative clones homozygous for a random series of EMS mutations were induced with *T155-Gal4>UAS-flp* (*T155>flp*) and stained with rhodamine-phalloidin to outline cell boundaries. Late third-instar wing imaginal discs were subsequently analyzed for clonal defects in epithelial morphogenesis (Fig. 1, A and B).

In the experimental line *EMS*<sup>4a21</sup>, mutant clones in medial regions of the wing disc exhibited defects in the ability to establish or maintain the pseudostratified columnar cell shape, resulting in their retraction from the apical epithelial surface and subsequent basal extrusion (Fig. 1, C and D). Counts of clone frequency relative to twin spot controls indicated that many clones induced in the presumptive medial blade territory were not recovered, presumably as a result of cell death, but those that we did observe consistently presented as cystlike epithelial extrusions. In addition, a large number of extruding clones were observed in the presumptive hinge and notum regions of experimental discs, with a fraction of these protruding apically rather than extruding basally (4). We conclude that loss of the *EMS*<sup>4a21</sup> gene product caused defective morphogenesis and clone extrusion, a phenotype intermittently associated with cell death in the medial wing blade territory.

To determine the genetic defect underlying extrusion, we mapped the embryonic lethality of *EMS*<sup>4a21</sup> to cytological interval 25D-25F, which includes the transforming growth factor  $\beta$  (TGF- $\beta$ ) type I receptor *thickveins* (*tkv*) (5). As a transmembrane receptor for DPP/BMP ligand, TKV is crucial for imaginal disc development (6–13) and other developmental processes such as adult thorax closure and embryonic dorsal closure (14, 15). Consistent with *EMS*<sup>4a21</sup> representing an allele of *tkv*, *EMS*<sup>4a21</sup> homozygotes exhibited embryonic

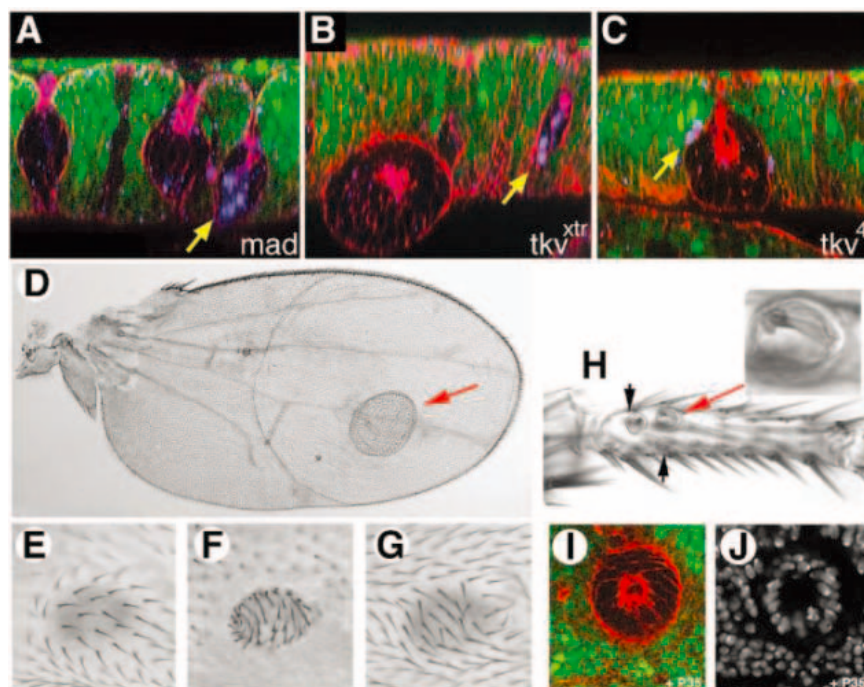


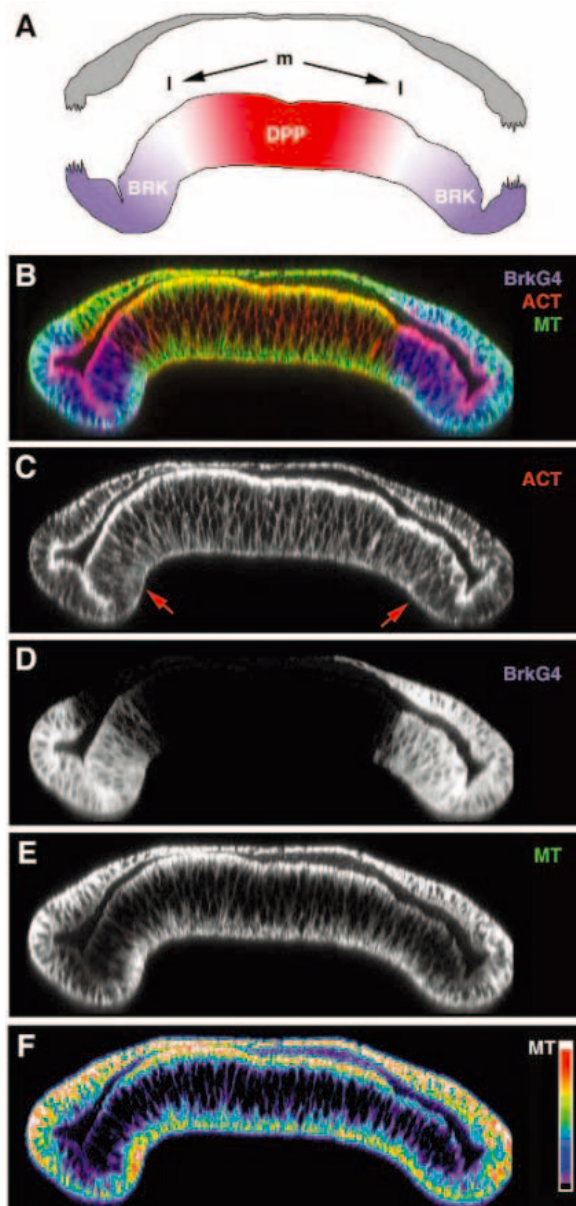
**Fig. 2.** Extrusion is independent of cell death. (A to C) Cleaved Caspase-3 staining (blue; CS3) does not correlate with (A) *mad*<sup>12</sup>, (B) *tkv*<sup>xtr</sup>, and (C) *tkv*<sup>4</sup> clones marked by loss of GFP (green) and stained with phalloidin (red; ACT). Although some CS3-positive cells are indeed present (yellow arrows), many extruding clones show no evidence of cell death. (D) Adult wing containing a large *tkv*<sup>xtr</sup> clone (red arrow). (E to G) Extruded cuticular vesicle (F) lodged between the dorsal (E) and ventral (G) wing surfaces. (H) *tkv*<sup>xtr</sup> extrusions in the adult leg (arrows). The vesicle indicated by a red arrow contains a sensory bristle (inset), consistent with a high level of cellular functioning in extruded clones. (I) Extrusion of clones from the wing disc is not rescued by blocking apoptosis with *T155-Gal4>UAS-p35*. (J) DNA stain (DAPI; 4',6'-diamidino-2-phenylindole) confirms normal nuclear morphology within the extruded clone shown in (I).

lethal phenotypes reminiscent of known *tkv* mutations (16), and *EMS*<sup>4a21</sup> failed to complement the previously identified alleles *tkv*<sup>7</sup> (*n* = 413), *tkv*<sup>4</sup> (*n* = 386), and *tkv*<sup>K16159</sup> (*n* = 319) (5). Confirming *EMS*<sup>4a21</sup> as a *tkv* allele, a *UAS-tkv* construct expressed globally under *tubulin-Gal4* rescued *EMS*<sup>4a21</sup> homozygotes to adult eclosion (4). More importantly, expression of *UAS-tkv* under *T155-Gal4* fully rescued *EMS*<sup>4a21</sup> clone extrusion (Fig. 1, E and

F), as did clone-autonomous expression of *UAS-tkv* using the MARCM system (fig. S2). These experiments demonstrate that clone extrusion was caused by loss of *tkv*, and we have therefore designated *EMS*<sup>4a21</sup> as *tkv*<sup>extruded</sup> (*tkv*<sup>xtr</sup>).

We next used *T155Gal4>flp* to induce clones of the amorphic allele *tkv*<sup>4</sup> (5) as well as an allele of the downstream signal transducer encoded by *mothers against DPP* (*mad*<sup>12</sup>)

**Fig. 3.** A gradient of epithelial architecture spans the wing disc. (A) DPP represses *brk* throughout medial (m) wing disc cells. (B to E) *brk-Gal4>UAS-srcEGFP* (blue) disc stained for F-actin (ACT, red) and microtubules (MT, green). (B) The overlap between apical MTs and ACT appears as an apical yellow band that terminates in *brk*<sup>+</sup> cells owing to the absence of apical microtubules. (C) Apical ACT is consistent along the medial-to-lateral axis, but ACT association with the basolateral cortex weakens laterally (red arrows). (D) *brk-Gal4>srcEGFP* demarcates the lateral domains where DPP signaling is low. (E) Apical microtubule densities are robust in medial columnar cells where DPP/BMP signal is high but weaken in lateral *brk* domains. (F) Pixel intensity plot of (E) illustrates an apical-specific gradient in microtubule intensity, because basal MT staining is consistent along the medial-lateral axis.



(5). In both cases, extrusion was routinely observed (Fig. 1, G and H, and Fig. 2A), linking this phenotype to general defects in DPP/BMP signaling and not some unique effect of the *tkv*<sup>xtr</sup> allele. These results contrast with the current interpretation of DPP/BMP as a cell survival factor, which is based on the observation that *tkv* mutant cells are eliminated from the wing by proapoptotic c-Jun N-terminal kinase (JNK) signaling (17–20). We thus considered whether extrusion might reflect a preliminary stage of apoptosis, similar to the basal extrusion of vertebrate epithelial cells destined for death (21). However, four observations provide evidence against this idea. (i) Clonal loss of *mad12*, *tkv*<sup>xtr</sup>, or *tkv4* consistently caused extrusion, but this phenotype did not necessarily correlate with apoptosis indicated by Caspase-3 activation (Fig. 2, A to C). (ii) Extruded *tkv*<sup>xtr</sup> and *tkv4* clones

often grew to an appreciable size (Fig. 1, D and H, and Fig. 2B) and contained mitotic figures (fig. S3), which is inconsistent with their active engagement in an apoptotic pathway. (iii) Many extruded clones survived metamorphosis and differentiated inverted cuticular vesicles lodged between the dorsal and ventral surfaces of the adult wing or leg (Fig. 2, D to H), demonstrating that *tkv* loss can disrupt epithelial organization without compromising cell viability. (iv) Extrusion was unaffected by ectopic expression of the apoptosis inhibitor p35 (Fig. 2, I and J), confirming that this phenotype is not simply a secondary consequence of cell death.

Together, these results challenge the view of DPP/BMP as a survival factor, favoring instead a more direct role for this pathway in controlling epithelial morphogenesis. This interpretation has the advantage of unifying the

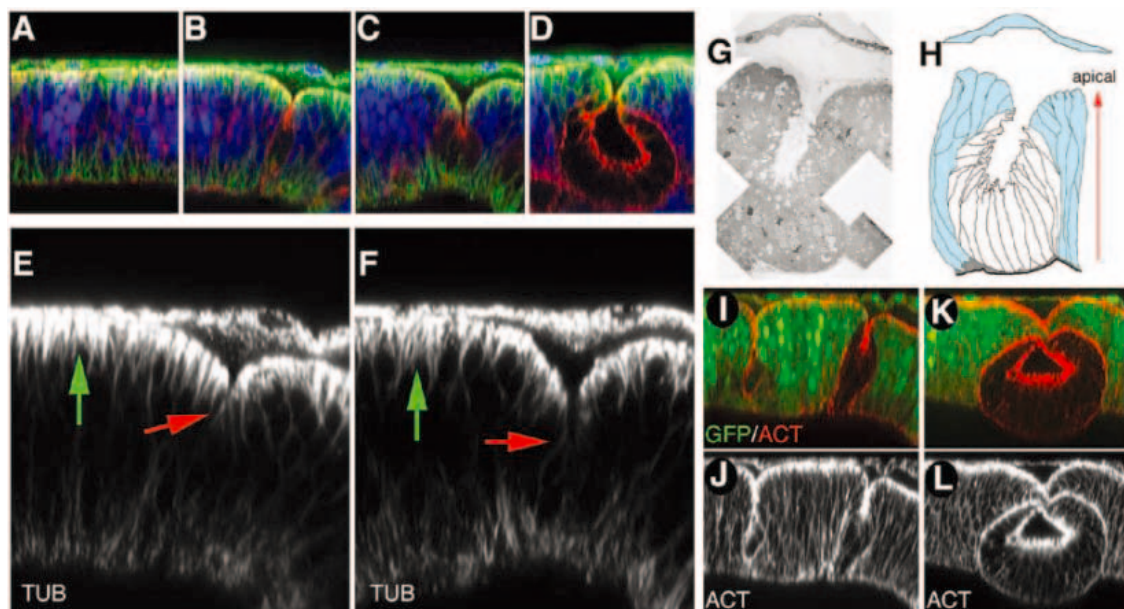
role of DPP/BMP as a pattern morphogen in imaginal discs with its role as an agent of morphogenesis in other developmental contexts. Nevertheless, the large phenotypic discrepancy between clone extrusion and clone death necessitated a closer consideration of why our results differed from previous reports. A major procedural difference in our experiments was the use of *T155>flp* to induce clones, instead of heat shock (*hs>flp*). Indeed, we confirmed that almost all heat shock-induced *tkv4* and *tkv*<sup>xtr</sup> clones were eliminated from the developing wing blade, as previously reported (4, 12). This indicates that either the *hs>flp* method enhanced *tkv* clone death, or alternatively, the *T155>flp* method somehow enhanced clone viability. Both of these possibilities could be explained by differential background activity of the JNK stress signaling pathway, because decreasing JNK activity is sufficient to rescue the lethality of some *hs>flp*-induced *tkv* clones (19). Conversely, when we used a single mutant allele of the regulatory phosphatase *puckered* to increase background JNK activity (18), *T155>flp*-induced *tkv*<sup>xtr</sup> clones were completely eliminated from the wing blade territory and extruding clones larger than 10 cells were not observed (fig. S4) ( $n = 15$  discs). This contrasts sharply with normal circumstances, where 78% of discs had one large *tkv*<sup>xtr</sup> extrusion greater than 10 cells in the wing blade and 50% had 2 or more ( $n = 32$  discs).

Based on the observations above, we infer that the primary phenotype of *tkv* clones is extrusion and propose that JNK-dependent cell death is a potent and confounding secondary effect, similar to a wound response. Current models suggest that *tkv* clone-dependent JNK activation is triggered by a morphogen-sensing mechanism designed to correct discontinuities in the total DPP/BMP gradient (19, 22). Our results suggest an alternative possibility: that the disruptive force of extrusion itself causes sufficient mechanical stress to activate JNK within and around *tkv* mutant cells (fig. S2C). Mechanical stretch, for example, activates JNK signaling in vertebrate cells (23), and mechanical disruption of the larval or adult epidermis causes localized JNK activation in *Drosophila* (24, 25). Extending these observations to the wing disc, we used a finely sharpened tungsten needle to stretch, then pierce the imaginal epithelium, mimicking the effect of extrusion. This manipulation elicited localized JNK reporter activity similar to that seen in wounded larval and adult epidermis (24, 25) and identical to that seen around *tkv* mutant clones (fig. S4).

Having concluded that the primary defect in *tkv* clones is extrusion and not death, we turned our attention to identifying position-specific aspects of epithelial morphogenesis that could be controlled by DPP/BMP signaling. During normal development, secreted



**Fig. 4.** Defective morphogenesis in extruding clones. (A to D) *tkv<sup>xtr</sup>* clones lacking GFP (blue) and stained for F-actin (ACT, red), and microtubules (TUB, green). (A) In the absence of mutant clones, pseudostratified wing columnar cells feature a highly regular apical surface; the overlap between ACT and TUB staining appears as a yellow band. (B to D) Extruding *tkv<sup>xtr</sup>* clones lose apical TUB, exposing red apical ACT. (E and F) Single-channel TUB staining from (B) and (C), respectively. Mutant cells (red arrows) autonomously lose the apical microtubule arrays present in neighboring control cells (green arrows). (G) Transmission electron microscopy sections confirm aberrant *tkv<sup>xtr</sup>* cell shape. (H) Interpretive tracing of (G). (I to L) *tkv<sup>4</sup>* clones show reduced basolateral cortical F-actin within the clone interior and ectopic F-actin accumulation at clone/nonclone boundaries.



DPP forms a medial-to-lateral gradient of signaling activity that antagonizes expression of the transcription factor encoded by *brinker* (*brk*) (Fig. 3A) (26). We made use of *brk-Gal4>UAS-srcEGFP* to mark the range of DPP/BMP signal and then examined cytoskeletal organization relative to the level of morphogen (Fig. 3, B to F). In confocal XZ sections through the wing disc, a gradation of columnar epithelial cell shape along the medial-lateral axis was immediately apparent, and this gradient of cell shape was further reflected in cytoskeletal organization. Although levels of F-actin localized to apical junctional complexes were fairly consistent across the disc, basolateral cortical F-actin levels were moderately reduced in lateral cells where DPP/BMP activity is low (Fig. 3C). Even more apparent, apical microtubule arrays were robust in medial cells where DPP/BMP is high, but tapered off to complete absence in the lateral *brk*-expressing domains (Fig. 3, D and E). Importantly, the density of basal microtubule arrays did not vary along the same axis, indicating that an apical-specific gradient of microtubule organization closely parallels the DPP/BMP morphogen gradient (Fig. 3E).

To test whether apical microtubule arrays, basolateral cortical F-actin, and epithelial cell shape were dependent on DPP/BMP signaling activity, we analyzed *T155>flp*-induced clones in greater detail (Fig. 4). Notably, the apical microtubule arrays were cell-autonomously eliminated in *tkv* mutant clones, even as basal microtubule networks were unperturbed (Fig. 4, B to F). Both large (early-induced) and small (late-induced) clones exhibited this phenotype, establishing the disruption of apical microtubule organization as an early and

specific consequence of defective DPP/BMP signaling. Mutant cells also featured a subtle yet consistent reduction of F-actin at the basolateral cortex of cells on the clone interior, transient ectopic accumulation of F-actin at the apical adherens junctions, and ectopic accumulation of F-actin at boundaries between mutant cells and their wild-type neighbors (Fig. 4, I to L). Ultrastructurally, these phenotypes correlated with a clone-autonomous transition from pseudostratification to a simple columnar epithelial modality (Fig. 4, G and H). We conclude that the DPP/BMP morphogen gradient both correlates with and is required for a parallel gradient of epithelial organization in the developing wing columnar epithelium.

The data summarized here provide an initial conceptual link between DPP/BMP-dependent wing patterning and the spatial regulation of epithelial morphogenesis. A logical next step will be to connect transcriptional targets of the DPP/BMP pathway to candidate effectors of morphogenesis, particularly molecules that could influence the integrity of the apical microtubule cytoskeleton or cortical F-actin meshwork. Although our results could support a direct cytoskeletal function for DPP/BMP in the wing disc [perhaps similar to its proposed role in dorsal closure and thorax closure (14, 15)], it is equally possible that DPP/BMP signaling drives epithelial morphogenesis by modulating cell adhesion. In this sense, the cell-autonomous disruption of apical microtubule arrays in *tkv* clones may be a result of abnormal apical cell-cell or cell-matrix adhesion. Consistent with this possibility, clonal loss of a chromosomal interval covering the DPP target *spalt* causes aberrant expression

of the leucine-rich repeat cell-adhesion proteins *capricious* and *tartan* and segregation of mutant cells away from the epithelium (20). Furthermore, we found that hyperactivated DPP signaling caused defective epithelial organization in lateral wing disc cells but was not alone sufficient to induce apical microtubule arrays (4). Clearly, the ability to distinguish adhesive versus cytoskeletal roles for DPP/BMP will require further study of downstream effectors during multiple developmental processes.

The extrusion of *tkv* clones from *Drosophila* epithelia presents an interesting parallel to juvenile polyposis, a human genetic disorder characterized by the formation of gastrointestinal polyps and cancer (27–30). Not only does the formation of extruded epithelial polyps bear some superficial similarity to the phenotypes described here, but heritable juvenile polyposis has been linked to mutations in two loci: a type I BMP receptor (27) and the SMAD4 signal transducer (28). In this regard, the present study not only demonstrates a morphogenetic function for DPP/BMP in the *Drosophila* wing but may also indicate a broadly conserved role for DPP/BMP signaling in the patterned morphogenesis of developing and adult epithelia.

#### References and Notes

1. S. M. Cohen, in *The Development of Drosophila melanogaster*, M. Bate, A. Martinez Arias, Eds. (Cold Spring Harbor Laboratory, Cold Spring Harbor, NY, 1993), vol. 2, pp. 747–841.
2. C. Auerbach, *Trans. R. Soc. Edinb.* **58**, 787 (1936).
3. J. B. Duffy, D. A. Harrison, N. Perrimon, *Development* **125**, 2263 (1998).
4. M. C. Gibson, N. Perrimon, data not shown.
5. The FlyBase Consortium, *Nucleic Acids Res.* **31**, 172 (2003).
6. A. Penton et al., *Cell* **78**, 239 (1994).
7. D. Nellen, M. Affolter, K. Basler, *Cell* **78**, 225 (1994).

8. T. J. Brummel *et al.*, *Cell* **78**, 251 (1994).
9. E. Ruberte, T. Marty, D. Nellen, M. Affolter, K. Basler, *Cell* **80**, 889 (1995).
10. D. Nellen, R. Burke, G. Struhl, K. Basler, *Cell* **85**, 357 (1996).
11. T. Lecuit *et al.*, *Nature* **381**, 387 (1996).
12. R. Burke, K. Basler, *Development* **122**, 2261 (1996).
13. M. A. Singer, A. Penton, V. Twombly, F. M. Hoffmann, W. M. Gelbart, *Development* **124**, 79 (1997).
14. E. Martin-Blanco, J. C. Pastor-Pareja, A. Garcia-Bellido, *Proc. Natl. Acad. Sci. U.S.A.* **97**, 7888 (2000).
15. M. G. Ricos, N. Harden, K. P. Sem, L. Lim, W. Chia, *J. Cell Sci.* **112**, 1225 (1999).
16. M. Affolter, D. Nellen, U. Nussbaumer, K. Basler, *Development* **120**, 3105 (1994).
17. E. Moreno, K. Basler, G. Morata, *Nature* **416**, 755 (2002).
18. T. Adachi-Yamada, K. Fujimura-Kamada, Y. Nishida, K. Matsumoto, *Nature* **400**, 166 (1999).
19. T. Adachi-Yamada, M. B. O'Connor, *Dev. Biol.* **251**, 74 (2002).
20. M. Milan, L. Perez, S. M. Cohen, *Dev. Cell* **2**, 797 (2002).
21. J. Rosenblatt, M. C. Raff, L. P. Cramer, *Curr. Biol.* **11**, 1847 (2001).
22. T. Adachi-Yamada, M. B. O'Connor, *J. Biochem. (Tokyo)* **136**, 13 (2004).
23. A. J. Ingram, L. James, H. Ly, K. Thai, J. W. Scholey, *Kidney Int.* **58**, 1431 (2000).
24. M. J. Gallo, M. A. Krasnow, *PLoS Biol.* **2**, E239 (2004).
25. M. Ramet, R. Lanot, D. Zachary, P. Manfrulli, *Dev. Biol.* **241**, 145 (2002).
26. G. Campbell, A. Tomlinson, *Cell* **96**, 553 (1999).
27. J. R. Howe *et al.*, *Nat. Genet.* **28**, 184 (2001).
28. J. R. Howe *et al.*, *Science* **280**, 1086 (1998).
29. A. P. Haramis *et al.*, *Science* **303**, 1684 (2004).
30. M. G. Sayed *et al.*, *Ann. Surg. Oncol.* **9**, 901 (2002).
31. We thank E. Benecchi for assistance with transmission electron microscopy; M. Schober and J. David Lambert

for critical readings of the manuscript; K. Gibson, S. Chery, and C. Micchelli for helpful discussions; and G. Campbell, T. Kornberg, L. Rafferty, K. Basler, R. Padgett, and the Bloomington *Drosophila* Stock Center for fly stocks. Our sincere apologies to colleagues whose work we were unable to cite owing to space constraints. N.P. is an Investigator of the Howard Hughes Medical Institute and M.C.G. is supported by the Jane Coffin Childs Memorial Fund for Cancer Research.

#### Supporting Online Material

[www.sciencemag.org/cgi/content/full/307/5716/1785/DC1](http://www.sciencemag.org/cgi/content/full/307/5716/1785/DC1)

Materials and Methods

Figs. S1 to S4

References and Notes

1 September 2004; accepted 11 January 2005

10.1126/science.1104751

## Extrusion of Cells with Inappropriate Dpp Signaling from *Drosophila* Wing Disc Epithelia

Jie Shen and Christian Dahmann\*

Decapentaplegic (Dpp) is a signaling molecule that controls growth and patterning of the developing *Drosophila* wing. Mutant cells lacking Dpp signal transduction have been shown to activate c-Jun amino-terminal kinase (JNK)-dependent apoptosis and to be lost from the wing disc epithelium. These observations have led to the hypothesis that Dpp promotes cell survival by preventing apoptosis. Here, we show that in the absence of JNK-dependent apoptosis, mutant cells lacking Dpp signal transduction can survive; however, they are still lost from the wing disc epithelium. This loss correlates with extensive cytoskeletal changes followed by basal epithelial extrusion. We propose that Dpp promotes cell survival within disc epithelia by affecting cytoskeletal organization.

Signaling by members of the transforming growth factor- $\beta$  (TGF- $\beta$ ) protein family is critical for epithelial growth and differentiation, and inappropriate signaling is common in cancer (1, 2). Dpp, a TGF- $\beta$  superfamily member related to bone morphogenetic protein (BMP) 2/4, is required for growth and patterning of the wing primordium (wing disc pouch) in *Drosophila* (3). Inappropriately reduced Dpp signaling leads to smaller wing size, activation of the JNK pathway, and apoptosis (4, 5). These and other observations have led to the hypothesis that Dpp acts as a survival factor for wing disc cells by preventing activation of the JNK-dependent apoptotic pathway (5–8).

To test this hypothesis, we analyzed the ability of cells mutant for the *Drosophila* gene *thickveins* (*tkv*), which encodes a receptor essential for Dpp signal transduction (3), and the gene *basket* (*bsk*), which encodes JNK (9), to survive within the developing wing disc

pouch. Marked “twinspots” composed of sibling double-mutant *tkv bsk* clones of cells and wild-type clones of cells were generated within the same wing disc by Flp-mediated mitotic recombination (10). The ratio of *tkv bsk* clones to sibling wild-type clones was determined and is referred to as the frequency of *tkv bsk* clone recovery. When clones were induced in first instar larvae, the frequency of *tkv bsk* clone recovery in the wing disc pouch of late-third instar larvae was only 24% ( $n = 187$ ), consistent with previous observations (6). Apoptosis was blocked in the mutant clones (fig. S1). *bsk* clones were recovered at high frequency (97%,  $n = 100$ ). The low frequency of *tkv bsk* clone recovery suggests that the loss of cells lacking Dpp signal transduction from the wing disc pouch is largely independent of JNK-mediated apoptosis (supporting online material text). Thus, Dpp must use additional mechanisms to prevent loss of cells from the wing disc pouch.

To elucidate these mechanisms, we generated *tkv bsk* clones in first instar larvae and analyzed their morphology in the wing disc pouch of late-third instar larvae. In the pseudostratified epithelium (Fig. 1A), *bsk* clones displayed a normal shape (Fig. 1B).

In contrast, *tkv bsk* clones were shorter along their apical-basal axis, had lost contact to the apical epithelial surface (Fig. 1C), and formed cyst-like structures with the apical cell membranes facing the center of the clone instead of the disc lumen (Fig. 1D). Furthermore, *tkv bsk* cells lost E-cadherin-based junctions to heterozygous neighboring cells and made E-cadherin-based junctions to other *tkv bsk* cells within the same clone (Fig. 1E). Clones mutant for both *mothers against dpp* (*mad*), which encodes a transcription factor essential for Dpp signal transduction (3), and *bsk* formed cyst-like structures similar to *tkv bsk* clones (fig. S2).

Epithelial cell shape is largely determined by the cytoskeleton. Cell shape changes leading to the formation of cyst-like structures could thus be due to cytoskeletal organization defects in *tkv bsk* cells. F-actin was enriched at the center of *tkv bsk* clones (Fig. 1F), whereas a dense apical network of microtubules, present in wild-type cells (11), was markedly reduced (Fig. 1, G and H). Basal microtubules appeared normal in *tkv bsk* cells (Fig. 1G). Both actin and microtubule cytoskeletons were normal in *bsk* clones (Fig. 1B) (12). These data indicate that Dpp signaling is required to maintain normal cytoskeletal organization in wing disc pouch cells. Furthermore, the presence of an apical microtubule network correlated with Dpp signaling activity along the anterior-posterior axis of wild-type wing discs (fig. S3), suggesting that Dpp signaling also plays a role in determining position-specific aspects of the microtubule cytoskeleton.

To test whether the loss of *tkv bsk* clones was through the formation of the cyst-like structures, we generated *tkv bsk* clones at different times during development and determined the number of cyst-like structures and the frequency of *tkv bsk* clone recovery in late-third instar larvae (Fig. 2A). Twenty-four hours after clone induction, 99% of *tkv bsk* clones were recovered ( $n = 93$ ) (Fig. 2B). Cells within clones still had contact to the apical epithelial surface, appeared to make normal E-cadherin-based junctions with

Max Planck Institute of Molecular Cell Biology and Genetics, Pfotenhauerstrasse 108, 01307 Dresden, Germany.

\*To whom correspondence should be addressed. E-mail: dahmann@mpi-cbg.de

neighboring cells (Fig. 2C), and had undetectable levels of Dpp signal transduction (fig. S4). Induction of *tkv<sup>-</sup>bsk<sup>-</sup>* clones earlier in development resulted in the recovery of

fewer clones (Fig. 2B). The *tkv<sup>-</sup>bsk<sup>-</sup>* clones that were recovered in the wing disc pouch of late-third instar larvae had formed cyst-like structures and were on average extruded farther

to the basal side of the epithelium (Fig. 2, B and C). At 96 hours after clone induction, only 20% of the clones were recovered ( $n = 44$ ), the majority of which had formed cyst-like structures and had been extruded from the basal side of the epithelium (Fig. 2, B to D). This suggests that the low frequency of *tkv<sup>-</sup>bsk<sup>-</sup>* clone recovery is due to the formation of cyst-like structures followed by extrusion from the basal side of the epithelium.

Some *tkv<sup>-</sup>bsk<sup>-</sup>* clones were observed in adult wings as extruded cyst-like structures located between the dorsal and ventral wing surfaces (Fig. 2, E to H), consistent with previous results (8, 13). These *tkv<sup>-</sup>bsk<sup>-</sup>* cells displayed hairs, characteristic structures of the adult epithelium, indicating that the extruded cells were alive and had undergone differentiation. Thus, in the absence of JNK, cells unable to transduce Dpp form cyst-like structures, are extruded from the wing disc epithelium, and can survive.

Our results suggest that Dpp signaling is involved in regulating cytoskeletal organization and is critical for normal cell morphology and integrity of wing disc epithelia. These functions of Dpp signaling are consistent with its role in embryonic dorsal closure and pupal thorax closure (14, 15). Hence, the regulation of cytoskeletal organization may be a more general function of Dpp not restricted to wing disc epithelia.

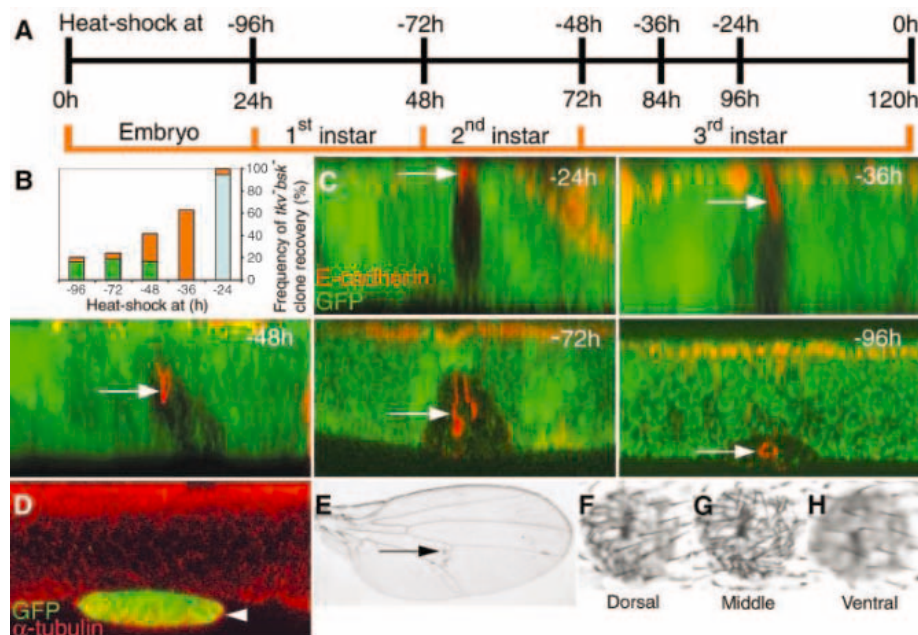
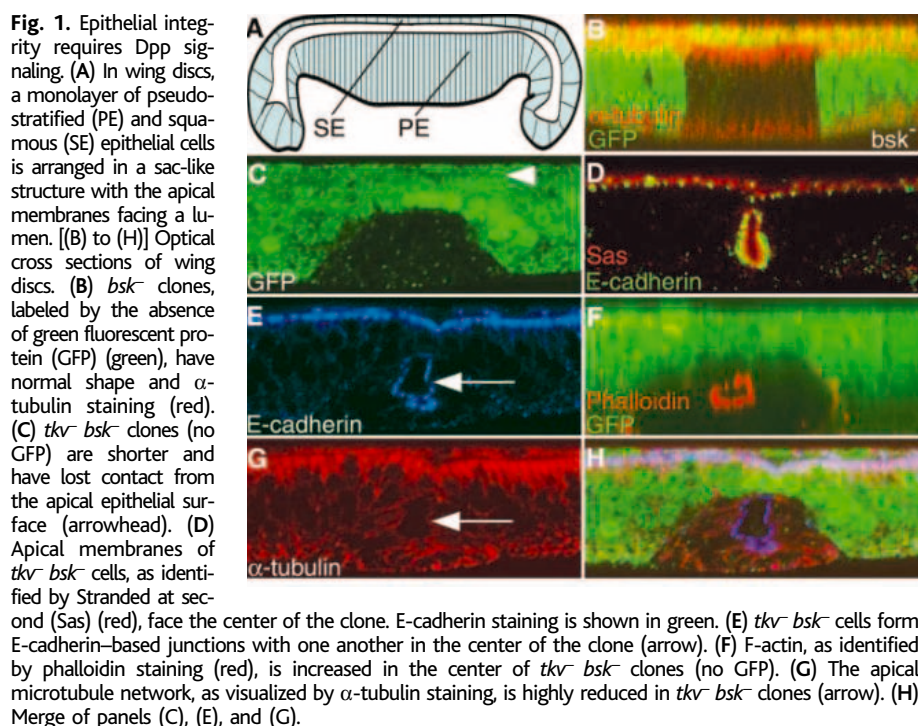


**Fig. 2.** Time course of extrusion of *tkv<sup>-</sup>bsk<sup>-</sup>* clones. (A) Timeline indicating how long before analysis larvae were heat shocked to induce clones. (B) Frequency of *tkv<sup>-</sup>bsk<sup>-</sup>* clone recovery expressed as a percentage. For each time point, the colors indicate the fraction of *tkv<sup>-</sup>bsk<sup>-</sup>* clones either with normal morphology (blue), constricted apically but still in contact with the apical epithelial surface (orange), or forming cyst-like structures that have lost contact from the apical epithelial surface (green). (C) Optical cross sections of wing discs with *tkv<sup>-</sup>bsk<sup>-</sup>* clones (no GFP, lack of green). Arrows point to E-cadherin staining (red) in mutant clones. Clones were induced at the indicated times before analysis. (D) Optical cross section of a wing disc with positively marked *tkv<sup>-</sup>bsk<sup>-</sup>* clones (arrowhead; GFP, green) induced 96 hours before analysis and stained for  $\alpha$ -tubulin (red). (E) *tkv<sup>-</sup>bsk<sup>-</sup>* clones form cyst-like structures in the adult wing (arrow). [(F) to (H)] Higher magnification of (F) dorsal, (G) middle, and (H) ventral views of the wing area marked by the arrow in (E).

References and Notes

1. Y. Shi, J. Massague, *Cell* **113**, 685 (2003).
2. P. M. Siegel, J. Massague, *Nature Rev. Cancer* **3**, 807 (2003).
3. L. A. Rafferty, D. J. Sutherland, *Dev. Biol.* **210**, 251 (1999).
4. P. J. Bryant, *Dev. Biol.* **128**, 386 (1988).
5. T. Adachi-Yamada, K. Fujimura-Kamada, Y. Nishida, K. Matsumoto, *Nature* **400**, 166 (1999).
6. T. Adachi-Yamada, M. B. O'Connor, *Dev. Biol.* **251**, 74 (2002).
7. E. Moreno, K. Basler, G. Morata, *Nature* **416**, 755 (2002).
8. M. Milan, L. Perez, S. M. Cohen, *Dev. Cell* **2**, 797 (2002).
9. J. R. Riesgo-Escovar, M. Jenni, A. Fritz, E. Hafen, *Genes Dev.* **10**, 2759 (1996).
10. Materials and methods are available as supporting material on Science Online.
11. S. Eaton, R. Wepf, K. Simons, *J. Cell Biol.* **135**, 1277 (1996).
12. J. Shen, C. Dahmann, data not shown.
13. N. Azpiazu, G. Morata, *Development* **127**, 2685 (2000).
14. M. G. Ricos, N. Harden, K. P. Sem, L. Lim, W. Chia, *J. Cell Sci.* **112**, 1225 (1999).
15. E. Martin-Blanco, J. C. Pastor-Pareja, A. Garcia-Bellido, *Proc. Natl. Acad. Sci. U.S.A.* **97**, 7888 (2000).
16. We thank T. Adachi-Yamada and K. Basler for fly stocks; K. Basler, S. Eaton, T. Hyman, K. Simons, and H. Thompson for comments on the manuscript; and M. Gibson and N. Perrimon for exchanging manuscripts before publication. This work was supported by the Max Planck Society.

Supporting Online Material

www.sciencemag.org/cgi/content/full/307/5716/1789/DC1  
 Materials and Methods  
 SOM Text  
 Figs. S1 to S4  
 References

2 September 2004; accepted 11 January 2005  
 10.1126/science.1104784

# NEW PRODUCTS

<http://science.labvelocity.com>

## DNA Plasmid Prep

The DNA Plasmid Prep Filter Plate Kit for preparation of high-quality plasmid DNA contains plates and seals for five 96-well preparations. The automation-friendly plates fit vacuum manifolds, centrifuges, and positive pressure devices. The pure DNA is suitable for downstream applications such as sequencing and restriction digestion.

**Nunc** For information 866-686-2548 [www.nuncbrand.com](http://www.nuncbrand.com)

## Red Fluorescent Protein

The BD Living Colors DsRed-Monomer Fluorescent Protein is a newly engineered mutant from *Discosoma* reef coral. It is suitable for multi-color applications in flow cytometry and fluorescence microscopy. The DsRed-Monomer protein is stable, allowing users to monitor fluorescence over extended periods of time. The chromophore matures rapidly and is readily detected 12 hours after transfection. The use of DsRed-Monomer as a fusion tag has been validated with a wide variety of proteins with diverse functions and subcellular locations. It is well-tolerated by mammalian cells and has been successfully used to create stably transfected, clonal cell lines.

**BD Biosciences** For information 877-232-8995 [www.bdbiosciences.com/clontech](http://www.bdbiosciences.com/clontech)

## Macroscopic Fluorescence System

The Leica MacroFluo is designed for large field-of-view, low-magnification (macro) fluorescence documentation and digital image stacking (multifocus or extended depth of field). The system is a unique combination of the long working distance and large field of view of a stereomicroscope with the vertical optical path of a classical light microscope. The design is suitable for imaging very large fields and increasing the accuracy of digital image processing, analysis, and measurement. The users who will benefit most from the MacroFluo are those conducting research on whole adult mice, fully developed zebrafish, chicken embryos, and *Xenopus*. Since these organisms tend to outgrow the field of view of standard stereomicroscopes, it is often difficult to attain high-quality, low-magnification images of them. In addition, the popularity of removing depth-of-field limitations from digital images via image stacking is increasing, and the on-axis MacroFluo will be useful to those labs wishing to capture publication-quality fluorescence images.

**Leica** For information 847-405-7026 [www.leica-microsystems.com](http://www.leica-microsystems.com)

## siRNA Design Service

HP Guaranteed siRNA is a small-interfering RNA (siRNA) design service. Four siRNAs targeting a gene of choice are designed using the innovative HiPerformance algorithm licensed from Novartis Pharmaceuticals, with a guarantee that at least two of them will result in efficient knockdown to the researcher's satisfaction.

**Qiagen** For information 800-426-8157 [www.qiagen.com](http://www.qiagen.com)

## Chromatography Medium

Capto Q, the first in a new family of chromatography media, is a medium for protein purification in downstream processing designed to meet the growing need in the biopharmaceutical market to process large feed volumes with high protein expression lev-

els. Capto Q is suitable for use in the capture and intermediate purification of high expression and high-volume feeds. The highly rigid matrix allows a wide working range of flow velocities, bed heights, and sample viscosities, all of which positively influence processing costs. High flow velocities increase volume throughput and reduce process time; longer bed heights eliminate the need for large equipment and keep footprints small; and high-flow processing of viscous samples means less dilution and shorter cycle times.

**GE Healthcare** For information +44 (0) 1494 498 050 [www.gehealthcare.com](http://www.gehealthcare.com)

## Automated Compound Storage and Retrieval

The MatriStore System is a compact, automated compound storage and retrieval system for pharmaceutical, biotechnology, genomic, and proteomic research laboratories. The modular design offers short installation times and the option to grow as storage needs grow. The MatriStore System has the capacity to store up to 40 million samples of chemical compounds, microorganisms, DNA, RNA, and other biological materials. It makes use of advanced robotics to pick and place samples at the rate of more than 20,000 per day. Housed in a cold-room environment, it operates from ambient to  $-20^{\circ}\text{C}$ . The system supports the large-scale storage of compounds held in varying plate and tube formats.



**Matrical** For information 509-343-6225 [www.matrical.com](http://www.matrical.com)

## Literature

The Upchurch Scientific 2005 *Catalog of Chromatography and Fluid Transfer Components* includes valves, pumps, and accessories for IDEX Corporation's precision flow products business units Rheodyne, Ismatec, and Micropump. The catalog offers a wide array of nanoscale to preparative scale fluidic components for analytical, biotechnology, and diagnostic lab applications. The catalog also includes application notes and technical resource information.

### Upchurch Scientific

For information 800-426-0191 [www.upchurch.com](http://www.upchurch.com)

*Ultrafiltration Handbook* includes 20 application notes and protocols for protein research, DNA sequencing, forensic, and clinical applications. The handbook's selection guide helps researchers choose the most appropriate ultrafiltration tool for a wide range of applica-

tions, including protein concentration, desalting, polymerase chain reaction clean-up, and sequencing reaction clean-up.

**Millipore** For information 800-MILLIPORE [www.millipore.com/proteinresearch](http://www.millipore.com/proteinresearch)

Newly offered instrumentation, apparatus, and laboratory materials of interest to researchers in all disciplines in academic, industrial, and government organizations are featured in this space. Emphasis is given to purpose, chief characteristics, and availability of products and materials. Endorsement by *Science* or AAAS of any products or materials mentioned is not implied. Additional information may be obtained from the manufacturer or supplier by visiting [www.science.labvelocity.com](http://www.science.labvelocity.com) on the Web, where you can request that the information be sent to you by e-mail, fax, mail, or telephone.

For more information visit **GetInfo**,  
*Science's* new online product index at  
<http://science.labvelocity.com>

From the pages of GetInfo, you can:

- Quickly find and request free information on products and services found in the pages of *Science*.
- Ask vendors to contact you with more information.
- Link directly to vendors' Web sites.